

Modern Approaches in Solid Earth Sciences

Andrew Y. Glikson
Franco Pirajno

Asteroids Impacts, Crustal Evolution and Related Mineral Systems with Special Reference to Australia

 Springer

Modern Approaches in Solid Earth Sciences

Volume 14

Series Editors

Yildirim Dilek, Department of Geology and Environmental Earth Sciences,
Miami University, Oxford, OH, U.S.A.

Franco Pirajno, The University of Western Australia, Perth, Australia

Brian Windley, Department of Geology, The University of Leicester, UK

More information about this series at <http://www.springer.com/series/7377>

Andrew Y. Glikson • Franco Pirajno

Asteroids Impacts, Crustal Evolution and Related Mineral Systems with Special Reference to Australia

 Springer

Andrew Y. Glikson
Planetary Science Institute
Australian National University
Canberra, ACT, Australia

Franco Pirajno
Centre for Exploration Targeting
The University of Western Australia
Crawley, WA, Australia

Responsible Series Editor: F. Pirajno

ISSN 1876-1682 ISSN 1876-1690 (electronic)
Modern Approaches in Solid Earth Sciences
ISBN 978-3-319-74544-2 ISBN 978-3-319-74545-9 (eBook)
<https://doi.org/10.1007/978-3-319-74545-9>

Library of Congress Control Number: 2018933184

© Springer International Publishing AG 2018

This work is subject to copyright. All rights are reserved by the Publisher, whether the whole or part of the material is concerned, specifically the rights of translation, reprinting, reuse of illustrations, recitation, broadcasting, reproduction on microfilms or in any other physical way, and transmission or information storage and retrieval, electronic adaptation, computer software, or by similar or dissimilar methodology now known or hereafter developed.

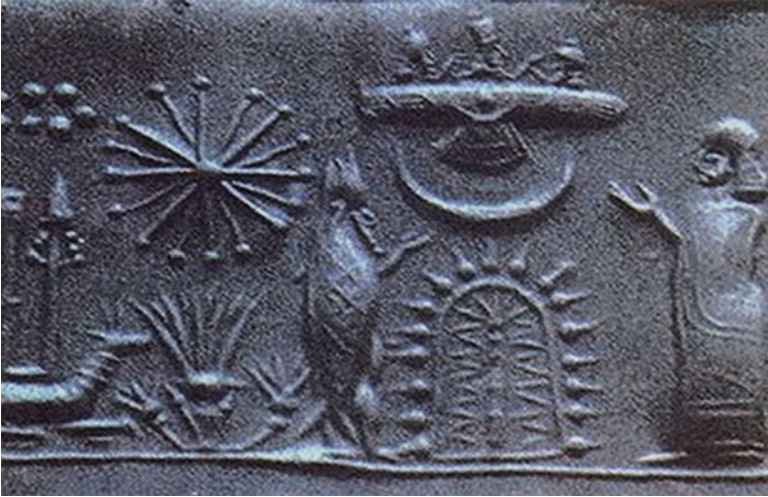
The use of general descriptive names, registered names, trademarks, service marks, etc. in this publication does not imply, even in the absence of a specific statement, that such names are exempt from the relevant protective laws and regulations and therefore free for general use.

The publisher, the authors and the editors are safe to assume that the advice and information in this book are believed to be true and accurate at the date of publication. Neither the publisher nor the authors or the editors give a warranty, express or implied, with respect to the material contained herein or for any errors or omissions that may have been made. The publisher remains neutral with regard to jurisdictional claims in published maps and institutional affiliations.

Printed on acid-free paper

This Springer imprint is published by the registered company Springer International Publishing AG part of Springer Nature.

The registered company address is: Gewerbestrasse 11, 6330 Cham, Switzerland



The Anunnaki, a group of deities that appear in the mythological traditions of the ancient Sumerians, Akkadians, Assyrians, and Babylonians, some of whom apparently represented the stars, i.e., the zodiac, or “heavenly host” worshipped by the Canaanites and Hebrews. Creative Commons (<https://www.flickr.com/photos/tortuga767/525162235/in/photolist-NpAri-qCtV4W-5YiNuT-7AdeWc-5YiPa6-ArwNvs-qs5Fjk-qawEF1-qavKvm-qawK6U-qawMu1-5YiNzH-bjqDs-c-dX9jVD-9R4bpo-7UKhQP-c5Vys1-NpfYf-LwTdSc-NpfYd-fzHbv9-5Yo3eN-5Yo3sA-3dEmny-5YiNMR-5Yo2LC-5YiNo2-5YiNQk-5Yo3a5-5YiNJM-5Yo36m-ecrYj1-n5ZZe-5Yo3xm-5YiNsF-9Wbk1t-5YiP48-5YiPeV-8VVgsj-5YiNEH-7u9hGF-8fAreF-qaEJtx-c3jWJS-ANDC5v-7udbsL-AWUNi1-qYiyFE-fU9Uwt-g3nwhA>)

*In honor of Eugene Merle Shoemaker and
Robert Sinclair Dietz: Pioneers of asteroid
impact research*

Preface

Thanks to their long-term geological stability, Precambrian and younger terrains in the Australian continent contain a large number of impact structures and probable impact structures. These include 38 confirmed asteroid impact structures and 43 ring structures, many of which constitute possible to probable asteroid impact structures. These structures have been the subject of more than half a century of studies by geologists from universities, geological surveys, and related institutions. The structures range from several tens of meter-large craters, such as the Henbury and Veevers craters, to buried structures larger than 100 km in diameter, such as the Woodleigh impact structure and the Warburton probable impact structure. Discoveries and research of many of these structures, notably by Peter Haines, Eugene and Caroline Shoemaker, John Gorter, Robert Iasky, Victor Gostin, George Williams, and others, published in the literature, are reviewed in the present book *“Asteroid Impacts, Crustal Evolution, and Mineral Systems with Reference to Australia.”* The book presents a compilation and a review of Australian impact structures, impact ejecta/fallout deposits, and related mineralization, including discussion of the significance of many of these structures for crustal evolution and for mineralization. The book further reviews asteroid impact ejecta/fallout units, mainly of Archaean age studied in the Pilbara Craton of Western Australia and also the late Proterozoic Bunyeroo impact layer in South Australia. Discoveries of impact fallout units in the Pilbara Craton by the US scientists, including Bruce Simonson, Scott Hassler, Don Lowe, and Gary Byerly, and their students and follow-up discoveries and research by Australian geologists have defined the Pilbara as one of the two best documented terrains where Archaean impact ejecta/fallout deposits are identified, the other terrain being the Kaapvaal Craton in southern Africa. A synthesis of evidence from both cratons indicates periods of large asteroid bombardments during ~3.47–2.48 billion years ago, including peak bombardment about 3.25–3.22 billion years ago. The latter period coincides with an abrupt transformation of an early Archaean granite–greenstone crust to mid- to late Archaean semi-continental crustal regimes, underpinning the significance of heavy asteroid impact events for crustal evolution. Thermal and hydrothermal processes associated with impact cratering bear important consequences for the formation of mineral deposits, such as Ni at

Sudbury and Pb–Zn at Siljan and Kentland. Impact structures may also provide sites for accumulation of hydrocarbons, whereas in some instances fracturing associated with impact structures allows outward migration of oil and gas.

Canberra, ACT, Australia
Crawley, WA, Australia

Andrew Y. Glikson
Franco Pirajno

Acknowledgments

We thank Arthur Hickman, Peter Haines, Bruce Simonson, Don Lowe, Gary Byerly, Victor Gostin, John Gorter, Alastair Stewart, Ken Mitchell, and the late Ian Williams for consultations and advice and Gary Byerly, Hugh Davies, John Gorter, Victor Gostin, Robert Iasky, Don Lowe and George Williams for reviews and Alastair Stewart for meticulous editing. Andrew is grateful to Alan Whitaker, Richard Blewett, Peter Milligan, Russell Korsch, Klajnik Krisztián, Tony Meixner, Ross Costello, and Michael Doublier of Geoscience Australia for their help with impact research and the compilation of an impact ARC-GIS. We acknowledge the contributions of the following geologists to the study of Australian asteroid and meteorite impacts: A. Abels, Alex Bevan, Alastair Stewart, Ann Therriault, Arthur Hickman, B. Rasmussen, Bruce Simonson, C. O'Neill, Caroline Shoemaker, Dan Milton, Don Lowe, Doug Guppy, Duane Hamacher, Duncan Dow, Eugene Shoemaker, Francis Macdonald, Gary Byerly, George Williams, Grant Boxer, H Zummersprekel, Ian Sweet, Ian Williams, J. Salisbury, J. Dunster, J. Plescia, Joe Harms, John Bunting, John Gorter, John Plescia, John Vickers, Ken McNamara, Ken Mitchell, Kieren Howard, Lutz Bischoff, Malcolm Wallace, Michael Dence, Michael Dentith, Paul Tonkin, Peter Haines, Phil Hawke, Robert Iasky, Robin Brett, T. Munson, Tonguc Uysal, Tony Yeates, and Victor Gostin, among others. We thank many other geologists and geophysicists for their help in our studies. Andrew is particularly grateful to the late Eugene Shoemaker for inspiration and encouragement and to John Vickers for long-term collaboration and help in the field.

Contents

1 Asteroid Impacts	1
1.1 Asteroids in Space and Time	1
1.2 Hadean to Early Archaean Impacts	10
1.3 Criteria for Identification of Asteroid Impacts	21
References	25
2 Australian Asteroid Ejecta/Fallout Units	31
2.1 c.3472 Ma Impacts	32
2.2 c.3460 Ma Impacts	37
2.3 Impact-Correlated Units c.3.3–3.227 Ga	39
2.4 Jeerinah c.2.63 Ga Impact Layer (JIL) and Carawine Dolomite Impact/Tsunami Megabreccia	41
2.5 Paraburdoo c. 2.57 Ga Spherule Layer	46
2.6 Spherule Marker Bed (SMB) c. 2.56 Ga Layer	47
2.7 Dales Gorge (DGS4) c.2.48 Ga Spherule Layer	50
2.8 Bunyeroo ~580 Ma Impact Ejecta	53
References	56
3 The World’s Largest Late to Post-Archaean Asteroid Impact Structures	61
3.1 Maniitsoq, South Greenland (D~ > 100 km) ~2975 Ma)	61
3.2 Vredefort, South Africa (D~298 km; 2023 ± 4 Ma)	62
3.3 Sudbury, Ontario (D~250 km; 1850 ± 3 Ma)	65
3.4 Chicxulub, Yucatan Peninsula, Mexico (D~170 km; 64.98 ± 0.05 Ma)	66
3.5 Popigai (D~100 km; 35.7 ± 0.2 Ma)	68
3.6 Warburton Twin Structures, South Australia (Each D~200 km; End-Carboniferous?)	70
3.7 Woodleigh (D = 120 km)	73
References	75

4	Australian Impact Structures >10 Km-Large	79
4.1	Exposed Impact Structures >10 km in Diameter	80
4.1.1	Acraman (D~30–90 km)	84
4.1.2	Yarrabubba (D~30–70 km)	85
4.1.3	Shoemaker (D~29–31 km)	86
4.1.4	Lawn Hill (D ~ 18–20 km)	88
4.1.5	Strangways (D~25–40 km)	89
4.1.6	Amelia Creek (D~20 × 12 km)	91
4.1.7	Cleanskin (D~15 km)	92
4.1.8	Glikson (D~14 km)	93
4.1.9	Gosses Bluff (D~12 km)	94
4.1.10	Kelly West (D~8–20 km)	97
4.1.11	Spider (D~11–13 km)	99
4.1.12	Goyder (D~9–12 km)	100
4.2	Buried Impact Structures	100
4.2.1	Warburton East (D ~ < 200 km)	102
4.2.2	Warburton West (D < 200 km)	102
4.2.3	Woodleigh (D = 120 km)	103
4.2.4	Talundilly (84 km)	103
4.2.5	Tookoonooka (D~55 km)	104
4.2.6	Gnargoo (D~75 km)	106
4.2.7	Mount Ashmore (>50 km)	107
4.2.8	Yallalie (D~12 km)	108
4.2.9	Lake Raeside (D~11 km)	109
4.3	Meteoritic Impact Craters	110
4.3.1	Goat Paddock (D~6 km)	110
4.3.2	Liverpool (D~1.6 km)	110
4.3.3	Darwin (D~1.2 km)	112
4.3.4	Wolfe Creek (D~0.88 km)	113
4.3.5	Hickman (D~0.36 km)	114
4.3.6	Boxhole (D~0.17 km)	116
4.3.7	Henbury Craters	117
	References	118
5	Ring and Dome Features, Possible and Probable Impact Structures	123
5.1	Structural Elements of Circular Features Suggestive of an Impact Origin	124
5.2	Morphological and Buried Ring Features	127
5.3	Magnetic and Gravity Ring Anomalies	141
5.4	Large Geophysical Multi-ring Features	150
5.5	Distribution Patterns of Ring and Dome Features	152
	References	154

- 6 Asteroids and Crustal Evolution** 157
 - 6.1 Significance of Archaean Impacts 157
 - 6.2 Significance of Proterozoic and Phanerozoic Impacts 166
 - References 167

- 7 Asteroids and Associated Mineral Systems** 173
 - 7.1 Introduction 174
 - 7.2 Asteroid and Cometary Impacts and Hydrothermal Circulation 175
 - 7.3 A Working Model 176
 - 7.4 Mineral Deposits and Impact Structures 178
 - 7.5 The Sudbury Hydrothermal System 180
 - 7.6 The Lockne Impact Structure 181
 - 7.7 The Vredefort Meteorite Impact and the Case for Witwatersrand Gold 182
 - 7.8 Australian Examples of Impact-Related Hydrothermal Activity 186
 - 7.9 Shoemaker Impact Structure 188
 - 7.10 Hydrothermal Alteration 190
 - 7.11 Yarrabubba Impact Structure 193
 - 7.12 Woodleigh Impact Structure 197
 - 7.13 Concluding Remarks 201
 - References 202

- Index** 207

Introduction

“Nature hides her secrets . . .” Albert Einstein

Humans have been looking at the stars, planets, comets, and falling meteorites and meteorite showers ever since, and much earlier than, the onset of civilization (Frontispiece). The terrestrial planets of the inner solar system—Mars, Earth, Venus, and Mercury—are all affected by asteroids deflected from the asteroid belt and comets falling off the Kuiper belt. However, when viewed from space planet Earth, although located in the trajectory of these bodies, displays little or no cratering. This impression is apparent rather than real, arising due to (1) the extension of the oceans over some two-thirds of the Earth’s surface and (2) the dynamic nature of Earth, including the accretion and subduction of tectonic plates as well as the intensive erosion processes. The asteroid impact record on Earth is thus to a large extent concealed and is the subject of extensive search using structural, geophysical, petrological, and geochemical methods. The cover-up of most oceanic impact records and erosion of orogenic mountain belts leave stable old cratons as the best sites for preservation of impact scars, including craters and their deep-seated roots and rebound dome structures. This book documents the impact records of the Australian continent and marine shelves, including impact ejecta/fallout units (Chap. 2), exposed impact structures (Sect. 4.1), buried impact structures (Sect. 4.2), meteorite craters (Sect. 4.3), and ring and dome geophysical anomalies of unproven origin (Chap. 5). A review of very large impact structures worldwide is given in Chap. 3.

Falling between the disciplines of astronomy, planetary science, and geology, the subject of asteroid impacts is only rarely taught in universities, remaining a focus of research by small teams. In Australia these notably included American scientists such as Eugene and Caroline Shoemaker, Don Lowe, Gary Byerly, Bruce Simonson, and Scott Hassler and Australian scientists including George Williams and Victor Gostin; geological survey scientists including P. Haines, P. Hawke, R. Iasky, F. Pirajno, and A. Hickman; and university and museum scientists including M. Dentith and A. Bevan and others. It was not until about 1981 when Louis and Walter Alvarez unearthed a telltale iridium-rich sedimentary horizon at the ~66 million-year-old (Ma) Cretaceous–Tertiary (K–T) boundary at Gubbio, Italy

(Alvarez et al. 1980, 1982; Alvarez 1997), that a paradigm shift took place in terms of the recognition of the significance of extraterrestrial impacts for K–T boundary mass extinction of species (Chap. 1, Fig. 1.9) and the effects of such impacts on terrestrial biological evolution. The spectre of the large dinosaurs extinguished by a large asteroid impact has fired the imagination of people like no extraterrestrial event has done before. The discovery reestablished the idea that much of Earth's history has been shaped by catastrophes, a theory promoted by Georges Cuvier and natural theologians which was preceded, but was largely supplanted, by Darwin's theory of evolution and by Hutton's and Lyell's geological uniformitarian and gradualism theory.

The geological antiquity of Australian land surfaces, in particular platform sediment and volcanic cover over Precambrian cratons in central and western parts of the continent, allows preservation of a range of circular features, including morphological and drainage rings, circular lakes, volcanic craters, tectonic domes, oval granite bodies, mafic igneous plugs, salt diapirs, and magnetic, gravity, and seismic anomalies of unknown origin. The criteria applied for recognition of asteroid impact structures and meteorite craters from geophysical evidence (Grieve and Pilkington 1996; Shoemaker and Shoemaker 1996; Glikson and Uysal 2010) and from petrological evidence for shock metamorphism (French 1998; French and Koeberl 2010) allow the identification of at least 38 impact structures on the Australian continent and surrounding continental shelf (Gorter 1998; Haines 2005; Bevan et al. 2012; Dunster et al. 2014; World Impacts Database) (Table 4.1). In addition 43 examples will be outlined of exposed and buried circular structures and features, including exposed ring and dome features and circular magnetic, gravity, and seismic anomalies of buried features (Table 5.1). The discussion will proceed in terms of examples of large geophysical multi-ring features including total magnetic intensity anomalies, circular gravity anomalies, and seismic domes.

The pressure–temperature field of shock metamorphism is distinct from that of terrestrial metamorphism, including the high-pressure eclogite facies. Central to the identification of extraterrestrial impact structures are criteria for shock metamorphism calibrated with laboratory experiments (French 1998) (Fig. 1.17). The static PT field of regional metamorphism is mostly below 10 GPa, whereas shock pressures inducing the graphite to diamond transformation, coesite to stishovite transformation, shatter cones, planar deformation features, diaplectic glass, and shock melting are higher than 10 GPa. Structural signatures of buried extraterrestrial impact structures are identified by cross-cutting relations with older structures, radial and oblique faulting, and tensional faulting at the rims and centripetal dome and thrust structures at the centers. Confirmation of an impact origin has to await petrofabric examination for intra-mineral deformation features, commonly planar deformation features (pdf) in quartz, solid-state vitrification to diaplectic glass, and melting of quartz to lechatelierite (French 1998).

Using these criteria, early discoveries included the Meteor Crater, Arizona (Roddy and Shoemaker 1995), and the Ries Crater, Germany (cf. Chao 1967, 1968). The pioneering studies of Robert Dietz have paved the way for the

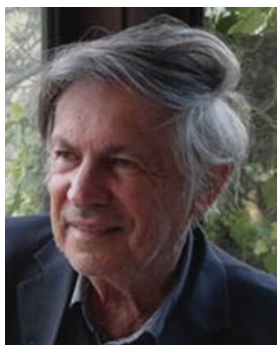
identification of giant impact structures, referred to as astroblemes (star scars), including Vredefort (289 km-diameter; $2,023 \pm 4$ Ma) (Dietz 1961) and Sudbury (~250 km; 1850 ± 3 Ma) (Dietz 1964). A number of factors militate against an origin of these structures due to deep-seated or cryptoexplosion mantle-derived processes (Nicolaysen and Ferguson 1990). These terrains contain shock metamorphic mineralogy and textures, including shatter cones, planar deformation features in quartz, high-pressure phases [coesite, stishovite], and shock vitrification products such as silica glass (lechatelierite), feldspar glass (maskelynite), impact melting, melt breccia, pseudotachylite veins, microbreccia dykes, and iridium anomalies. While melt rock abound, no volcanic rocks are associated with mega-impact structures. The shock metamorphic features indicate pressures of >10 GPa, exceeding pressures induced by volcanic explosions.

References

- Alvarez W (1997) *Tyranosaurus Rex and the crater of doom*. Princeton University Press, Princeton, p 185
- Alvarez L, Alvarez W, Asaro F, Michel HV (1980) Extraterrestrial cause for the Cretaceous-Tertiary extinction. *Science* 208:1095–1108
- Alvarez L, Alvarez W, Asaro F, Michel HV (1982) Iridium anomaly approximately synchronous with terminal Eocene extinctions. *Science* 216:886–888
- Bevan A, Bunting J, Freeman M (2012) Western Australian impact craters Field Excursion 20–29 August 2012. <http://museum.wa.gov.au/sites/default/files/Met-FT-2012.pdf>
- Chao ECT (1967) Shock effects in certain rock-forming minerals. *Science* 156:192–202
- Chao ECT (1968) Pressure and temperature histories of impact-metamorphosed rocks based on petrographic observations. In: French BM, Short NM (eds) *Shock metamorphism of natural materials*. Mono Book Corp, Baltimore. 135–158
- Dietz RS (1964) Sudbury structure as an astrobleme. *J Geol* 72:412–434
- Dunster JN, Haines PW, Munson TJ (2014) Meteorites and impact structures in the Northern Territory. Northern Territory Geological Survey Record 2014–007
- French BM (1998) Traces of catastrophe—a handbook of shock metamorphic effects in terrestrial meteorite impact structures. *Lunar Planet Sci Inst Contrib* 954:120
- French BM, Koeberl C (2010) The convincing identification of terrestrial meteorite impact structures: what works what doesn't and why. *Earth Sci Rev* 98:123–170
- Glikson AY, Uysal IT (2010) Evidence of impact shock metamorphism in basement granitoids, Cooper Basin (Abstract). In: *Proceedings of the Australian geothermal conference, Adelaide*. Geoscience Australia Record 2010/35
- Gortler JD (1998) The petroleum potential of Australian Phanerozoic impact structures. *APPEA J* 1998:159

- Grieve RAF, Pilkington M (1996) The signature of terrestrial impacts. *Aust Geol Surv J Aust Geol Geophys* 16:399–420
- Haines PW (2005) Impact cratering and distal ejecta: the Australian record. *Aust J Earth Sci* 52:481–507
- Nicolaysen LO, Ferguson J (1990) Cryptoexplosion structures shock deformation and siderophile concentration related to explosive venting of fluids associated with alkaline ultramafic magmas. *Tectonophysics* 171:303–335
- Roddy DJ, Shoemaker EM (1995) Meteor Crater (Barringer Meteorite Crater) Arizona: summary of impact conditions. *Meteoritics* 30:567
- Shoemaker EM, Shoemaker CS (1996) The Proterozoic impact record of Australia. *Aust Geol Surv Org J Aust Geol Geophys* 16:379–398
- World Impacts Database. <http://www.passc.net/EarthImpactDatabase/>

Authors' Biography



Andrew Yoram Glikson an Earth and paleo-climate scientist, studied geology at the University of Jerusalem and graduated at the University of Western Australia in 1968. He conducted geological studies of the oldest geological formations in Australia, South Africa, India, and Canada and studied large asteroid impacts, including effects on the atmosphere, oceans, and mass extinction of species. Between 1998 and 2014, this work included detailed studies of impact ejecta units in the Pilbara Craton, Western Australia, geochemical studies of impact ejecta units from South Africa, and the identification and study of several Australian buried impact structures, including Woodleigh, Gnargoo, Mount Ashmore, Talundilly, Warburton East and West, Hickman crater, and Lake Raeside jointly with Arthur Hickman, recently a 3.46 Ga twin impact ejecta and possibly the Diamantina anomaly. Currently, he is a Visiting Scientist in Geoscience Australia developing a catalogue and website of Australian confirmed and possible asteroid impact structures. Since 2005 he extended the studies of past mass extinctions to the effects of climate on human evolution, the discovery of fire and global warming.



Franco Pirajno Adjunct Professor at the Centre for Exploration Targeting (CET), University of Western Australia, is an authority on tectonics, ore deposit geology and mineral exploration, with experience in Europe, southern Africa, South East Asia, New Zealand, the southwest Pacific, China, Greenland, southern and eastern Siberia, and Australia. He joined the Geological Survey of Western Australia in 1993, following post-doctoral research at the Vesuvius Volcano Observatory, exploration with Anglo American Corporation, Chair of Economic Geology at Rhodes University, South Africa, with research activity

on precious metals and base metals mineral deposits in the southern African subcontinent. In the last 23 years Franco Pirajno has worked extensively in Western Australia's Proterozoic terranes and was instrumental in the discovery of a new large igneous province in Australia. He was a Visiting Professor at Peking University in 2003, China University of Geosciences, Beijing, in 2004, Distinguished Foreign Professor at Hefei University of Technology during September–October 2012, and Editor-in-Chief of *Ore Geology Reviews* since 2012. His principal research interests include Archaean granite greenstone terrane, Proterozoic intra-cratonic basins, rift associated mineral deposits, layered mafic-ultramafic complexes, metamorphic belts of Proterozoic age, alkaline complexes and an-orogenic magmatism, and carbonate rocks in passive margin settings.

Chapter 1

Asteroid Impacts



Abstract Mars, Earth, Venus and Mercury are all affected by asteroids deflected from the asteroid belt and comets falling off the Kuiper belt, but when the Earth is viewed from space it betrays little or no cratering by large impacts, despite the fact it is located in the trajectory of both asteroids and comets. This impression however is more apparent rather than real and constitutes the consequence of the coverage of the Earth's crust by oceans over some 2/3 of the surface. The other major factor is the dynamic nature of the Earth, including the accretion and subduction of tectonic plates as well the intensive erosional processes, which obscure its impact history. Thus asteroid impact records on Earth are mostly concealed and are the subject of extensive exploration, using structural, geophysical, petrological and geochemical methods. It is the stable cratons which cratons contain the best preserved impact records, including exposed and filled-in craters and deep-seated impact-rebound dome structures. Documentation of the impact records of the Australian continent and marine shelves includes impact ejecta/fallout units, exposed impact structures, buried impact structures, meteorite craters and ring and dome geophysical anomalies of unproven origin. The identification of impact structures and impact ejecta/fallout deposits is fraught with complications. Initial references to circular morphological and drainage patterns, round lakes and oval depressions may provide a hint to possible underlying ring or dome structures, requiring field tests or drilling. Where impact structures have been destroyed, the presence of impact ejecta/fallout in sediments allows further insights into the impact history of the Earth.

1.1 Asteroids in Space and Time

Nearly two million asteroids – stony and dust aggregates accreted from relics of the solar disc and fragmented during subsequent collisions form the main asteroid belt between Jupiter and Mars at 2.15–3.3 AU (255–600 million km) and from the Trojan asteroid belt (Figs. 1.1, 1.2, 1.3 and 1.4), as well as comets (Fig. 1.5) falling off the Oort cloud at the outer fringe of the solar system, impinge on the inner planets. The total mass of asteroids would form a body of ~1500 km diameter. The size distribution includes

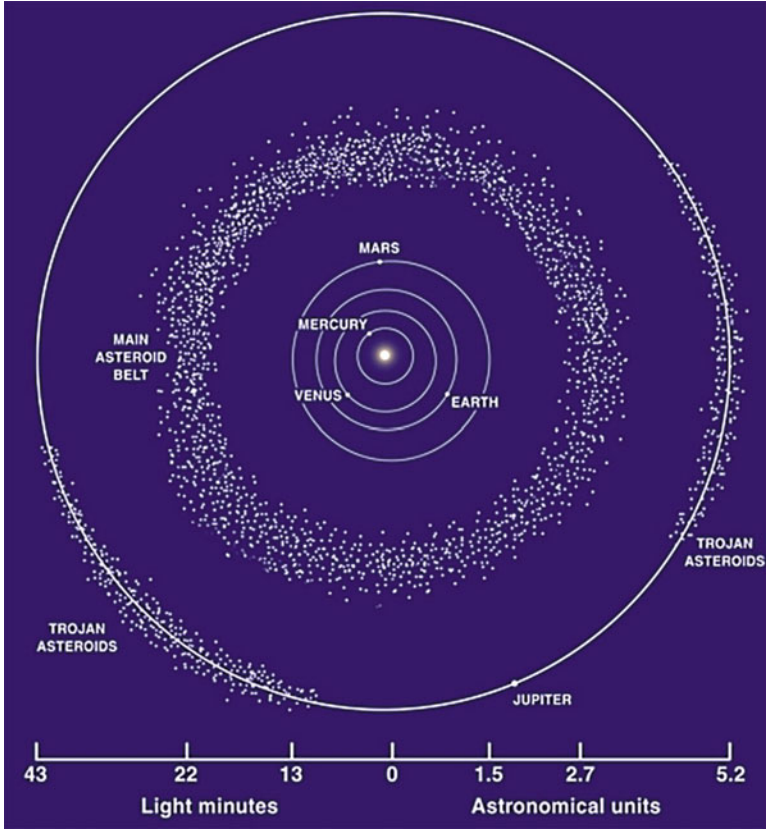


Fig. 1.1 Asteroids are material left over from the formation of the solar system. One theory suggests that they are the remains of a planet that was destroyed in a massive collision long ago. More likely, asteroids are material that never coalesced into a planet. If the estimated total mass of all asteroids was gathered into a single object, the object would be less than 1500 km across, less than half the diameter of our moon. NASA (<https://solarsystem.nasa.gov/galleries/the-asteroid-belt>)

12 asteroids of diameters 250 km or larger. Asteroid orbits are elliptical at the same direction as Earth and taking 3–6 years for a full orbit around the Sun. Near Earth asteroids (NEA) at orbits of about 1.3 AU (~195.106 km) include (a) Amor class asteroids crossing the Mars orbit, the typical one being Eros; (b) Apollo class asteroids crossing Earth's orbit with a period greater than 1 year, such as Geographos; (c) Aten class asteroids cross Earth's orbit with a period less than 1 year, an example being Ra-Shalom. NEA with orbits of 0.983 to 1.3 astronomical units (AU) pose a potential impact risk for Earth. With over 90% of NEA larger than 1 km already discovered (Fig. 1.2), the number now tops 15,000, with an average of 30 new discoveries added each week. This milestone marks a 50% increase in the number of known NEAs since 2013, when discoveries reached 10,000 in August of that year. In 2017 the NEA Program is focusing on finding 90% of the NEA population larger than 140 m. Many

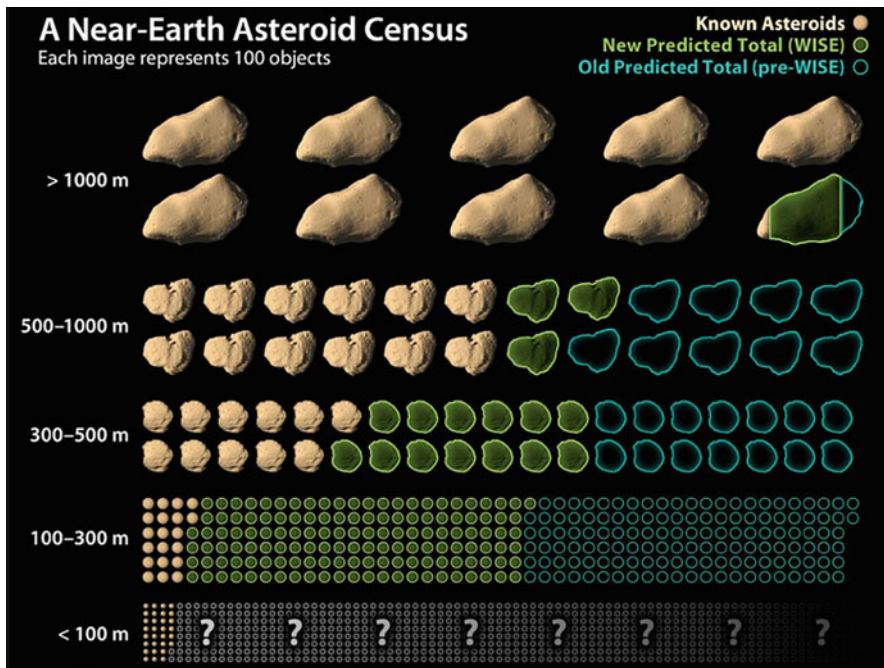


Fig. 1.2 WISE revises numbers of asteroids near earth. This chart shows how data from NASA’s wide-field infrared survey explorer, or WISE, has led to revisions in the estimated population of near-earth asteroids. The infrared-sensing telescope performed the most accurate survey to date of a slice of this population as part of project called NEOWISE. This allowed the science team to make new estimates of the total numbers of the objects in different size categories. NEOWISE observed more than 500 objects larger than 100-m (330-ft) wide – what can be thought of as medium to large-size asteroids. Near-earth asteroids smaller than this size range were not studied, and near-earth comets will be analyzed at a later time. Asteroid sizes are not drawn to scale in the chart. Each asteroid image represents about 100 actual objects. Near-earth asteroids that have already been found are filled in and appear brown. An entire row of asteroid images through the blue outlines shows how many total objects were thought to exist before the NEOWISE survey. The green outlines show the reduced new estimates based on the NEOWISE data. As the graphic reveals, only a small difference was observed in the estimated total numbers of the largest asteroids – the ones with the potential for global consequences should they impact earth. For the medium-sized asteroids, which could still destroy a metropolitan area, new estimates predict fewer space rocks than previously thought. Details are listed below. –For the largest asteroids, larger than 1000 m (3300 ft), NEOWISE data revises the total population down to 981 from a prior estimate of about 1000. While this is not a dramatic difference, the findings show that NASA has met an initial near-earth asteroid goal agreed to with Congress in 1998, calling for at least 90% of the largest objects to be found. There are an estimated 911 objects of this size range known, which means that NASA has found 93%. That leaves roughly 70 of these bodies left to find. The NEOWISE data reveals an approximately 44% decline in the estimated numbers of medium-sized asteroids, which are defined as those objects between 100 and 1000 m (330 and 3300 ft). Estimates now indicate about 19,500, whereas 35,000 were thought to exist before. The study does not apply to objects smaller than 100 m (330 ft), but it is estimated that there are more than a million in this size range based on previous studies. NASA/JPL-Caltech. NASA (https://www.nasa.gov/mission_pages/WISE/multi-media/gallery/neowise/pia14734.html)

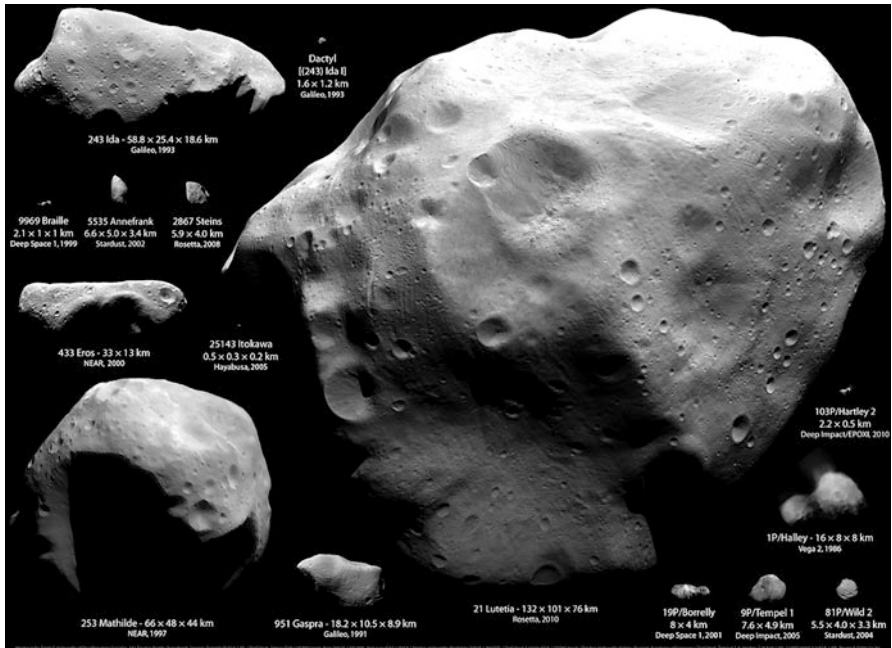


Fig. 1.3 All asteroids and comets visited by spacecraft as of November 2010 Credits: Montage by Emily Lakdawalla. Ida, Dactyl, Braille, Annefrank, Gaspra, Borrelly: NASA/JPL/Ted Stryk. Steins: ESA/OSIRIS team. Eros: NASA/JHUAPL. Itokawa: ISAS/JAXA/Emily Lakdawalla. Mathilde: NASA/JHUAPL/Ted Stryk. Lutetia: ESA/OSIRIS team/Emily Lakdawalla. Halley: Russian Academy of Sciences/Ted Stryk. Tempel 1, Hartley 2: NASA/JPL/UMD (<https://www.universetoday.com/37425/what-are-asteroids-made-of/>)

of the data depend on diameters that can only be roughly inferred from an asteroid's estimated absolute magnitude (H) and an assumed reflectivity, or albedo.

The asteroid belt includes over 50% of large asteroids – Ceres (950 km), Vesta (530 km), Pallas (530–565 km) and Hygiea (350–500 km) (Fig. 1.3), over 200 asteroids are more than 100 km in diameter and 700,000–1,700,000 asteroids exceed 1 km, the rest forming dust particles. Asteroids include:

- A. Carbonaceous (C-type) chondrites inhabit the main belt's outer regions, include more than 75% of known asteroids, have low albedo (0.03–0.09), with chemical ratios akin to solar composition and depleted in hydrogen and helium.
- B. Siliceous (S-type) asteroids occupy the inner asteroid belt, include about 17% of known asteroids, show high albedo of 0.10–0.22, consist of metallic iron mixed with iron and magnesium-silicates. S-type asteroids display various degrees of melting and segregation of metal from silicate.
- C. Metallic (M-type) inhabit the middle part of the asteroid belt, display high albedo (0.10–0.18) and consist of metallic iron.

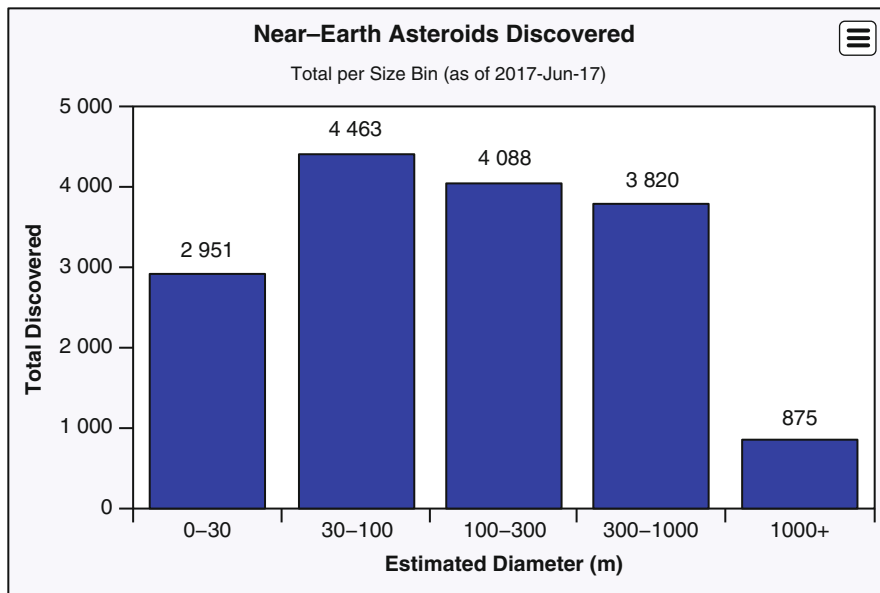


Fig. 1.4 Current total number of known NEAs grouped according to their estimated sizes. The first size bin represents NEAs smaller than ~ 30 m in diameter. The last bin represents NEAs with diameters larger than ~ 1 km. NASA (<https://cneos.jpl.nasa.gov/stats/size.html>)

By June 2017 total near Earth asteroids (NEA) discovered included 875 bodies of >1 km, 3820 of 0.3–1.0 km, 4088 of 0.1–0.3 km, 4463 of 30–100 m and 2951 of 0–30 m in diameter (Figs. 1.2, 1.3 and 1.4).

Comets made of silicate dust and ice fall at about half the speed of asteroids ($\sim 25\text{--}30$ km s^{-1}) from the Oort cloud located on the outer margins of the Solar system on short-lived elliptical trajectories. Although comets may retain solid cratered surfaces such as the comet Wilde-2 (Fig. 1.5) they contain vapor tails emanating from evaporating ice. The huge gravity pull of Jupiter (24.79 m/s², compared to the Earth's 9.78 m/s²) induces collisions between and sweeps most of the fragments as observed by the Shoemaker-Levy-9 comet impact (Figs. 1.6a and 1.6b). Whereas the inner planets are heavily bombarded by asteroids and comets (Figs. 1.7a, 1.7b, 1.7c and 1.7d), had it not been for the gravity effect of Jupiter the impact incidence would have reduced the probability of life on Earth – a metaphoric validation for the Romans' view of their god Jupiter as protector of the State. However, when viewed from space, although located in the trajectory of these bodies, planet Earth displays little or no cratering (Fig. 1.8), a consequence of the buried nature of some of the larger impact structures, detected through geophysical methods (Chap. 4), fallout/ejecta units (Chap. 2) and mass extinction events (Fig. 1.9).

Early views on the origin of the asteroid belt were advanced in terms of the breakdown of a small planet such as Vesta and Ceres under the strong gravity effect

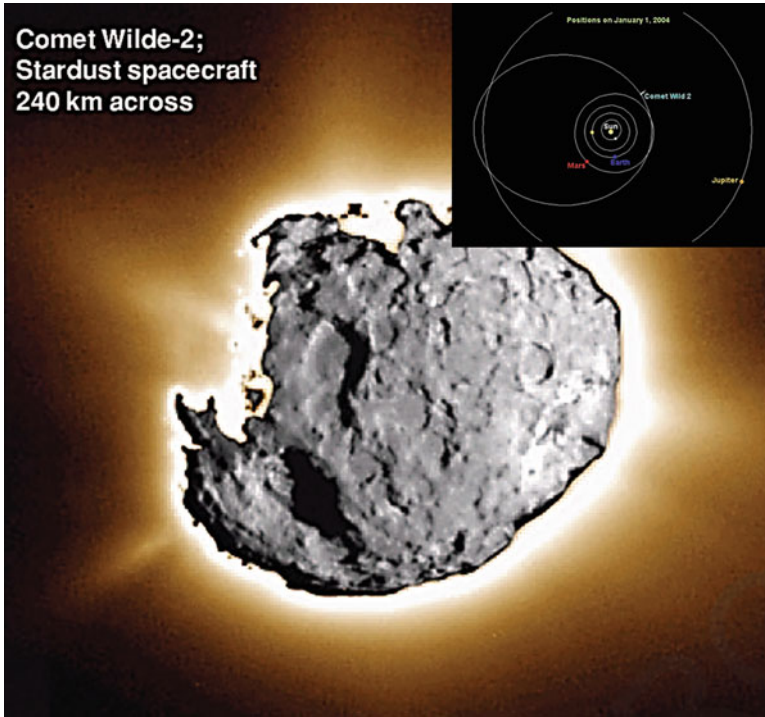


Fig. 1.5 Comet Wilde-2 from stardust spacecraft 240 km-across. Note the released gas jets. NASA (https://stardust.jpl.nasa.gov/highres/jets_release_03_12_04_1.jpg). Inset: https://www.windows2universe.org/comets/wild_2/wild_2.html)



Fig. 1.6a Fragments of the Shoemaker-Levy comet approaching the planet Jupiter. NASA (https://en.wikipedia.org/wiki/Comet_Shoemaker%E2%80%93Levy_9#/media/File:Shoemaker-Levy_9_on_1994-05-17.png)

of Jupiter, whereas modern views based on the compositional diversity of asteroids suggest the asteroid belt formed during the first 10 million years of solar history by gravitational accretion from the primitive solar disc, aggregation, melting and fractionation. The NEAR Shoemaker mission observing Eros, its surface features,



Fig. 1.6b Fragments of comet Shoemaker-Levy 9 (SL9) impacting Jupiter. NASA (<https://www2.jpl.nasa.gov/sl9>)

Fig. 1.7a The multiring 360 km-diameter impact structure Valhalla on Calisto, one of Jupiter’s moons. Public domain ([https://en.wikipedia.org/wiki/Valhalla_\(crater\)#/media/File:Valhalla_crater_on_Callisto.jpg](https://en.wikipedia.org/wiki/Valhalla_(crater)#/media/File:Valhalla_crater_on_Callisto.jpg))

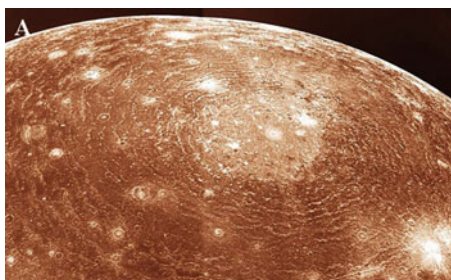


Fig. 1.7b Impact structures on Mars. Creative commons (https://en.wikipedia.org/wiki/Mars#/media/File:Eso1509a_-_Mars_planet.jpg)



chemistry, mineral composition, spin state, magnetic field and the effects of the solar wind, carried 56 kg of equipment, including an X-ray/gamma ray spectrometer, a near-infrared spectrograph, a multispectral camera, a laser range finder and a magnetometer. Eros is an S-type asteroid, namely a body dominated by silicate minerals. Although NEAR Shoemaker was not designed as a Lander, the craft’s gamma-ray spectrometer continued to collect data for 2 weeks on the elemental composition of Eros. The spacecraft made its last call to Earth on 28 February 2001. Several space encounters with asteroids and comets followed, including the Japanese Hayabusa probe which collected asteroid debris from the asteroid Itokawa (640 × 270 m) on 12 September 2005. NASA’s Deep Impact probe encountered the cratered nucleus

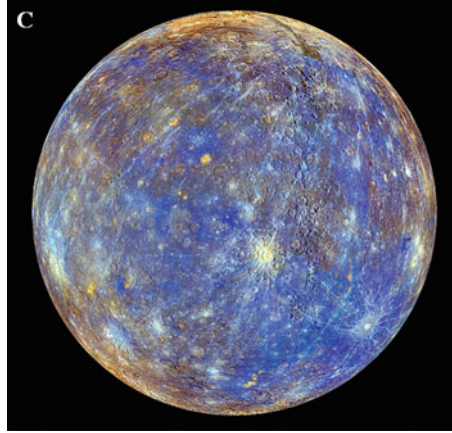
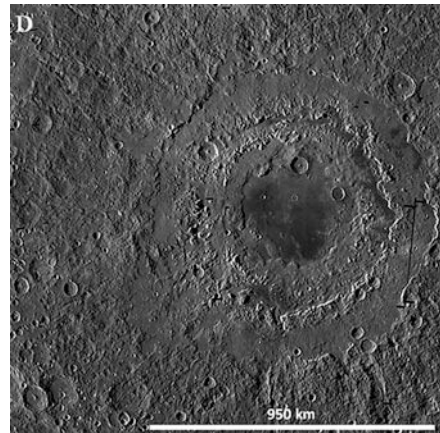


Fig. 1.7c The heavily cratered surface of Mercury. NASA (<https://www.flickr.com/photos/gsfcr/8497942353/in/photolist-dWWbct-UzQvA4-fxNrc7-cuFQK5-9VBmCt-9uAd7r-9uD599-nU1F6q-je2T6P-TeQEq9-cUb6nY-dWW6Nt-6EJfcx-dWW6LV-9JykQx-79BYNQ-6uQD9B-Rt8eWy-VcUxYB-azggbR-nfR6sF-9rfVkw-naFfE3-4mPJrB-Uc6537-6hF13r-qWwmuH-kCmUA8-mjsSN6-mEEbyW-kyCZse-cuFR37-GFcMfp-mh6bRX-dxkgAE-nuPh7A-nrJRDv-bXjnXB-cuFR4Q-mw9vPZ-r3WEGa-nfV9So-nhEL9W-9ApJzR-fbWoWk-neuPuo-a7NNSv-VaFwhJ-UYNAWG-9unbvZ>)

Fig. 1.7d The 950 km-diameter Mare Orientale on the Moon. NASA ([https://en.wikipedia.org/wiki/Mare_Orientale#/media/File:Mare_Orientale_\(Lunar_Orbiter_4.png\)](https://en.wikipedia.org/wiki/Mare_Orientale#/media/File:Mare_Orientale_(Lunar_Orbiter_4.png)))



of comet Tempel-1 (100–200 m.) on 4 July 2005. On 10 July this year, the European Space Agency’s probe Rosetta passed 3162 km from the asteroid Lutetia (long axis 134 km) at a speed of 15 km/s. Rosetta’s OSIRIS images of Lutetia, taken with both wide-angle and narrow-angle cameras, with resolution to 60 m, show large, eroded craters imprinted by young, well-defined craters. Lutetia shows spectral characteristics intermediate between those of C-Type asteroids and M-Type asteroids.

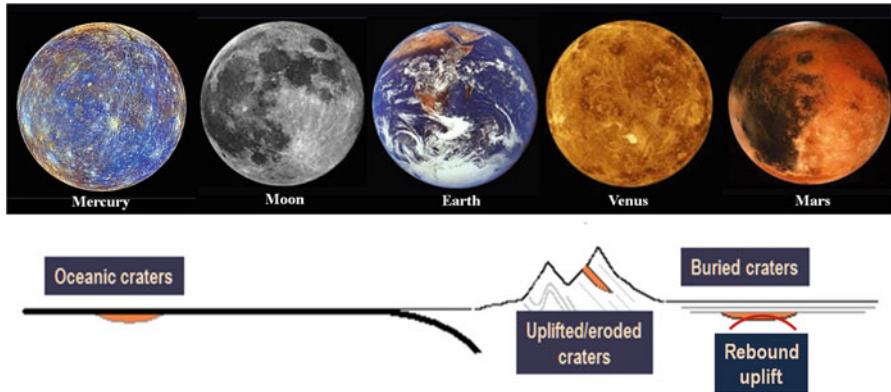


Fig. 1.8 The surfaces of the inner planets: Mars, Venus, Earth, Moon and Mercury and a diagram displaying the elimination of impact craters of the earth’s oceans and orogenic belts vs their preservation in cratons. NASA



Fig. 1.9 Artist’s depiction of the end-Cretaceous impact event Public domain (https://en.wikipedia.org/wiki/Timeline_of_Cretaceous%E2%80%93Paleogene_extinction_event_research); 1.9 (inset) *Tyrannosaurus rex* specimen at the Carnegie Museum of Natural History, Pittsburgh. Wikipedia commons (https://en.wikipedia.org/wiki/Tyrannosaurus#/media/File:Tyrannosaurus_Rex_Holo_type.jpg)

1.2 Hadean to Early Archaean Impacts

Following accretion of chondritic fragments and cosmic dust in the solar nebula, gravitational collapse and melting (Chyba 1993; Chyba and Sagan 1996; Delsemme 2000), an emergence of felsic igneous rocks is indicated by <4.4 Ga zircons (Mojzsis and Harrison 2000), signifying two-stage mantle melting processes and hydrous melting of mafic-ultramafic crust (Green and Ringwood 1967). From $^{18}\text{O}/^{16}\text{O}$ evidence from ~4.4 Ga-old zircons low temperature conditions allowed presence of liquid water at the surface (Wilde et al. 2001; Peck et al. 2001; Mojzsis et al. 2001). During a Late Heavy Bombardment of Earth (~3.95–3.85 Ga), exposure to cosmic radiation, electric and thermal flash associated with large asteroid impacts, clouding effects and acid rain would have annihilated any photosynthesizing bacterial colonies at the surface (Zahnle and Greenspoon 1990; Zahnle and Sleep 1997; Chyba 1993; Chyba and Sagan 1996), possibly with the exception of extremophile chemotrophic bacteria residing around ‘black chimneys’ and ‘nanobes’ (Uwins 1998) in faults and fractures. Earliest replicating cells probably required only 20 or so elements at submarine hot springs (da Silva and Williams 1991), and as many fundamental organic molecular components (Wald 1964). Traces of $^{13}\text{C}/^{12}\text{C}$ isotopically light graphite within apatite in 3.85 Ga banded iron formation in southwestern Greenland were suggested as possible clues for such habitat (Mojzsis et al. 1996; Mojzsis and Harrison 2000), but according to other workers the graphite, dispersed through the rock represents later contamination (Nutman and Friend 2006). Continuous accretion of cosmic dust from about 3.8 Ga, estimated from deep ocean pelagic sediment cores to have occurred at the rate of 60,000 tons/year (Kyte 2002), contributed a small fraction of about $0.2 \cdot 10^{-7}$ of the Earth mass. Geochemical hints for early biological activity is detected in Isua ~3.7 Ga dolomitic meta-sediments where low Al_2O_3 (<0.5%) and TiO_2 (<0.05%) levels Ca-Mg-Fe ratios correspond to those of ferroan dolomite – siderite – Fe-oxide sediments with REE + Y profiles showing La, Ce, Eu and Y positive anomalies, corresponding to the signature of sea water (Bolhar et al. 2004). This is consistent with experimental evidence for anoxic microbial origin of low-temperature dolomites (Nutman et al. 2010; Vasconcelos et al. 1995; Roberts et al. 2004), and the likely precipitation of banded iron formations either by microbial oxidation or by photolysis by ultraviolet radiation under the ozone-poor or ozone-free Archaean atmosphere (Konhauser et al. 2002).

Prior to the Apollo missions of 1963–1972 some interpreted the lunar craters as volcanic in origin, an idea laid to rest by the shock-metamorphic state of the lunar samples. Whereas early pre-4.0 Ga impact basins are recorded on the Lunar Highlands, peak 3.95–3.85 Ga bombardment, forming the large lunar mare (cf. Imbrium, Oceanus Procellarum Serenitatis, Tranquilitatis, Orientalis, Fecunditatis, Nectaris, Crisium) (Figs. 1.10 and 1.11), is termed the Late Heavy Bombardment (LHB) with an impact incidence of $4\text{--}9 \cdot 10^{-13} \text{ km}^{-2} \text{ year}^{-1}$ on the Moon (for craters >18 km). An early interpretation in terms of the tail-end of planetary accretion (Baldwin 1985) has been replaced by views favoring a temporally distinct bombardment episode (Ryder 1990, 1991, 1997) in view of a scarcity of pre-LHB ejecta in the lunar highlands. Principal craters formed during the LHB include Imbrium (outer ring – 1300 km), Orientale

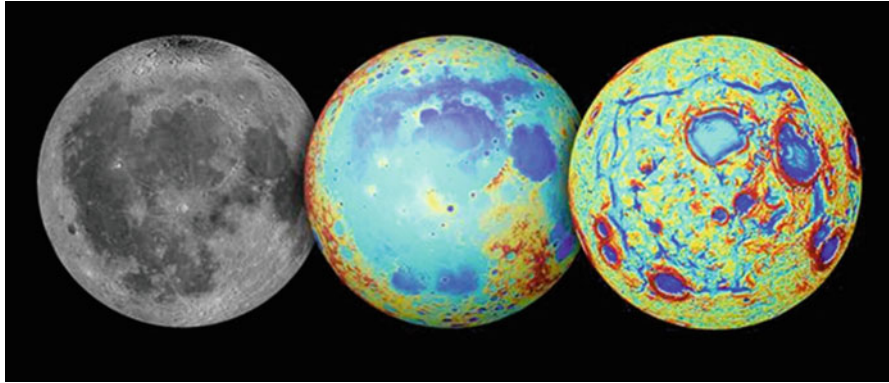


Fig. 1.10 Earth’s moon as observed in visible light (left), topography (center, where red is high and blue is low), and the GRAIL gravity gradients (right). The Procellarum region is a broad region of low topography covered in dark mare basalt. The gravity gradients reveal a giant rectangular pattern of structures surrounding the region. Public domain (https://en.wikipedia.org/wiki/Lunar_mare#/media/File:14-236-LunarGrailMission-OceanusProcellarum-Rifts-Overall-20141001.jpg)

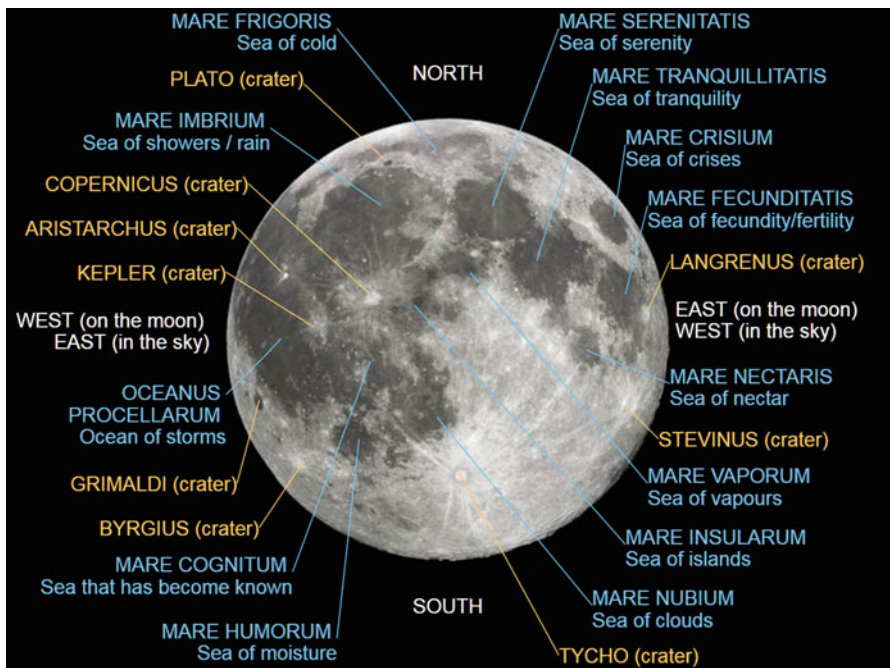


Fig. 1.11 Principal impact features on the face of the moon. Wikimedia commons (https://upload.wikimedia.org/wikipedia/commons/6/61/Moon_names.svg)

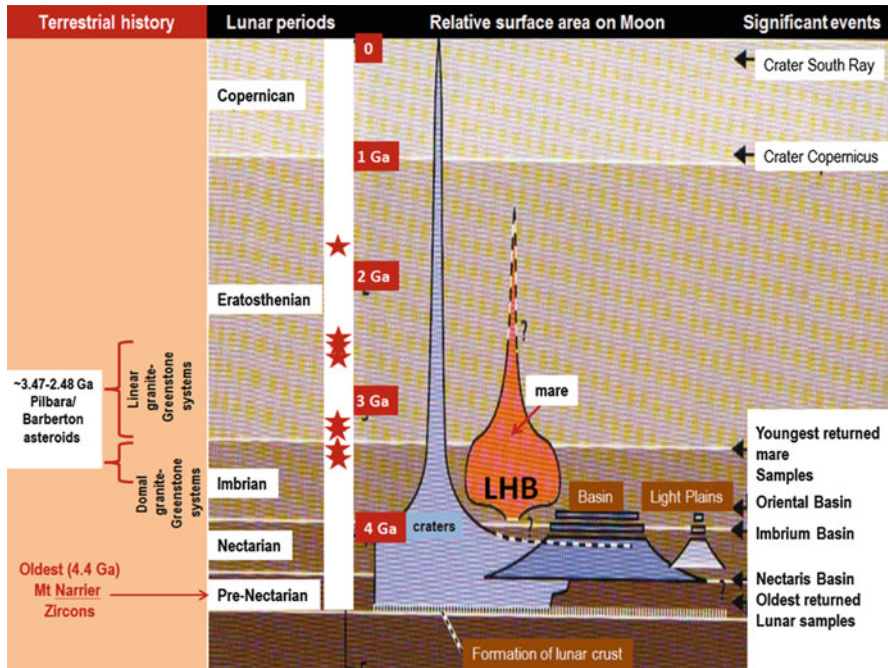


Fig. 1.12 Broad stratigraphy of the Moon with the early earth, marking the distribution of the lunar basins, light plains, craters and mare, correlated with Archaean stages and events on earth (Data source: NASA. Lunar events (LHB – Late Heavy Bombardment). NASA Atlas of the Moon. NASA (<https://www.bookdepository.com/Compact-NASA-Atlas-Solar-System-Ronald-Greeley/9780521806336>))

(930 km), Tranquillitatis (873 km), Serenitatis (707 km), Crisium (605 km) and Smythii (373 km). The Lunar impact history is classified in terms of several stages (Wilhelms 1987) (Fig. 1.12):

- I. Pre-Nectarian era (>3.9 Ga).
- II. Nectarian era (3.92–3.85 Ga, named after the Nectaris impact basin – 333 km).
- III. Imbrian era (3.85–3.2 Ga).
- IV. Eratosthenian era (3.2–1.2 Ga).
- V. Copernican era (1.1–0 Ga).

Craters of the two latter periods, imprinted on the surfaces of the large lunar mare, display radial ejecta rays, i.e. Tycho, Copernicus. Mare basins may contain low-Ti basalts, which likely represent impact-triggered volcanic activity (Ryder 1997), including 3.85 ± 0.03 Ga-old K, REE, and P-rich-basalts (KREEP) in Mare Imbrium (BVTP 1981), Oceanus Procellarum 3.29–3.08 Ga basalts and Hadley Apennines 3.37–3.21 Ga basalts (BVTP 1981). Recent laser $^{40}\text{Ar}/^{39}\text{Ar}$ analyses of lunar impact spherules from, Fra Mauro Formation (Apollo 14) (Culler et al. 2000), tentatively indicate large errors in the ~ 3.87 , ~ 3.83 , ~ 3.66 , ~ 3.53 and ~ 3.47 Ga

age peaks, An age spike occurs at ~ 3.18 Ga near the boundary of the Late Imbrian (~ 3.85 – 3.2 Ga) and the post-mare Eratosthenian (~ 3.2 – 1.2 Ga) defined by the cratering record (Wilhelms 1987). 34 lunar impact spherules yield a mean age of 3188 ± 198 Ma (median 3181 Ma) and spherule ages with error < 100 m.y. yield a mean age of 3178 ± 80 Ma (median 3186 Ma), hinting at a broad overlap with an Archaean 3.26–3.22 Ga impact cluster in the Barberton Mountain Land, Transvaal.

Although coupling of the Earth-Moon system about ~ 4.5 Ga remains beyond reasonable doubt (Ringwood 1986), to date no definitive evidence of the 3.95–3.85 Ga impacts on the Earth has been detected, despite extensive records of ~ 3.8 – 4.4 Ga-old zircons in Archaean gneisses and derived clastic sediments (Wilde et al. 2001). No shock metamorphic planar deformation features (PDF) were observed to date in zircons of these early gneisses, nor have significant siderophile element anomalies been detected, with the exception of Tungsten isotope anomalies in Greenland gneisses (Schoenberg et al. 2002). Evidence such as PDF in quartz has likely been obliterated by high grade metamorphism. On the other hand growing evidence of multiple impact fallout/ejecta units intercalated with ~ 3.47 – 3.22 Ga sediments in Archaean greenstone belts in the Kaapvaal and Pilbara cratons (Simonson and Glass 2004; Lowe et al. 2003; Glikson and Vickers 2006) has been interpreted by Lowe and Byerly (2010) in terms of a prolongation of the LHB.

Following the Late Heavy Bombardment of ~ 3.95 – 3.85 Ga, impacts by very large asteroids and comets in the inner solar system declined from a flux of 4 – $9 \cdot 10^{-13}$ km² year⁻¹ (for craters $D_c \geq 18$ km) to a flux of 3.8 – $6.3 \cdot 10^{-15}$ km² year⁻¹ (for craters $D_c \geq 20$ km) (Grieve and Dence 1979; Baldwin 1985; Ryder 1990). Post-LHB impact rates on Earth extrapolated from lunar crater counts are similar at a rate of $5.9 \pm 3.5 \cdot 10^{-15}$ km⁻² year⁻¹ (for craters $D_c \geq 20$ km), consistent with observations of near-Earth asteroids (NEA) and comets. Shoemaker and Shoemaker (1996) estimated an impact flux of $N \propto D_c^{-1.8}$ to $N \propto D_c^{-2.0}$ (N = cumulative number of craters with diameters larger than D_c ; D_c = crater diameter). Plots of crater size versus cumulative crater size frequency as projected from the Moon (Fig. 1.13) allow estimates of impact incidence since the LHB, as follows:

- A. >600 craters of $D_c \geq 100$ km
- B. >100 craters of $D_c \geq 300$ km
- C. >50 craters of $D_c \geq 500$ km

To date 3 large Archaean to early Proterozoic impact structures (Maniitsoq, ~ 2975 Ma; Garde et al. 2012; Vredefort, 2023 Ma, Gibson and Reimold 2001; Sudbury, 1850 Ma, Theriault et al. 1997) (Table 4.1) were identified and near-16 impacts by asteroids >10 km in diameter recorded from microkrystite spherule units [~ 3472 (2), ~ 3460 (2), ~ 3445 , ~ 3416 , ~ 3334 , ~ 3256 , ~ 3243 , ~ 3225 (2), ~ 2630 , ~ 2570 , ~ 2560 (2), ~ 2480 Ma) (Table 5.1). The total of ~ 20 implies that about one fifth of the very large ($D > = 300$ km) asteroids estimated from the lunar flux (>100 craters of $D_c \geq 300$ km) (Fig. 1.13) have been identified on Earth to date. These estimates do not take into account probable and possible but as yet unproven impact structures such as the Warburton shock metamorphic terrain and palimpsest ring feature on the Earth such as the Deniliquin-Booligal and Winton/Diamantina (Sect. 5.3) circular features,

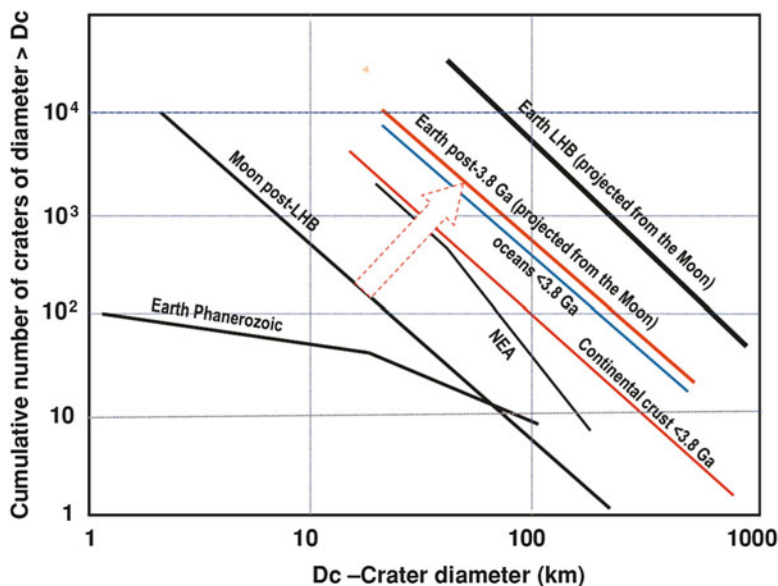


Fig. 1.13 Crater diameter versus cumulative number of craters of diameters $< D_c$ for (1) Late heavy bombardment of Earth, extrapolated from lunar data of Barlow (1990); (2) Lunar post-Late Heavy Bombardment (LHB); (3) Earth post 3.8 Ga (projected from the moon as indicated by the arrow); (4) Earth oceans (~80% of the earth's surface); earth continental crust (~20% of the earth surface); (5) Phanerozoic impact rates displaying erosional loss of small craters (Modified after Grieve and Dence 1979) (<http://www.springer.com/gp/book/9789400763272>)

conceivably signifying pre-existing or deeply buried ring structures. Such a surprising high rate of preservation is explained by the crustal depth of major impact craters and rebound domes and thereby their good preservation. Likewise thick ejecta units are more readily identified than thin fallout layers.

According to the Earth Impact Database nearly 190 impact structures have been confirmed to date (Figs. 1.14, 1.15a and 1.15b), many of which displaying clear explosion-type craters (Fig. 1.16) and some identified thanks to their impact metamorphic features such as shatter cones and planar deformation features (Fig. 1.17). Post-LHB asteroids and comet flux can be roughly estimated from the impact frequency/size distribution (Fig. 1.13), leading to expect ~150–250 impact structures >100 km in diameter, ~15–25 impact structures ~300 km in diameter and ~2–4 impact structures ~500 km in diameter. From the commonly chlorite-rich composition of, and the scarcity of shocked quartz grains in, Archaean and early Proterozoic impact spherules, the majority of these impacts are likely to have impinged on basic oceanic crust (Simonson et al. 1998; Glikson and Allen 2004). This suggestion agrees with rare earth-based growth estimates of the continental crust with time (Taylor and McLennan 1983) and Sm–Nd isotopes (McCulloch and Bennett 1994). Age distribution patterns suggest impacts tended to occur episodically in clusters. Metamorphism and anatexis in high-grade terrains obscures Early Precambrian

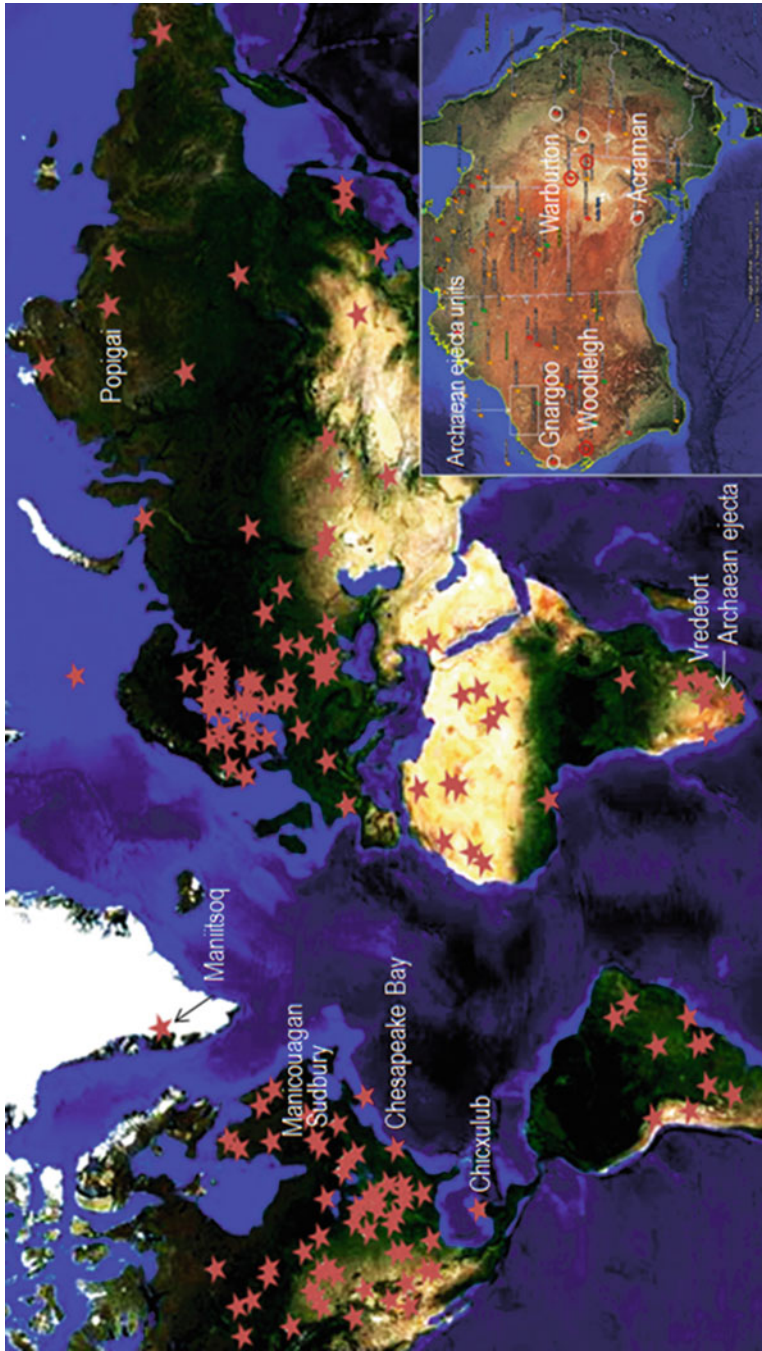


Fig. 1.14 NASA global map (<https://visibleearth.nasa.gov/view.php?id=57752>) including location of the larger (>70 km diameter) impact structures discussed in Chap. 3, including Warburton, Woodleigh, Gnargoo, Acraman and Talundilly. Stars indicate smaller impact structures (<http://www.passc.net/EarthImpactDatabase/>)

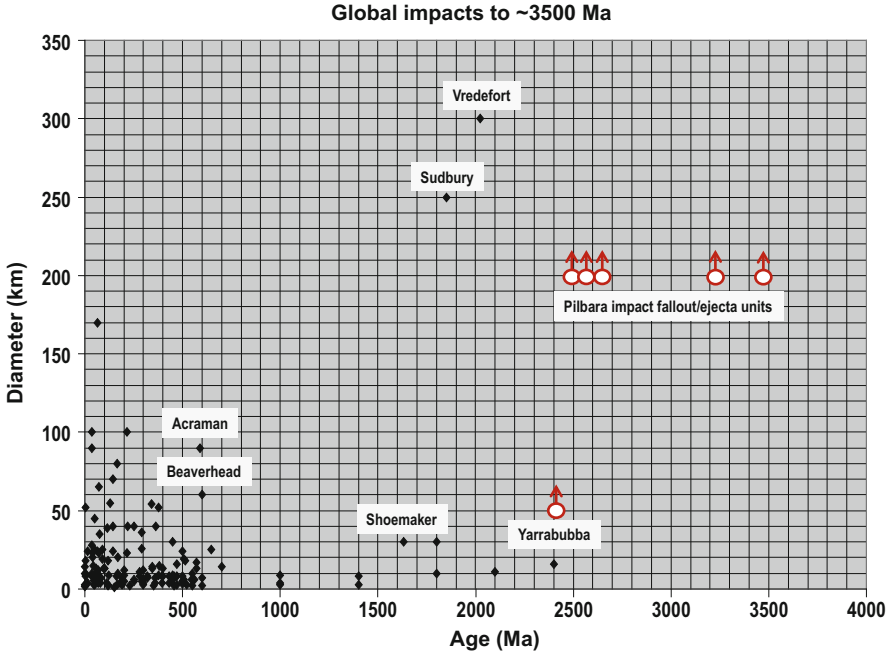


Fig. 1.15a Age versus diameter of global impact structures and impact ejecta units to 3500 Ma

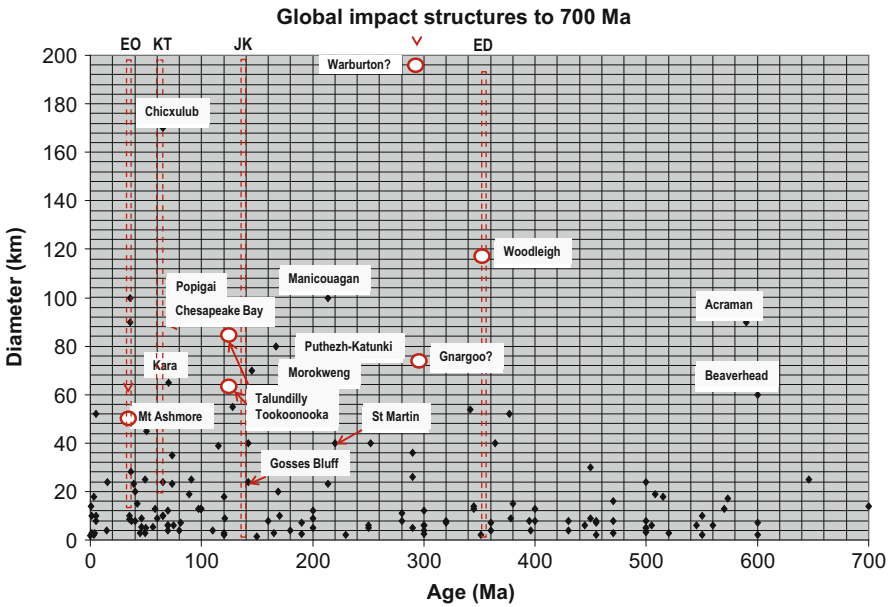


Fig. 1.15b Age versus diameter of global impact structures younger than 700 Ma, highlighting large impact structures

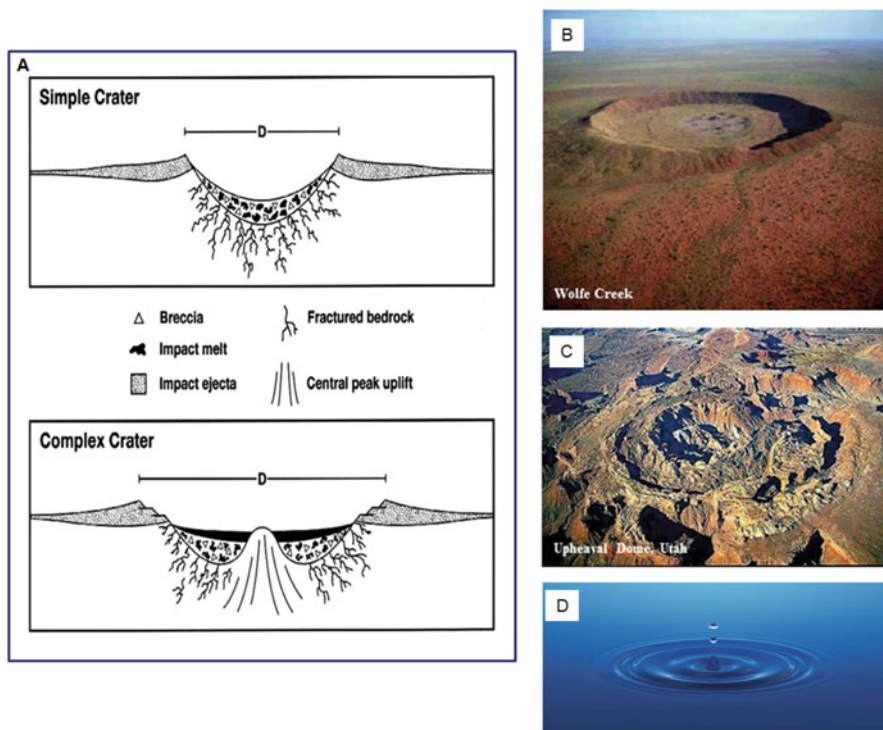


Fig. 1.16 (a) Development of a complex impact structure. Creative commons (<https://commons.wikimedia.org/wiki/File:Craterstructure.gif>); (b) Simple crater: Wolfe Creek, Kimberley (Dainis Dravins, by permission); (c) Upheaval Dome, Utah (Jim Wark, by permission). (d) Ripple effect of a pebble thrown into water A water drop ejected by elastic rebound – an analogy with an impact event

impactites, with the exception of well-preserved terrains such as the Barberton Greenstone Belt (BGB) in South Africa and the Pilbara Craton Western Australia (Chap. 2).

While the paucity of Archaean impact signatures on Earth prior to the 1980s may have suggested an abrupt cessation of the LHB, the identification by Lowe, Byerly, Simonson and Hassler of impact ejecta/fallout spherules in ~3.47 and 2.56 Ga sediments in the Kaapvaal Craton and the Pilbara Craton (Lowe and Byerly, 1986; Simonson 1992), heralded the discoveries of ejecta/fallout units of at least 14 large to very large Archaean to early Proterozoic impact events in Archaean terrains (Simonson and Hassler 1997; Lowe et al. 2003; Simonson and Glass 2004; Hassler et al. 2011; Glikson 2008; Glikson et al. 2016) and of at least 2 in early Proterozoic terrains. This breakthrough was allowed by the identification of millimeter-scale originally glassy spherules in sediments of the KT impact boundary termed microkrystites (Glass and Burns 1988) characterized by inward radiating quench crystallites, chromium spinels and platinum group element anomalies, markedly

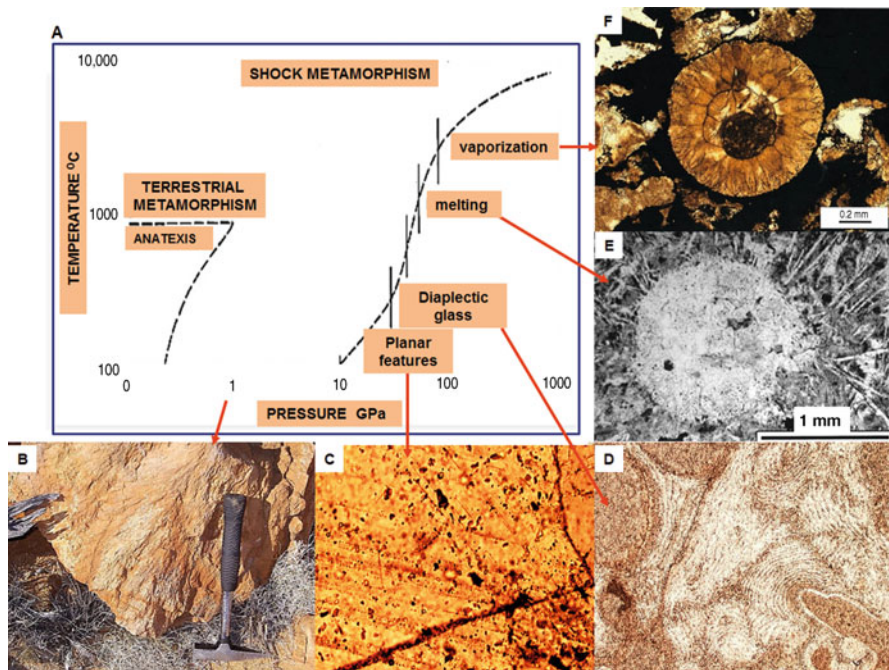


Fig. 1.17 (a) Pressure–temperature diagram comparing conditions of shock metamorphism and conditions of endogenic crustal metamorphism. The shock-metamorphic field (from ~ 7 to >100 GPa) is distinct from the endogenic field ($P < 5$ GPa, $T < 1000$ °C). Stability curves for high-pressure minerals (coesite, diamond, stishovite) (<https://curator.jsc.nasa.gov/education/lpets/metamorphism.cfm>); (b) a shatter cone; (c) planar deformation features in quartz in Yarrabubba Granite; (d) devitrified impact glass; (e) granophyre core and radiating crystallites (Macdonald et al. 2003; Elsevier with permission); (f) a microkrystite spherule formed by condensation of impact-released vapor (Jeerinah impact layer)

high iridium levels (Glikson 2005 (Figs. 1.18 and 1.19). Geochemistry and isotopes--based estimates and spherule size-frequency analyses suggest 20–50 km-large asteroids (Melosh and Vickery 1991; Byerly and Lowe 1994; Shukolyukov et al. 2000; Kyte et al. 2003; Glikson and Allen 2004).

Impact spherules are produced from the condensation in the atmosphere of vapor, ejected from large impact craters, where the target rocks are shattered, fragmented, fused and vaporized. The underlying sub-crater crust undergoes elastic rebound, forming a dome, by analogy to the ejection of a water drop from a pond hit by a stone. Dispersal of the vapor in the atmosphere driven by winds leads to cooling, condensation and settling of myriad droplets as glassy spheres, preserved in marine sediments. In the Barberton greenstone belt ejecta units are dated at ~ 3.472 , ~ 3.445 , ~ 3.416 , ~ 3.334 , ~ 3.256 , ~ 3.243 and ~ 3.225 Ga (2 units) (Lowe and Byerly 2010). In the Pilbara greenstone belts ejecta units are dated at ~ 3.47 Ga (2 fallout units), ~ 3.46 (2 fallout units) ~ 2.63 Ga, ~ 2.57 Ga, ~ 2.56 Ga (2 units) and ~ 2.48 Ga. A spherule

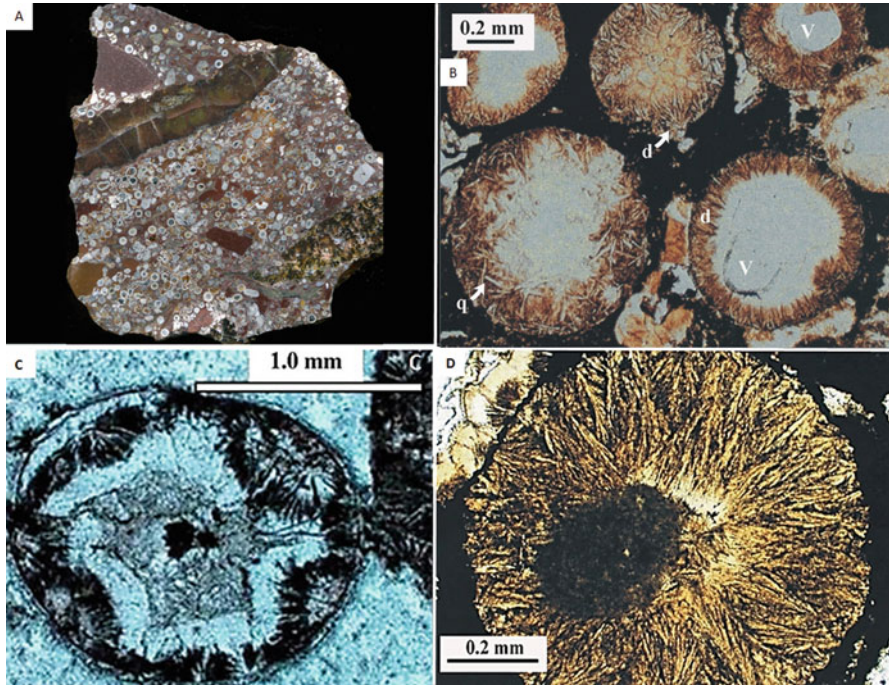


Fig. 1.18 Microkrystite impact spherules: (a) ~2.63 Ga Jeerinah Impact layer, Hesta Siding, Fortescue Basin, Pilbara Craton (courtesy B.M. Simonson); (b) 2.56 Ga Bee Gorge Member, Wittenoom Formation; (c) 3.259 Ga S2 (base of Fig Tree Group) spherules, Barberton Greenstone Belt; (d) ~2.63 Ga Jeerinah Impact layer, Hesta Siding, Pilbara Craton

unit 1.85–2.13 Ga-old is reported from Greenland (Chadwick et al. 2000) and spherule units ~1.850 Ga-old are reported from Ontario, Minnesota and Michigan (Addison et al. 2005; Cannon et al. 2010). The 580 Ma Bunyerroo impact ejecta in the Adelaide and Officer Basins has been confidently related to the ~40–90 km-large Acraman impact structure (Williams 1986; Williams et al. 1996; Williams and Gostin 2005, 2010; Grey et al. 2003; Williams and Wallace 2003; Hill et al. 2004).

Given the difficulty in identifying spherule units in the field, impact frequencies documented to date represent the minimum asteroid flux or ‘tip of the iceberg’, yielding further support to Lowe and Byerly (2010) suggested extension of the LHB. Lowe and Byerly (2010) observed juxtaposition between multiple ~3.26 to 3.22 Ga-old impact ejecta units in the Barberton greenstone belt, South Africa, and unconformities separating underlying mafic-ultramafic-volcanic sequences and overlying semi-continental arenites, siliceous volcanics, banded ironstone and conglomerate (Lowe et al. 1989; Byerly et al. 1996). Impact ejecta units may display fracture systems and dykes representing the effects of seismic shock and tsunami waves prior to settling of the impact spherules (Lowe 2013). Near-contemporaneous ~3.26–3.22 Ga sequences in the central Pilbara Craton uncover major breaks between mafic-ultramafic volcanic units

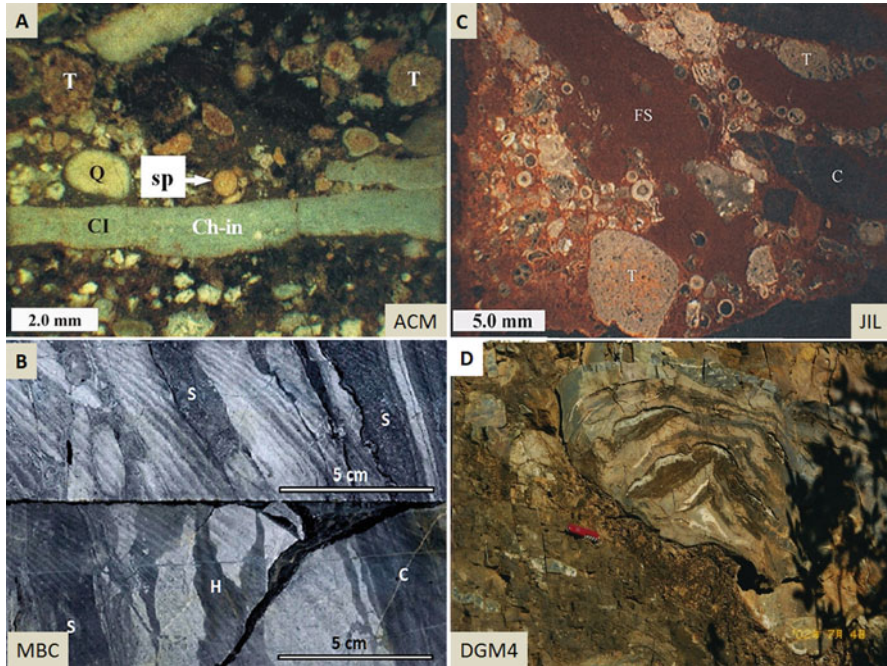


Fig. 1.19 Fragmental and tsunami deposits associated with impact ejecta. (a) Chert plate interspersed with spherule-bearing arenite, 3.47 Ga Antarctic Chert Member, Mount Ada Basalt, central Pilbara; (b) Core: Chert plates interspersed with spherule-bearing arenite, 3.46 Ga Marble Bar Chert Member, S – spherule-rich arenite; H – hybrid arenite-spherule units; (c) – impact spherules and tectonites (T) mixed with fragments of ferruginous shale (FS). Jeerinah Impact layer, Pilbara Craton.; (d) A block of folded layered chert set in spherule-rich clay and tuff of the Dales Gorge Member, Brockman iron formation, Hamersley Basin

and semi-continental sediments, including arenite, conglomerate and major boulder deposits, including blocks up to 250 m large (Glikson and Vickers 2006). This time interval was associated with plutonic granitic activity in both the Kaapvaal and Pilbara cratons, hinting at possible genetic relations between the impacts and plutonic magmatism. It follows the impact cluster may have triggered the abrupt transformation in crustal conditions, terminating the development of komatiite-rich basaltic oceanic-like crustal conditions and initiating felsic plutonic and volcanic magmatism and emerging semi-continental environments.

Possible evidence for mafic volcanism triggered by impacts is observed where impact ejecta/fallout units are overlain by either mafic volcanics or/and banded iron formations (Glikson 2006; Glikson and Vickers 2007; Glikson and Hickman 2014). Principal examples of impact units overlain by either mafic volcanics or banded iron formations include: In the Pilbara ~3.26–2.56 Ga-old impact ejecta/fallout layers are commonly capped by iron-rich chert and banded iron formations, some of which are the source of Pilbara iron ores, hinting at the existence of large volcanic terrains from

which the iron could be leached under the anoxic atmospheric conditions during the Archaean (Cloud 1973). In the Barberton greenstone belt such units include (Table 1.1):

1. 3334 ± 3 Ma Spherule K-3 unit in the Kromberg Fm is overlain by mafic volcanic + chert of the Mendon Fm and Weltevreden Formations;
2. 3243 ± 4 Ma to 3225 ± 3 Ma silica-sericite spherules; BGB-S2 spherule unit occurs at the base of the Mapepe Formation, Fig Tree Group, is overlain by iron-rich sediments of the Ulundi Formation in the northern part of the BGB;
3. 3258 ± 3 Ma silica-sericite BGB-S2 spherule unit occurs at the base of Manzimnyama Jaspilite Member (<20 m) and shale of the Mapepe Formation, Fig Tree Group

The oldest Archaean impact structure identified to date is Maniitsoq, southern Greenland, forming a > 100 km-diameter deformed zone within high grade Archaean metamorphic terrain and marked by a large aeromagnetic anomaly (Garde et al. 2012). The rocks considered to be exhumed from a depth of 20–25 km below the surface and have undergone regional hydrothermal alteration under amphibolite-facies conditions. The structure includes a central 35×50 km-large core of crushed recrystallized gneisses and quartzo-feldspathic rocks cut by fractures, fracture cleavage and breccia. Planar deformation features (PDF) in quartz display multiple intersecting planar sets including Miller indices {0001}, {10–14}, {10–13}, {10–12}, {10–11}, {10–22}, {11–21} and {31–41} with narrow planar spacing of ~2–5 microns, confirming a shock metamorphic origin of the structure (Garde and Glikson 2011). The PDF-bearing quartz grains may be re-deformed, displaying undulose extinction and curved or kinked PDFs which preserve near-original crystallographic orientations. Other features include fluidized micro-breccia and K-feldspar and plagioclase melting in migmatized rocks. The structure is cut by ultramafic intrusions showing crustal contamination and yielding a U–Pb zircon age of 2975 ± 6 Ma.

1.3 Criteria for Identification of Asteroid Impacts

The identification of impact structures and impact ejecta/fallout deposits is fraught with complications. Initial references to circular morphological and drainage patterns, round lakes and oval depressions may provide a hint to possible underlying ring or dome structures, requiring field tests or drilling where no outcrop occurs (Grieve and Pilkington 1996; Glikson and Uysal 2013). Structural domes and near-circular fold structures may be mistaken for impact structures, as are basins of approximately circular or slightly elongate pattern and plutonic domes such as oval granite intrusions, laccoliths and gabbro plugs. In orogenic belts domes may be produced by compression and associated folding, including fold sets with different trends producing domes at the culminations of crossing anticlines. Diapirs cored by relatively low-density rocks may be initially mistaken for impact structures, examples being granite domes uplifted relative denser country rocks.

Table 1.1 Archaean impact ejecta associated with ferruginous sediments and banded iron- formations in the Pilbara and Southern Africa

Age	Asteroid impact ejecta	Overlying ferruginous sediments or/and volcanics	References
3470.1 ± 1.9 Ma	Microkrystite spherules and spherule-bearing conglomerate. Antarctic Creek Member, Mount Ada Basalt, Pilbara Craton.	Jaspilite unit	Byerly et al. (2002) and Glikson et al. (2004)
3459 ± 2 Ma	Two spherule units within the Marble Bar Chert Member of the Duffer Formation, Marble Bar, central Pilbara Craton	Overlying Marble Bar Jaspilite in turn overlain by komatiites of the Apex Basalt.	Glikson et al. (2016)
3258 ± 3 Ma	Silica-sericite spherules; BGB–S2 spherule unit at the base of the Mapepe Formation, Fig Tree Group, Kaapvaal Craton	Manzimnyama Jaspilite Member (<20 m) and shale above BGB–S2	Lowe et al. (2003)
3243 ± 4 Ma to 3225 ± 3 Ma	S3. 10–15 cm-thick to locally 2- to 3-m-thick silica–Cr sericite–chlorite spherules; S4–15 cm-thick arenite with chlorite-rich spherules. Lower part of Mapepe Fm. Fig Tree Group, Kaapvaal Craton	BGB–S3 is overlain by iron-rich sediments	Lowe et al. (2003)
3235 ± 3 Ma	Olistostrome, base Soanesville Group, Pilbara Craton	Arenite, felsic tuff and BIF	Glikson and Vickers (2006)
3334 ± 3 Ma	Spherule unit, Kromberg Fm K-3	Overlying mafic volcanic + chert Mendon Fm and Weltevreden Fm	Glikson and Hickman (2014)
2630 ± 6 Ma	Spherule-bearing Carawine Dolomite Megabreccia	Spherule-bearing carbonate and chert boulders in carbonate matrix	Simonson (1992) and Glikson (2004)
2629 ± 5 Ma	JIL - Jeerinah Impact Layer, top Jeerinah Formation, Fortescue Basin, Pilbara	Marra Mamba Iron-Formation	Simonson et al. (2000) and Hurst et al. (2013)
2562 ± 6 Ma	SMB-1 Ma/Bee Gorge Member, upper Wittenoom Formation, Hamersley Basin, Pilbara	2 cycles of microkrystite spherules, turbidites and tsunami units, followed by ferruginous carbonate & shale	Simonson (1992), Glikson (2004) and Glikson and Vickers (2007)

(continued)

Table 1.1 (continued)

Age	Asteroid impact ejecta	Overlying ferruginous sediments or/and volcanics	References
2501 ± 8 Ma	Fragmentals/intraclast unit – Top Mt. McRae Shale, Hamersley Basin, Pilbara	Dales Gorge Member	This paper
2481 ± 4 Ma	~20 cm spherule unit, DGS4 S-Macroband, Dales Gorge Member, Brockman Iron Formation, Hamersley Basin, Pilbara	Banded iron-formation	Simonson (1992) and Glikson and Allen (2004)

Structural elements of circular features suggestive of an impact cratering and elastic rebound of underlying rocks (Fig. 1.16) include:

- Intersections of older structures by external rings of the circular feature, as displayed for example by the *Chicxulub* impact structure (Sharpton et al. 1996), the *Woodleigh* impact structure (Glikson et al. 2005a, b), the *Gnargoo* probable impact structure (Iasky and Glikson 2005; Glikson and Uysal 2013) and the *Shoemaker* impact structure (Pirajno et al. 2003). Whereas structurally discordant intersections are displayed by volcanic diatremes, igneous plugs and salt domes, a presence of a central uplift core or dome fringed by a ring syncline is consistent with diagnostic features of impact structures;
- The central uplifts of impact structures are defined in seismic reflection sections where the uplift is commonly associated with inward-verging thrust faults, as in the *Woodleigh* impact structure (Iasky et al. 2001) and the *Spider* impact structure (Abels 2005).
- An intersection of the top of the dome or a basement uplift by unconformably overlying post-impact sediments is typical of impact structures, as demonstrated in the *Woodleigh*, *Gnargoo*, *Mount Ashmore* and *Tookoonooka* structures. Post-impact isostatic vertical movements are indicated where the central uplift pierces through the unconformity, as in the *Mount Ashmore* structure.

Where the core of the structure consists of sedimentary strata, a structural dome is outlined containing chaotically disrupted core zones which display a loss of seismic markers associated with mega-brecciation, as in the *Mount Ashmore* probable impact structure (Glikson et al. 2010). By contrast to thrust faults around and within central core zones, ring synclines and outer rims of impact structures display inward-dipping normal faults. These structural patterns represent centripetal and upward block movements involving compression around the uplifted core or plug and inward collapse of the crater rim, evident in the *Woodleigh*, *Gnargoo* and *Talundilly* structures. In addition, some impact structures and probable impact structures display uplift of crystalline basement below impacted sediments, as in the

Woodleigh impact structure (), the *Mount Ashmore* probable impact structure (Glikson et al. 2010) and as magnetic highs at the centres of the *Warburton* impact structures (Glikson et al. 2013, 2015).

Microstructural features are central to the identification of shock metamorphic features and the pressure-temperature conditions associated with asteroid impacts, the most commonly used being planar deformation features in quartz (PDF/Qz). Other criteria include solid state vitrification to diaplectic glass and melting of quartz to lechatelierite which occur above 10 GPa and the graphite to diamond and coesite to stishovite transformations (French 1998) (Fig. 1.17).

Distinctions between Planar Deformation Features in quartz (PDF/Qz) indicative of shock metamorphism within established impact structures on the one hand, and proposed Metamorphic Deformation Lamellae (MDL/Qz) of supposed purely endogenic origin on the other hand, are extensively discussed in the literature (Carter 1965, 1968; Carter et al. 1986; Alexopoulos et al. 1988; Lyons et al. 1993; Grieve et al. 1990; Vernooij and Langenhorst 2005; Spray and Trepmann 2006; Ferriere et al. 2009; French and Koeberl 2010; Hamers and Drury 2011). Criteria suggested in this regard include:

- A. PDF/Qz lamellae are defined by diagnostic Miller indices correlated with specific shock levels, in particular the {10–11}, {10–12} and {10–13} planes (French 1998). Planar features referred to as MDL/Qz display a wide scatter, including low C_{OAQz}^{PDF} (the angle between the Optic Axis and the pole of planar deformation features) on frequency distribution plots (Lyons et al. 1993; French 1998).
- B. PDF/Qz lamellae forms multiple planar sets in shock metamorphosed rocks (Robertson et al. 1968; Stöffler and Langenhorst 1994; Grieve et al. 1990), but planar features referred to as MDL/Qz consist mostly of only one set of lamellae within any one quartz grain (French and Koeberl 2010), commonly forming basal {0001} planes, which represent ~8–10 GPa shock pressures (French 1998), such as in explosive volcanic units, cf. Toba ignimbrites (Carter et al. 1986).
- C. PDF/Qz lamellae can be 1–2 μm -thick whereas planar features referred to as MDL/Qz consist of segments usually 2–4 μm thick.
- D. PDF/Qz lamellae are originally perfectly planar whereas planar features referred to as MDL/Qz commonly display undulation, bending and wavy patterns.
- E. Transmission Electron Microscopy (TEM) studies indicate little-deformed segments of PDF/Qz lamellae with optical continuity between bordering intracrystalline segments displaying no subgrain boundaries. On the other hand planar features referred to as MDL/Qz display irregular/undulating boundaries and optical discontinuities between separate subgrains where optic orientations depart by $\leq 5^\circ$ from each other and from the orientation of the host quartz (Glikson et al. 2013).

- F. TEM studies show PDF/Qz lamellae are amorphous or composed of quartz with low dislocation densities. On the other hand planar features described as MDL/Qz are commonly altered and display high dislocation densities (Goltrant et al. 1991).
- G. PDF/Qz lamellae in SEM–Cathode Luminescence form straight, narrow, well-defined features, whereas tectonic deformation lamellae are thicker and are slightly curved (Hamers and Drury 2011).

Based on these and other criteria a large number of impact structures and probable impact structures have been identified (Table 4.1).

The identification of impact ejecta/fallout units within sedimentary sequences requires another set of criteria, including detection of millimetre-scale meta-glass spherules originally recognized in the KT impact boundary, termed microkrystites (Glass and Burns 1988). Microkrystites are characterized by inward radiating quench crystallites, chromium spinels and platinum group element anomalies, and markedly high iridium levels (Glikson 2005). From geochemical Ir-based and Cr isotopes--based estimates and from spherule size-frequency analyses projectile diameters of 20–50 km-large asteroids have been suggested (Melosh and Vickery 1991; Byerly and Lowe 1994; Shukolyukov et al. 2000; Kyte et al. 2003; Glikson and Allen 2004). Commonly the microkrystites are closely associated with impact-induced tsunami breccia (Fig. 1.19).

References

- Abels A (2005) Spider impact structure, Kimberley Plateau, Western Australia: interpretations of formation mechanism and age based on integrated map-scale data. *Aust J Earth Sci* 52:653–663
- Addison WD, Brumpton GR, Vallini DA, McNaughton NJ, Davis DW, Kissin SA, Fralick PW, Hammond AL (2005) Discovery of distal ejecta from the 1850 Ma Sudbury impact event. *Geology* 33:193–196
- Alexopoulos JS, Grieve RAF, Robertson PB (1988) Microscopic lamellar deformation features in quartz: discriminative characteristics of shock-generated varieties. *Geology* 16:796–799
- Baldwin RB (1985) Relative and absolute ages of individual craters and the rates of in-falls on the moon in the post-imbrium period. *Icarus* 61:63–91
- Barlow NG (1990) Estimating the terrestrial crater production rate during the late heavy bombardment period. *Lunar Planet Inst Contrib* 746:4–7
- Bolhar R, Kamber BS, Moorbath S, Fedo CM, Whitehouse MJ (2004) Characterization of early Archaean chemical sediments by trace element signatures. *Earth Planet Sci Lett* 222:43–60
- BVTP (1981) Basaltic volcanism on the terrestrial planets. The Lunar and Planetary Institute/Pergamon Press, Inc., Houston/New York
- Byerly GR, Lowe DR (1994) Spinel from archaean impact spherules. *Geochim Cosmochim Acta* 58:3469–3486
- Byerly GR, Kröner A, Lowe DR, Todt W, Walsh MM (1996) Prolonged magmatism and time constraints for sediments deposition in the early archaean Barberton greenstone belt: evidence from the Upper Onverwacht and Fig Tree Groups. *Precambrian Res* 78:125–138
- Byerly GR, Lowe DR, Wooden JL, Xie X (2002) An archaean impact layer from the Pilbara and Kaapvaal Cratons. *Science* 297:1325–1327

- Cannon WF, Schulz KJ, Wright J, Horton D, Kring A (2010) The Sudbury impact layer in the Paleoproterozoic iron ranges of Northern Michigan, USA. *Geol Soc Am Bull* 122:50–75
- Carter NL (1965) Basal quartz deformation lamellae – a criterion for recognition of impactites. *Am J Sci* 263:786–806
- Carter NL (1968) Meteoritic impact and deformation of quartz. *Science* 160:526–528
- Carter NL, Officer CB, Chesner A, Rose WI (1986) Dynamic deformation of volcanic ejecta from the Toba caldera: possible relevance to cretaceous/tertiary boundary phenomena. *Geology* 14:380–383
- Chadwick B, Claeys P, Simonson BM (2000) New evidence for a large palaeoproterozoic impact spherules in a dolomite layer in the Ketilidian orogen South Greenland. *J Geol Soc Lond* 158:331–340
- Chyba CF (1993) The violent environment of the origin of life: progress and uncertainties. *Geochim et Cosmochim Acta* 57:3351–3358
- Chyba CF, Sagan C (1996) Comets as the source of prebiotic organic molecules for the early Earth. In: Thomas PJ, Chyba CF, McKay CP (eds) *Comets and the origin and evolution of life*. Springer, New York, pp 147–174
- Cloud P (1973) Paleocological significance of the banded iron formation. *Econ Geol* 68:1135–1143
- Culler TS, Becker TA, Muller RA, Renne PR (2000) Lunar impact history from $^{39}\text{Ar}/^{40}\text{Ar}$ dating of glass spherules. *Science* 287:1785–1789
- Da Silva JJRF, Williams RJP (1991) *The biological chemistry of the elements: the inorganic chemistry of life*. Oxford University Press, Oxford, p 600
- Delsemme AH (2000) Cometary origin of the biosphere: 1999 Kuiper prize lecture. *Icarus* 146:313–325
- Ferriere L, Morrow JR, Amgaa T, Koeberl C (2009) Systematic study of universal-stage measurements of planar deformation features in shocked quartz: implications for statistical significance and representation of results. *Meteor Planet Sci* 44:925–940
- French BM (1998) *Traces of catastrophe – a handbook of shock metamorphic effects in terrestrial meteorite impact structures*. Lunar Planet Sci Inst Contrib 954:120
- French BM, Koeberl C (2010) The convincing identification of terrestrial meteorite impact structures: what works what doesn't and why. *Earth Sci Rev* 98:123–170
- Garde AA, Glikson AY (2011) Poster: recognition of re-deformed planar deformation features (PDFs) in large impact structures Maniitsoq impact structure and planar deformation features orientations. <http://www.lpi.usra.edu/meetings/metsoc2011/pdf/5246.pdf>
- Garde AA, McDonald I, Dyck B, Keulen N (2012) Searching for giant ancient impact structures on Earth: the Meso-Archaeon Maniitsoq structure, West Greenland. *Earth Planet Sci Lett* 337:197–210
- Gibson RL, Reimold WU (2001) *The Vredefort impact structure South Africa: the scientific evidence and a two-day excursion guide*. Council Geosci Mem 92:111
- Glass BP, Burns CA (1988) Microkrystites: a new term for impact-produced glassy spherules containing primary crystallites. *Proc Lunar Planet Sci Conf XVIII*:455–458
- Glikson AY (2004) Early Precambrian asteroid impact-triggered tsunamis: excavated seabed debris flows exotic boulders and turbulence features associated with 3.47–2.47 Ga-old asteroid impact fallout units, Pilbara Craton, Western Australia. *Astrobiology* 4:1–32
- Glikson AY (2005) Geochemical and isotopic signatures of archaean to early proterozoic extraterrestrial impact ejecta/fallout units. *Aust J Earth Sci* 52:785–799
- Glikson AY (2006) Asteroid impact ejecta units overlain by iron rich sediments in 3.5–2.4 Ga terrains Pilbara and Kaapvaal Cratons: accidental or cause–effect relationships? *Earth Planet Sci Lett* 246:149–160
- Glikson AY (2008) Field evidence of Eros-scale asteroids and impact-forcing of Precambrian geodynamic episodes, Kaapvaal (South Africa) and Pilbara (Western Australia) Cratons. *Earth Planet Sci Lett* 267:558–570

- Glikson AY, Allen C (2004) Iridium anomalies and fractionated siderophile element patterns in impact ejecta, Brockman Iron Formation, Hamersley Basin, Western Australia: evidence for a major asteroid impact in simatic crustal regions of the early proterozoic earth. *Earth Planet Sci Lett* 220:247–264
- Glikson AY, Hickman AH (2014) Coupled asteroid impacts and banded iron-formations, Fortescue and Hamersley groups, Pilbara, Western Australia. *Aust J Earth Sci* 61:689–701
- Glikson AY, Uysal IT (2013) Geophysical and structural criteria for the identification of buried impact structures, with reference to Australia. *Earth-Sci Rev* 125:114–122
- Glikson AY, Vickers J (2006) The 3.26–3.24 Ga Barberton asteroid impact cluster: tests of tectonic and magmatic consequences Pilbara Craton Western Australia. *Earth Planet Sci Lett* 241:11–20
- Glikson AY, Vickers J (2007) Asteroid mega-impacts and Precambrian banded iron formations: 2.63 Ga and 2.56 Ga impact ejecta/fallout at the base of BIF/argillite units, Hamersley Basin, Pilbara Craton, Western Australia. *Earth Planet Sci Lett* 254:214–226
- Glikson AY, Allen C, Vickers J (2004) Multiple 3.47-Ga-old asteroid impact fallout units, Pilbara Craton, Western Australia. *Earth Planet Sci Lett* 221:383–396
- Glikson AY, Eggins S, Golding S, Haines P, Iasky RP, Mernagh TP, Mory AJ, Pirajno F, Uysal IT (2005a) Microchemistry and microstructures of hydrothermally altered shock-metamorphosed basement gneiss, Woodleigh impact structure, Southern Carnarvon Basin, Western Australia. *Aust J Earth Sci* 52:555–573
- Glikson A, Mory AJ, Iasky R, Pirajno F, Golding S, Uysal IT (2005b) Woodleigh, Southern Carnarvon Basin, Western Australia: history of discovery late devonian age and geophysical and morphometric evidence for a 120 km-diameter impact structure. *Aust J Earth Sci* 52:545–553
- Glikson AY, Jablonski D, Westlake S (2010) Origin of the Mount Ashmore structural dome West Bonaparte Basin Timor Sea. *Aust J Earth Sci* 57:411–430
- Glikson AY, Uysal IT, Fitz Gerald JD, Saygin E (2013) Geophysical anomalies and quartz microstructures, Eastern Warburton Basin, North-east South Australia: tectonic or impact shock metamorphic origin? *Tectonophysics* 589:57–76
- Glikson AY, Meixner AJ, Radke B, Uysal IT, Saygin E, Vickers J, Mernagh TP (2015) Geophysical anomalies and quartz deformation of the Warburton West structure, Central Australia. *Tectonophysics* 643:55–72
- Glikson AY, Hickman AH, Evans NJ, Kirkland CI, Jung-WP RR, Romano S (2016) A new 3.46 Ga asteroid impact ejecta unit at Marble Bar, Pilbara Craton, Western Australia: a petrological, microprobe and laser ablation ICPMS study. *Precamb Res* 279:103–122
- Goltrant O, Cordier P, Doukhan JC (1991) Planar deformation features in shocked quartz: a transmission electron microscopy investigation. *Earth Planet Sci Lett* 106:103–115
- Green DH, Ringwood AE (1967) An experimental investigation of the gabbro to eclogite transformation and its petrological applications. *Geochim Cosmochim Acta* 31:767–833
- Grey K, Walter MR, Calver CR (2003) Neoproterozoic biotic diversification: snowball earth or aftermath of the Acraman impact? *Geology* 31:469–472
- Grieve RAF, Dence MR (1979) The terrestrial cratering record: II the crater production rate. *Icarus* 38:230–242
- Grieve RAF, Pilkington M (1996) The signature of terrestrial impacts. *Aust Geol Surv J Aust Geol Geophys* 16:399–420
- Grieve RAF, Corderre JM, Robertson PB, Alexopoulos J (1990) Microscopic planar deformation features in quartz of the Vredefort structure: anomalous but still suggestive of an impact origin. *Tectonophysics* 171:185–200
- Hamers MF, Drury MR (2011) Scanning electron microscope cathod-luminescence (SEM-CL) imaging of planar deformation features and tectonic deformation lamellae in quartz. *Meteor Planet Sci* 46(181):1814
- Hassler SW, Simonson BM, Sumner DY, Bodin L (2011) Paraburdoo spherule layer (Hamersley Basin, Western Australia): distal ejecta from a fourth large impact near the archaean-proterozoic boundary. *Geology* 39:307–310

- Hill AC, Grey K, Gostin VA, Webster LJ (2004) New records of late Neoproterozoic Acraman ejecta in the Officer Basin. *Austral J Earth Sci* 51:47–51
- Hurst J, Krapez B, Hawke P (2013) Stratigraphy of the Marra Mamba Iron Formation within the Chichester range and its implications for Iron Ore Genesis at Roy Hill – evidence from Deep Diamond Drill Holes within the East Fortescue Valley. *Iron Ore, Aus IMM The Minerals Institute* 2013, p 95
- Iasky RP, Glikson AY (2005) Gnargoo: a possible 75 km-diameter post-early permian – pre-cretaceous buried impact structure Carnarvon Basin Western Australia. *Aust J Earth Sci* 52:577–586
- Iasky RP, Mory AJ, Blundell KA (2001) The geophysical interpretation of the Woodleigh impact structure Southern Carnarvon Basin. Western Australia, *Geol Surv of West Aust Rep* 79:41
- Konhauser K, Hamada T, Raiswell R, Morris R, Ferris F, Southam G, Canfield D (2002) Could bacteria have formed the precambrian banded iron-formations? *Geology* 30:1079–1082
- Kyte FT (2002) Tracers of extraterrestrial components in sediments and inferences for earth's accretion history. *Geol Soc Am Spec Pap* 356:21–38
- Kyte FT, Shukolyukov A, Lugmair GW, Lowe DR, Byerly GR (2003) Early Archaean spherule beds: chromium isotopes confirm origin through multiple impacts of projectiles of carbonaceous chondrite type. *Geology* 31:283–286
- Lowe DR (2013) Crustal fracturing and chert dike formation triggered by large meteorite impacts, ca. 3.260 Ga, Barberton Greenstone Belt, South Africa. *Geol Soc Am Bull* 125:894–912
- Lowe DR, Byerly GR (1986) Early archaean silicate spherules of probable impact origin, South Africa and Western Australia. *Geology* 14:83–86
- Lowe DR, Byerly GR (2010) Did the LHB end not with a bang but with a whimper? 41st Lunar Planet Sci Conf 2563pdf
- Lowe DR, Byerly GR, Asaro F, Kyte FJ (1989) Geological and geochemical record of 3400 million year old terrestrial meteorite impacts. *Science* 245:959–962
- Lowe DR, Byerly GR, Kyte FT, Shukolyukov A, Asaro F, Krull A (2003) Characteristics, origin, and implications of archaean impact-produced spherule beds, 3.47–3.22 Ga, in the Barberton Greenstone Belt, South Africa: keys to the role of large impacts on the evolution of the early earth. *Astrobiology* 3:7–48
- Lyons JB, Officer CB, Borella PE, Lahodinsky R (1993) Planar lamellar substructures in quartz. *Earth Planet Sci Lett* 119:431–440
- Macdonald FA, Bunting JA, Cina SE (2003) Yarrabubba—a large deeply eroded impact structure in the Yilgarn Craton Western Australia. *Earth Planet Sci Lett* 213:235–247
- McCulloch MT, Bennett VC (1994) Progressive growth of the Earth's continental crust and depleted mantle: geochemical constraints. *Geochim Cosmochim Acta* 58:4717–4738
- Melosh HJ, Vickery AM (1991) Melt droplet formation in energetic impact events. *Nature* 350:494–497
- Mojzsis SJ, Harrison TM (2000) Vestiges of a beginnings: clues to the emergent biosphere recorded in the oldest known rocks. *Geol Soc Am Today* 10:1–6
- Mojzsis SJ, Harrison TM, Pidgeon RT (2001) Oxygen-isotope evidence from ancient zircons for liquid water at the earth's surface 4,300 Myr ago. *Nature* 409:178–180
- Mojzsis SJ, Arrhenius G, McKeegan KD, Harrison TM, Friend CRL (1996) Evidence for life on Earth before 3800 million years ago. *Nature* 270:43–45
- Nutman AP, Friend CRL (2006) Re-evaluation of oldest life evidence: infrared absorbance spectroscopy and petrography of apatites in ancient metasediments, Akilia, W. Greenland. *Precambrian Res* 147:100–106
- Nutman AP, Clark Friend RL, Bennett VC, Wright D, Norman MD (2010) 3700 Ma metamorphic dolomite formed by microbial mediation in the Isua supracrustal belt (W. Greenland): simple evidence for early life? *Precambrian Res* 183:725–737
- Peck WH, Valley JW, Wilde SA, Graham CM (2001) Oxygen isotope ratios and rare earth elements in 3.3 to 4.4 Ga zircons: ion microprobe evidence for high 18 O continental crust and oceans in the early archaean. *Geochim Cosmochim Acta* 65:4215–4229

- Pirajno F, Hawke P, Glikson AY, Haines PW, Uysal T (2003) Shoemaker impact structure Western Australia. *Aust J Earth Sci* 50:775
- Ringwood AE (1986) Origin of the Earth and Moon. *Nature* 322:323–328
- Roberts JA, Bennett PC, González LA, Macpherson GL, Milliken KL (2004) Microbial precipitation of dolomite in methanogenic groundwater. *Geology* 32:277–280
- Robertson PB, Dence MR, Vos MA (1968) Deformation in rock-forming minerals from Canadian craters. In: French BM, Short NM (eds) *Shock metamorphism of natural materials*. Mono Book Corp, Baltimore, pp 433–452
- Ryder G (1990) Lunar samples lunar accretion and the early bombardment of the Moon. *EOS Trans Am Geophys Union* 71:313–322
- Ryder G (1991) Accretion and bombardment in the Earth–Moon system: the lunar record. *Lunar Planet Sci Instit Contrib* 746:42–43
- Ryder G (1997) Coincidence in the time of the Imbrium Basin impact and apollo 15 creep volcanic series: impact induced melting? *Lunar Planet Sci Instit Contrib* 790:61–62
- Schoenberg R, Kamber B, Collerson KD, Moorbath (2002) Tungsten isotope evidence from ~3.8 Gyr metamorphosed sediments for early meteorite bombardment of the Earth. *Nature* 418:403–405
- Sharpton V, Martin E, Carney JL, Lees S, Ryder G, Schuraytz BC, Sikora P, Spudis PD (1996) A model of the Chicxulub impact basin based on the evaluation of geophysical data, well logs and drill core samples. *Geol Soc Am Special Paper* 307:55–74
- Shoemaker EM, Shoemaker CS (1996) The Proterozoic impact record of Australia. *Aust Geol Surv Org J Aust Geol Geophys* 16:379–398
- Shukolyukov A, Kyte FT, Lugmair GW, Lowe DR, Byerly GR (2000) The oldest impact deposits on Earth. In: Koeberl C, Gilmour I (eds) *Lecture notes in Earth science 92: impacts and the early Earth*. Springer, Berlin, pp 99–116
- Simonson BM (1992) Geological evidence for an early precambrian microtektite strewn field in the Hamersley Basin of Western Australia. *Geol Soc Am Bull* 104:829–839
- Simonson BM, Glass BP (2004) Spherule layers – records of ancient impacts. *Annu Rev Earth Planet Sci* 32:329–361
- Simonson BM, Hassler SW (1997) Revised correlations in the early Precambrian Hamersley Basin based on a horizon of re-sedimented impact spherules. *Aust J Earth Sci* 44:37–48
- Simonson BM, Davies D, Wallace M, Reeves S, Hassler SW (1998) Iridium anomaly but no shocked quartz from Late archaean microkrystite layer: oceanic impact ejecta? *Geology* 26:195–198
- Simonson BM, Davies D, Hassler SW (2000) Discovery of a layer of probable impact melt spherules in the late Archaean Jeerinah Formation, Fortescue Group, Western Australia. *Aust J Earth Sci* 47:315–325
- Spray JG, Trepmann CA (2006) Shock-induced crystal-plastic deformation and postshock annealing of quartz. *Eur J Mineral* 18:161–173
- Stoffler D, Langenhorst F (1994) Shock metamorphism of quartz in nature and experiment: I. Basic observation and theory. *Meteoritics* 29:155–181
- Taylor SR, McLennan SM (1983) Geochemistry of early proterozoic sedimentary rocks and the archaean – proterozoic boundary. *Geol Soc Am Mem* 161:119–113
- Therriault AM, Grieve RAF, Reimold WU (1997) The vredefort structure: original size and significance for geologic evolution of the Witwatersrand Basin. *Meteoritics* 32:71–77
- Uwins PJR (1998) Novel nano-organisms from Australian sandstones. *Am Mineral* 83:1541–1550
- Vasconcelos C, McKenzie JA, Bernasconi S, Grujic D, Tien AJ (1995) Microbial mediation as a possible mechanism for natural dolomite at low temperatures. *Nature* 377:220–222
- Vernooij MJC, Langenhorst F (2005) Experimental reproduction of tectonic deformation lamellae in quartz and comparison to shock-induced planar deformation features. *Meteorit Planet Sci* 40:1353–1361
- Wald G (1964) The origin of life. *Proc Natl Acad Sci USA* 52:595–611

- Wilde SA, Valley JW, Peck WH, Graham CM (2001) Evidence from detrital zircons for the existence of continental crust and oceans on the earth 4.4 Gyr ago. *Nature* 409:175–178
- Wilhelms DE (1987) The geological history of the Moon. US Geol Surv Prof Pap 1348
- Williams GE (1986) The Acraman impact structure; source of ejecta in late precambrian shales, South Australia. *Science* 233:200–203
- Williams GE, Gostin VA (2005) The Acraman – Bunyeroo impact event (Ediacaran) South Australia and environmental consequences: 25 years on. *Aust J Earth Sci* 52:607–620
- Williams GE, Gostin VA (2010) Geomorphology of the Acraman impact structure, Gawler Ranges, South Australia. *Cadernos Laboratorio Xeoloxico de Laxe* 35:209–220
- Williams GE, Wallace MW (2003) The Acraman asteroid impact South Australia: magnitude and implications for the late vendian environment. *J Geol Soc Lond* 160:545–554
- Williams GE, Schmidt PW, Boyd DM (1996) Magnetic signature and morphology of the Acraman impact structure South Australia. *Aust Geol Surv Org J Aust Geol Geophys* 16:431–442
- World Impacts Database. <http://www.passc.net/EarthImpactDatabase/>
- Zahnle K, Grinspoon D (1990) Comet dust as a source of amino acids at the Cretaceous/Tertiary boundary. *Nature* 348:157–160
- Zahnle K, Sleep NH (1997) Impacts and the early evolution of life. In: Thomas P, Chyba C, McKay C (eds) *Comets and the origin of life*. Springer, Dordrecht, pp 175–208

Chapter 2

Australian Asteroid Ejecta/Fallout Units



Abstract Geochronological U-Pb zircon dates are increasingly indicative of an episodic nature of the evolution of lithosphere and crust, including tectonic and thermal episodes associated with large asteroid impacts. Documented Archaean and early Proterozoic impacts at ~ 3.47 , ~ 2.63 , ~ 2.57 , ~ 2.56 , ~ 2.48 , ~ 2.023 Ga (Vredefort) and 1.85 Ga (Sudbury) are considered to represent a minimum impact incidence due to gaps in stratigraphic sequences and the difficulty in identifying impact ejecta/fallout units. Evidence for major dynamic and thermal effects of large impact clusters on the early Precambrian crust is provided by ejecta/fallout units associated with: unconformities, tsunami boulder debris, compositional contrasts between supracrustal sequences that underlie and overlie ejecta units; including an onset of iron-rich sedimentation; and near-contemporaneous intrusion of granitoid magmas. A prime example is a ~ 3.26 – 3.24 Ga impact cluster whose fallout units, documented in the Barberton greenstone belt, South Africa, are associated with unconformities. The unconformities constitute abrupt breaks between underlying mafic-ultramafic volcanic sequences and overlying continental sediments which include granitoid detritus, representing granite felsic igneous activity. Geochronologically correlated unconformities and olistostrome mega-breccia are observed in the Pilbara Craton, Western Australia. In these terrains a > 300 Ma-long period of greenstone–granite evolution is abruptly terminated by unconformities overlain by impact ejecta, turbidite and banded iron-formation and associated with major faulting, uplift, erosion, and the onset of high-energy sedimentation including detrital components derived from contemporaneous and older granites. Onset of iron-rich sedimentation, including banded iron-formation, in the wake of these impacts is indicative of weathering and soluble transport of ferrous oxide under low-oxidation atmosphere and hydrosphere conditions, likely representing mafic volcanic activity triggered by the impacts. Depending on the site of the ~ 2.48 Ga impact, extensive injection of mafic dykes during 2.48–2.42 Ga (Matachewan, Scourie, Karelian, Widgiemooltha, Bangalore, Antarctica dykes) may have been related to deep crust/mantle fractures triggered by mega-impacts.

2.1 c.3472 Ma Impacts

The Archaean greenstone belts of the Pilbara granite-greenstone Craton display close stratigraphic analogies with the Barberton greenstone belt of the East Kaapvaal shield, South Africa (Fig. 2.1). This includes a lower mafic-ultramafic +/- felsic volcanic and chert units of the Warrawoona Supergroup (Figs. 2.2 and 2.3) and an upper predominantly sedimentary clastic succession of the Gorge Creek Group and Lalla Rookh conglomerate and quartzite formation. Unconformably overlying the early to middle Archaean sequences and related granitoids are the Fortescue Group (2.7–2.63 Ga) and Hamersley Group (2.63–2.4 Ga) (Fig. 2.7). Table 2.1 presents a summary of Archaean to early Proterozoic asteroid impact ejecta/fallout units in the Pilbara, Kaapvaal Craton and elsewhere.

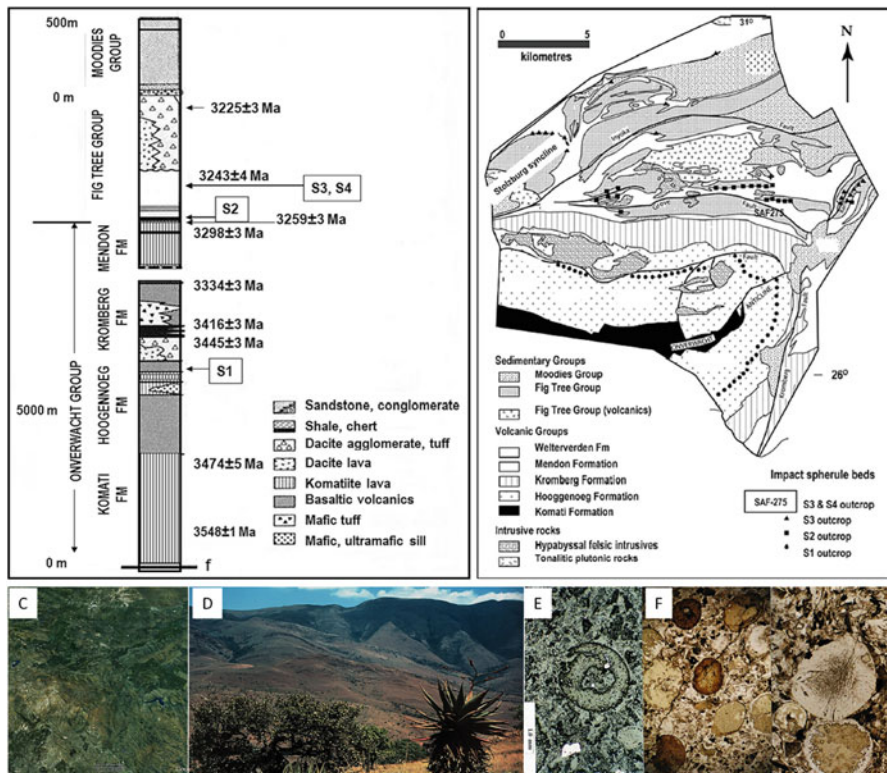


Fig. 2.1 (a) Schematic stratigraphy and impact ejecta units in the Barberton greenstone belt, Eastern Transvaal (After Lowe and Byerly 2010) (EPSL with permission). <http://www.lpi.usra.edu/meetings/lpsc2010/pdf/2563.pdf>; (b) Geological sketch map of the southwestern Barberton Greenstone Belt, east Kaapvaal Craton, South Africa (From Lowe et al. 2003); (c) Satellite image of the Barberton Mountain Land (EPSL with permission); (d) View of the Stolzberg syncline and the Pig Ridge in the Barberton Mountain Land; (e and f) Microkrystite impact spherules, S2 ejecta unit, Barberton greenstone belt

Lowe and Byerly (1986) reported millimeter to sub-millimeter scale silicified spherules displaying quench-crystallization and devitrified glass textures in a chert/arenite unit in the Antarctic Chert Member, upper Mount Ada Basalt, tracing this unit about 1 km along strike (Fig. 2.4). The Mount Ada Basalt, as defined by Hickman (1983, 2012), Van Kranendonk (2000) and Van Kranendonk and Morant (1998), consists of carbonated pillowed tholeiitic and high-Mg basalt, dolerite sills, minor volcanoclastic rocks and ~1–10 m-scale intercalations of chert, chert/arenite and minor intraclast chert pebble-dominated conglomerate. The isotopic age of the Mount Ada Basalt is constrained in the adjacent Marble Bar greenstone belt to the east by the age of the underlying Duffer Formation (~3471–3463 Ma) and the age of the overlying Panorama Formation (~3458–3454 Ma) (Van Kranendonk et al. 2002; Hickman 2012). The thickest (5–20 m) sedimentary intercalation within the Mount Ada Basalt, the Antarctic Creek Member, consists of felsic volcanoclastics, mafic tuff silicified argillite, chert, arenite and jaspilite intruded by dolerite. Spherules within chert retain high to very high sphericity and internal radiating quench textures, allowing their positive identification

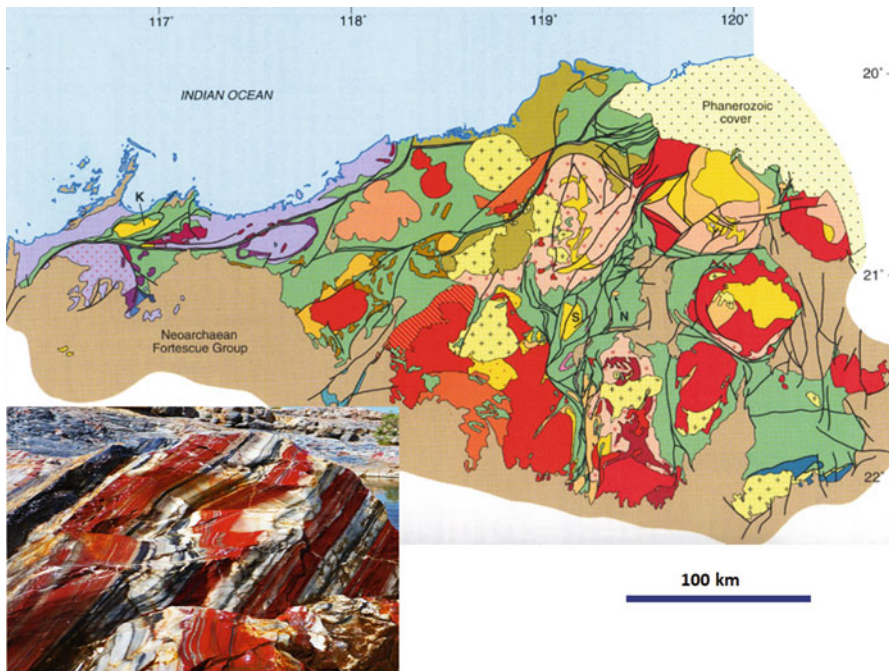


Fig. 2.2 Geological sketch map of the Pilbara Craton, Western Australia (Geological Survey of Western Australia; gsdar2003–04. MVK521; GSWA with permission). Inset: Marble Bar Chert Member

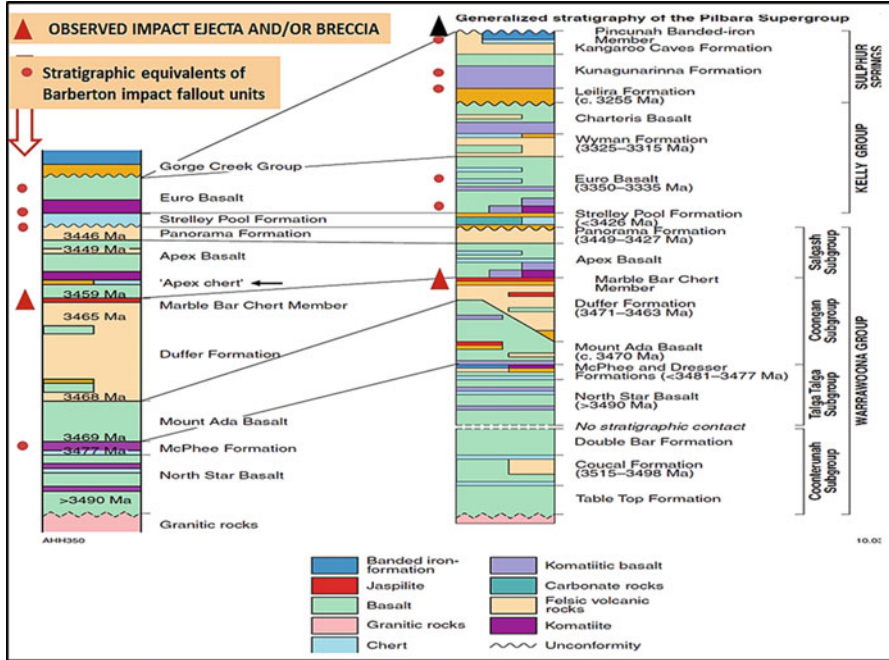


Fig. 2.3 Stratigraphy and isotopic ages of the Marble Bar greenstone belt. Red dots represent units correlated with stratigraphic units of the Barberton Greenstone Belt containing impact ejecta deposits. Geological Survey of Western Australia, Record 2011/7; GSWA with permission

as microkrystite spherules (Glikson et al. 2004) as defined by Glass and Burns (1988). Byerly et al. (2002) reported a $^{207/206}$ Pb age of 3470.1 ± 1.9 Ma for euhedral zircons derived from the spherule bearing unit, i.e. within error from the age of the Duffer Formation (3467 ± 4 , Van Kranendonk et al. 2002). Byerly et al. (2002) correlate the spherule-bearing unit with a similar S1 unit in the Hoogenoeg Formation, Barberton Greenstone belt, Kaapvaal Craton, South Africa, which yielded a $^{207/206}$ Pb zircon age of 3470.4 ± 2.3 Ma. The microkrystite-bearing units of the Antarctic Chert Member may represent three impacts or, alternatively, redeposition of spherules from a single impact. The microkrystite spherules are discriminated by their high sphericities, inward-radiating fans of sericite pseudomorphs after K-feldspar, relic quench textures and Ni-Cr-Co relations. Scanning Electron Microscopy coupled with E-probe (EDS) and laser ICPMS analysis indicate high Ni and Cr in sericite-dominated spherules, suggesting mafic composition of source. Ni/Cr and Ni/Co ratios of the spherules are higher than in

Table 2.1 Archaean to Proterozoic impact ejecta/fallout units and impact structures

Geological unit	composition	Age	References
ACM-1 Mt Ada Basalt, Warrawoona Group, Pilbara Craton	Silica–sericite spherules in m-thick chert breccia/conglomerate. Overlain by felsic hypabyssal/volcanics	3470.1 ± 1.9 Ma	Byerly et al. (2002)
ACM-2, Mt Ada Basalt, Warrawoona Group, Pilbara Craton	Silica-sericite spherules within ~14 m-thick chert, arenite. Overlain by ~10 m-thick jaspilite overlying spherule unit ACM-1	3470.1 ± 1.9 Ma	Byerly et al. (2002)
BGB-S1A & BGB-S1B, upper Hoogenoeg Formation, Onverwacht Group, Kaapvaal Craton	Two units of silica–chert spherules within 30–300 cm-thick unit of chert and arenite.	3470.4 ± 2.3 Ma	Byerly et al. (2002)
BGB-S2, base of the Mapepe Formation, Fig Tree Group, Kaapvaal Craton	310 cm-thick silica–sericite spherules. Overlain by Manzimnyama Jaspilite Member: BIF/jaspilite/ferruginous shale (520 m) and shale above BGB-S2	3258 ± 3 Ma	Lowe et al. (2003)
BGB-S3 and BGB-4 lower Mapepe Formation, Fig Tree Group, Kaapvaal Craton	S3: 10–15 cm-thick to locally 2–3 m-thick silica–Cr-sericite–chlorite spherules, overlain by ferruginous sediments of the Ulundi Formation in the northern part of the BGB.	3243 ± 4 to 3225 ± 3 Ma	Lowe et al. (2003)
	S4: 15 cm-thick arenite with chlorite-rich spherules		
Maniitsoq impact structure, SW Greenland	A central crush zone enveloped by gneiss and cut by mafic bodies.	~2975 ± 6 Ga	Garde et al. (2012)
JIL, top Jeerinah Formation, Fortescue Group, Hamersley Basin.	Hesta: 80 cm-thick carbonate–chlorite spherules and spherule-bearing breccia; 60 cm thick overlying debris flow; overlain by Marra Mamba Iron-formation, immediately above ~60 cm-thick shale unit overlying JIL	<2629 ± 5 Ma, >2597 ± 5 Ma	Simonson et al. (2000a) and Trendall et al. (2004)
Base of Carawine Dolomite, Hamersley Group, Hamersley Basin	Carbonate megabreccia-hosted microkrystite spherules; K-feldspar–carbonate–chlorite spherules in tsunami-generated carbonate–chert megabreccia	2630 ± 6 Ma	Simonson and Hassler (1997) and Rasmussen et al. (2005)

(continued)

Table 2.1 (continued)

Geological unit	composition	Age	References
Monteville Formation, West Griqualand Basin, west Kaapvaal Craton	5 cm-thick spherule layer. Carbonate hosted	<2650 ± 8 Ma ~2647 ± 30 Ma	Simonson and Glass (2004) and Simonson et al. (2010)
Reivilo Formation, West Griqualand Basin, western Kaapvaal Craton.	1.8 cm-thick spherule unit. Carbonate-hosted .	>2581 ± 9 Ma <2588 ± 6	Simonson et al. (2010)
Paraburdoo Spherule Layer, Hamersley Basin, Western Australia	2 cm-thick altered spherule unit in carbonates.	>2561 ± 8 Ma <2597 ± 5 Ma	Simonson et al. (2010)
SMB-1, top of Bee Gorge Member, upper Wittenoom Formation, Hamersley Group, Hamersley Basin	5 cm-thick K-feldspar–carbonate–chlorite spherules in carbonate turbidite. Overlain by ferruginous siltstone (Sylvia Formation), banded iron-formation (Bruno Member)	2541 ± 18/ 16 Ma	Simonson et al. (2010), Glikson (2004) and Trendall et al. (2004)
SMB-2, top of Bee Gorge Member, upper Wittenoom Formation, Hamersley Group, Hamersley Basin	20 cm-thick K-feldspar–carbonate–chlorite spherules within turbidite. Overlain by ferruginous siltstone (Sylvia Formation), banded iron-formation (Bruno Member)	2541 ± 18/ 16 Ma	Glikson (2004) and Trendall et al. (2004)
S4 Shale Macroband, Dales Gorge Member, Brockman Iron-Formation Hamersley Group, Hamersley Basin	10–20 cm K-feldspar–stipnomelane spherules at top of 2–3 m of ferruginous volcanic tuffs. Located 38 m above the base of the Brockman	2481 ± 4 Ma	Trendall et al. (2004) and Simonson et al. (2010)
lower Kuruman Formation, West Griqualand Basin, west Kaapvaal Craton	1 cm-thick spherule unit overlain by 80 cm breccia. Located 37 m above base of banded ironstones	<2516 ± 4 Ma	Simonson et al. (2010)
Graensco, Vallen, Ketilidean, southwest Greenland	20 cm-thick spherule unit. Carbonate-hosted spherules	~2.13–1.85 Ga	Chadwick et al. (2000)
Ejecta from the Sudbury impact structure	D~250 km	1850 ± 1 Ma	Addison et al. (2005)

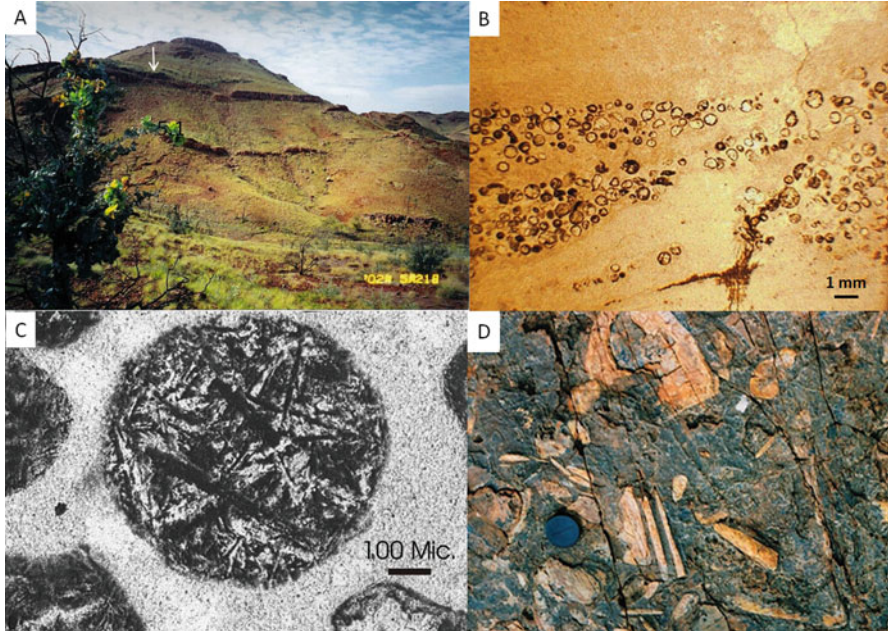


Fig. 2.4 Microkrystite spherules in chert and arenite intercalations in the ~3.47 Ga Antarctic Creek Chert Member, Mount Ada Basalt, Miralga Creek. **(a)** Outcrops of the Antarctic Creek Chert Member. Arrow points to chert bank containing impact ejecta units; **(b)** Lens of impact spherules within chert; **(c)** microkrystite spherule showing quench textures of clouded altered needles probably representing primary Fe-Mg minerals; **(d)** Chert breccia containing impact spherules

associated Archaean tholeiitic basalts and high-Mg basalts, rendering possible contamination by high Ni/Cr and Ni/Co chondritic components. Only a minor proportion of spherules are broken and the near-perfect sphericities of chert-hosted spherules and arenite-hosted spherules constrain the extent of shallow water winnowing of the originally delicate glass spherules. It follows the spherules were either protected by rapid burial or, alternatively, disturbance was limited to a short term high energy perturbation such as may have been affected by a deep-amplitude impact-triggered tsunami wave.

2.2 c.3460 Ma Impacts

Two units of impact spherules intermixed with chert fragments have been identified in the Marble Bar Chert Member (MBCM), dated as 3459 ± 2 Ma-old by U–Pb zircon (Glikson et al. 2016) (Fig. 2.5). The ejecta unit, observed in a drill core (ABDP 1) ~4 km south-southwest of Marble Bar, consists of multiple lenses and

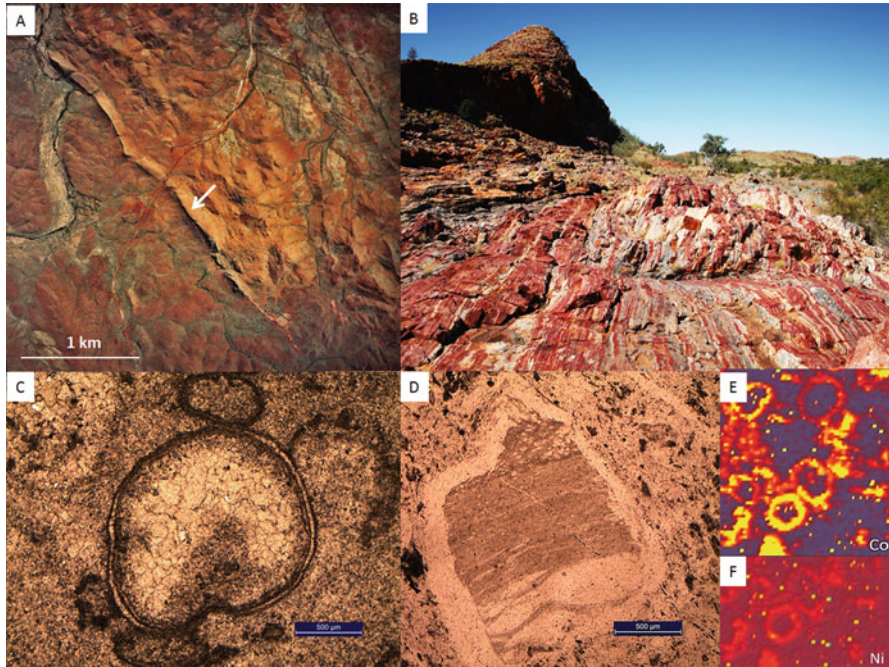


Fig. 2.5 The ~3.46 Ga Marble Bar Chert Member: (a) Air photograph of the MBCM (arrow) underlain by felsic volcanics of the Duffer Formation and overlain by mafic volcanics of the Apex Basalt and Mount Roe Basalt; (b) Jaspilite outcrops of the MBCM, Coongan River; (c) microkrystite impact spherule, displaying quartz-rich interior and iron-rich rims; (d) Microtektite displaying flow texture and enveloped by quartz mantle; (e). Laser-ICPMS image of cobalt levels in microkrystites; (f) Laser-ICPMS image of Nickel levels in microkrystite (After Glikson et al. 2016; Elsevier, with permission (<http://www.sciencedirect.com/science/article/pii/S0301926816300511>))

bands of almost totally silicified impact spherules 1–2 mm in diameter. All internal primary textures of the spherules have been destroyed. Nonetheless, Fe-rich spherule rims, largely composed of secondary siderite, are well preserved. Chemical analyses of the rims reveal iron-magnesium carbonate displaying high Fe, Mg, Ni, Co and Zn. Whole-rock and in-situ analyses, including X-ray fluorescence, Inductively Coupled Plasma Mass Spectrometry (ICPMS), electron-microprobe (EMP) and EMP-calibrated laser ICPMS, reveal the spherule rims contain high Ni abundances and high Ni/Cr ratios (<50). The spherules are separated by an arenite matrix and spherule lenses occur also within bedded chert. The spherules are particularly common over some 14 m of stratigraphic thickness in which chert breccia is interpreted to represent a tsunami-generated diamictite affected by hydrothermal fragmentation and veining. Despite the almost total silicification of the MBCM whole-rock analysis by NIS Fire Assay and ICPMS indicates high Ir (2 ppb) and a low Pd/Ir ratio (2.0), consistent with geochemical features of impact ejecta units.

Dense concentrations of spherules at the 57–58 m level and the 77 m level of the core, separated by banded chert, raise the possibility of two distinct impact events. Stratigraphic and isotopic age data distinguish between the 3459–3449 Ma age of the MBCM ejecta unit and 3470.1 ± 1.9 Ma impact ejecta units in the Antarctic Creek Member, Mount Ada Basalt, about 40 km to the west of Marble Bar. In combination with a 3472 ± 2.3 Ma impact unit in the Barberton greenstone belt, these impact ejecta units record large Paleoproterozoic asteroid impacts, significant for understanding early bombardment rates on Earth and early crustal evolution.

2.3 Impact-Related Units c.3.3–3.227 Ga

Three impact spherule-bearing units (S1–S3) in the Barberton Greenstone Belt (BGB) have been identified at the base to lower part of the Fig Tree Group by quench textures, iridium anomalies and Cr isotopic data (Lowe and Byerly 1986; Lowe et al. 1989, 2003; Byerly and Lowe 1994; Byerly et al. 2002; Kyte 2002; Kyte et al. 1992, 2003; Shukolyukov et al. 2000; Glikson 2007). Significant analogies pertain between sequences in the BGB and East Pilbara greenstone belts, including likely correlations between stratigraphic/unconformity breaks about 3.3–3.22 Ga (Glikson and Vickers 2006, 2010) (Fig. 2.6) including:

- (a) The hiatus between the ultramafic to mafic/felsic volcanic Onverwacht Group in the BGB (Mendon Formation 3298 ± 3 Ma) and turbidite/felsic volcanics of the Fig Tree Group (Mapepe Formation – 3258 ± 3 – 3225 ± 3 Ma) (U-Pb zircon ages after Kröner et al. 1991a, b and Byerly et al. 1996).
- (b) The break between the ultramafic to felsic volcanic Sulphur Springs Group in the central Pilbara (U-Pb zircon ages of 3550–3235 Ma) and overlying megabreccia (olistostrome), ferruginous argillite/turbidite/felsic volcanic and BIF of the Gorge Creek Group, Pilbara Craton (Fig. 2.6) (Van Kranendonk and Morant 1998; Van Kranendonk 2000; Buick et al. 2002)

The ~3.255–3.235 Ga Sulphur Springs Group (SSG) is dominated by a volcanic succession which includes a basal conglomerate, wackes and felsic volcanic rocks (~3255 Ma Leilira Formation), through komatiite (Kunagunarinna Formation), to a unit of basalt-andesite and rhyolite, with interbedded chert horizons (3235 Ma Kangaroo Caves Formation). The volcanic rocks are overlain by an up to 50 m thick chert unit (Fig. 2.6) associated with the emplacement of the syn-volcanic Strelley Granite laccolith and precipitation of volcanogenic massive sulphide deposits (Vearncombe et al. 1998; Brauhart et al. 1998). The chert is overlain by an olistostrome breccia (Fig. 2.6a, b) and ferruginous clastic and locally chemical sedimentary rocks of the Pincunah Hill Formation (Gorge Creek Group), including felsic tuff lenses.

The correlation between the BGB and central Pilbara successions has led to a search for impact fallout units at the base of the Gorge Creek Group (Glikson and Vickers 2006). To date however no microkrystites have been identified. Volcanic varioles and amygdales are widespread in felsic to intermediate metavolcanic rocks and in pyroclastic rocks and are distinguished from impact spherules by (1) occurrence of resorbed quartz microphenocrysts in the volcanic fragments; (2) outward-radiating textures in varioles, as contrasted with inward radiating and quench textures in impact-condensation spherules (microkrystites); (3) poor sorting and occurrence of >5 mm-scale spherules in volcanic deposits, contrasted with the highly uniform size distribution and mostly mm to sub-mm-scale of impact spherules. It is likely that the arenite-dominated composition of the Leilira Formation and basal Soanesville Group resulted in corrosion and destruction of the originally glassy microkrystite spherules. The olistostrome (Fig. 2.6a, b) may have been associated with the end of felsic volcanic activity and caldera collapse (Van Kranendonk et al. 2002). On the other hand the location of the megabreccia/olistostrome at a

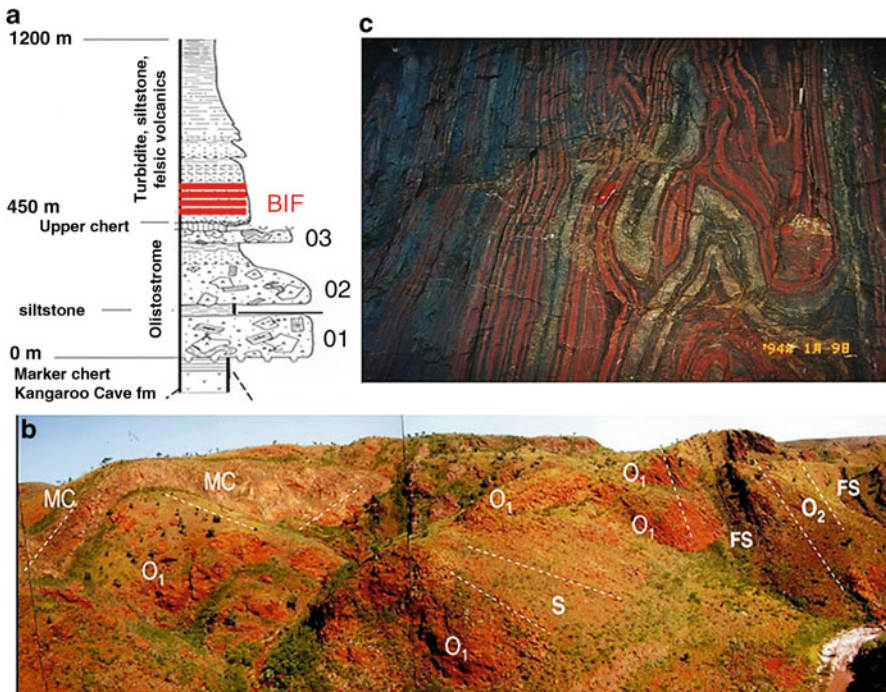


Fig. 2.6 ~3.2 olistostrome and banded iron formations, Sulphur Springs area, central Pilbara Craton: (a) Schematic cross section showing the basal unconformity of the olistostrome over volcanics of the Sulphur Springs Group, multiple olistostrome units and overlying banded iron formations, turbidites and felsic volcanics of the Soanesville Group; (b) A view of olistostrome units (O1, O2), intercalated siltstone (S) and ferruginous siltstone (FS) and the underlying Marker Chert (MC) signifying the top of the Sulphur Springs Group; (c) Banded iron formation of the Gorge Creek Group (From Glikson 2006; Elsevier, with permission (<http://www.sciencedirect.com/science/article/pii/S0012821X06002809>))

stratigraphic level correlated with the Barberton impact spherules, and the size of the blocks (olistoliths), conceivably hint at contemporaneous seismic/earthquakes effects related to impacts.

2.4 Jeerinah c.2.63 Ga Impact Layer (JIL) and Carawine Dolomite Impact/Tsunami Megabreccia

A thin ~6 mm layer of microkrystite spherules occurs in the Ilbiana Well FVG-1 drill hole at the top of the JIL black shale sequence (Simonson et al. 2000a, b. The JIL (2684 ± 6 Ma – 2629 ± 5 Ma) (Arndt et al. 1991; Nelson 1999). The layer is located 2.7 m below the top of the Jeerinah Formation which underlies the Marra Mamba Iron Formation (2597 ± 5 Ma) (Fig. 2.7). An exposure of the JIL located by B.M. Simonson at Hesta railway siding (Simonson et al. 2001) (Fig. 2.8a, b) displays the transition from laminated argillite to argillite-chert (~ 5 m) to a ~1 m-thick zone of microkrystite spherules-bearing breccia with siltstone and chert (Fig. 2.8c), a massive zone of spherules with fewer argillite and chert intraclasts and overlying microkrystite

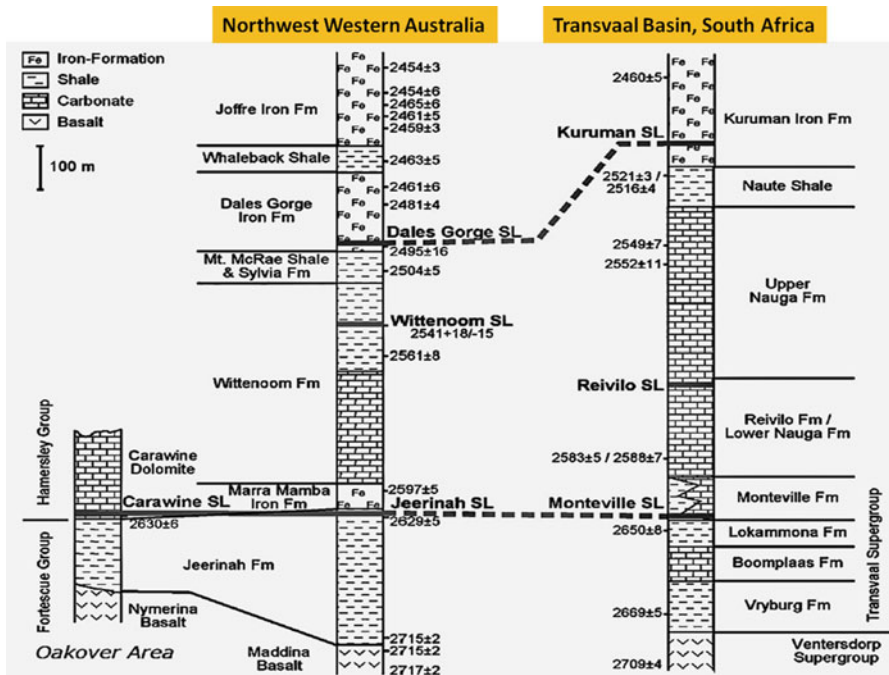


Fig. 2.7 Stratigraphy of ejecta of large impacts around the Archaean-Proterozoic boundary: schematic columns of the Hamersley and Transvaal successions showing the stratigraphic locations and proposed correlations of impact spherule layers (Simonson et al. 2009a, b; Elsevier with permission (<http://www.sciencedirect.com/science/article/pii/S0301926808002635>))

spherules-poor breccia dominated by angular to rounded chert cobbles and boulders (Fig. 2.8c). The impact fallout unit overlain by a boulder deposit likely representing tsunami effects (Fig. 2.8d). Microkrystite spherules display inward radiating fibrous K-feldspars and centrally offset vesicles (Fig. 2.8e). Irregular-shaped fragments reaching 2–4 mm in size contain feldspar microlites in microcrystalline matrix and showing flow banding and quartz-filled vesicles are regarded as microtektites (Figs. 2.8f) compared with Muong Nong type microtektites such as described from tsunami-disrupted carbonate-chert unit located at the contemporaneous Carawine Dolomite (Simonson et al. 2000a, b, 2001; Glikson 2004). Ni levels of JIL microkrystites are analogous to basaltic

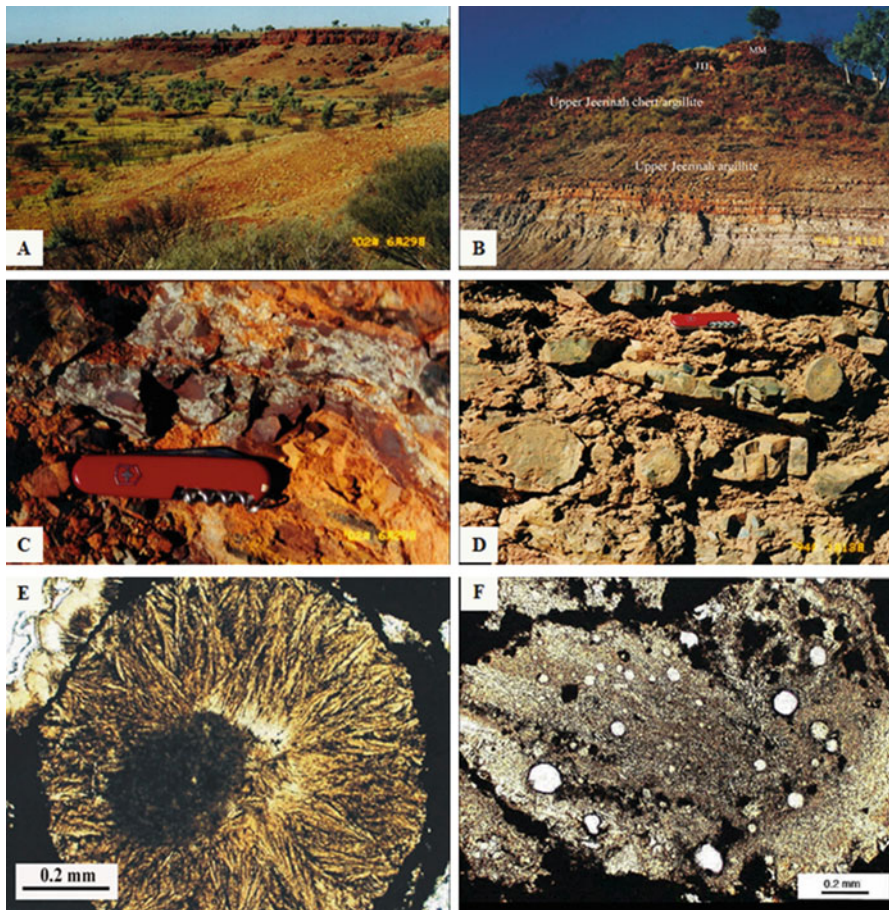


Fig. 2.8 Impact ejecta of the 2.63 Ga Jeerinah Impact Layer (JIL) in the classic Hesta outcrop, central Pilbara Craton. (a) Outcrops of the JIL; (b) Exposure of the Hesta outcrops of Jeerinah Formation siltstone, JIL layer and overlying laterite top; (c) Outcrop of the JIL consisting of impact spherules-bearing siltstone; (d) Boulder breccia overlying the JIL; (e) A quench textured inward radiating microkrystite spherules with a centrally offset vesicle; (f) microtektite fragments displaying weak flow texture and gas bubbles

compositions and Pd/Ir ratios are low (~ 0.8 – 2.1) consistent with depletion of volatile PGE relative to refractory PGE in microkrystite spherules during condensation (Glikson and Allen 2004; Glikson 2007). Following the criteria of O’Keefe and Aherns (1982) and Melosh and Vickery (1991) the sizes of some spherules above 1 mm correlate with impacts by asteroids on the scale of 10–20 km. Rasmussen and Koeberl (2004) report an Ir concentration of 15.5 ppb in JIL spherules and an angular quartz grain containing planar deformation features (PDF), indicating the impact affected some quartz-bearing rocks. However the prevalence of chlorite in spherule interiors and the paucity of shocked quartz grains are suggestive of a basaltic/oceanic composition of the target crust, consistent with observations pertaining to microkrystites of the Wittenoom Formation and the Carawine Dolomite.

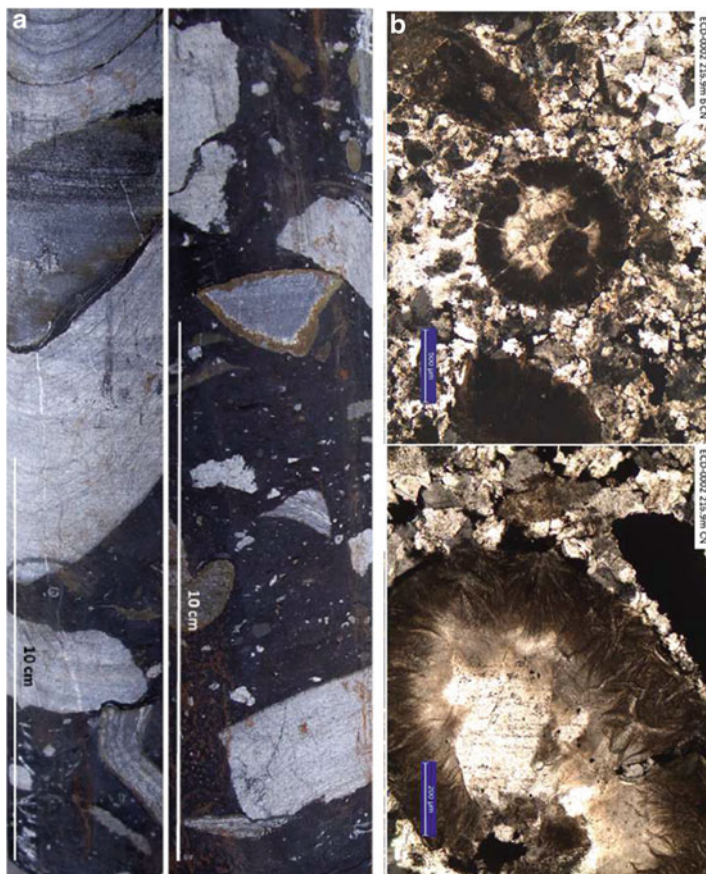


Fig. 2.9 (a) Chert, carbonate and sulfide fragments and boulders within carbonate-spotted black carbonaceous shale within the tsunami deposit incorporating the JIL in the ECD-0002 drill core, within the Roy Hill Member of the Jeerinah Formation. Note the sulfide rims and blebs in the upper frame. For stratigraphy refer to Fig. 5.5; (b and c): Microkrystite spherules within the JIL, drill core ECD-0002. Note the inward-radiating quench crystallite fans in (c), diagnostic of quenching of impact spherules (AJES with permission)

Impact spherules correlated with the ~2.63 Ga Jeerinah Impact layer (JIL) are observed within an over 100 meters-thick fragmental-intraclast breccia in Roy Hill drill holes, East Hamersley Basin (Hurst et al. 2013) (Fig. 2.9a–c), representing major thickening of the impact/tsunami unit relative to the JIL type section at Hesta and also relative to the 20–30 m-thick ~2.63 Ga Carawine Dolomite spherule bearing mega-breccia (CDMB), Oakover River to the East. The latter, identified in the Oakover Valley (Simonson 1992) and Woodie-Woodie (Hassler et al. 2000), extends over a strike distance of 98 km (Figs. 2.10a, 2.10b). It consists of chert and dolomite clasts and mega-clasts on scales ranging up to several meters and derived from an autochthonous to sub-autochthonous lithologically distinct chert- dolomite unit (Fig. 2.10b). Ductile deformation of bed segments is observed on a range of scales, for example in layered chert-carbonate blocks, within individual boulders and as small folded concretions. Multiple veins of breccia and microbreccia injected across and along bedding planes of carbonates underlying the megabreccia may contain microkrystites and microtektites whose preservation is interpreted in terms of tsunami-induced hydraulic pressures, minimizing mechanical grinding effects (Glikson 2004). Microtektite and microkrystite concentrations are concentrated toward the top, where the breccia is conformably overlain in sharp contact by well layered carbonate.

Salient features relevant to the origin of the CDMB include the following (Glikson 2004) (Fig. 2.10b):

1. The megabreccia forms a stratigraphically unique time/event marker horizon, allowing the identification of lateral and vertical facies and thickness controls in the Carawine Dolomite.
2. The dominantly irregular structure, unsorted fragments and near-random orientation of blocks and fragments militates autochthonous to near-autochthonous derivation of the fragments.
3. The absence of stromatolite-facies fragments within the megabreccia is consistent with an autochthonous nature of the brecciation.
4. The size of blocks, observed up to <7 m, and the common excavation of the base of the CDMB provide evidence for high-energy disruption of the sea bed.
5. The location of the CDMB in below-wave-base carbonate-siltstone units suggests the disruption originated by high-amplitude waves.
6. Models regarding the origin of the CDMB must take into account the constraints imposed by the near-perfect preservation of underlying and overlying carbonate sediments and overlying and injected microkrystite spherules.

Impact-triggered mega-tsunami-generated autochthonous to sub-autochthonous breccia account for much of the observed evidence (Simonson 1992), Simonson and Hassler 1997, Hassler et al. 2000 and Hassler and Simonson 2001. Similar features have been described in the vicinity of the Chicxulub impact structure at Belize, Mexico (Pope et al. 1997). Sharp variations in the thickness of the CDMB where megabreccia sections about 12 m thick are juxtaposed with megabreccia sections about 4 m-thick, indicate faulting. A model supported here involves: (1) Arrival of the tsunami impinging on bottom sediments with consequent dispersal of a mud cloud in the submarine environment

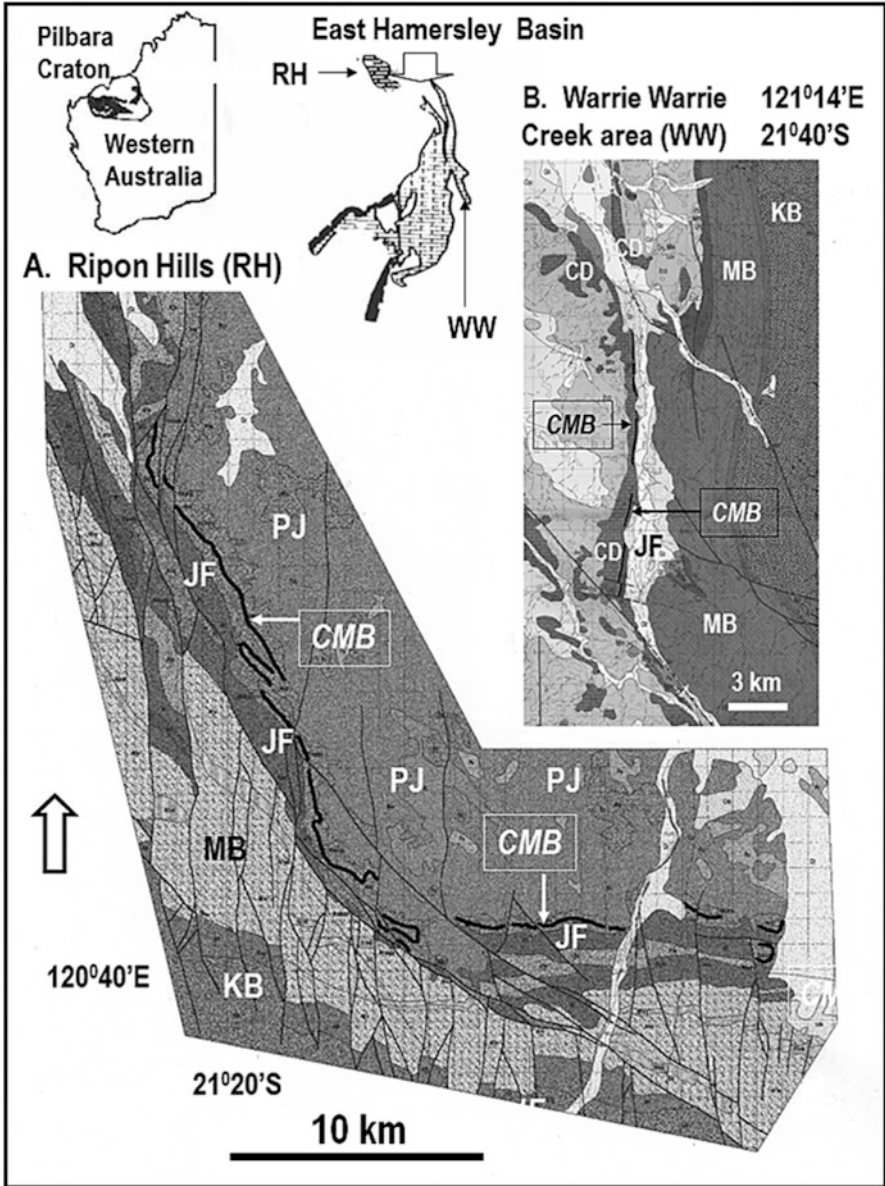


Fig. 2.10a A geological sketch map of the Eastern Hamersley Basin, indicating the distribution of the Carawine Dolomite Megabreccia (CMB). KB Kylena Basalt, MB Maddina Basalt, JF Jeerinah Formation 2.629 Ga, PJ Pinjian Chert (silicified breccia), GR Gregory Range, WW Warrie Warrie Creek belt, RH Ripon Hills. The CMB unit is shown as a thick black line (After Glikson 2004)

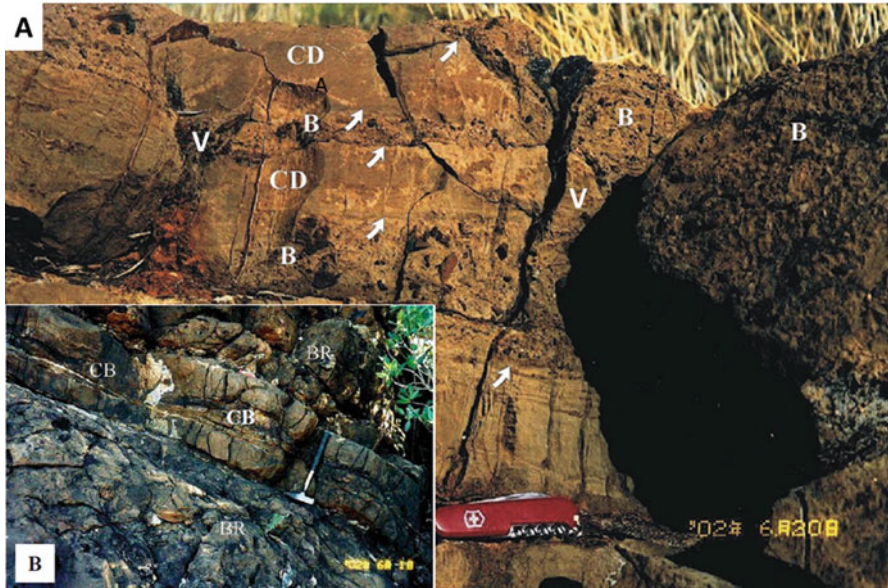


Fig. 2.10b Carawine Megabreccia (CDMB): **A.** conformable breccia (labelled B) intercalated between horizontal slabs of Carawine Dolomite (CD) and vein breccia (arrows) injected across layering. **B.** Mega-breccia plates overlying medium-scale breccia

(2) Deformation of ductile sea bed sediments as evidenced by ductile deformed/folded layers and fragments; (3) Excavation, fracturing and chaotic disruption of the solid substratum below the soft sedimentary column; (4) Settling of microkrystite spherules and microtektite glass fragments from the impact-released cloud, forming a top spherule layer; (5) Continuing seismic-triggered tsunami waves and injection of parts of the subaqueous spherule-bearing mud into the breccia substratum, resulting in preservation of the microkrystite spherules in veins.

2.5 Paraburdoo c. 2.57 Ga Spherule Layer

The PSL unit of the Wittenoom Formation is hosted by thin-bedded dolomite deposited in a deep shelf off-platform environment (Hassler et al. 2011) (Fig. 2.11a). It consists of a < 2 cm-thick spherule layer located ~55 m below the top of the member and ~86 m below a marker tuff horizon dated as 2561 ± 8 Ma (Hassler et al. 2011). Another tuff horizon located hundreds of meters below the PSL was dated as 2597 ± 5 Ma (Trendall et al. 1998), leading Hassler et al. (2011) to estimate an age of 2.57 Ga for the PSL. The unit consists of packed spherules set in

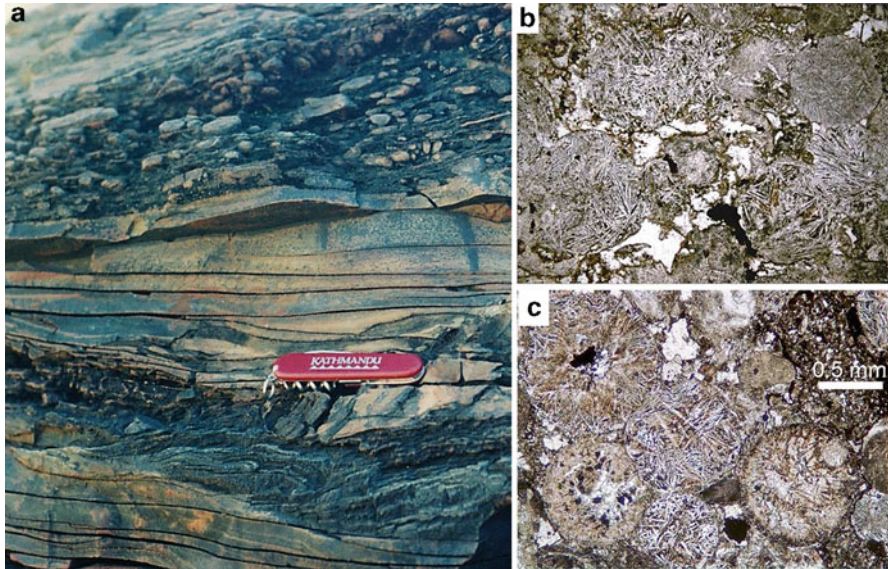


Fig. 2.11 The 2.57 Ga Paraburdoo impact layer: (a) Tsunami deposits outcrops in Bee Gorge, Hamersley Range; (b and c) Well preserved microkrystite spherules displaying quench textures (After Hassler et al. 2011 (<https://pubs.geoscienceworld.org/geology/article-abstract/39/4/307/130511/paraburdoo-spherule-layer-hamersley-basin-western>)) (Geology, with permission)

~4% intergranular carbonate matrix. The spherules are internally recrystallized. K-feldspar crystallites and phlogopite-type crystals at either random orientations or branching clusters and skeletal textures (Fig. 2.11b, c). Hassler et al. (2011) regard the K-feldspar crystallites as alteration products of quench crystallized plagioclase crystallites, compared to K-feldspar replacement of plagioclase in mafic Hamersley tuffs (Hassler 1993). An absence of current reworking in the PSL suggests below-wave deposition. These authors correlate the PSL with the Reivilo Spherule Layer (RSL), Transvaal Basin. Laser-ICPMS analyses of Paraburdoo spherules determined Ni levels of up to 404 ppm, Ir levels of up to 357 ppb and low Pd/Ir ratios in the range of 0.1–0.67 (Goderis et al. 2013).

2.6 Spherule Marker Bed (SMB) c. 2.56 Ga Layer

The Spherule Marker Bed (SMB), located within the ~230 m-thick siltstone-carbonate Bee Gorge Member, upper Wittenoom Formation, and identified by Simonson (1992) at Wittenoom Gorge, is a microtektite-bearing turbidite unit about 0.5–1.0 m-thick (Figs. 2.12a, b, 2.12c and 2.13). The SMB extends over an area ~16,000 km², with thickness variations from centimetre-scale layers to several decimetre-thick turbidite units (Simonson 1992). Sedimentological studies of

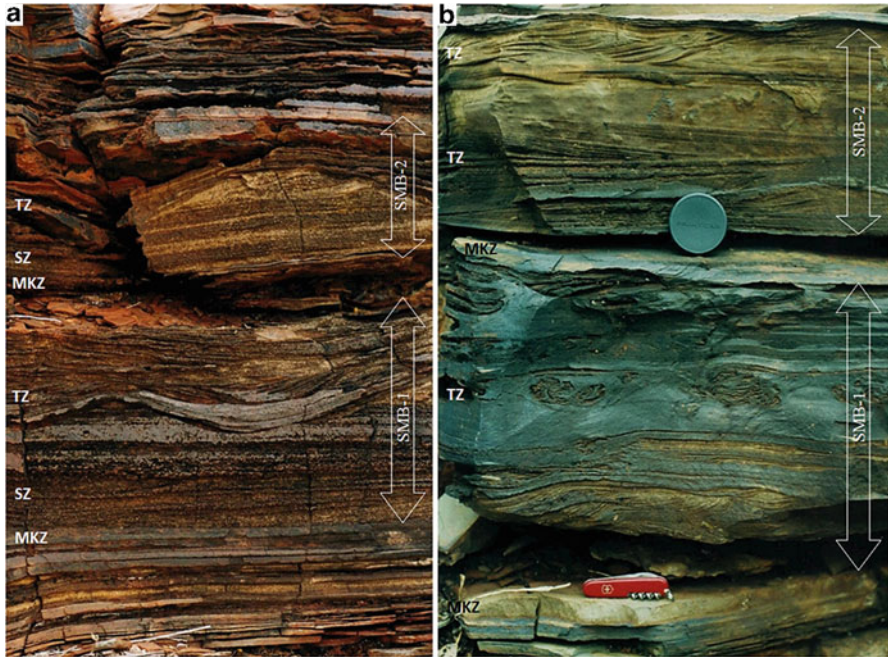


Fig. 2.12a, b ~2.56 Ga microkrystite spherule marker bed (SMB), showing two impact cycles, SMB-1 and SMB-2, overlain and underlain by carbonate, siltstone, and chert. Each cycle includes a basal layer or series of lenses of microkrystite spherules (MKZ) overlain by rhythmic turbidites (seismic zone, SZ), overlain by a cross-rippled tsunami zone (TZ). The two cycles are separated by a stratigraphically consistent layer of silicified black siltstone denoted as a ‘Quiet Zone’ (a. Munjina Gorge; b. Wittenoom Gorge) (Springer, 2014. by permission)

15 sections of the SMB (Simonson 1992; Hassler et al. 2000; Hassler and Simonson 2001) suggest a slope or deep shelf environment, persisting below and above the impact fallout layer. A tsunami origin of the SMB is indicated by the close association of bedforms with microkrystite and microtektite-bearing units accumulated below wave-base position, indicating wave amplitudes exceeding those of wind-driven wave systems (Hassler et al. 2000). U-Pb zircon ages reported as 2561 ± 8 Ma or 2565 ± 9 Ma (Trendall et al. 1998; Trendall et al. 2004) are somewhat older than carbonate whole rock Pb-Pb ages (Woodhead et al. 1998) as $2541 + 18/-15$ Ma.

Simonson (1992) documented splitting of the SMB at its westernmost occurrences into two parts, as is also observed in the Wittenoom and Munjina gorges (Glikson 2004) (Fig. 2.12a, b and 2.12c): The lower cycle contains at its base a cm-scale spherule-rich horizon or discontinuous <5 cm-thick spherule-rich lenses, while in many areas spherules are missing. The spherule-rich unit is overlain by a graded bedded Bouma-type cycle arenite-turbidites, in turn overlain by cross layered arenite, or by siltstone capped by convolute current turbulence climbing cross-



Fig. 2.12c The lower cycle (SMB-1) at Munjina Gorge, displaying the “Fire Layer” of microkrystite spherules, “seismic zone” of seismic-generated turbidites and “Tsunami Layer” of cross-layered turbidites

bedding and ‘ball-and-pillow’ structures. Major recumbent over-folds, representing switching current directions, occur at the top of SMB-1, in turn overlain by tens of cm-thick little-disturbed stratigraphically consistent argillite of SMB-2. The upper cycle locally includes a thick (<20 cm) densely packed spherule unit or isolated microkrystite-bearing carbonate bands. The close coupling of spherule deposition and high-energy currents as two cycles represent two distinct temporally related impact events, possibly the fragments of a single asteroid.

Microkrystites of the SMB display

1. Inward-radiating fibrous/acicular K-feldspar which either form shells, shells and mantles, or completely fill the spherules (Fig. 2.13b, c)
2. Internal vesicles filled with quartz, carbonate, chlorite, sericite and Fe-oxides.
3. Composite particles consisting of agglutinated microkrystite spherules and microtektites (Fig. 2.13c)
4. Some microkrystites have both inward-radiating K-feldspar fans and randomly oriented K-feldspar needles, showing transitional characteristics with microtektites.

Siderophile elements (Ni, Co, Cr, Zn) and Platinum Group Element (PGE) (Simonson et al. 1998) disclose weak anomalies consistent with a meteoritic derivation of the microkrystite spherules and microtektite-rich sediments. Chondrite-normalized abundance profiles for the elements Ir, Ru, Pt, Pd, Au, Ni, Co, V and Cr – corresponding to progressive enrichment sequence in Pyrolite model mantle (Ringwood 1975) relative to C1-chondrite (McDonough and Sun 1995) indicate:

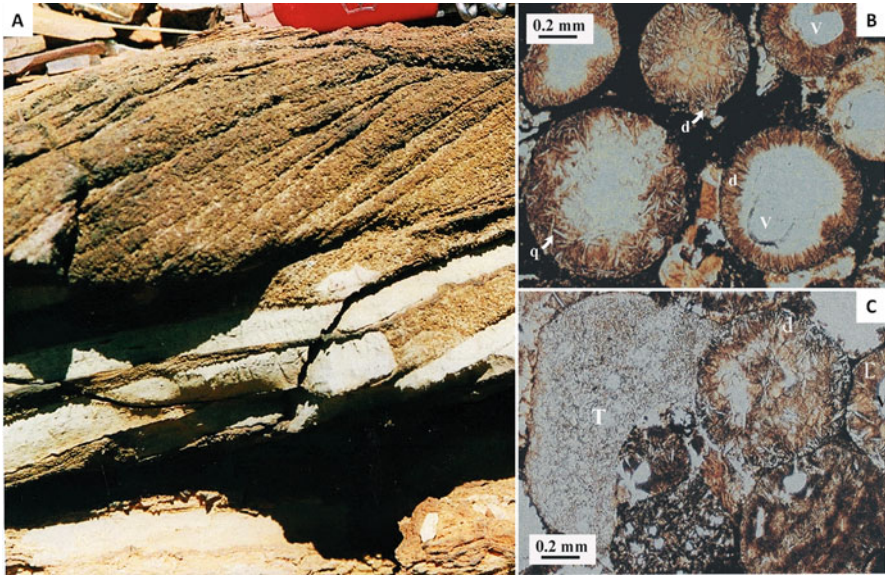


Fig. 2.13 Impact fallout units of the Spherule Marker Bed: (a) Massive spherule-rich layers of east of Bee Gorge; (b) Microkrystite spherules displaying quench rims formed of K-feldspar surrounding quartz-rich cores; (c) A tektite (T) and quench textured microkrystite spherules

1. The Ir levels of microkrystite spherule-rich sediments (mean Ir = 0.496 ppb) are about an order of magnitude higher than in background sediments (mean Ir = 0.0033 ppb) associated with the SMB.
2. Pd/Ir, Pt/Ir are lower than those of spherule-poor sediments and background sediments and are closer to chondritic values, consistent with preferential condensation of the refractory PGE relative to volatile PGEs (Glikson and Allen 2004; Glikson 2007).

However the abundances of Ni (mean = 36 ppm) and Co (mean = 18 ppm) in spherule-bearing sediments are similar to background sediments (mean Ni = 31 ppm, mean Co = 20 ppm), while the mean Cr values of the spherule-rich sediments (100 ppm) is about double that of background sediments (mean ~47 ppm) (Simonson et al. 1998).

2.7 Dales Gorge (DGS4) c.2.48 Ga Spherule Layer

Millimetre-scale spherulitic textures documented by LaBerge (1966) within the Shale-unit-4 (DGS4) of the lower Dales Gorge Member, Brockman Iron Formation) can be traced at least 30 km in the Dales Gorge-Wittenoom Gorge area forming a



Fig. 2.14a A. Dales Gorge, Hamersley Range. The white arrow points to the Dales Gorge Shale 4-hosted impact spherule unit; B. A boulder of folded chert set in the spherule-rich DGS4 impact unit, Mines Pool, Wittenoorn Gorge, Hamersley Range

1–2 m-thick soft zone consisting which forms a distinct recess within cliff-forming banded iron (Fig. 2.14aA). The spherule-bearing unit forms a stratiform zone within ferruginous siltstone/shale and varies in thickness from about 20–30 cm at Dales Gorge to 110 cm at Wittenoorn Gorge. Simonson (1992) has shown the spherules

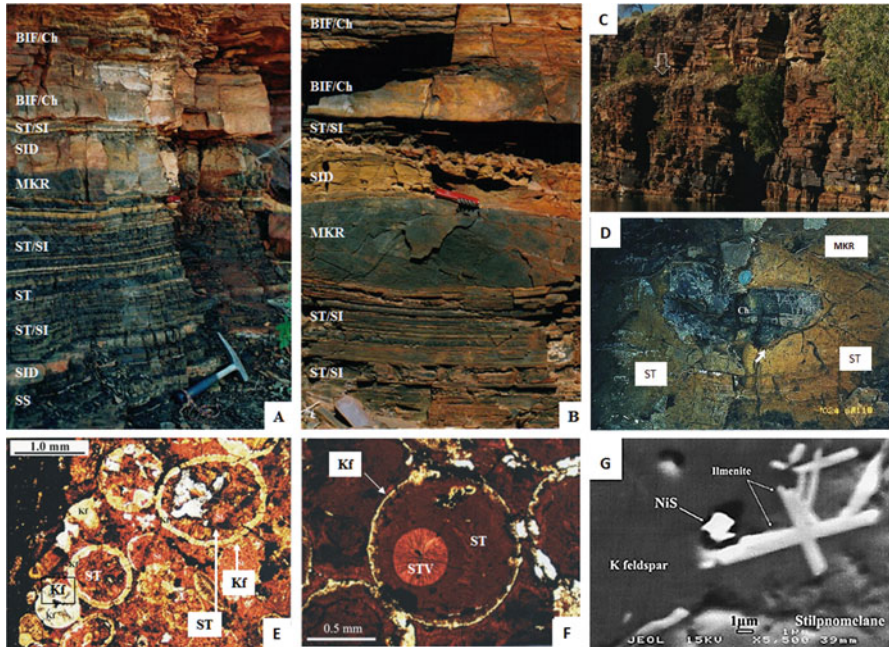


Fig. 2.14b Outcrops and microphotographs of the DGS4 impact unit, Hamersley Range: **A**. Outcrop of the DGS4 at Yampire Gorge. MKR-Microkrystite spherule layer; SID – siderite; ST – stilpnomelane-rich layer; BIF – banded iron formation; Ch – chert; **B**. DGS4 spherule unit in Dales Gorge. Symbols as in **A**; **C**. The DGS4 forming a soft bank underlain and overlain by banded iron formations, near Mine Pool, Wittenoom Gorge; **D**. A tsunami-transported block of chert in DGS4 near Mine Pool; **E**. DGS4 microkrystite spherules consisting of stilpnomelane rimmed by K-feldspar; **F**. A stilpnomelane-dominated microkrystite spherule rimmed by K-feldspar and containing an offset bubble; **G**. Ilmenite crystals and NiS grain within K-feldspar in a microkrystite spherule

constitute impact microkrystites (Fig. 2.14bE, F), dated by Trendall et al. 1998; Thorne and Trendall 2001 and Trendall and Blockley 1970) as 2479 Ma-old. The spherules display high sphericities, elongate and dumbbell-shaped spherules as long as 2.5 mm are present ($D_{\text{mean}} \sim 0.7$ mm; $D_{\text{max}} < 1.8$ mm) and consist of inward radiating K-feldspar fans surrounding stilpnomelane-dominated interiors. Petrological and geochemical studies establish a chondrite-related composition (Glikson and Allen 2004).

A distinct feature of the DGS4 unit is the presence of isolated angular to sub-rounded fragments and meter-scale rafts of chert and banded ferruginous chert (Figs. 2.14aB, 2.14bD) (Hassler and Simonson 2001; Glikson and Allen 2004; Glikson 2004). The mega-clasts rest at a variety of angles to the overall layering, including near-vertical orientations and appear to have been incorporated contemporaneously or shortly following deposition of the spherule-rich material, leading to their interpretation in terms of

exotic tsunami-transported blocks ripped off submarine scarps. The spherules consist of stilpnomelane rimmed by shells of K-feldspar (Fig. 2.14bE, F). Spherule morphologies include oblate, disc-shaped and near dumbbell-like forms. Spherule interiors may contain central to offset vesicles filled with randomly oriented fans of stilpnomelane. Secondary micro-spherules of stilpnomelane may occur within K-feldspar shells and mantles. The K-feldspar appears to display little effects of alteration. Micron-scale ilmenite needles within K-feldspar include Ni-metal, Ni-oxide, Ni-sulphide and Ni-arsenide (Fig. 2.14bG). SEM analysis resolves a common occurrence of euhedral ~5–10 µm-long ilmenite needles within K-feldspar spherule shells, including near-pure Ni-metal (Ni < 84.7%), Ni-S-As particles, Ni-Co-As-S particles and NiS particles. A chondritic affinity is further indicated by high Ni abundances, high Ni/Co and Ni/Cr ratios in stilpnomelane spherule interiors, low Pd/Ir, Pt/Ir and Pd/Pt ratios in stilpnomelane spherule interiors and to a lesser extent in K-feldspar shells (Glikson and Allen 2004).

Whole rock PGE analyses by solution ICPMS yield high abundances of Ir (~1–18 ppb), Pt (~2–42 ppb) and distinctly low Pd (~0.64–25.1 ppb), and thereby low Pd/Ir ratios (0.56–1.4) as compared to terrestrial mafic rocks (range 3.4–3.7). The relative depletion in volatile PGEs is consistent with PGE patterns in microkrystite spherules from other impact ejecta units (Glikson and Allen 2004; Simonson et al. 2009a, b), as contrasted with the enrichment of volatile PGEs (Pd, Au) in terrestrial materials, with the notable exception of refractory harzburgites (Chou 1978). The DGS4 impact fallout unit includes large microkrystite spherules in the range of <1.4 mm and long axes of oblate and dumbbell-shaped spherules up to <2.2 mm. According to thermodynamic estimates by O’Keefe and Aherns (1982) and Melosh and Vickery 1991 impact spherules on this scale represent projectile diameters in the order of 15–25 km. Likely equivalents of DGS4 were encountered in a drill hole ~30 km south of Griquaastad, western Transvaal Basin, where a ~1 cm-thick spherule layer is located within a 2 m-thick shale unit near the base of the Kuruman Iron Formation, about 37 m above Gamahuann carbonates and below a ~80 cm-thick breccia unit.

2.8 Bunyeroo ~580 Ma Impact Ejecta

The Late Proterozoic (Ediacaran) Bunyeroo impact ejecta, exposed in the Flinders Ranges (Fig. 2.15) and cored in the Dey-Dey Mudstone Beds under the Office Basin, South Australia (Wallace et al. 1990, 1996; Hill et al. 2004) (Fig. 2.16), and dated as ~580 Ma, has been correlated with the Acraman impact structure. The correlation is further supported by the lateral variation in clast size in the ejecta and the palaeomagnetism of melt rock from the central impact area and the ejecta-hosting Bunyeroo Formation (Williams and Schmidt 2015). The structure is expressed by a ~30 km diameter depression in the Gawler Ranges of South Australia, with a possible



Fig. 2.15 The Bunyeroo impact layer at Bunyeroo Gorge, Flinders Ranges, containing fragments of dacite ejected from the Acraman crater (Photo: courtesy of Victor Gostin)

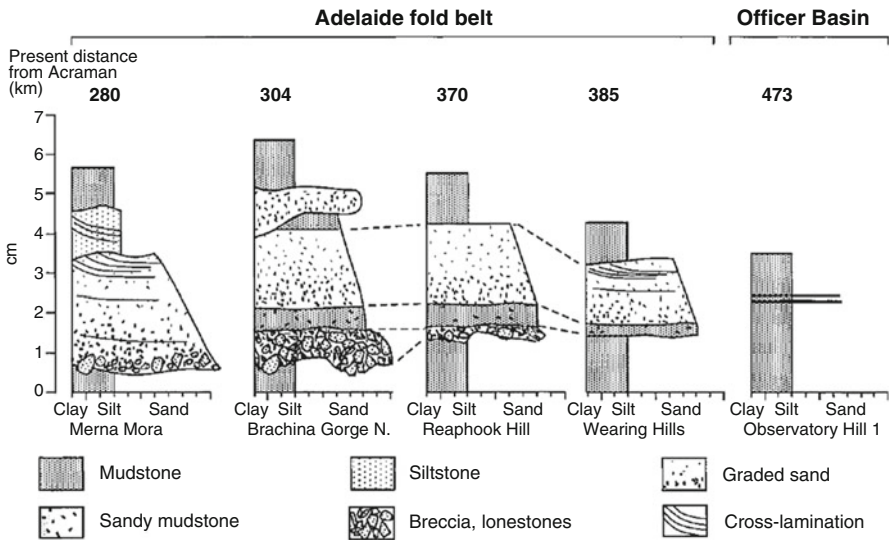


Fig. 2.16 Sections typical of the Acraman impact ejecta horizon in the Adelaide fold belt and Officer Basin, South Australia, arranged according to present distance from the center of Acraman (After Williams and Wallace 2003) (The Geological Society, with permission)

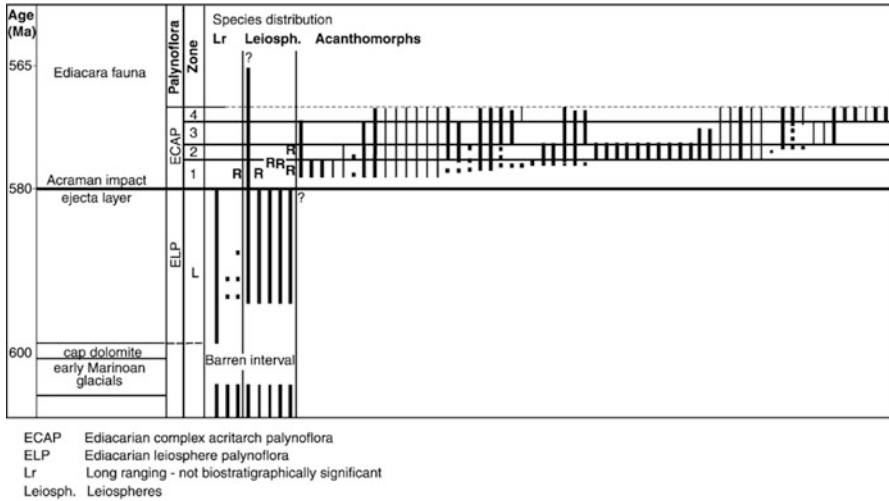


Fig. 2.17 Generalized ranges of Ediacaran palynomorphs. Distributions plotted by zone (highest degree of refinement currently possible). Note change at ELPECAP boundary and rapid increase in diversity of acanthomorphs above Acraman impact ejecta layer. ARC–Adelaide Rift Complex (After Grey et al. 2003 (<https://pubs.geoscienceworld.org/geology/article-abstract/31/5/459/198279/neoproterozoic-biotic-diversification-snowball?redirectedFrom=fulltext>)) (Geology, with permission)

85–90 km-diameter, (Williams 1986; Williams and Gostin 2005, 2010) (Sect. 2.8) and a possible outer limit of the structural disturbance of 150 km (Williams and Wallace 2003). Wallace et al. (1996) documented the stratigraphy and sedimentology of the up to 40 cm-thick ejecta unit which contains felsic volcanic fragments ejected from the mid-Proterozoic Yardea Dacite (Gawler Volcanics) as well as altered melt particles. The original area covered by the ejecta is estimated as over 10⁶km². The ejecta is marked by two different facies: (1) a graded lone-stone/breccia-arenite-mudstone sequence (Fig. 2.16) and (2) a poorly sorted facies with weak normal grading and cross lamination. The ejecta contain anomalous Iridium levels as well as Au, Pt, Pd, Ru and Cr and initial ¹⁸⁷Os/¹⁸⁸Os of 0.10 of chondritic character, consistent with a meteoritic source. Keays et al. (2004).

Bio-stratigraphic and Chemo-stratigraphic research discloses contemporaneous relations between a relationship a palyno-floral change, a negative excursion in carbon isotope composition of kerogen, and ejecta from the c.580 Ma Acraman impact event (Grey et al. 2003). Palynomorphs changed from an assemblage dominated by long-ranging simple spheroids to a more diverse assemblage characterized by short-ranging, large, complex, process-bearing acanthomorph acritarchs, with a first appearance of 57 species (Fig. 2.17). A marked negative carbon isotope excursion was followed by a steady rise coinciding with acanthomorph radiation. This global extinction and recovery event may have been associated with the Acraman impact.

References

- Addison WD, Brumpton GR, Vallini DA, McNaughton NJ, Davis DW, Kissin SA, Fralick PW, Hammond AL (2005) Discovery of distal ejecta from the 1850 Ma Sudbury impact event. *Geology* 33:193–196
- Arndt NT, Nelson DR, Compston W, Trendall AF, Thorne AM (1991) The age of the Fortescue group, Hamersley basin Western Australia from ion microprobe zircon U-Pb results. *Aust J Earth Sci* 38:261–281
- Brauhart CW, Groves DI, Morant P (1998) Regional alteration systems associated with volcanogenic massive sulfide mineralization at Panorama, Pilbara, Western Australia. *Econ Geol* 93:292–302
- Buick R, Brauhart CW, Morant P (2002) Geochronology and stratigraphic relationships of the Sulphur Springs Group and Strelley Granite: a temporally distinct igneous province in the Archaean Pilbara Craton, Australia. *Precambrian Res* 114:87–120
- Byerly GR, Lowe DR (1994) Spinel from Archaean impact spherules. *Geochim Cosmochim Acta* 58:3469–3486
- Byerly GR, Kröner A, Lowe DR, Todt W, Walsh MM (1996) Prolonged magmatism and time constraints for sediments deposition in the early Archaean Barberton greenstone belt: evidence from the upper overwacht and fig tree groups. *Precambrian Res* 78:125–138
- Byerly GR, Lowe DR, Wooden JL, Xie X (2002) An archaean impact layer from the Pilbara and Kaapvaal Cratons. *Science* 297:1325–1327
- Chadwick B, Claeys P, Simonson BM (2000) New evidence for a large Palaeoproterozoic impact Spherules in a dolomite layer in the Ketilidian orogen South Greenland. *J Geol Soc Lond* 158:331–340
- Chou CL (1978) Fractionation of siderophile elements in the Earth's upper mantle. In: *Proc Lunar Planet Sci Conf 9th*. pp 219–230
- Garde AA, McDonald I, Dyck B, Keulen N (2012) Searching for giant ancient impact structures on Earth: the Meso-Archaean Maniitsoq structure, West Greenland. *Earth Planet Sci Lett* 2012:337–338
- Glass BP, Burns CA (1988) Microkrystites: a new term for impact-produced glassy spherules containing primary crystallites. *Proc Lunar Planet Sci Conf XVIII*:455–458
- Glikson AY (2004) Early Precambrian asteroid impact-triggered tsunamis: excavated seabed debris flows exotic boulders and turbulence features associated with 3.47–2.47 Ga-old asteroid impact fallout units, Pilbara Craton, Western Australia. *Astrobiology* 4:1–32
- Glikson AY (2006) Asteroid impact ejecta units overlain by iron rich sediments in 3.5–2.4 Ga 507 terrains Pilbara and Kaapvaal Cratons: accidental or cause–effect relationships? *Earth Planet Sci Lett* 246:149–160
- Glikson AY (2007) Siderophile element patterns, PGE nuggets and vapor condensation effects in Ni-rich quench chromite-bearing microkrystite spherules, 3.24 Ga S3 impact unit, Barberton greenstone belt, Kaapvaal Craton, South Africa. *Earth Planet Sci Lett* 253:1–16
- Glikson AY, Allen C (2004) Iridium anomalies and fractionated siderophile element patterns in impact ejecta, Brockman Iron Formation, Hamersley Basin, Western Australia: evidence for a major asteroid impact in simatic crustal regions of the early Proterozoic earth. *Earth Planet Sci Lett* 20:247–264
- Glikson AY, Vickers J (2006) The 3.26–3.24 Ga Barberton asteroid impact cluster: tests of tectonic and magmatic consequences, Pilbara Craton, Western Australia. *Earth Planet Sci Lett* 241:11–20
- Glikson AY, Vickers J (2010) Asteroid impact connections of crustal evolution. *Aust J Earth Sci* 57:79–95
- Glikson AY, Allen C, Vickers J (2004) Multiple 3.47-Ga-old asteroid impact fallout units, Pilbara Craton, Western Australia. *Earth Planet Sci Lett* 221:383–396
- Glikson AY, Hickman AH, Evans NJ, Kirkland CI, Jung-WP RR, Romano S (2016) A new 3.46 Ga asteroid impact ejecta unit at Marble Bar, Pilbara Craton, Western Australia: a petrological, microprobe and laser ablation ICPMS study. *Precamb Res* 279:103–122

- Goderis S, Tagle R, Smit J, Montanari A, Vanhaecke F, Erzinger J, Claeys PH (2013) Reevaluation of siderophile element abundances and ratios across the Cretaceous–Paleogene (K–Pg) boundary: Implications for the nature of the projectile. *Geochim Cosmochim Acta* 120:417–446
- Grey K, Walter MR, Calver CR (2003) Neoproterozoic biotic diversification: snowball Earth or aftermath of the Acraman impact? *Geology* (5):459–462
- Hassler SW (1993) Depositional history of the Main Tuff Interval of the Wittenoom Formation, late Archaean–early Proterozoic Hamersley Group, Western Australia. *Precambrian Res* 60:337–359
- Hassler SW, Simonson BM (2001) The sedimentary record of extraterrestrial impacts in deep shelf environments evidence from the early Precambrian. *J Geol* 109:1–19
- Hassler SW, Robey HF, Simonson BM (2000) Bedforms produced by impact-generated tsunami, 2.6 Ga Hamersley basin, Western Australia. *Sediment Geol* 135:283–294
- Hassler SW, Simonson BM, Sumner DY, Bodin L (2011) Paraburdoo spherule layer, Hamersley Basin, Western Australia: distal ejecta from a fourth large impact near the Archaean–Proterozoic boundary. *Geology* 39:307–310
- Hickman AH (1983) Geology of the Pilbara Block and its environs, West Australia geological survey Bulletin 127. *Geol Surv W Aust, Perth*, 268 pp
- Hickman AH (2012) Review of the Pilbara Craton and Fortescue Basin, Western Australia: crustal evolution providing environments for early life. *Island Arc* 21:1–31
- Hill AC, Grey K, Gostin VA, Webster LJ (2004) New records of late neoproterozoic Acraman ejecta in the officer basin. *Aust J Earth Sci* 51:47–51
- Hurst J, Krapez B, Hawke P (2013) Stratigraphy of the Marra Mamba iron formation within the Chichester Range and its implications for iron ore genesis at Roy Hill – evidence from deep diamond drill holes within the East Fortescue Valley. *Iron Ore, Australian Institute of Mining Metal paper* 95
- Keays R, Schaefer B, Wallace M, Lambert D (2004) The Acraman impact event horizon: relative contributions of meteoritic, diagenetic and host rock Cu and PGE from Re–Os Isotopes, 17th Australian Geological Convention, Hobart, Tasmania 8–13th Feb 2004
- Kröner A, Byerly GR, Lowe DR (1991a) Chronology of early Archaean granite–greenstone evolution in the Barberton Mountain Land, South Africa, based on precise dating by single grain zircon evaporation. *Earth Planet Sci Lett* 103:41–54
- Kröner A, Wendt JI, Tegtmeier AR, Milisenda C, Compston W (1991b) Geochronology of the Ancient Gneiss Complex, Swaziland, and implications for crustal evolution. In: Ashwal LD (ed) *Two cratons and an orogen – excursion guidebook and review articles for a field workshop through selected Archaean terrains of Swaziland, South Africa, and Zimbabwe, IGCP project 280*. Department of Geology, University of the Witwatersrand, Johannesburg, pp 8–31
- Kyte FT (2002) Tracers of extraterrestrial components in sediments and inferences for Earth's accretion history. *Geol Soc Am Spec Pap* 356:21–38
- Kyte FT, Zhou L, Lowe DR (1992) Noble metal abundances in an early Archaean impact deposit. *Geochim Cosmochim Acta* 56:1365–1372
- Kyte FT, Shukolyukov A, Lugmair GW, Lowe DR, Byerly GR (2003) Early Archaean spherule beds: chromium isotopes confirm origin through multiple impacts of projectiles of carbonaceous chondrite type. *Geology* 31:283–286
- LaBerge GL (1966) Altered pyroclastic rocks in iron formation in the Hamersley Range, Western Australia. *Econ Geol* 61:147–161
- Lowe DR, Byerly GR (1986) Early Archaean silicate spherules of probable impact origin, South Africa and Western Australia. *Geology* 14:83–86
- Lowe DR, Byerly GR (2010) Did the LHB end not with a bang but with a whimper? 41st lunar planet science conference 2563pdf
- Lowe DR, Byerly GR, Asaro F, Kyte FJ (1989) Geological and geochemical record of 3400 million year old terrestrial meteorite impacts. *Science* 245:959–962
- Lowe DR, Byerly GR, Kyte FT, Shukolyukov A, Asaro F, Krull A (2003) Characteristics, origin, and implications of Archaean impact-produced spherule beds, 3.47–3.22 Ga, in the Barberton

- Greenstone Belt, South Africa: keys to the role of large impacts on the evolution of the early Earth. *Astrobiology* 3:7–48
- McDonough WE, Sun S (1995) The composition of the Earth. *Chem Geol* 120:223–253
- Melosh HJ, Vickery AM (1991) Melt droplet formation in energetic impact events. *Nature* 350:494–497
- Nelson DR (1999) Compilation of SHRIMP U-Pb Zircon Geochronology Data, 1998. Western Australia Geological Survey Record 1999/2
- O’Keefe JD, Aherns TJ (1982) Interaction of the Cretaceous/Tertiary extinction bolide with the atmosphere. *Geol Soc Am Spec Pap* 190:103–120
- Pope KO, Baines KH, Ocampo AC, Ivanov BA (1997) Energy volatile production and climatic effects of the Chicxulub Cretaceous/Tertiary impact. *J Geophys Res* 102:21645–21664
- Rasmussen B, Koeberl C (2004) Iridium anomalies and shocked quartz in a Late Archean spherule layer from the Pilbara Craton: new evidence for a major asteroid impact at 2.63 Ga. *Geology* 32:1029–1032
- Rasmussen B, Blake TS, Fletcher IR (2005) U-Pb zircon age constraints on the Hamersley spherule beds: evidence for a single 2.63 Ga Jeerinah-Carawine impact ejecta layer. *Geology* 33:725–728
- Ringwood AE (1975) Composition and petrology of the Earth’s mantle. McGraw-Hill, New York
- Shukolyukov A, Kyte FT, Lugmair GW, Lowe DR, Byerly GR (2000) The oldest impact deposits on Earth. In: Koeberl C, Gilmour I (eds) *Lecture notes in Earth science 92: impacts and the early Earth*. Springer, Berlin, pp 99–116
- Simonson BM (1992) Geological evidence for an early Precambrian microtektite strewn field in the Hamersley Basin of Western Australia. *Geol Soc Am Bull* 104:829–839
- Simonson BM, Glass BP (2004) Spherule layers – records of ancient impacts. *Annu Rev Earth Planet Sci* 32:329–361
- Simonson BM, Hassler SW (1997) Revised correlations in the early Precambrian Hamersley Basin based on a horizon of re-sedimented impact spherules. *Aust J Earth Sci* 44:37–48
- Simonson BM, Davies D, Wallace M, Reeves S, Hassler SW (1998) Iridium anomaly but no shocked quartz from Late Archaean microkrystite layer: oceanic impact ejecta? *Geology* 26:195–198
- Simonson BM, Davies D, Hassler SW (2000a) Discovery of a layer of probable impact melt spherules in the late Archaean Jeerinah Formation, Fortescue Group, Western Australia. *Aust J Earth Sci* 47:315–325
- Simonson BM, Hornstein M, Hassler SW (2000b) Particles in late Archaean Carawine Dolomite, Western Australia, resemble Muong Nong-type tektites. In: Gilmour I, Koeberl C (eds) *Impacts and the early earth*. Springer, Berlin, pp 181–214
- Simonson BM, Cardiff M, Schubel KA (2001) New evidence that a spherule layer in the late Archaean Jeerinah Formation of Western Australia was produced by a major impact. In: 32nd lunar planetary science conference abstracts, lunar and planetary institute contribution 1080, Houston
- Simonson BM, McDonald I, Shukolyukov A, Koeberl C, Reimold WU, Lugmair GW (2009a) Geochemistry of 2.63–2.49 Ga impact spherule layers and implications for stratigraphic correlations and impact processes. *Precambrian Res* 175:51–76
- Simonson BM, Sumner DY, Beukes NJ, Johnson S, Gutzmer J (2009b) Correlating multiple Neoproterozoic–Paleoproterozoic impact spherule layers between South Africa and Western Australia. *Precambrian Res* 169:100–111. Elsevier with permission. <http://www.sciencedirect.com/science/article/pii/S0301926808002635>
- Simonson BM, Hassler SW, Beukes NJ, Sumner DY (2010) Large impacts around the Archaean-Proterozoic boundary—an update. 41st Lunar Planet Sci Conf, 2386.pdf
- Thorne AM, Trendall AM (2001) Geology of the Fortescue Group, Pilbara Craton, Western Australia. *Geol Surv Bull* 144:249p
- Trendall AF, Blockley JG (1970) The iron formations of the Precambrian Hamersley group, Western Australia. *Geol Surv West Aust Bull* 119:365 pp

- Trendall AF, Nelson DR, deLaeter JR, Hassler SW (1998) Precise zircon U-Pb ages from the Marra Mamba iron formation and wittenoom formation, Hamersley group, Western Australia. *Aust J Earth Sci* 45:137–142
- Trendall AF, Compston W, Nelson DR, De Laeter JR, Bennett VC (2004) SHRIMP zircon ages constraining the depositional chronology of the Hamersley group, Western Australia. *Aust J Earth Sci* 51:621–644
- Van Kranendonk MJ (2000) Geology of the North Shaw 1:100,000 sheet, Western Australia Geological Survey 1:100,000 series explanatory notes. Geological Survey of Western Australia, Perth, 89 pp
- Van Kranendonk MJ, Morant P (1998) Revised Archaean stratigraphy of the North Shaw 1:100 000 sheet, Pilbara Craton. *Geol Surv West Aust Ann Rev 1997–1998*:55–62
- Van Kranendonk MJ, Hickman AH, Smithies RH, Nelson D (2002) Geology and tectonic evolution of the Archaean North Pilbara Terrain, Pilbara Craton, Western Australia. *Econ Geol* 97:695–732
- Vearncombe S, Vearncombe JR, Barley ME (1998) Fault and stratigraphic controls on volcanogenic massive sulphide deposits in the Strelley Belt, Pilbara Craton, Western Australia. *Precambrian Res* 88:67–82
- Wallace MW, Gostin VA, Keays RR (1990) Spherules and shard-like clasts from the late Proterozoic Acraman impact ejecta horizon, South Australia. *Meteoritics* 25:161–165
- Wallace MW, Gostin VA, Keays RR (1996) Sedimentology of the Neoproterozoic Acraman impact-ejecta horizon, South Australia. *AGSO J Aust Geol Geophys* 16:443–451
- Williams GE (1986) The Acraman impact structure; source of ejecta in late Precambrian shales, South Australia. *Science* 233:200–203
- Williams GE, Gostin VA (2005) The Acraman – Bunyeroo impact event (Ediacaran), South Australia, and environmental consequences: 25 years on. *Aust J Earth Sci* 52:607–620
- Williams GE, Gostin VA (2010) Geomorphology of the Acraman impact structure, Gawler Ranges, South Australia. *Cad Lab Xeol Laxe* 35:209–220
- Williams GE, Schmidt PW (2015) Low paleolatitude for the late Cryogenian interglacial succession, South Australia: paleomagnetism of the Angepena Formation, Adelaide Geosyncline. *Aust J Earth Sci* 62:243–253
- Williams GE, Wallace MW (2003) The Acraman asteroid impact, South Australia: magnitude and implications for the late Vendian environment. *J Geol Soc Lond* 160:545–554
- Woodhead JD, Hergt JM, Simonson BM (1998) Isotopic dating of an Archaean bolide impact horizon, Hamersley Basin, Western Australia. *Geology* 26:47–50

Chapter 3

The World's Largest Late to Post-Archaean Asteroid Impact Structures



Abstract As distinct from small to medium-size impact events, large asteroid impacts producing explosions more powerful than 10^7 TNT-equivalent, represented by craters and rebound domes larger than about 100 km in diameter have major consequences including the triggering of major seismic events, tsunami events and extinction episodes. Such events are manifested by the Archaean ~ 3.25 – 3.24 Ga impact cluster and associated transformation from greenstone-granite terrains to semi-continental assemblages (Glikson AY, Vickers J, *Earth Planet Sci Lett* 241:11–20, 2006). These impact events are considered in Chap. 6. The oldest identified mega-impact is the ~ 3 Ga Maniitsoq structure in southwest Greenland, while younger mega-impact structures >100 km in diameter include the Vredefort and Sudbury structures. Phanerozoic mega-impacts include the Woodleigh impact structure, Warburton twin structures, Chicxulub and Popigai structures. The global tectonic consequences of some of these mega-impacts are yet to be elucidated.

3.1 Maniitsoq, South Greenland ($D \sim > 100$ km, ~ 2975 Ma)

The Maniitsoq impact structure, south Greenland (Garde and Glikson 2011; Garde et al. 2012), represents the deep seated root zone of the oldest known impact structure. The >100 km-diameter deformed zone is cored by a central 35×50 km-large crushed recrystallized gneisses and quartzo-feldspathic material (Fig. 3.1a). Regional-scale hydrothermal alteration occurred under amphibolite-facies conditions. The deformed zone is cut by widespread fractures, intense fracture cleavage, breccia and micro breccia (Fig. 3.1b). The shock metamorphic origin is confirmed by planar deformation features (PDF) in quartz (Garde and Glikson 2011), displaying Miller indices {0001}, {10–14}, {10–13}, {10–12}, {10–11}, {10–22}, {11–21} and {31–41}, with narrow planar spacing of ~ 2 – 5 microns (Fig. 3.1c, d). Re-deformed quartz grains display undulose extinction and curved or kinked PDFs which may preserve near-original crystallographic orientations. Other features of the shock metamorphosed rocks include fluidization of micro-breccia and evidence of direct K-feldspar and plagioclase melting. The Maniitsoq

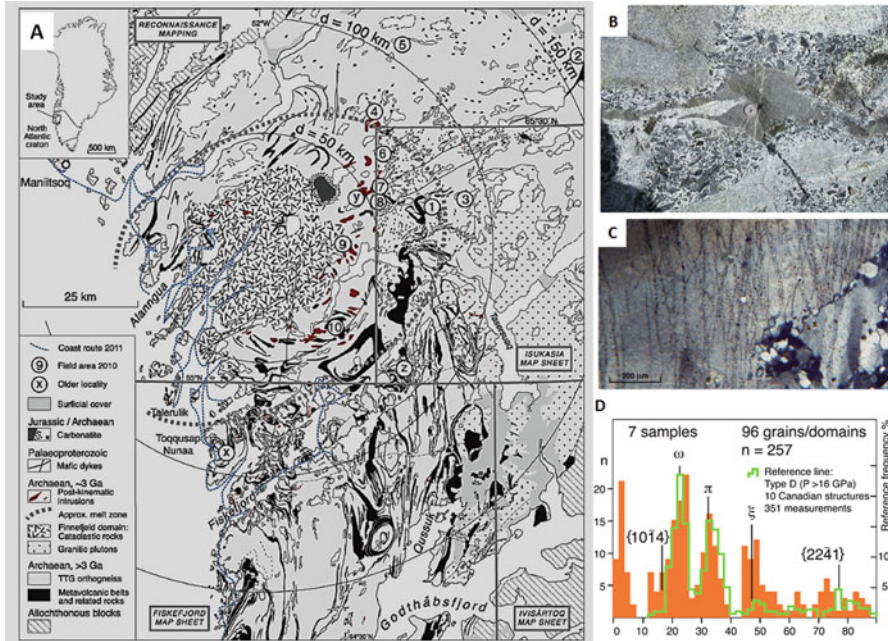


Fig. 3.1 The Maniitsoq structure is interpreted as a giant, 2975 Ma old impact structure. The present, deeply eroded craton is exposed at ~20–25 km below the surface, in amphibolite- to granulite-orthogneiss with intercalated metamorphic belts; (a) Simplified geological map of the Maniitsoq region, with index map showing position in Greenland, and reference circles of $d = 50$, 100 and 150 km; (b) agmatite consisting of amphibolite fragments in felsic matrix; (c) deformed planar deformation features; (d) Orientations of planar elements at Maniitsoq, showing pole angles from c-axis (Garde et al. 2012) (Elsevier, with permission) (<http://www.sciencedirect.com/science/article/pii/S0012821X12001938>)

structure is injected by ultramafic intrusions, yielding a U–Pb zircon age of 2975 ± 6 Ma and showing evidence of crustal contamination. The gneisses are considered to have been exhumed from a depth of 20–25 km. To date no fallout ejecta corresponding to the Maniitsoq impact has been identified.

3.2 Vredefort, South Africa (D~298 km; 2023 ± 4 Ma)

An impact origin for the Vredefort structure was initially proposed by Hargraves (1961) and Dietz (1961), an interpretation questioned by Nicolaysen and Ferguson (1990). The structure includes a 80–90 km diameter central plug of Archaean gneisses enveloped by an annular ring of Proterozoic sediments with a total outer diameter of ~298 km (Fig. 3.2a) (Therriault et al. 1997; Grieve et al. 2008; McCarthy et al. 1990; Gibson and Reimold 2001; Reimold and Gibson 2005, 2006). The central dome is enveloped by concentric folds and widespread occurrences of breccia and

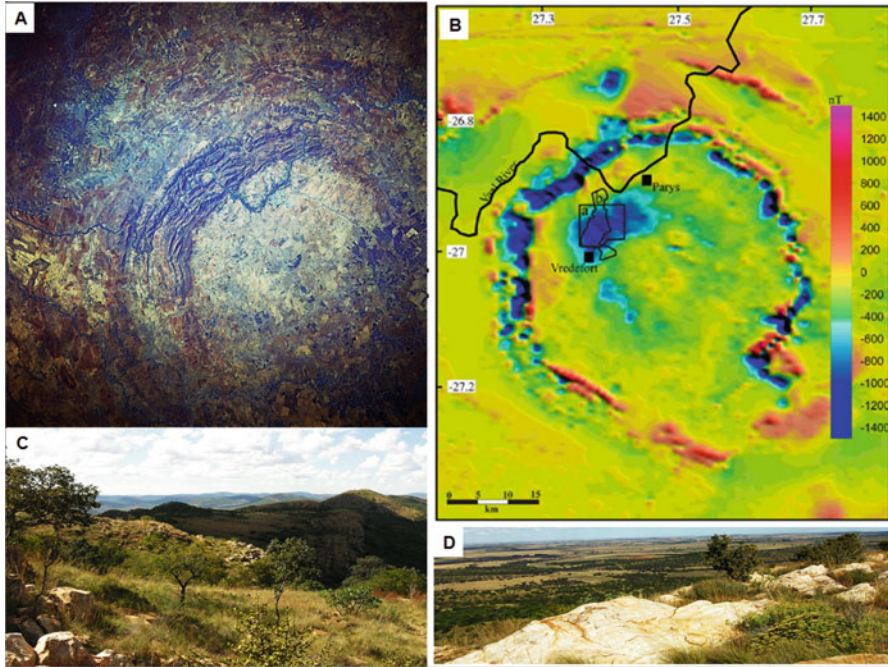


Fig. 3.2 The Vredefort impact structure, Orange Free State, South Africa. (a) Landsat image (https://en.wikipedia.org/wiki/Vredefort_crater#/media/File:Vredefort_Dome_STS51I-33-56AA.jpg); (b) Aeromagnetic anomaly map. Outer negative anomaly corresponds to the iron-rich shales of the Witwatersrand basin, and the inner negative anomaly is centered on the amphibolite – granulite transition in the basement (Muundjua 2007) (Elsevier, with permission). (c) View of the rim around the Vredefort dome (https://commons.wikimedia.org/wiki/File:Vredefort_Dome-113482.jpg); (d) View at the center of the Vredefort dome (https://commons.wikimedia.org/wiki/File:Vredefort_Dome-113487.jpg)

pseudotachylite veins which extend as far as the northern and northwest sector of the Witwatersrand Basin (McCarthy et al. 1986, 1990; Killick et al. 1988; Reimold and Gibson 2001). Uplift of the central core is estimated as 20–30 km accounting for the removal of the original transient crater (Therriault et al. 1997) and is well represented by annular magnetic anomalies corresponding to upfolded sedimentary units including Fe-rich shales (Fig. 3.2b). The collar of up-folded supracrustal rocks outside the central plug displays outward-directed thrusting whereas outermost sectors display inward-directed normal faulting as far as some 60 km north of the basement core. Seismic data identifies deformed circular sectors around the entire structure. Brink et al. (1997) and Lana et al. (2004) suggested that displacements within the central granitoid core occurred by mm to cm-scale differential rotations and slip and by movements along zones of pseudotachylite.

The basement is cut by nine several km-long radial dykes consisting of impact melt denoted as *Vredefort Granophyre* (Fig. 3.3b, c) and by radial fractures, mylonitic zones and breccia-bearing pseudotachylite vein systems concentrated

along the margin (Buchanan and Reimold 2002) (Fig. 3.3b). Kamo et al. (1996) determined a U–Pb zircon age of 2020 ± 5 Ma of the granophyre. Shock metamorphic features include shatter cones (Hargraves 1961) (Fig. 3.3a), planar deformation features in quartz (Leroux et al. 1994), shock deformation in zircon (Kamo et al. 1996), coesite and stishovite (Martini 1978) and extra-terrestrial geochemical signatures. Trace element studies of the pseudotachylite indicate significant enrichment in Iridium relative to Vredefort granitic rocks (French et al. 1988). Gibson and Reimold (2001) identified paleo-temperatures ranging from 700 to 1000 °C in the inner core to ~300 °C in the outer collar zone, reflecting pre-impact geothermal gradient, preceding the shock heating. Deformation due to compression in the NW–SE direction and deposition of the Karoo Supergroup over the southeast part of the structure post-date the impact.

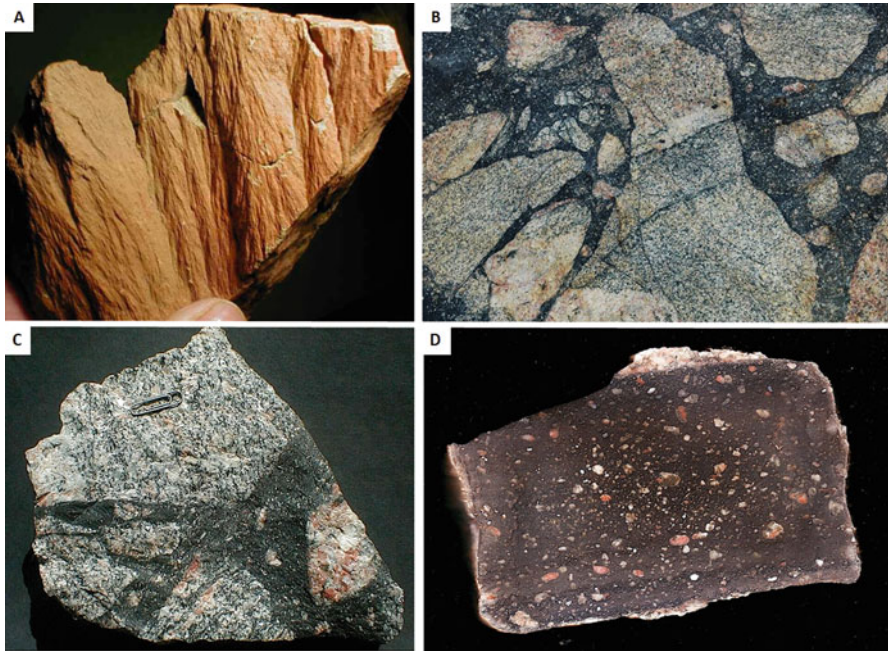


Fig. 3.3 Shock metamorphic features: (a) Shatter cones (<http://www.impact-structures.com/impact-rocks-impactites/the-shatter-cone-page/shatter-cones-from-impact-structures-worldwide/Vredefort>); (b) pseudotachylite breccia of Vredefort in South Africa. Light-colored granite in dark-colored pseudotachylite. Photo scale: about 1 meter across from left to right (https://commons.wikimedia.org/wiki/File:Pseudotachylite_Breccia_of_Vredefort_in_South_Africa.jpg); (c) Pseudotachylite (the black veins), maximum size <19 cm> (<http://www.impact-structures.com/wp-content/uploads/2011/12/50-vrede.jpg>); (d) Melt rock (granophyre) (<http://www.impact-structures.com/impact-rocks-impactites/Impact>); <12 cm> (<http://www.impact-structures.com/impact-rocks-impactites/the-shatter-cone-page/shatter-cones-from-impact-structures-worldwide/Vredefort>) (Ernstson & Claudin (<http://www.impact-structures.com/>), with permission)

3.3 Sudbury, Ontario (D~250 km; 1850 ± 3 Ma)

The Sudbury impact structure (Dietz 1964), dated as 1850 ± 1 Ma (Krogh et al. 1984), comprises a ~60 × 27-km-large, 2.5–3.0 km-thick differentiated layered igneous sheet which includes granodiorite, granophyre, quartz gabbro and norite, termed Sudbury Igneous Complex (SIC) (Fig. 3.4a), set within fractured and brecciated Archaean basement terrain and eroded to a depth of about 5–6 km (Dietz 1968; Naldrett et al. 1970; French 1968; Giblin 1984; Pye et al. 1984; Grieve et al. 1991; Thompson et al. 1998; Tuchscherer and Spray 2002; Therriault et al. 2002; Grieve 2006; Lightfoot 2016). An overall diameter of ~260 km is suggested by geophysical data, including a N–S LITHOPROBE geophysical transect (Tuchscherer and Spray 2002; Spray et al. 2004), indicating thrust faults and ductile shears related to post-impact deformation. Despite of NW–SE shortening by the Penokean orogeny (Rousell 1984; Riller 2005) the impacted basement, the SIC, the overlying melt breccia of the Onaping Formation, overlying Whitewater shale and radial dikes of impact melt of an overall noritic composition, are well preserved.

Shock metamorphic evidence is provided by shatter cones in the surrounding quartzite (Guy-Bray 1966) (Fig. 3.4b), planar deformation features in quartz and

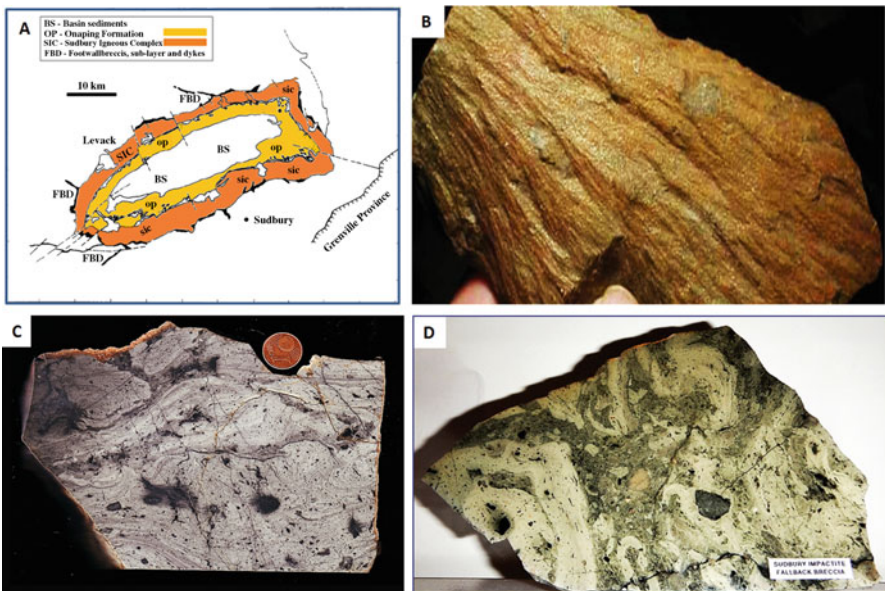


Fig. 3.4 (a) A geological sketch map of the Sudbury impact structure (<http://www.springer.com/gp/book/9789400763272>); (b) Shatter cones in quartzite (<http://www.impact-structures.com/impact-rocks-impactites/the-shatter-cone-page/shatter-cones-from-impact-structures-worldwide>); (c) Impact melt rock. Coin diameter 16 mm (<http://www.impact-structures.com/wp-content/uploads/2011/12/18-sud.jpg>); (d) Melt breccia/Suevite (Ernstson & Claudin, with permission (https://upload.wikimedia.org/wikipedia/commons/3/3a/Melted_Chaos_from_Sudbury_Impact_Crater.jpg)))

feldspar in the basement, and impact melt in the overlying Onaping Formation (French 1968; Dence 1972) (Fig. 3.4c, d). Breccia occurrences are concentrated about 5–15 km from the SIC but are also found as far as 80 km from the SIC (Spray 1997). Spray et al. (2004) delineated four breccia rings at 90, 130, 180 and 260 km north of the SIC corresponding to LANDSAT lineament analysis by Butler (1994). A hydrous composition of parent melt of the SIC is suggested by the dominance of amphibole and biotite, granophyre and deuteric alteration. Segregations of sulfide precipitated from the melt and from hydrothermal fluids represent advanced magmatic differentiation of the SIC. The SIC is distinguished from layered intrusions elsewhere by its intermediate composition, hydrous nature, crustal/granitic isotopic values, presence of normative corundum, prevalence of granophyre, presence of plagioclase xenocrysts showing complex twinning and planar deformation features and presence of PDF in quartz xenocrysts (Therriault et al. 2002).

The SIC is overlain in part by 1.4–1.6 km-thick breccia and melt breccia of the Onaping Formation, containing shock metamorphosed and hydrothermally altered lithic clasts and glass fragments and flows, analogous to suevite breccia of the Ries Crater (Chao 1967). Allochthonous ejecta containing shock-induced PDF in quartz and altered devitrified glass and/or accretionary lapilli and dated as 1875–1830 Ma, corresponding to the Sudbury impact in Ontario (Addison et al. 2005), Minnesota and northern Michigan, 500–700 km east of Sudbury (Cannon et al. 2010).

3.4 Chicxulub, Yucatan Peninsula, Mexico (D~170 km; 64.98 ± 0.05 Ma)

The Chicxulub impact structure, buried under 2 km-thick Tertiary sediments in the Yucatan Peninsula, Mexico, and identified by Glen Penfield (Hildebrand et al. 1991) thanks to its ~170 km-diameter multiring Bouguer anomaly that intersects an older north–south gravity ridge (Sharpton et al. 1993; Pilkington et al. 1994; Hildebrand et al. 1995). (Fig. 3.5a) has turned out to be the source of the K-T boundary mass extinction event which has decimated some 75% of terrestrial and marine fauna. Ar–Ar ages on melt fractions and on tektite suggest a 64.98 ± 0.05 Ma (Swisher et al. 1992). The Bouguer anomaly coincides with multi-ring magnetic anomalies, including an inner high-amplitude (>500 nT) anomaly of ~40 km-diameter which coincides with a gravity high and a high seismic velocity of 6.0–6.3 km/s, reflecting a ~3 km deep crystalline basement uplift (Pilkington and Hildebrand 2000). An outer ~90 km-diameter magnetic zone overlaps an inward dipping seismic reflector forming a boundary between an inner breccia zone and an outer intact zone (Morgan et al. 2000). The outer Bouguer ring coincides with a 160 km-diameter ring of Cenote sinkholes (Pope et al. 1993). Outer limits of the structure are indicated by a marine seismic reflection survey, defining a peak ring which rises approximately 600 meters above the apparent crater floor and is surrounded by circular faults at diameters of ~195 and ~240 km (Morgan et al. 1997).

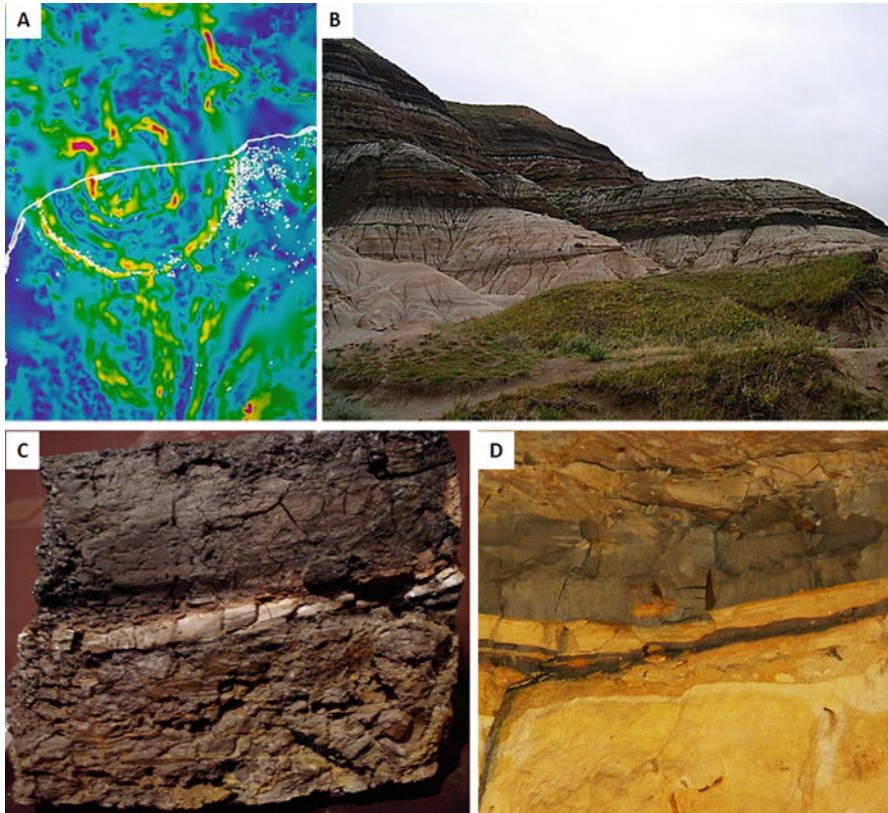


Fig. 3.5 The Chicxulub impact structure and K-T boundary deposits. (a) Gravity anomaly map. The coastline is shown as a white line. A striking series of concentric features reveals the location of the crater. White dots represent water-filled sinkholes (solution-collapse features common in the limestone rocks of the region) called cenotes. Wikimedia Commons (https://en.wikipedia.org/wiki/Chicxulub_crater#/media/File:Chicxulub-Anomaly.jpg); (b) Badlands near Drumheller, Alberta, Canada, where glacial and post-glacial erosion have exposed the K–T boundary. Wikimedia Commons (https://en.wikipedia.org/wiki/Cretaceous%E2%80%93Paleogene_boundary#/media/File:KT_boundary_054.jpg); (c) The K-T boundary layer in Wyoming, USA. The intermediate claystone layer contains 1000 times more iridium than the upper and lower layers (<https://commons.wikimedia.org/wiki/File:K-T-boundary.JPG>); (d) Complex Cretaceous-Paleogene clay layer (gray) in the Geulhemmergroeve tunnels near Geulhem, the Netherlands. Wikimedia Commons (https://en.wikipedia.org/wiki/Cretaceous%E2%80%93Paleogene_boundary#/media/File:Cretaceous_Paleogene_clay_at_Geulhemmergroeve.jpg)

The peak ring is surrounded by thick breccia deposits (Hildebrand et al. 1998; Morgan et al. 2000) and is underlain by a steeply dipping low velocity seismic zone interpreted as injected breccia overlying fractured crystalline basement (Vermeesch and Morgan 2004). Around the peak ring is a 490 meters-thick zone of melt breccia above brecciated dolomite. The Impact breccia displays shock metamorphic features and impact melting (Sharpton et al. 1996; Stöffler et al. 2004).

The Cretaceous-Paleocene boundary is exposed in several continents (Figs 3.5b, c, d). In the Umbrian Apennines, Italy, it forms a para-conformity that represents a hiatus across which foraminifera-rich a white limestone facies containing large-scale *Globotruncana contusa* is abruptly replaced by overlying clay-rich red limestone termed Scaglia rossa containing smaller foraminifera (*Globigerina eugubina*) and micron-scale algal coccoliths (Alvarez et al. 1980). At the Gubbio locality a ~1 cm-thick boundary clay layer includes a lower ~5 mm-thick grey clay zone dominated by clastic material and an upper ~5 mm-thick red clay zone denoted the 'fire layer' marked by an iridium anomaly of up to ~9 ppb, coinciding with a geomagnetic reversal. KT boundary impact ejecta, best preserved in deep water environments, has been identified along the Maastrichtian–Danian boundary in more than 101 sites and Iridium anomaly in over 85 sites around the globe (Claeys et al. 2002).

In and around the Gulf of Mexico the K-T boundary ejecta coincides with erosion of Maastrichtian sediments and onset of clastic sediments and breccia attributable to seismic and tsunami effects. Several studies indicate the severe environmental effects of the impact, including seismic mega-earthquakes, faulting, cratering, crustal rebound, fragmentation, fusion, vaporization of rocks, an ejecta blanket, atmospheric and stratospheric dusting, vapor clouding, atmospheric chemical reactions, acid rain, destruction of ozone, release of CO₂ from target materials and ensuing greenhouse effects and biological mass extinction. Aerosol clouding reducing sunlight and thereby arresting photosynthesis would affect the base of the terrestrial and marine food chain, followed by extreme warming induced by released greenhouse gases. According to Beerling et al. (2002) Late Cretaceous background CO₂ levels of 350–500 ppm increased to at least 2300 ppm within 10,000 years of the KT impact, due to instantaneous transfer of approximately ~4600 billion ton carbon (GtC) with consequent rise in greenhouse radiative forcing of + 12 W/m², raising surface temperatures by ~7.5 °C, accounting for the mass extinction of ~44% of genera (Keller 2005).

3.5 Popigai (D~100 km; 35.7 ± 0.2 Ma)

Preceding the end-Eocene (~34 Ma) an impact cluster of at least three large asteroids and a strewn tektite field resulted in the Popigai, Siberia (D ~ 100 km; 35.7 ± 0.2 Ma) (Masaitis 1998) (Figs. 3.6a, 3.6b), Chesapeake Bay, off-shore Virginia (D ~ 85 km; 35.3 ± 0.1 Ma) and Mount Ashmore (Timor Sea, end-Eocene, D > 50 km) (Fig. 4.22) (Glikson et al. 2010) impact structures and in approximately ~10% extinction and associated radiation of species. Popigai is located about 100 km from the Laptev Sea, a branch of the Arctic Sea. Ejecta from these impacts including tektites, microtektites, microkrystites, shocked minerals including impact diamonds dispersed over large areas and representing high-pressure transition from graphite contained in the target basement gneisses. The ejecta deposits were produced by excavation flows, ballistic ejections, ground surges, pyroclastic flows, base surges and impact melt spheroids and condensates

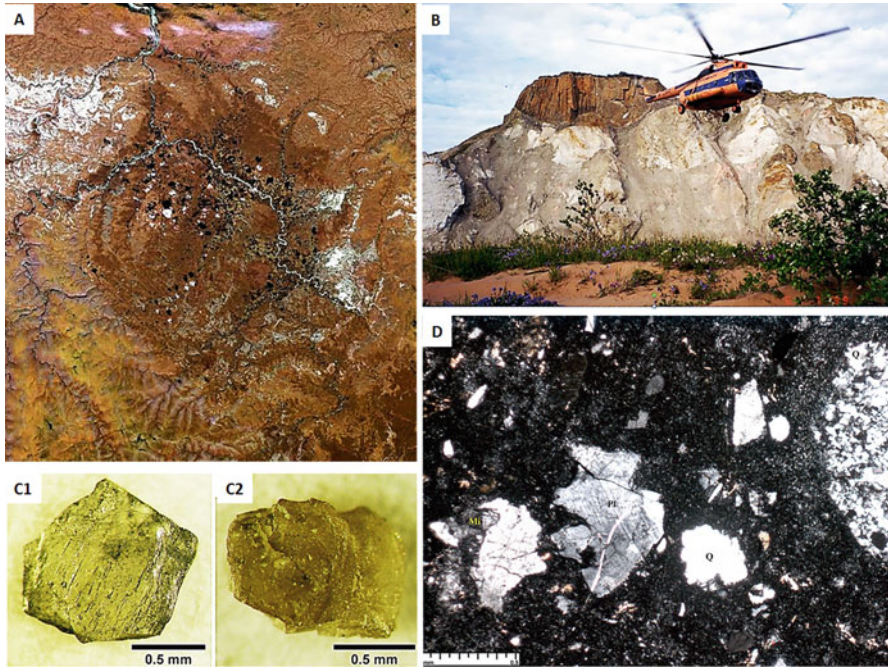


Fig. 3.6a The Popigai impact structure, Siberia. **A.** A satellite image https://en.wikipedia.org/wiki/Popigai_crater#/media/File:Popigai_crater_russia.jpg; **B.** Mega-breccia outcrops and overlying tagamite (Suevite/melt breccia) of the Popigai crater (geology.mines.edu/faculty/Klee/Popigai.pdf, by permission); **C1&C2.** Popigai microdiamonds; **D.** Tagamite/crystal-vitroclastic suevite. Angular clasts are mainly composed of chilled impact glass; matrix consists of partly altered small particles of the same glass and crystal fragments (Courtesy victor Masaitis 2017)

(Masaitis 1998). Distal effects of the impacts due to earthquakes, blast waves, thermal radiation, ballistic ejecta, storms, and by giant tsunami are found at distances of about 2000–3000 km, accounting for global climate changes and extinctions.

The Popigai impact is attributed to a chondrite projectile of ~5–8 km diameter depositing about 1.7×10^{23} Joule of energy (Masaitis 1998) The crater floor has a low topographic high in the center surrounded by an outer synform. Geophysical signatures include magnetic and gravity lows and a central gravity high. The basement gneisses display shatter cones, planar deformation features, lechatelierite, diaplectic glasses, coesite and stishovite. Shock pressures transformed graphite to diamond within 13.6 km of ground zero. The crater is filled with 2–2.5 km thick impact deposits dominated by suevite and Tagamite (melt rock) (Fig. 3.6aD). The consequences of the impact included (1) formation of a transient cavity ~8–10 km deep through 1.5-km-thick cover into Archean graphite-garnet gneisses; (2) peak pressure of ~624 GPa; (3) melting of ~1750 km³ of rock; (4) vaporization of the projectile and target rocks as a vapor-melt cloud; (5) shock metamorphism forming shatter cones, PDFs, coesite, stishovite and diaplectic glasses and transforming graphite to diamond within 13.6 km of ground zero (Fig. 3.6aC); (6) bedrock was shattered into blocks forming mega-breccia; (7) gneisses



[POPIGAI IMPACT STRUCTURE OVERVIEW About 36 million years ...
geology.mines.edu/faculty/Klee/Popigai.pdf](http://geology.mines.edu/faculty/Klee/Popigai.pdf)

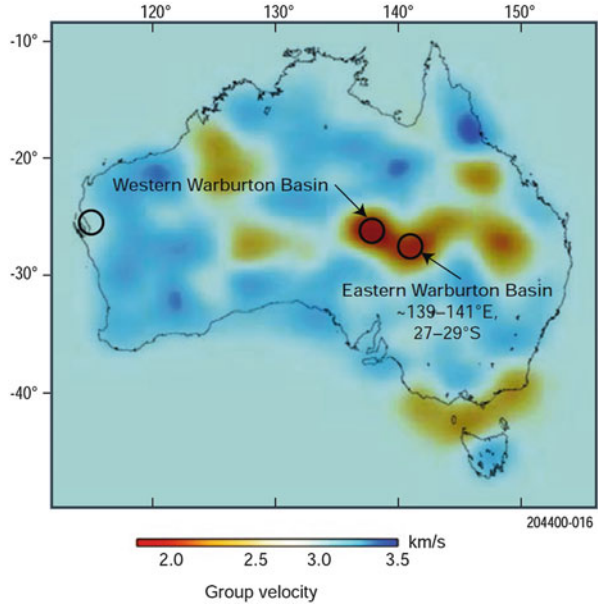
Fig. 3.6b (Enlargement of Fig. 3.6a, b)

fused into melt sheets covering large parts of the cavity floor over the mega-breccia (Fig. 3.6b) and (8) clouds of fragmental ejecta, vapor, and melt were ejected from the crater were ejected as far as 70 km.

3.6 Warburton Twin Structures, South Australia (Each D~200 km; End-Carboniferous?)

Several lines of evidence combine to suggest the existence of two very large asteroid impact structures in north-eastern South Australia and the southern Northern Territory, based on drill core evidence for shock metamorphism in the early Palaeozoic Warburton Basin and on magnetic and seismic tomographic anomalies (Fig. 3.7a). The eastern Warburton Basin underlies the Carboniferous–Permian Cooper Basin and the western Warburton Basin underlies the Carboniferous– Permian Pedirka Basin and Triassic Simpson Basin (Meixner et al. 1999, 2000; Radke 2009; Glikson et al. 2013, 2015). Two remarkable seismic tomography anomalies, the strongest on the continent, overlapping magnetic anomalies, and in one instance a Bouguer gravity anomaly, are outlined. The occurrence of planar deformation features (PDFs) in quartz indicative of shock metamorphism in both areas requires consideration of possible post-Late Carboniferous impact by large asteroids.

Fig. 3.7a Warburton twin impacts, South Australia. Seismic velocity tomography anomalies of the upper crust of the Australian continent (After Saygin and Kennett 2010) (Elsevier with permission)



The Eastern Warburton Basin, northeast South Australia, features major geophysical anomalies, including a magnetic high of near-200 nT centered on a ~25 km-wide magnetic low (~100 nT), interpreted in terms of a magmatic body below 6 km depth. A distinct seismic tomographic low velocity anomaly may reflect its thick (9.5 km) sedimentary section, high temperatures and possible deep fracturing. Scanning electron microscope (SEM) analyses of granites resolves microbreccia veins consisting of micron-scale particles injected into resorbed quartz grains. Planar and sub-planar elements in quartz grains (Qz/PE) occur in granites, volcanics and sediments of the >30,000 km²-large Eastern Warburton Basin as well as the western Warburton Basin. The Qz/PE include multiple intersecting planar to curved sub-planar elements with relic lamellae less than 2 μm wide with spacing of 4–5 μm. Qz/PE are commonly re-deformed, displaying bent and wavy patterns accompanied with fluid inclusions (Fig. 3.7bA, C). U-stage measurements of a total of 243 planar sets in 157 quartz grains indicate dominance of $\Pi\{10-12\}$, $\omega\{10-13\}$ and subsidiary $\{\{11-22\}, \{22-41\}, m\{10-11\}$ and $x\{51-61\}$ planes. Transmission Electron Microscopy (TEM) analysis displays relic narrow ≤ 1 μm-wide lamellae and relic non-sub grain boundaries where crystal segments maintain optical continuity. Extensive sericite alteration of feldspar suggests hydrothermal alteration to a depth of ~500 m below the unconformity which overlies the Qz/PE-bearing Warburton Basin terrain. The data are discussed in terms of (A) Tectonic–metamorphic deformation and (B) impact shock metamorphism producing planar deformation features (Qz/PDF). Deformed Qz/PE are compared to re-deformed Qz/PDFs in the Sudbury, Vredefort, Manicouagan and Charlevoix impact structures. A 4–5 km uplift of the Big Lake Granite Suite during ~298–295 Ma is consistent

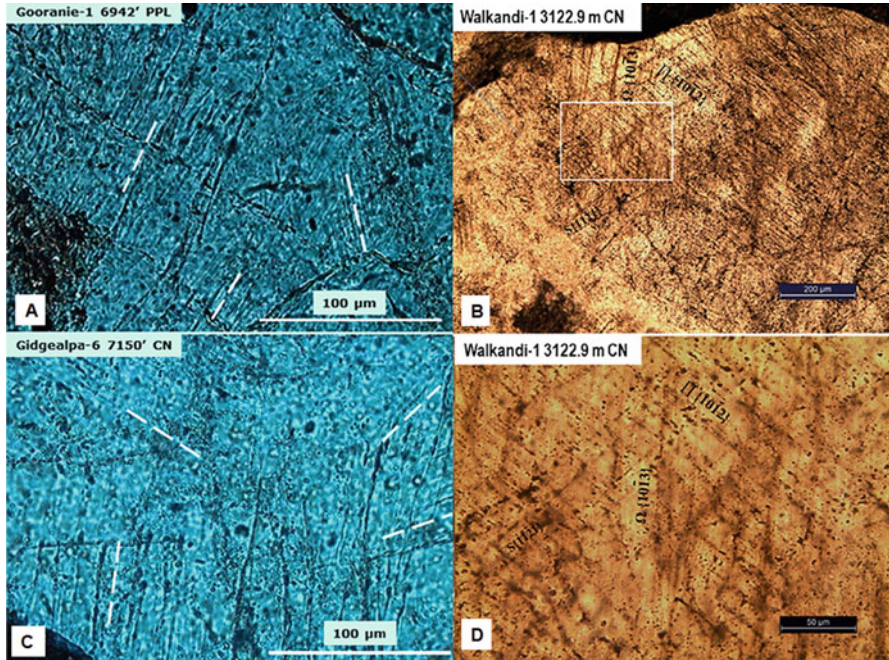


Fig. 3.7b Deformed planar deformation features, Warburton east and west impact structures. **A & C.** Warburton East structure: Gooranie and Gidgealpa drill holes; **B & D** Warburton West structure: Walkandie drill hole

with missing of upper Ordovician to Devonian strata and possible impact rebound. The occurrence of circular seismic tomography anomalies below the east Warburton Basin, the Poolowana Basin and the Woodleigh impact structure signifies a potential diagnostic nature of circular tomographic anomalies.

In the Warburton West Basin a large magnetic body of $SI = 0.030$ is modelled below ~10 km, with a large positive gravity anomaly offset to the north of the magnetic anomaly. In both the Warburton East and Warburton West the deep crustal fracturing suggested by the low velocity seismic tomography complicates interpretations of the gravity data. Universal Stage measurements of quartz lamellae suggest presence of both planar deformation features of shock metamorphic derivation and deformed planar lamella (Fig. 3.7bB, D). The latter may be attributed either to re-deformation of impact-generated lamella, impact rebound deformation or/and post impact tectonic deformation. The magnetic anomalies in the Warburton East and West sub-basins are interpreted in terms of (1) presence of deep seated central mafic bodies; (2) deep crustal fracturing and (3) removal of Devonian and Carboniferous strata associated with rebound of a central uplift consequent on large asteroid impact. Further tests of the Warburton structures require deep crustal seismic transects.

Outstanding problems regarding the Warburton twin structures include: (1) the impacted rocks of the Warburton Basin are located some 2–3 km below the surface, rendering the documentation of their structure complicated; (2) To date no ejecta from the Warburton impact has been disclosed, nor has such been searched for in any detail; (3) no major mass extinction is known from the Carboniferous-Permian boundary. To a large extent the latter problem may reflect the uncertainties in determining the age of the Warburton impacts (t).

3.7 Woodleigh (D = 120 km)

The identification of the Woodleigh impact structure as a multi-ring structure of likely impact origin (Iasky et al. 1998, 2001; Mory et al. 2000a, b), initially hinging on geophysical data, namely the truncation of the regional Ajana –Wandagee gravity ridges by the outer Bouguer anomaly ring of the Woodleigh structure (Fig. 3.8a), and subsequently confirmed by drilling demonstrates a 120 km-diameter impact structure (Glikson et al. 2005). The evidence includes an arcuate magnetic anomaly along the eastern part of the structure and seismic-reflection data indicating a central 37 km-diameter dome (Fig. 3.8a), corroborated by a seismic tomographic low (Fig. 3.8b). Drill core evidence resolves planar deformation features in quartz (Fig. 3.8c, d) and feldspar, shock-induced melting and diaplectic transformations, partly masked by alteration of the shocked gneisses to montmorillonite-dominated clay assemblage, accounting for the high MgO and low K₂O of cryptocrystalline components. A possible contamination of sub-crater levels of the Woodleigh impact structure by meteoritic components, suggested by high Ni, Co, Cr, Ni/Co and Ni/Cr ratios, requires further siderophile element analyses of vein materials. Pervasive hydrothermal activity dated by K – Ar isotopes of illite–smectite suggests an age of 359 ± 4 Ma (Uysal et al. 2001, 2002), consistent with stratigraphic age constraints of post-Middle Devonian to pre-Early Jurassic.

Hydrothermally altered shock-metamorphosed gneisses consist of relic igneous biotite – K-feldspar/Na-rich alkali feldspar/plagioclase/quartz assemblages (+/– accessory garnet, corundum, titanite, monazite, zircon), showing extensive replacement by montmorillonite, illite, sericite, and to a lesser extent chlorite, calcite, epidote, zoisite and pyrite. Spatial Universal stage analysis of quartz-hosted planar deformation features (PDFs) indicates a majority of indexed sets parallel to planar {1013} (Fig. 3.8d), a less common occurrence of planar {1012}, and some sets parallel to the basal plane (0001) and {1011} consistent with pressures about or over 20 GPa. Feldspar-hosted PDFs form reticulate vein networks displaying checkerboard-like to irregular and serrated patterns attributable to preferential replacement of shock-damaged PDFs and/or perthitic twin lamella by clay minerals. The gneisses are pervaded by clay-dominated intergranular and intra-granular veins of cryptocrystalline material that display marked departures from bulk-rock

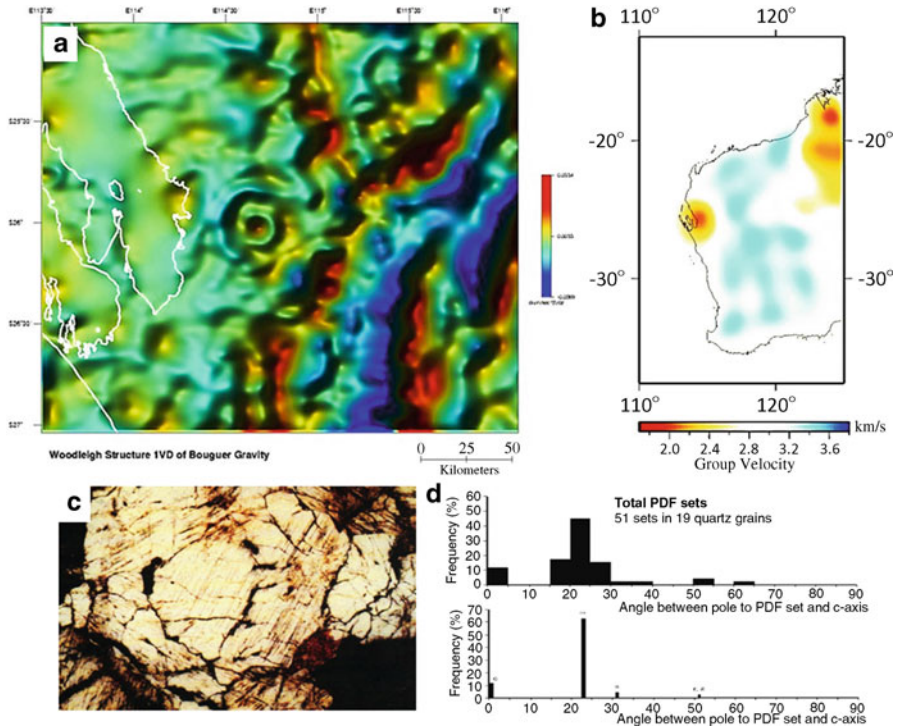


Fig. 3.8 Woodleigh impact structure, Gascoyne Platform, southern Carnarvon Basin, Western Australia. (a) First Vertical Derivative Bouguer anomaly, displaying the central peak ring, inner ring and intersection of the outer ring at 120 km diameter (after Iasky et al. 2001, GSWA with permission). (b) Seismic velocity tomography anomaly overlapping with the Woodleigh impact structure (after Saygin and Kennett 2010; Elsevier, with permission); (c) Planar deformation features (PDF) in quartz in a Woodleigh drill core; (d) Distribution of pdfs in quartz in Woodleigh core. Note the concentration about 23° from the C axis (After Glikson et al. 2005; AJES, with permission)

chemistry and from mineral compositions. XRD analysis identifies the cryptocrystalline components as illite – montmorillonite, illite and chlorite, while laser Raman analysis identifies high-fluorescence sub-micrometer clay assemblage, feldspar, quartz and minor mica. SEM/EDS-probe and laser-ICPMS analysis indicate low-K high-Mg clay mineral compositions consistent with montmorillonite. Quartz PDF-hosted cryptocrystalline laminae display distinct enrichments in Al, Mg, Ca and K. Altered intergranular veins and feldspar-hosted cryptocrystalline components show consistent enrichment in the relatively refractory elements (Al, Ca, Mg, Fe) and depletion in relatively volatile elements (Si, K, Na). The clay alteration retards determination whether clay-dominated vein networks represent altered shock-induced pseudotachylite veins or result from purely mineralogical and chemical differentiation affected by hydrothermal fluids. Overall enrichment of the shocked gneiss and of the cryptocrystalline components in Mg and trace ferromagnesian

elements (Ni, Co, Cr) may be attributed alternatively to introduction of siderophile element-rich fluid from the projectile, or/and contamination of hydrothermal fluids by MgO from dolomites surrounding the basement uplift. High Ni/Co and Ni/Cr and anomalous PGE (platinum group elements) may support the former model (Glikson et al. 2005).

References

- Addison WD, Brumpton GR, Vallini DA, McNaughton NJ, Davis DW, Kissin SA, Fralick PW, Hammond AL (2005) Discovery of distal ejecta from the 1850 Ma Sudbury impact event. *Geology* 33:193–196
- Alvarez L, Alvarez W, Asaro F, Michel HV (1980) Extraterrestrial cause for the Cretaceous-Tertiary extinction. *Science* 208:1095–1108
- Beerling DJ, Lomax BH, Royer DL, Upchurch GR, Kump LR (2002) An atmospheric pCO₂ reconstruction across the Cretaceous-Tertiary boundary from leaf mega fossils. *Proc Natl Acad Sci USA* 99:7836–7840
- Brink MC, Wanders FB, Bisschoff AA (1997) Vredefort: a model for the anatomy of an astrobleme. *Tectonophysics* 270:83–114
- Buchanan PC, Reimold WU (2002) Impact-related features in lithic clasts from the Vredefort Granophyre, South Africa. *Meteoritics* 36, 9, Supplement pg. 31
- Butler HR (1994) Lineament analysis of the Sudbury multiring impact structure. *Geol Soc Am Sp Pap* 293:319–329
- Cannon WF, Schulz KJ, Wright J, Horton D, Kring A (2010) The Sudbury impact layer in the Paleoproterozoic iron ranges of northern Michigan, USA. *Geol Soc Am Bull* 122:50–75
- Chao ECT (1967) Shock effects in certain rock-forming minerals. *Science* 156:192–202
- Claeys P, Kiessling W, Alvarez W (2002) Distribution of Chicxulub ejecta at the Cretaceous-Tertiary boundary. In: Koeberl C, MacLeod KG (eds) *Catastrophic events and mass extinctions: impacts and beyond*. Special Papers 356. Geological Society of America, Boulder, pp 55–68
- Dence MR (1972) Meteorite impact craters and the structure of the Sudbury basin. *Geol Assoc Canada Sp Pap* 10:7–18
- Dietz RS (1961) Vredefort ring structure: meteorite impact scar? *J Geol* 69:496–505
- Dietz RS (1964) Sudbury structure as an astrobleme. *J Geol* 72:412–434
- Dietz RS (1968) Shatter cones in cryptoexplosion structures. In: French BM, Short NM (eds) *Shock metamorphism of natural materials*. Mono Book Corp, Baltimore, pp 267–285
- French BM (1968) Sudbury structure Ontario: some petrographic evidence for an origin by meteorite impact. In: French BM, Short NM (eds) *Shock metamorphism of natural materials*. Mono Books, Baltimore, pp 383–412
- French BM, Orth CJ, Quintana LR (1988) Iridium in the Vredefort Bronzite Granophyre—impact melting and limits on a possible extraterrestrial component. *Lunar and Planetary Science Conference 19th Houston TX* 14–18, pp 733–744
- Garde AA, Glikson AY (2011) Recognition of re-deformed planar deformation features (PDF) in large impact structures. 74th Ann Meteor Soc Meet, 5246 pdf
- Garde AA, McDonald I, Dyck B, Keulen N (2012) Searching for giant ancient impact structures on Earth: the Meso-Archaeon Maniitsoq structure, West Greenland. *Earth Planet Sci Lett* 2012:337–338
- Giblin PE (1984) History of exploration and development of geological studies and development of geological concepts. In: Pye E, Naldrett AJ, Giblin PE (eds) *The geology and ore deposits of the Sudbury structure*. Ontario Geological Survey, Toronto, pp 3–24
- Gibson RL, Reimold WU (2001) The Vredefort impact structure South Africa: the scientific evidence and a two-day excursion guide. *Council Geosci Mem* 92:111 p

- Glikson AY, Vickers J (2006) The 3.26–3.24 Ga Barberton asteroid impact cluster: tests of tectonic and magmatic consequences, Pilbara Craton, Western Australia. *Earth Planet Sci Lett* 241:11–20
- Glikson AY, Eggins S, Golding S, Haines P, Iasky RP, Mernagh TP, Mory AJ, Pirajno F, Uysal IT (2005) Microchemistry and microstructures of hydrothermally altered shock-metamorphosed basement gneiss, Woodleigh impact structure, Southern Carnarvon Basin, Western Australia. *Aust J Earth Sci* 52:555–573
- Glikson AY, Jablonski D, Westlake S (2010) Origin of the Mount Ashmore structural dome west 661 Bonaparte basin Timor Sea. *Aust J Earth Sci* 57:411–430
- Glikson AY, Uysal IT, Fitz Gerald JD, Saygin E (2013) Geophysical anomalies and quartz microstructures, Eastern Warburton Basin, North-east South Australia: Tectonic or impact shock metamorphic origin? *Tectonophysics* 589:57–76
- Glikson AY, Meixner AJ, Radke B, Uysal IT, Saygin E, Vickers J, Mernagh TP (2015) Geophysical anomalies and quartz deformation of the Warburton West structure, central Australia. *Tectonophysics* 643:55–72
- Grieve RAF (2006) Impact structures in Canada. Geological Association of Canada, St. John's, p 210
- Grieve RAF, Stöffer D, Deutsch A (1991) The sudbury structure: controversial or misunderstood? *J Geophys Res* 96:22753–22764
- Grieve RAF, Reimold WU, Morgan J, Riller U, Pilkington M (2008) Observations and interpretations at Vredefort, Sudbury and Chicxulub: towards an empirical model of terrestrial impact basin formation. *Meteorit Planet Sci* 43:855–882
- Guy-Bray J (1966) Shatter cones at Sudbury. *J Geol* 74:243–245
- Hargraves RB (1961) Shatter cones in the rocks of the Vredefort ring. *Geol Soc S Afr Trans* 64:147–154
- Hildebrand AR, Penfield GT, Kring DA, Pilkington M, Camargo ZA, Jacobsen SB, Boynton WV (1991) A possible Cretaceous-Tertiary boundary impact crater on the Yucatan Peninsula, Mexico. *Geology* 19:867–871
- Hildebrand AR, Pilkington M, Connors M, Ortiz-Aleman C, Chavez RE (1995) Size and structure of the Chicxulub crater revealed by horizontal gravity gradients and cenotes. *Nature* 376:415–417
- Hildebrand AR, Pilkington M, Ortiz-Aleman C, Chavez RE, Urrutia-Fucugauchi J, Connors M, Graniel-Castro E, Camarago ZA, Halpenny JF, Niehaus D (1998) Mapping Chicxulub crater structure with gravity and seismic reflection data. In: *Meteorites flux with time and impact effects*, Special publication, vol 140. Geological Society, London, pp 153–173
- Iasky RP, Mory AJ, Shevchenko SI (1998) A structural interpretation of the Gascoyne platform Southern Carnarvon basin West Australia In: Purcell PG, Purcell RR (eds) *The sedimentary basins of West Australia*. Proc Petrol Explor Soc Aust Symp, Perth, pp 589–598
- Iasky RP, Mory AJ, Blundell KA (2001) The geophysical signature of the Woodleigh impact structure Southern Carnarvon basin, Western Australia. *Geol Surv West Aust Rep* 79, 41 p
- Kamo SL, Reimold WU, Krogh TE, Colliston WP (1996) A 2.023 Ga age for the Vredefort impact event and a first report of shock metamorphosed zircons in pseudotachylitic breccias and granophyre. *Earth Planet Sci Lett* 144:369–387
- Keller G (2005) Impacts volcanism and mass extinction: random coincidence or cause and effect? *Aust J Earth Sci* 52:725–757
- Killick AM, Thaites AM, Germs GJB, Schoch AE (1988) Pseudotachylite associated with a bedding-parallel fault zone between the Witwatersrand and Ventersdorp supergroup South Africa. *Geolo Rund* 77:329–344
- Krogh TE, Davis DW, Corfu F (1984) Precise U-Pb zircon and Baddeleyite ages for the Sudbury area. In: *The geology and ore deposits of the Sudbury structure*, Special volume 1. Ontario Geological Survey, Sudbury, pp 431–448

- Lana C, Reimold WU, Gibson R, Koeberl C, Siegesmund S (2004) Nature of the Archean midcrust in the core of the Vredefort Dome, Central Kaapvaal Craton, South Africa. *Geochim Cosmochim Acta* 68:623–642
- Leroux H, Reimold WU, Doukhan JC (1994) A TEM investigation of shock metamorphism in quartz from the Vredefort Dome South Africa. *Tectonophysics* 230:223–239
- Lightfoot P (2016) Nickel sulfide ores and impact melts – Origin of the Sudbury Igneous Complex. Elsevier, Amsterdam, 662pp
- Martini JEJ (1978) Coesite and stishovite in the Vredefort Dome South Africa. *Nature* 272:715–717
- Masaitis VL (1998) Popigai crater: origin and distribution of diamond-bearing impactites. *Meteorit Planet Sci* 33:349–359
- McCarthy TS, Charlesworth EG, Stanistreet IG (1986) Post-Transvaal structural features of the northern portion of the Witwatersrand basin. *Trans Geol Soc S Afr* 89:311–324
- McCarthy TS, Stanistreet IG, Robb LJ (1990) Geological studies related to the origin of the Witwatersrand basin and its mineralization—an introduction and a strategy for research and exploration. *S Afr J Geol* 93:1–4
- Meixner AJ, Boucher RK, Yeates AN, Gunn PJ, Richardson LM, Frears RA (1999) Interpretation of geophysical and geological data sets, Cooper Basin region. South Australia: Australian Geological Survey Organization, Record, 1999/22
- Meixner TJ, Gunn PJ, Boucher RK, Yeates AN, Murray L, Yeates TN, Richardson LM, Freares RA (2000) The nature of the basement to the Cooper Basin region. South Australia. *Explor Geophys* 31:024–032
- Morgan JV, Warner M, Chicxulub Working Group (1997) Size and morphology of the Chicxulub impact crater. *Nature* 390:472–476
- Morgan JV, Warner MR, Collins GS, Melosh HJ, Christeson GL (2000) Peak ring formation in large impact craters. *Earth Planet Sci Lett* 183:347–354
- Mory AJ, Iasky RP, Glikson AY, Pirajno F (2000a) Woodleigh Carnarvon basin, Western Australia: a new 120 km-diameter impact structure. *Earth Planet Sci Lett* 177:119–128
- Mory AJ, Iasky RP, Glikson AY, Pirajno F (2000b) Response to ‘Critical comment on AJ Mory et al. (2000) Woodleigh Carnarvon basin Western Australia: a new 120 km diameter impact structure. *Earth Planet Sci Lett* 184:359–365
- Muundjua M (2007) Magnetic imaging of the Vredefort impact crater, South Africa. *Earth Planet Sci Lett* 261:456–468
- Naldrett AJ, Bray JG, Gasparrini EL, Podolsky T, Rucklidge JC (1970) Cryptic variation and the petrology of the Sudbury nickel irruptive. *Econ Geol* 65:122–155
- Nicolaysen LO, Ferguson J (1990) Cryptoexplosion structures shock deformation and siderophile concentration related to explosive venting of fluids associated with alkaline ultramafic magmas. *Tectonophysics* 171:303–335
- Pilkington M, Hildebrand AR (2000) Three-dimensional magnetic imaging of the Chicxulub crater. *J Geophys Res* 105:23479–23491
- Pilkington M, Hildebrand AR, Ortiz-Aleman C (1994) Gravity and magnetic field modeling and structure of the Chicxulub crater, Mexico. *J Geophys Res* 99:13147–13162
- Pope KO, Ocampo AC, Duller CE (1993) Surficial geology of the Chicxulub impact crater Yucatán Mexico. *Earth Moon Planet* 63:93–104
- Pye EG, Naldrett AJ, Giblin PE (eds) (1984) The geology and ore deposits of the Sudbury structure, Special volume 1. Ontario Geological Survey, Toronto, 604 p
- Radke B (2009) Hydrocarbon and geothermal prospectivity of sedimentary basins in Central Australia Warburton, Cooper, Pedirka, Galilee, Simpson and Eromanga Basins. *Geoscience Australia Record* 2009/25
- Reimold WU, Gibson RL (2005) Meteorite impact! The danger from space and South Africa’s mega-impact – the Vredefort structure. Chris van Resnburg Publications Ltd, Johannesburg, 319pp

- Reimold WU, Gibson RL (2006) The melt rocks of the Vredefort impact structure–Vredefort granophyre and pseudotachylitic breccias: implications for impact cratering and the evolution of the Witwatersrand Basin. *Chemie der Erde Geochem* 66:1–35
- Riller U (2005) Structural characteristics of the Sudbury impact structure Canada: impact induced and orogenic deformation—a review. *Meteorit Planet Sci* 40:1723–1740
- Rousell DH (1984) Structural geology of the Sudbury basin. In: Pye E, Naldrett AJ, Giblin PE (eds) *The geology and ore deposits of the Sudbury structure, Special volume 1*. Ontario Geological Survey, Sudbury, pp 83–96
- Saygin E, Kennett BLN (2010) Ancient seismic tomography of the Australian continent. *Tectonophysics* 481:116–125
- Sharpton VL, Burke K, Camargo Z, Hall SA, Lee DS, Marin LE, Suárez R, Quezada M, Spudis PD, Urrutia-Fucugauchi J (1993) Chicxulub multi-ring impact basin: size and other characteristics derived from gravity analysis. *Science* 261:1564–1567
- Sharpton VL, Martin LE, Carney JL, Lees S, Ryder G, Schuraytz BC, Sikora P, Spudis PD (1996) A model of the Chicxulub impact basin based on the evaluation of geophysical data well logs and drill core samples. *Geol Soc of Am Sp Pap* 307:55–74
- Spray JG (1997) Superfaults. *Geology* 25:627–630
- Spray JG, Butler HR, Thompson LM (2004) Tectonic influences on the morphometry of the Sudbury impact structure: implications for terrestrial cratering and modeling. *Meteorit Planet Sci* 39:287–301
- Stöffler D, Artemieva A, Ivanov B, Hecht L, Kenkmann T, Schmitt RT, Tagle RA, Wittmann A (2004) Origin and emplacement of the impact formations at Chicxulub Mexico as revealed by the ICDP deep drilling at Yaxcopoil-1 and by numerical modeling. *Meteorit Planet Sci* 39:1035–1067
- Swisher CC, Grahales-Nishimura JM, Montanari A, Margolis SV, Claeys P, Alvarez W, Renne P, Cedillo-Pardo E, Florentin JM, Maurasse R, Curtis GH, Smit J, McWilliams MO (1992) Coeval $^{39}\text{Ar}/^{40}\text{Ar}$ ages of 66 million years ago from Chicxulub crater melt rock and Cretaceous-Tertiary boundary tektites. *Science* 257:954–958
- Therriault AM, Grieve RAF, Reimold WU (1997) The Vredefort Structure: original size and significance for geologic evolution of the Witwatersrand Basin. *Meteoritics* 32:71–77
- Therriault AM, Anthony D, Flower R, Grieve RAF (2002) The Sudbury igneous complex: a differentiated impact melt sheet. *Econ Geol* 97:1521–1540
- Thompson LM, Spray JG, Kelley SP (1998) Laser probe argon-40/argon-39 dating of pseudotachylite from the Sudbury structure: evidence for post-impact thermal overprinting in the North range. *Meteorit Planet Sci* 33:1259–1269
- Tuchscherer MG, Spray JG (2002) Geology mineralization and emplacement of the Foy offset dike, Sudbury. *Econ Geol* 97:1377–1398
- Uysal T, Golding SD, Glikson AY, Mory AJ, Glikson M (2001) K–Ar evidence from illitic clays of a Late Devonian age for the 120 km diameter Woodleigh impact structure, southern Carnarvon Basin, Western Australia. *Earth Planet Sci Lett* 192:281–289
- Uysal T, Golding SD, Glikson AY, Mory AJ, Glikson M, Iasky RP, Pirajno (2002) Reply to “Comment on: ‘K–Ar evidence from illitic clays of a Late Devonian age for the 120 km diameter’”. *Earth Planet Sci Lett* 201:253–260
- Vermeesch PM, Morgan JV (2004) Chicxulub central crater structure: Initial results from physical property measurements and combined velocity and gravity modeling. *Meteorit Planet Sci* 39:1019–1034

Chapter 4

Australian Impact Structures >10 Km-Large



Abstract The geological antiquity of Australian land surfaces and the sedimentary and volcanic cover of Precambrian cratons in the central and western parts of the continent, allow preservation of a range of circular features, including morphological and drainage rings, circular lakes, volcanic craters, tectonic domes, oval granite bodies, mafic igneous plugs, salt diapirs, and magnetic, gravity and seismic anomalies of unknown origin. These include 38 confirmed asteroid and meteorite impact structures and craters and more than 40 ring, dome and crater features of unknown origin. Many of these structures display structural and geophysical elements consistent with impacts. Exposed features include circular crater-like morphological patterns which may intersect pre-existing linear structural features, central morphological highs and unique thrust and fault patterns. Buried circular features include single or multi-ring magnetic patterns, circular magnetic quiet zones, corresponding gravity patterns and low velocity and non-reflective seismic zones. Discrimination between impact structures and igneous plugs, volcanic caldera and salt domes requires field work possibly drilling. Large circular structures such as Mount Ashmore and Gnargoo are considered to have convincing structural deformation features to warrant classification as likely impact structures. Examples of crater-form features containing elements consistent with, but unproven to be of, impact origin include Auvergne, Delamere, Fiery Creek, Monte Christo, Mount Moffatt, Tanami East, Youngerina, Tingha. Examples of buried multi-ring features of possible to probable impact origin include Augathella, Balfour Downs, Calvert Hills, Camooweal, Green Swamp Well, Herbert, Ikybon River, Ilkurka, Lennis, McLarty Hills, Mount Davies, Mulkara, Neale, Sheridan Creek, Oodjuongari and Renehan. The origin of the very large circular magnetic and gravity pattern of the Diamantina River drainage feature and the multiple TMI ring pattern of the Deniliquin-Booligal region remains unresolved. Compared with frequency distribution patterns of extra-terrestrial impact structures worldwide, the Australian record displays a relatively a common occurrence of large impact structures and relative depletion in small impact structures and craters, explained by the better preservation of large structures at deep crustal zones as compared to the erosion of small craters, and a good geophysical coverage of large parts of the continent.

4.1 Exposed Impact Structures >10 km in Diameter

The distribution of 38 confirmed impact structures and 42 ring structures of unknown, possible and probable impact origin is displayed in Fig. 4.1. Table 4.1 lists confirmed and probable impact structures located on the Australian continent and continental shelf, including geographic location, province, diameter, age or possible age, notes and references. The list and following summaries of individual structures are based on numerous references, in particular compilations by Shoemaker and Shoemaker (1996, 1997), Bevan (1996), Haines (2005), Boxer (2014) and Dunster et al. (2014). Below summary accounts are presented for impact structures larger than 10 km in diameter.

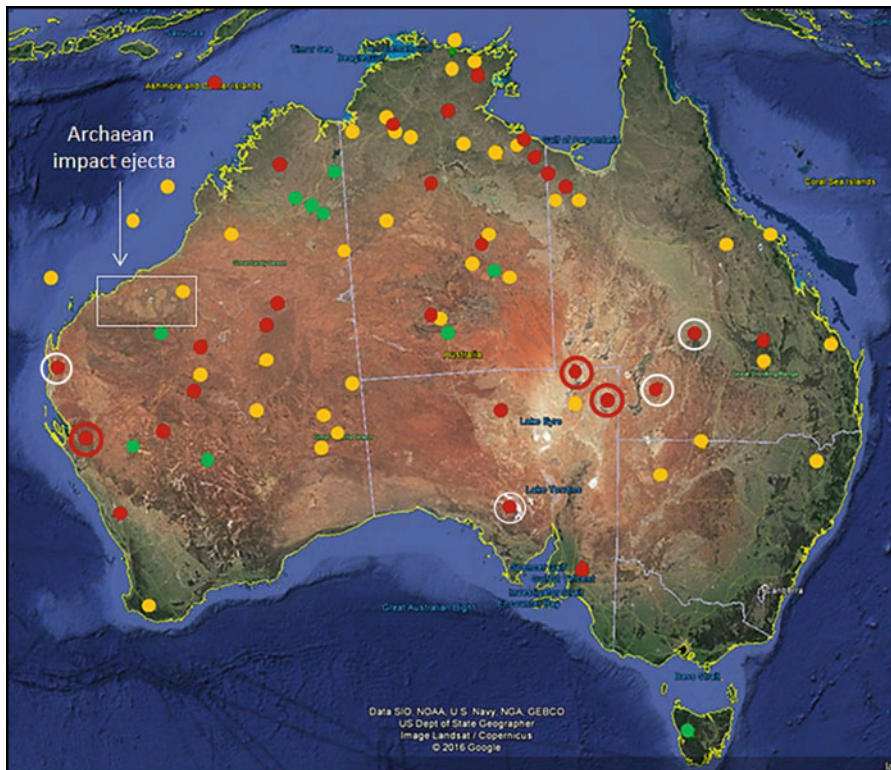


Fig. 4.1 Impact structures and ring structures of possible to probable impact origin on the Australian continent and offshore. Red circles – confirmed impact structures; green circles – impact craters; yellow circles – possible to probable ring structures; red circled red circles – impact structures >100 km in diameter; white circled red circles – impact structures >50 km (Elsevier, with permission)

Table 4.1 38 Confirmed and probable impact structures and craters on the Australian continent and continental shelf

Name	Long/Lat	province	Diameter km	Age	Notes	References
Acraman	135.44E32.019S	Gawler Craton, SA	40–90	580 Ma	Confirmed impact structure	Williams (1986), Williams and Wallace (2003)
Amelia Creek	134.83E20.92S	Davenport Ranges, NT	~20x12	1640–600	Confirmed impact structure	Macdonald et al. (2005)
Boxhole Crater	135.1952E 22.613S,	NT	~0.17	5.4 + 1.5	Confirmed impact crater	Madigan (1937)
Calvert Hills	137.466E; 17.344S	McArthur Basin, NT	≥4	Post-Mesoproterozoic	TMI ring, confirmed impact structure	Macdonald and Mitchell (2004) and Dunster et al. (2014)
Cleonskin	137.937E18.163S	NT-Qld border	15	post 1400 Ma pre-Cretaceous	Tmi, Radiometric, morphology; Confirmed impact structure	Haines et al. (2012)
Connolly Basin	124.758E23.537S	Gibson Desert, WA	~9	Paleocene	Confirmed impact structure	Shoemaker and Shoemaker (1986)
Dalgaranga	117.283E27.634S	WA	0.02	0.27 Ma	Confirmed impact crater	Nisinger and Huss (1960)
Darwin	145.665E 42.308S	Tasmania	1.2	0.816 ± 0.007	Confirmed impact crater	Fudali and Ford (1979)
Flaxman & Crawford	139.056E34.611S 139.033E34.724S	South Australia	3.5–8.5	Late Eocene to early Oligocene?	Presence of shock metamorphic features	Haines et al. (1999)
Foelsche	136.783E16.672S	McArthur Basin	~6	Neo-Proterozoic	Confirmed impact structure	Haines and Rawlings (2002)
Glikson	121.56E23.982S	Savory Basin, WA	14	<508	Confirmed impact structure	Shoemaker and Shoemaker (1997) and Macdonald et al. (2005)
Gnargoo	114.026E23.626S	Carnarvon Basin, WA	~75	<300	Structure near-identical to Woodleigh including a central uplift	Iasky and Glikson (2005)

(continued)

Table 4.1 (continued)

Name	Long/Lat	province	Diameter km	Age	Notes	References
Goat Paddock	126.675E 18.336S	West Kimberley, WA	~5	Early Eocene	Confirmed impact structure	Milton and Macdonald (2005)
Gosses Bluff	132.308E23.817S	Amadeus Basin, NT	14	142.4 ± 0.8 Ma	Confirmed impact structure	Milton et al. (1972)
Goyder	135.043'E 13.468'S	McArthur Basin, NT	9–12	1325–150 Ma	Confirmed impact structure	Haines (1996)
Henbury Craters	133.148E24.572S	Amadeus Basin, NT	0.06–0.18	4.2 ± 1.9 kyr	Confirmed impact craters	Milton (1972)
Hickman	119.683E23.037S	Hammersley Basin, WA	0.36	Quaternary	Confirmed impact crater	Glikson et al. (2008)
Kelly West	133.957E19.931S	NT	8–20	1640–550 Ma	Confirmed impact structure	Tonkin (1973)
Lake Raeside	120.964E28.792S	Yilgarn Craton, WA	~11	Tertiary	Confirmed buried impact crater	Glikson et al. (2016)
Lawn Hill	138.647E18.69S	NW Qld	18	Post-Cambrian	Confirmed impact structure	Stewart and Mitchell (1987)
Liverpool	134.0476E12.396S	Northern NT	1.6	NeoProterozoic	Confirmed impact structure	Guppy et al. (1971) and Shoemaker et al. (2005)
Matt Wilson	131.181E15.498S	Gregory National Part, NT	5.5	NeoProterozoic	Confirmed impact structure	Sweet et al. (2005)
Mount Ashmore	123.2075E12.5586S	Timor Sea	> 50	Eocene-Oligocene boundary	seismic dome, probable impact structure	Glikson et al. (2010)
Mount Toondina	135.359E27.944S		3–4	Cretaceous to Paleogene	Confirmed impact structure	Youles (1976)
Piccaninny	128.43E17.42S	Kimberley, WA	7	<360 Ma	Confirmed impact structure	Beere (1983)
Renehan	132.664E18.309S	South Lake Woods, NT	≥10	Post-Middle Cambrian	TMI ring; probable impact structure	Dunster et al. (2014)
Shoemaker	120.888E25.859S	Nabberu Basin, WA	29–31	<568 Ma	Confirmed impact structure	Pirajno et al. (2003)
Spider	126.091E16.742S	Kimberley, WA	11–13	900–600 Ma	Confirmed impact structure	Abels (2005)

Strangways	133.59E15.203S	McArthur Basin, NT	25–40	642 ± 46 Ma	Confirmed impact structure	Zummersprekel and Bischoff (2005)
Talundilly	144.482E24.862S	Eromanga Basin, Qld	84	125 ± 1	Confirmed impact structure	Gorter and Glikson (2012)
Tookoonooka	142.681E27.105S	Eromanga Basin, Qld	55	125 ± 1	Confirmed impact structure	Gostin and Theriault (1997).
Veevers	125.3727E22.9699S	Canning Basin, WA	70 m	~4 kyr	Confirmed impact crater	Yeates et al. (1976)
Warburton East	140.407E27.656S	Warburton Basin east	<200	~300	Probable impact structure	Glikson et al. (2013)
Warburton West	138.799E26.434S	Warburton Basin west	<200	~300	Probable impact structure	Glikson et al. (2015)
Wolfe Creek	127.795E19.171S	Kimberley, WA	0.88	30 kyr	Confirmed impact crater	Guppy and Matherson (1950)
Woodleigh	114.840E26.803S	Carnarvon Basin, WA	120	359.2 ± 2.5	Confirmed impact structure	Iasky et al. (2001)
Yallalie	115.76E30.446S	Perth Basin, WA	12	Cretaceous	Confirmed impact structure	Dentith et al. (1999)
Yarrabubba	118.83E27.183S	Murchison, Yilgarn Craton, WA	>30–70	Proterozoic	Confirmed impact structure	Macdonald et al. (2003)

4.1.1 Acraman ($D \sim 30\text{--}90\text{ km}$)

The Acraman impact structure in the Gawler Ranges of northern Eyre Peninsula, South Australia (Williams 1986; Williams and Gostin 2005) is expressed by a $\sim 30\text{ km}$ -diameter depression occupied by a $\sim 20\text{ km}$ diameter sub-circular salt lake, Lake Acraman (Fig. 4.2a, b). The structure has a distinctive aeromagnetic signature with circular magnetic low, subdued magnetic relief 20 km in diameter and a central high-amplitude dipole anomaly (Williams et al. 1996; Hawke 2003) (Fig. 4.2b). Target rocks of the c.1590 Ma Yardea Dacite, Gawler Range felsic volcanics display shatter cones (Fig. 4.2c), planar deformation features in quartz and melt textures (Fig. 4.2d). The impact has been correlated with 580 Ma distal ejecta deposits located in the Bunyeroo Formation of the Adelaide geosyncline and in the Officer Basin (Gostin et al. 1986; Wallace et al. 1990, 1996; Hill et al. 2004; Williams and Schmidt 2015). K-Ar and Ar-Ar dating of melt rock from Acraman yielded an age of $\sim 450\text{ Ma}$ interpreted as the age of recrystallisation of K-feldspars subsequent to the impact (Williams and Schmidt 2015). Apatite fission track and geomorphic evidence suggest erosion of $>2.5\text{ km}$ (Williams and Wallace 2003). Shoemaker and Shoemaker (1996) suggested an original crater of $35\text{--}40\text{ km}$ diameter, Hawke (2003)

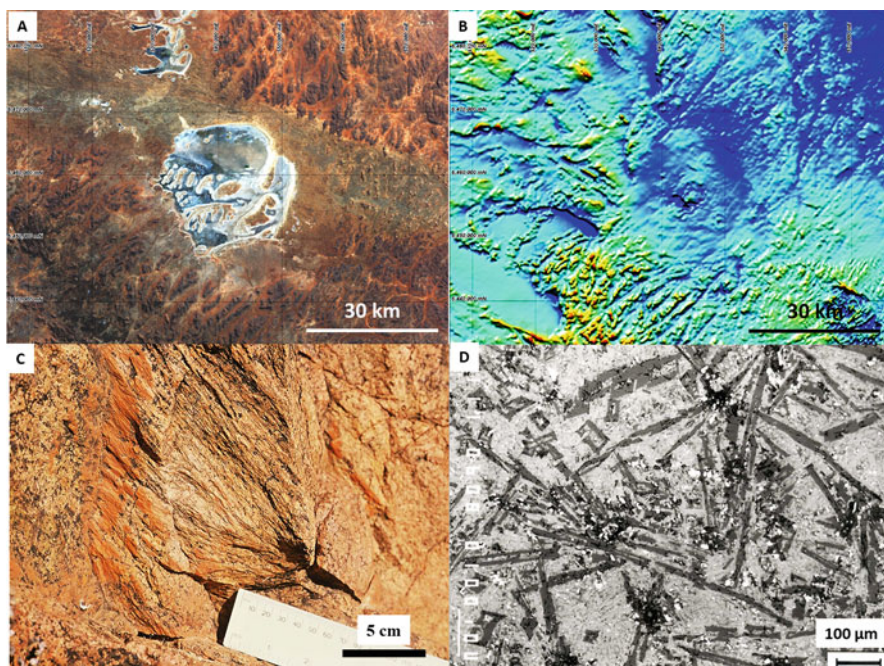


Fig. 4.2 Acraman impact structure, South Australia. (a) Landsat 8 image South (NASA); (b) Shaded Total Magnetic Intensity image (note circular de-magnetized zone (GA Creative Commons)); (c) Shatter cone in the Yardea Dacite (courtesy George Williams and Victor Gostin); (d) Quench textures in impact melt (Courtesy George Williams and Victor Gostin)

inferred a diameter of 55 km from aeromagnetic data, while Gostin and Zbik (1999) inferred a transient crater of 30–40 km. According to Williams and Wallace (2003) the original crater comprised a transient cavity or excavated area up to c.40 km in diameter, a central uplift and a possible final structural rim of 85–90 km diameter, while Williams et al. (1996) extended the rim to ~150 km from geomorphic evidence. K–Ar and Ar–Ar dating yielded age estimates of c.580 Ma (Williams and Wallace 2003; Hill et al. 2004), determined from the stratigraphic position of the distal eject layer (Sect. 2.8) (Haines 2005) and coinciding with major extinction and radiation event of Acritarch microfossils (Grey et al. 2003).

4.1.2 *Yarrabubba (D~30–70 km)*

Given the antiquity of up to 4404 \pm 8 Ma (for detrital zircons) and large dimension of the Yilgarn Craton (65,000 km²) in Western Australia, the craton can be expected to contain a significant number of impact structures and crater, yet to date only few have been identified. These include small craters (D~0.17 km; 30 \pm 5 kyr), medium-size buried craters (Lake Raeside, D~11 km, Tertiary to Quaternary (Glikson et al. 2016) and larger structures such as Yarrabubba (D~30–70 km; Proterozoic age). The paucity of impact structures in the Yilgarn Craton can be accounted for primarily due to the overprinting of Yilgarn granitoid-greenstone structures by strong north-northwest oriented shears and faults and in part due to very poor outcrop.

This is the case with the Yarrabubba impact structure (Macdonald et al. 2003) (Fig. 4.3a), displaying NNW-elongation parallel with regional trends and cropping out weakly with the exception of the Barlangi Hill granophyre at its core (Fig. 4.3b). Aeromagnetic images show an elliptical ~11 \times 15 km magnetically quiet region, interpreted as resulting from impact-induced demagnetisation, with an elliptical ring-like central high coinciding in part with outcrops of the Barlangi Granophyre. It is mainly thanks to Will Libby's (Geological Survey of Western Australia) keen eyes that planar deformation features (Fig. 4.3d) were discovered in the surrounding Yarrabubba granitoid. In addition the presence of shatter cones (Fig. 4.3c), rectangular cleavage, melt features in the granite (Fig. 4.4a), planar deformation features (Fig. 4.4b) quench features in the Barlangi granophyre (Fig. 4.4c, d) and pseudotachylite veins in the Yarrabubba Granite attest to shock metamorphism.

The Barlangi Granophyre, which intrudes the Yarrabubba Granite, is interpreted as an impact melt injected along faults and fractures into the shocked granite (Macdonald et al. 2003). These authors referred to an original crater diameter in the range 30–70 km. The age of Yarrabubba is uncertain, with the 2.65 Ga age of the Yarrabubba Granite providing a maximum constraint (Macdonald et al. 2003). Linear dykes postdating the impact event are visible on aeromagnetic images and only partly crop out in the terrain and are probably of Proterozoic age. Pirajno (2005) reported an Ar–Ar date of 1134 \pm 26 Ma from pseudotachylite veins in the granite, providing a possible minimum age estimate for the impact event.

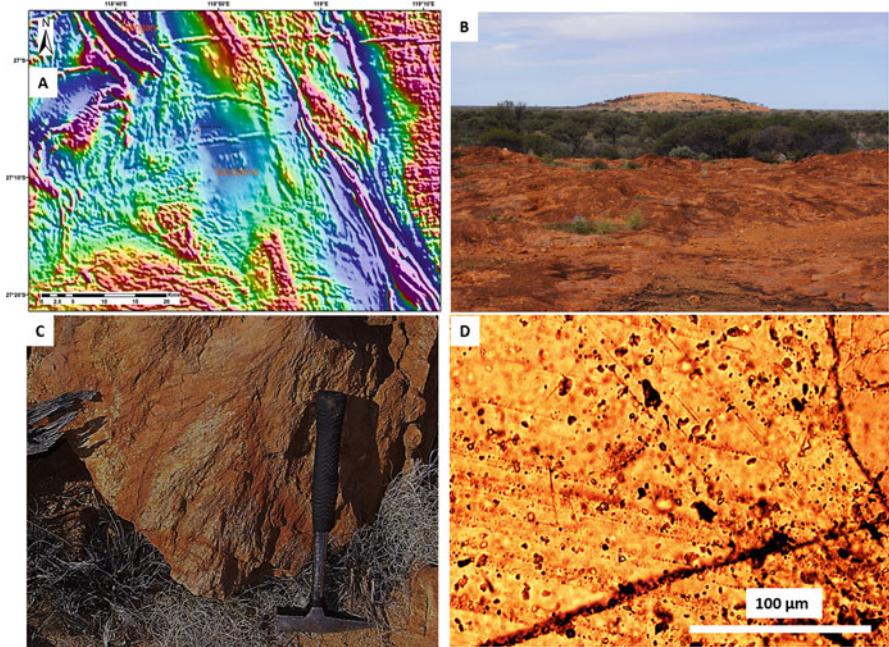


Fig. 4.3 Yarrabubba impact structure, Western Australia. (a) Total magnetic intensity image displaying the low TMI core of the structure, re-deformed by the NNW tectonic trend of the greenstone-granite system, and cut by East-West dykes (GA Creative Commons); (b) View of Barlangi Hill, consisting of granophyre at the core of the Yarrabubba impact structure; (c) Shatter cones in the Yarrabubba Granite north of Barlangi Hill; (d) Planar deformation features in quartz of Yarrabubba Granite

4.1.3 Shoemaker ($D \sim 29\text{--}31\text{ km}$)

The Shoemaker Impact Structure, earlier named Teague Lake structure and renamed in honour of Eugene M. Shoemaker (1928–1997) (Pirajno and Glikson 1998), forms a prominent circular feature on satellite images and maps. It constitutes a 30 km-diameter multi-ring morphological feature and a geophysical anomalies (Figs. 4.5 and 4.6a) intersecting a WNW-trending ridge of the Frere Iron Formation in the early Proterozoic Earahedy Basin. The structure is manifest by concentric ring synclines and anticlines of sedimentary rocks cored by 12 km-diameter granitoid uplift, attributed to an approximately 1.63 billion years-old impact (Butler 1974; Bunting et al. 1980; Pirajno and Glikson 1998; Pirajno et al. 2003; Hawke 2003. Bunting et al. 1980 reported shatter cones, PDFs in quartz and pseudotachylite veins in the central Teague Granite. During 1986 and 1995 Gene and Carolyn Shoemaker identified the feature as a deeply eroded complex impact structure (Shoemaker and Shoemaker 1996). The Teague Granite has an unusual alkali-rich syenitic

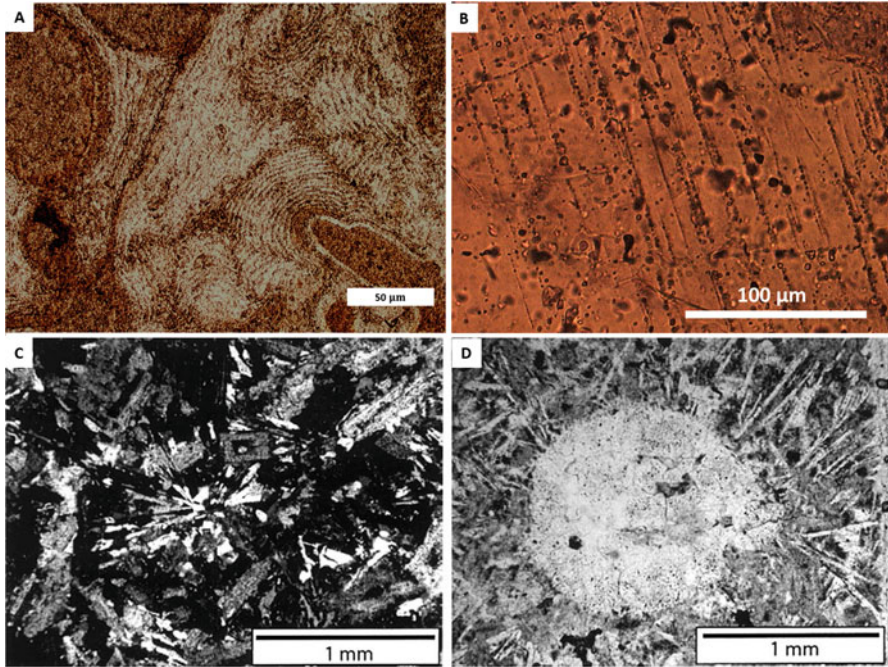


Fig. 4.4 Yarrabubba impact structure, Western Australia. (a) Flow textures in devitrified glass within melt breccia vein; (b) Planar deformation features in quartz in Yarrabubba Granite; (c) Radiating quartz textures in Barlangi Granophyre (Macdonald et al. 2003, Elsevier, with permission); (d) Spherulitic texture in the Barlangi Granophyre (Macdonald et al. 2003; C&D Elsevier, with permission)

composition, possibly representing alkali metasomatism related to impact-induced hydrothermal activity (Pirajno et al. 2003; Pirajno 2005). The circular magnetic and Bouguer anomaly patterns (Figs 4.6a) represent the magnetic response of different target lithologies, particularly the distribution of the Frere Iron Formation and possibly also hydrothermal activity (Hawke 2003; Pirajno et al. 2003). A central negative Bouguer anomaly coinciding with the central uplift (Plescia 1999) reveals a low density of the central Teague Granite.

Maximum ages for the impact are defined by 2648 ± 8 Ma age of the Teague Granite (Pirajno et al. 2003) and 2027 ± 23 Ma detrital zircons within the sedimentary Yelma Formation (Pirajno et al. 2003). A minimum age may be provided by two whole-rock Rb – Sr isochron ages of c.1630 Ma and c.1260 Ma of altered granite of the central uplift Teague Granite (Bunting et al. 1980). K– Ar dating of illite and smectite in the Teague Granite yields inconsistent ages of 694 ± 25 and 568 ± 20 Ma (Pirajno et al. 2003). Pirajno et al. (2003) raised the possibility that the younger age may reflect Late Neoproterozoic impact-induced hydrothermal activity.

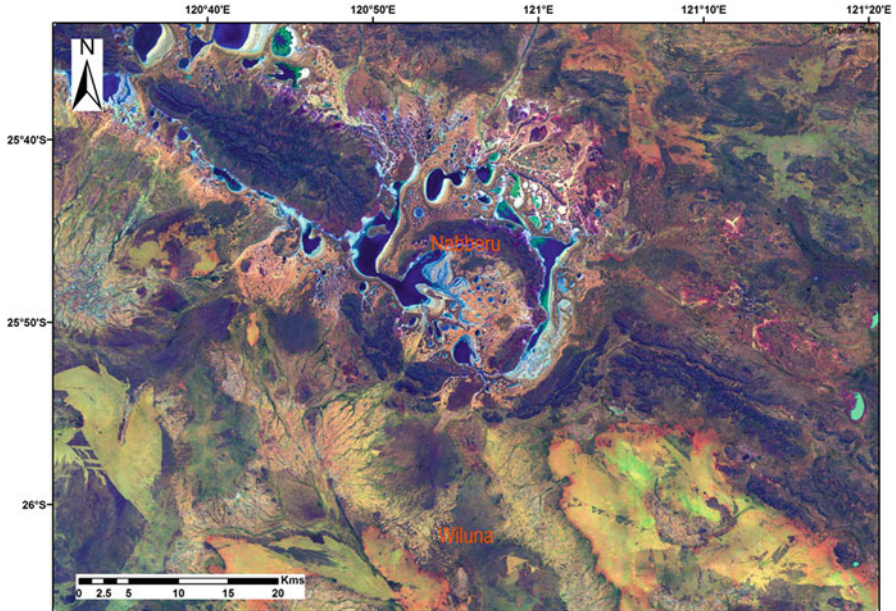


Fig. 4.5 LANDSAT RGB-741 image of the Shoemaker (formerly Teague) impact structure, Naberu Basin, Western Australia (NASA)

4.1.4 Lawn Hill ($D \sim 18\text{--}20\text{ km}$)

The Lawn Hill structure is located within Middle Cambrian carbonates of the Lawn Hill Platform in north-western Queensland (Fig. 4.7a, b). Stewart and Mitchell (1987) identified shatter cones (Fig. 4.7c), planar deformation features in quartz and melt breccia (suevite) (Fig. 4.8a, b, c) with impact-melted clasts of siltstone and sandstone at the centre of the structure, demonstrating an impact origin. Possible microdiamonds were later identified (Fig. 4.8d) (Salisbury et al. 2008). Mapping of the structure by Shoemaker and Shoemaker (1996) defined a $\sim 8\text{ km}$ -diameter central uplift enveloped by steeply plunging faulted blocks repeated along a series of small thrusts, consistent with patterns observed in impact structures. These authors considered the impact predated the Cambrian limestones. However, M. Dence (cited in Haines 2005) considered that the brecciation of the limestone to be related to impact. Subsequent studies confirmed this interpretation showing the block structures and brecciation related to the impact (Salisbury et al. 2008).

Salisbury et al. (2008) studied the relations between the Lawn Hill impact and the Meso-Proterozoic Century Zn – Pb deposit located on the margin of the impact structure to the southwest. The effects of the impact on the Cambrian limestone comprise veins of brecciated limestone injected hundreds of metres into the Mesoproterozoic basement and contorted bedding and convoluted flow structures (Fig. 4.8c) in the limestone and shale

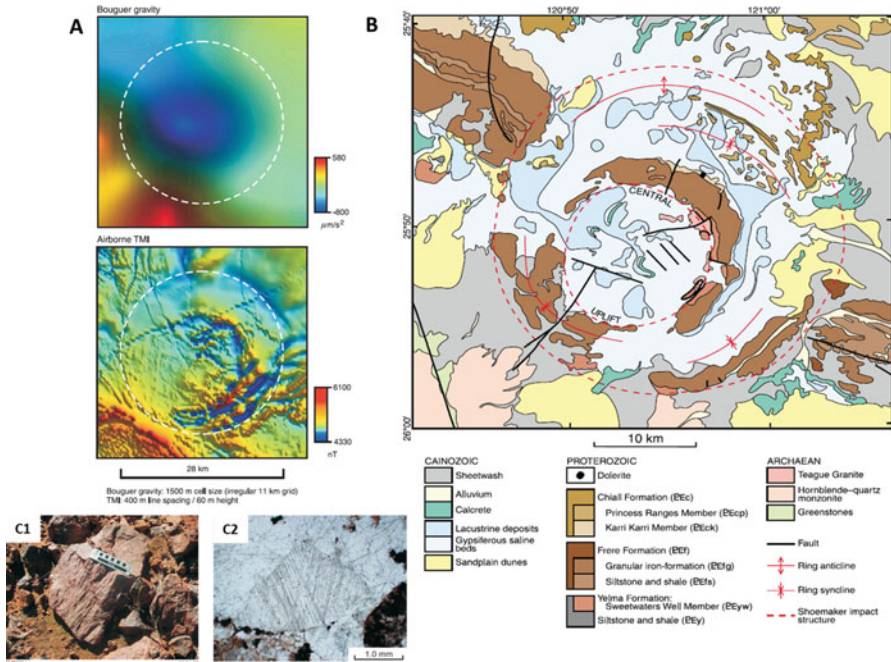


Fig. 4.6 Shoemaker impact structure. (a) Bouguer gravity and Total Magnetic Intensity values. Geological Survey of Western Australia Report 82: Geology of the Shoemaker impact structure, Western Australia, by F. Pirajno; (b) geological sketch map of the Shoemaker impact structure. (Pirajno et al. 2003; AJES with permission); (c1) shatter cones in granular iron-formation of the Frere Formation on the northern rim of the Shoemaker impact structure; (c2) planar deformation features; in quartz crystals from the Teague Granite (plane-polarized light). GSWA Report 82, with permission

annulus, suggesting contemporaneity between carbonate deposition during 520–510 Ma and the impact. The impact affected macro-scale remobilisation of large ore fragments induced by lateral and vertical injection of limestone into the Meso-Proterozoic basement. Darlington et al. (2016) reported ^{40}Ar - ^{39}Ar ages for impact-related melt particles suggesting an Ordovician (472 +/- 8 Ma) age, during which the Georgina Basin was an active depositional center.

4.1.5 Strangways ($D \sim 25\text{--}40\text{ km}$)

The Strangways impact structure, which affected Mesoproterozoic sediments with interlayered dolerite sills of the McArthur Basin and underlying granitic basement, stands out on geophysical and satellite maps (Fig. 4.9a-c). The exposed diameter of

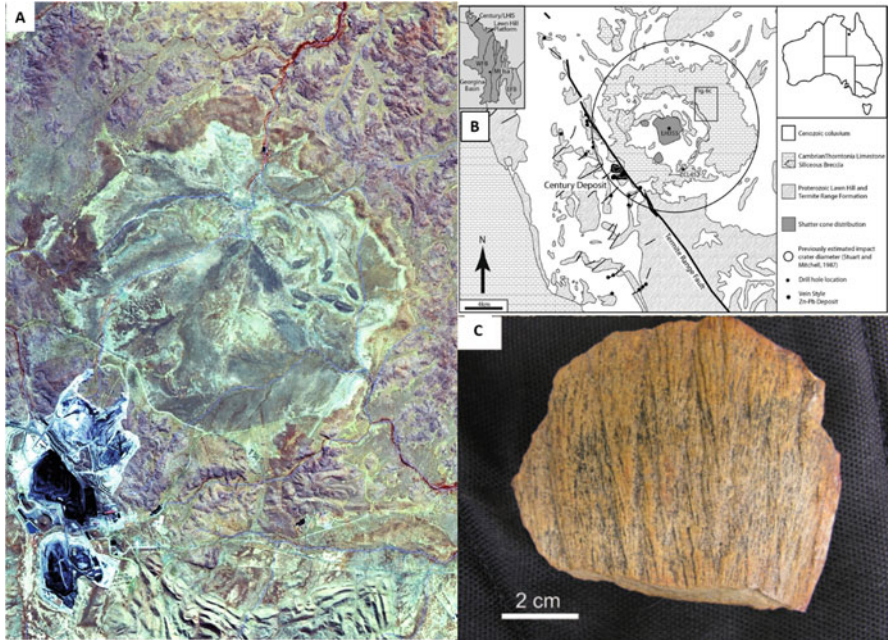


Fig. 4.7 Lawn Hill impact structure. (a) LANDSAT image of the Lawn Hill structure, NASA. Note the Century Zn mine in the southwest; (b) geological sketch map (Salisbury et al. 2008); (c) shatter cone (Salisbury et al. 2008; AJES with permission)

the Strangways structure is about 16 km whereas the original size of the crater rim was interpreted as 40 km or more by Shoemaker and Shoemaker (1996). Spray et al. (1999) and Zummersprekel and Bischoff (2005) suggested a diameter of 24 to 26 km and an uplift of 2.4 to 2.7 km. The structure, originally regarded as igneous in origin was identified by Guppy et al. (1971) as an impact structure from the presence of shatter cones, melt breccia (suevite) and shocked minerals. Further documentation of the structure was conducted by Shoemaker and Shoemaker (1996), Spray et al. (1999), Haines (2005), Zummersprekel and Bischoff (2005) and Dunster et al. (2014). The melt breccia overlies granite breccia, shattered granite, brecciated, mega-brecciated or shock melted granite, and consists of shock-melted fragments of quartzite, shale and granite, some clasts being larger than a meter and some display plastic deformation and viscous flow (Shoemaker and Shoemaker 1996). Melt fractions located close to the center of the structure contain high Ni, Cr, Ir, Os and Pd likely derived from the projectile, Ni is enriched 60 times and Ir 20 times relative to background values (Shoemaker and Shoemaker 1996). The age of the impact is indicated by infrared laser $^{40}\text{Ar}/^{39}\text{Ar}$ analysis of impact melt and shocked breccia clast yielding an age of 646 ± 42 Ma, consistent with the overlap of un-deformed early Cambrian Antrim Plateau Volcanics (Spray et al. 1999).

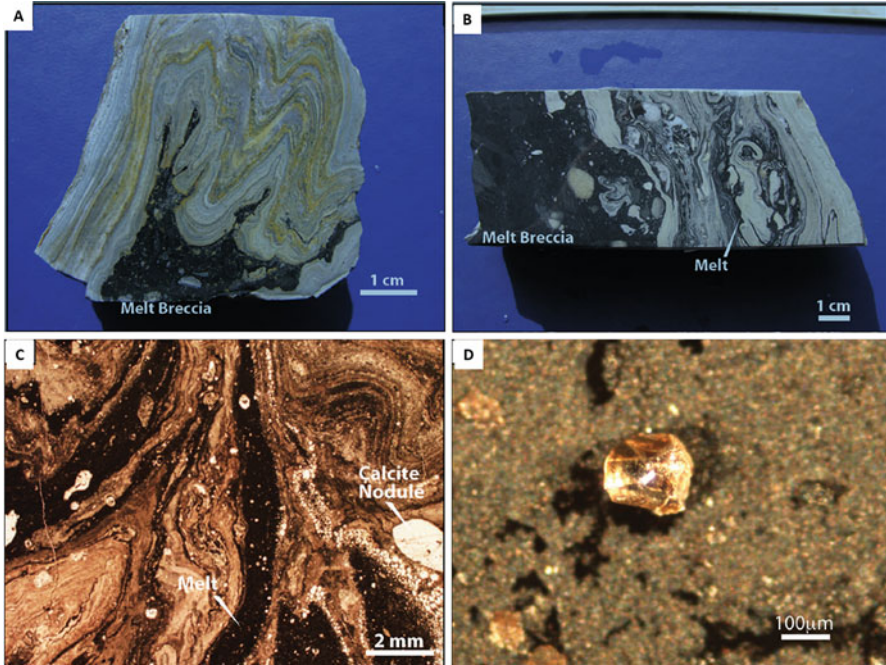


Fig. 4.8 Lawn Hill impact structure. Samples from drill hole LH355 drilled into the aeromagnetic anomaly at the center of the Lawn Hill impact structure, and photomicrographs of textures therein. (a) glass cemented breccia in well-bedded and strongly deformed shale at 171.6 m depth. (b) more devitrified glass than developed in A at 172 m depth. (c) partial melting and melt-lubricated folding in well-bedded shale; a calcite nodule is also evident plane-polarized light). (d) diamond separated from shatter cone-bearing carbonaceous shale at the center of the structure. Salisbury et al. 2008 (AJES with permission)

4.1.6 Amelia Creek ($D \sim 20 \times 12$ km)

The Amelia Creek impact structure in the Davenport Ranges, Northern Territory, where shatter cones were first identified by A.J. Stewart in 1981 in the Wauchope Subgroup of the Palaeoproterozoic Hatches Creek Group, tectonically deformed prior to impact. The structure was further mapped by Macdonald and Mitchell 2003. The asymmetrical structure is deeply eroded, weakly defined and superposed on complex fold structures of the Davenport Province (Figs 4.10a, b and 4.11). The dimensions are estimated as 20×12 km in diameter (Macdonald et al. 2005). The asymmetry of the overall structure may indicate an oblique impact. The structure is marked by a positive magnetic anomaly of 100 nT at the center (Fig. 4.10c). Shatter cones are ubiquitous in the Unimbra Sandstone as well as in felsic volcanic rocks and in the Yeeradgi Sandstone (Dunster et al. 2014). The shatter cones are accompanied by feather-like microstructures, possibly incipient planar deformation features in quartz grains of the target sandstone, distinct from tectonic fractures and typical of

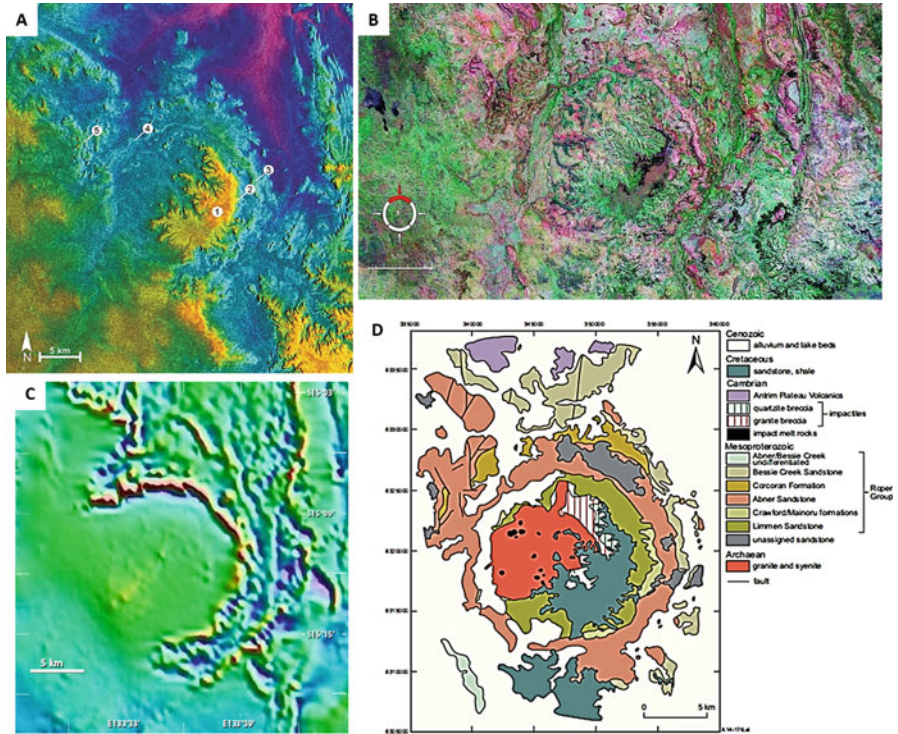


Fig. 4.9 Strangways impact structure. (a) Digital elevation model with an exaggeration factor of 10 and an artificial illumination from the east merged with an ERS radar scene. 1, Cretaceous Mullamen beds; 2, Limmen Sandstone; 3, Abner Sandstone; 4, arcuate ridges of Abner sandstone possibly indicating gentle folding; 5, lineations cutting through Abner Sandstone (remnants of terraced rim area) (Zummersprekel and Bischoff 2005) (AJES with permission); (b) false color LANDSAT image (Wikipedia commons) (https://en.wikipedia.org/wiki/Strangways_crater#/media/File:Strangways_crater.jpg) (c) Strangways total magnetic image (After Shoemaker and Shoemaker 1996 (<http://www.geoscience.nt.gov.au/gemis/ntgsjspui/handle/1/82468>)) (NTGS with permission); (d) Geological sketch map (After Shoemaker and Shoemaker 1996)

quartz grains in impact structures. Large autogenic breccia clasts occur along fault lines. Clastic dikes are present. An age range of 1640–600 Ma is constrained by unconformably overlying Neoproterozoic rocks.

4.1.7 Cleanskin (D~15 km)

The Cleanskin impact structure constitutes a 15 km-diameter deformed zone in the Constance Sandstone of the early Mesoproterozoic South Nicholson Group, Queensland-Northern Territory border zone, partly underlying Cretaceous cover, and identified by Ian Sweet and Ken Mitchell (Haines 2005; Dunster et al. 2014) (Fig. 4.12a).

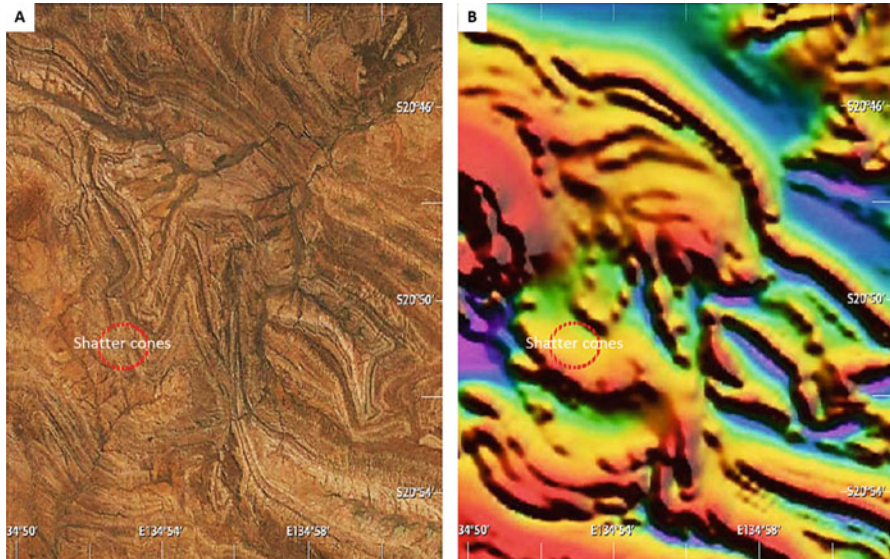


Fig. 4.10 Amelia Creek impact structure; red outline indicates approximate area of pervasive shatter-coning. (a) Satellite image (Google Earth, Digital Globe, CNES/Spot Image 2014); (b) Aeromagnetic anomaly (Dunster et al. 2014; NTGS with permission)

An impact origin is confirmed by shatter cones (Fig. 4.12b) and possible planar deformation features in quartz (Fig. 4.12c). The structure includes a central dome faulted by circumferential reverse faults. Shatter cones in sandstones 3.5 km from the centre are associated with bands of brecciated sandstone and siltstone tens of metres large. The quartz grains reveal multiple planar fracturing, feather features, grain mosaicism, and possible planar deformation features. The overall low levels of shock metamorphism suggest the structure is deeply eroded by at least 1–3 km, implying the original crater could have been approximately 20 km in diameter (Dunster et al. 2014). The target sediments of the impact are estimated as 1400–1500 Ma old whereas the impact event is pre-Cretaceous and is believed to have post-dated regional deformation and occurred prior to the Cambrian, relegating the likely age to between about 1400 Ma and the early Cambrian (Dunster et al. 2014).

4.1.8 Glikson ($D \sim 14$ km)

The Glikson impact structure located in little-deformed ~800 Ma-old Neoproterozoic sediments of the north-western Officer Basin was originally identified from TMI maps by A. Whittaker on the basis of a perfectly circular 14 km-diameter magnetic ring (Fig. 4.13a) and studied by Shoemaker and Shoemaker (1997) and Macdonald et al. (2005). The TMI ring envelopes poorly outcropping

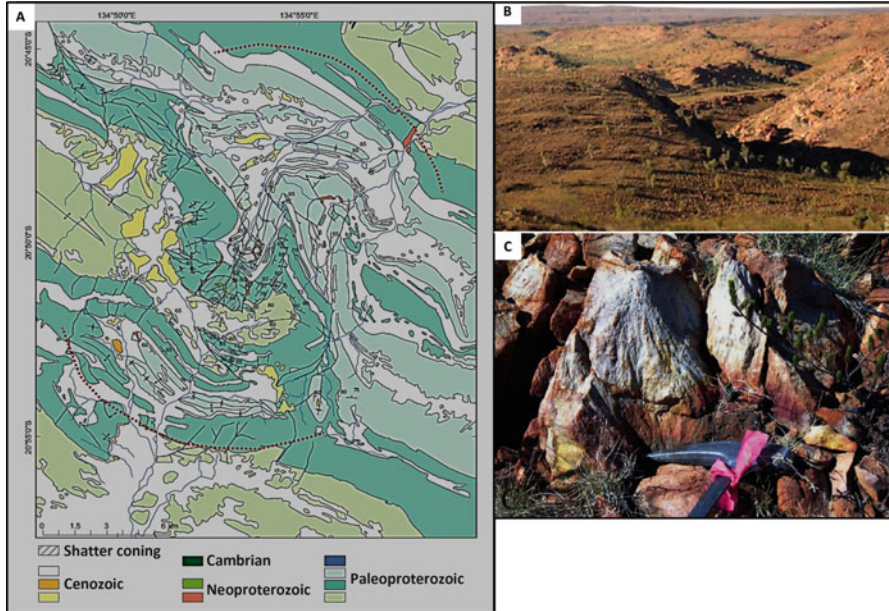


Fig. 4.11 Amelia Creek impact structure. (a) Geological sketch map (Shoemaker et al. 2005; Macdonald et al. 2005; Dunster et al. 2014) (<http://www.geoscience.nt.gov.au/gemis/ntgsjspui/handle/1/82468>); (b) Central syncline viewed from a sandstone ridge to the southwest (<http://www.tandfonline.com/doi/pdf/10.1080/08120090500170401>). (c) Shatter cones in the Unimbra Sandstone with apices pointing nearly upward (20851.1°S, 134853.0°E) (<http://www.geoscience.nt.gov.au/gemis/ntgsjspui/handle/1/82468>). (NTGS with permission)

arenites containing impact evidence including a circular uplift exposing lower stratigraphic levels at the centre (Fig. 4.13b) and shatter cones (Fig. 4.13c). Macdonald and Mitchell (2003) and Macdonald et al. (2005) extended the deformed zones to a diameter of 19 km. The magnetic ring (Fig. 4.13a) likely represents a dolerite sill uptilted by the impact. A SHRIMP U–Pb baddeleyite and zircon age of 508 ± 5 Ma (Middle Cambrian) for a dolerite located 25 km south of the Glikson structure (Macdonald et al. 2005) may correlate with the ring dolerite surrounding the impact structure.

4.1.9 Gosses Bluff (D~12 km)

Gosses Bluff constitutes one of the most complete and at its centre well exposed medium-size impact structures in the world, originally thought to be ~24 km in diameter (Milton et al. 1996a, b) but revised as ~14 km with a central uplift ~5 km in diameter (Fig. 4.14a, b) overlapped by a well expressed Bouguer anomaly

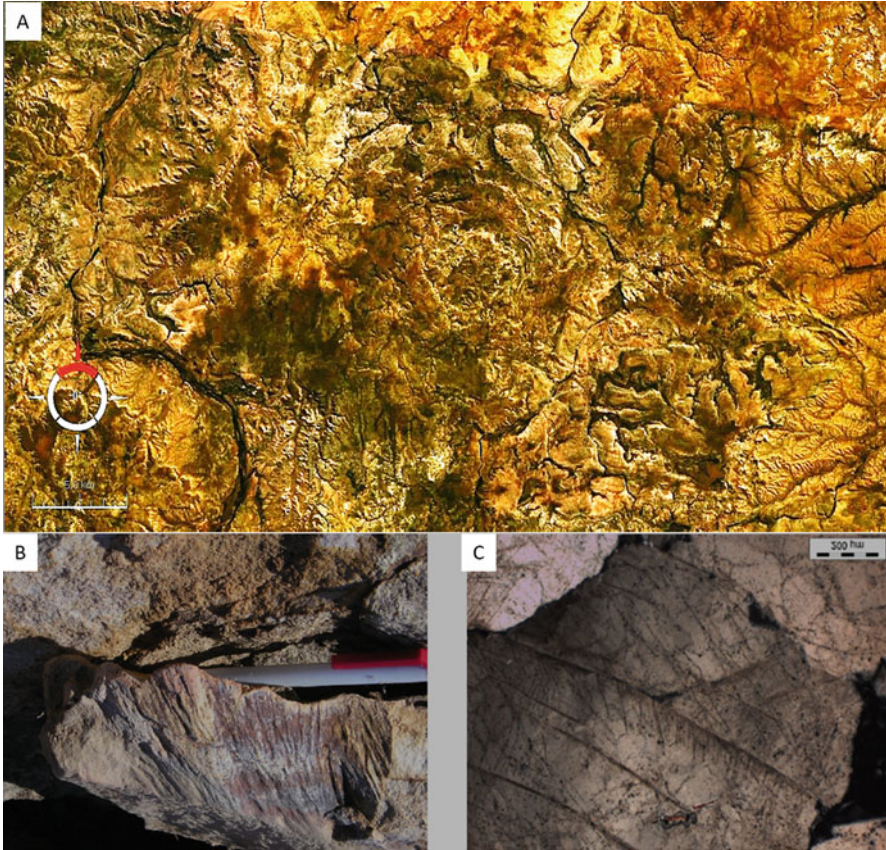


Fig. 4.12 (a) Cleanskin structure, Landsat imagery (b) Shatter cones in sandstone. Photomicrograph of multiple planar fractures with feather features in quartz; (c) Deformed planar deformation features in quartz. B and C (Haines et al. 2012 (<https://www.lpi.usra.edu/meetings/metsoc2012/pdf/5176.pdf>); Dunster et al. 2014 (NTGS with permission)

(Fig. 4.14c). The well-exposed central uplift includes at its core soft arenites and shale ensuing in a central morphological depression. The impact affected flat lying mostly Ordovician to Devonian arenites of the Amadeus Basin An impact origin was considered by Crook and Cook (1966), with Cook preferred a cryptovolcanic origin and Crook favouring an impact origin, confirmed when shatter cones (Fig. 4.14e) were discovered. A joint study by the Australian Bureau of Mineral Resources and the United States Geological Survey during 1968–1969 (Glikson 1969; Milton et al. 1972, 1996a, b) identified a wide range of impact features, including a centripetal sense of deformation, overturned blocks (Fig. 4.14d) melt breccia and planar deformation features in quartz (Milton et al. 1972, Milton et al. 1996a, b). The central uplift was drilled by two petroleum exploration wells but no significant

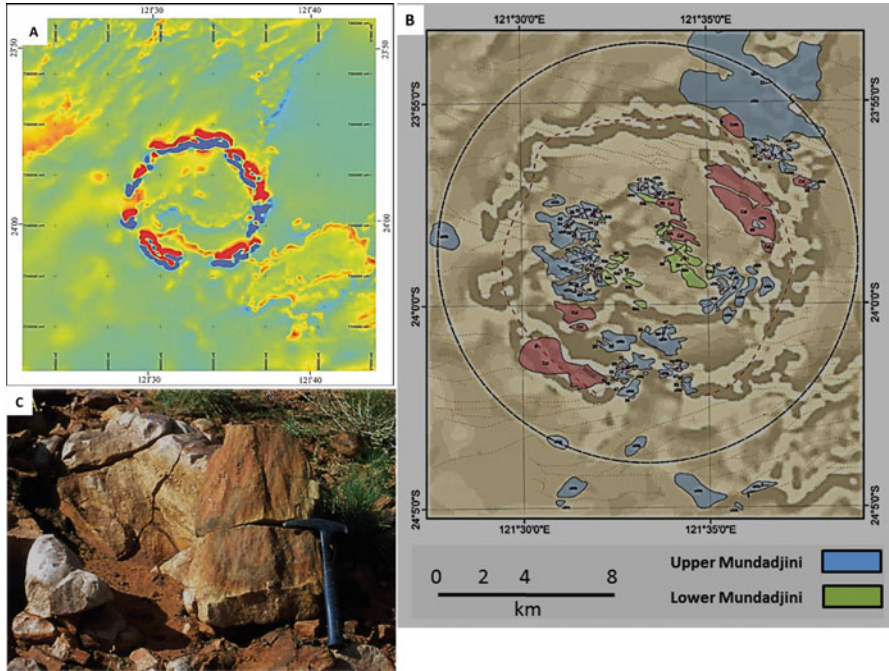


Fig. 4.13 Glikson impact structure (Macdonald et al. 2005). (a) Regional total magnetic intensity (TMI) image. The line spacing of the airborne survey is 300 m and flying height 80 m. Intensity values decrease from red to dark blue; (b) Geological sketch map with first-derivative aeromagnetic drape in the background. Outcrops on the western collar of the central uplift and the northeast rim of the structure are excellent, whereas most other mapped outcrops are not well exposed; (c) Shatter cone from discovery locality ~3 km northwest of the center of the structure (AJES with permission)

accumulations of petroleum were detected. Detailed imaging by several seismic lines (Brown 1973; Milton et al. 1996a) and close spaced gravity measurements (Fig. 4.14c) (Milton et al. 1996a) allow a 3-D structural analysis of the structure. Remnant melt breccia was identified at Mount Pyroclast in the outer ring syncline south of the central uplift (Milton et al. 1996b). The melt breccia consists of partly melted fragments of recrystallised arenite and recrystallized arenite containing devitrified silica glass in a flow-banded matrix (Milton et al. 1996b). ³⁹Ar/⁴⁰Ar age determination of melt fractions yielded an age of 142.5 ± 0.8 Ma (Milton and Sutter 1987), namely close to the Jurassic – Cretaceous boundary (145.5 ± 4.0 Ma: Gradstein et al. 2004). In this context Gosses Bluff belongs to a cluster of asteroid impacts’ including Morokweng (145.0 ± 0.8; D = 70 km) and Mjøltnir (142.0 ± 2.6 Ma; D = 40 km).

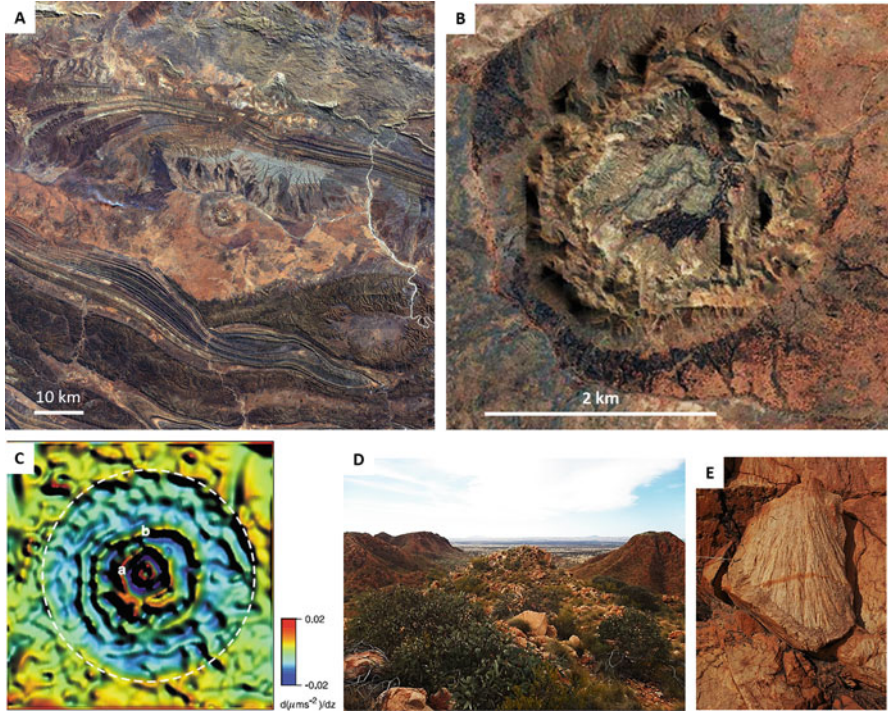


Fig. 4.14 Gosses Bluff impact structure. (a & b) Location at the center of the Missionary Plane syncline. Google Earth satellite images; (c) First vertical derivative Bouguer anomaly. Iasky et al. 2001 (GSWA with permission); (d) View of overturned white quartzite of the Middle Devonian Merreenie Formation above up-tilted rim of late Devonian Pertnjara Sandstone; (e) Shatter cones in Pitjantjatjara sandstone

4.1.10 Kelly West ($D \sim 8-20$ km)

The Kelly West impact structure (Fig. 4.15a, b), about 40 km south-southwest of Tennant Creek, identified thanks to the presence of shatter cones in its central uplift (Tonkin 1973), was estimated by Shoemaker and Shoemaker (1996) as at least 8 km and less than 20 km in diameter. Shatter cones are distributed over the entire 2 km long exposure of target. There are no exposed geological constraints on the location of the original rim (Dunster et al. 2014). A gravity survey indicates the centre of the structure coincides with a + 0.8 mGal annular gravity high (Plescia 2006) and magnetic data indicates annular disruption of the magnetic response (Hawke 2003). Based on the geophysical data an original diameter of 6.6 km is inferred. Hawke (2003) and Plescia (2006) inferred uplift of Hatches Creek Group quartz sandstone target rocks, as also indicated by rotation of shatter-cone axes and

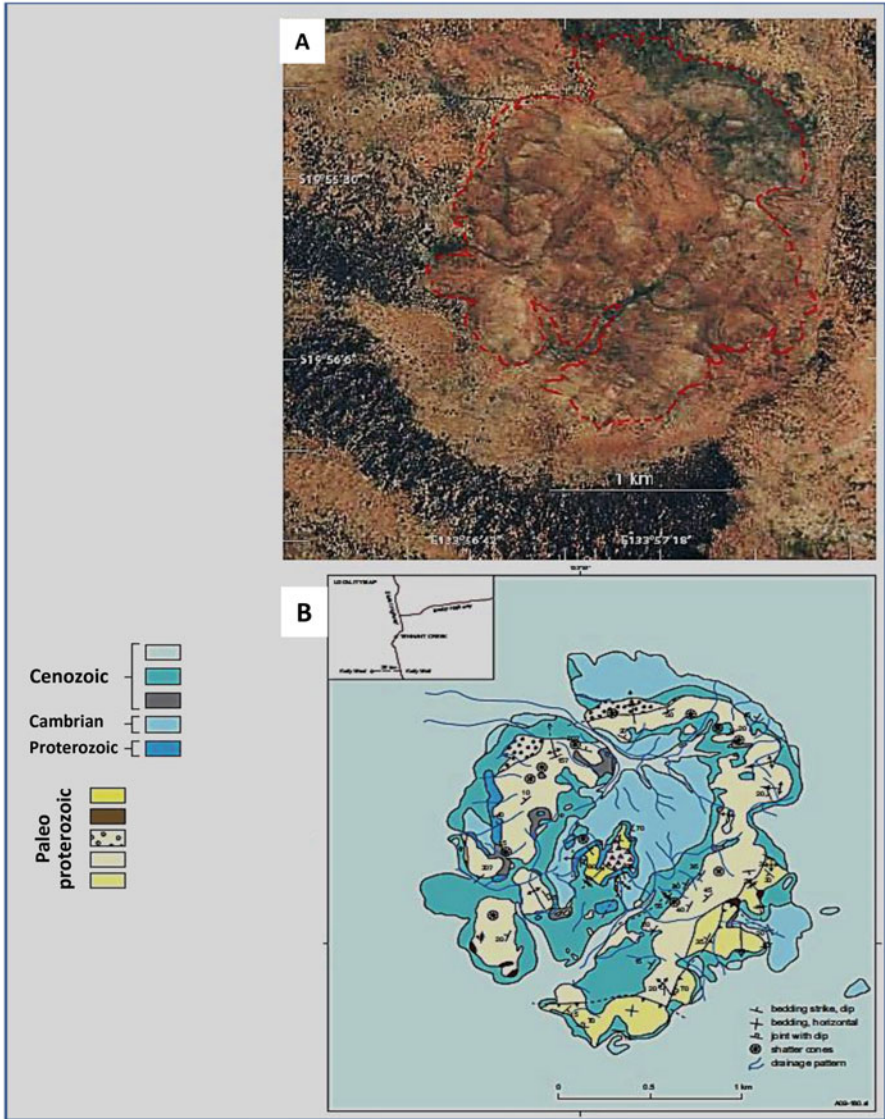


Fig. 4.15 Kelly West impact structure. (a) Satellite image. Google Earth; B. LANDSAT 741 imager of Kelly West; (b) Geological sketch map after Tonkin (1973) and Shoemaker and Shoemaker (1996). Dunster et al. (2014). (NTGS with permission)

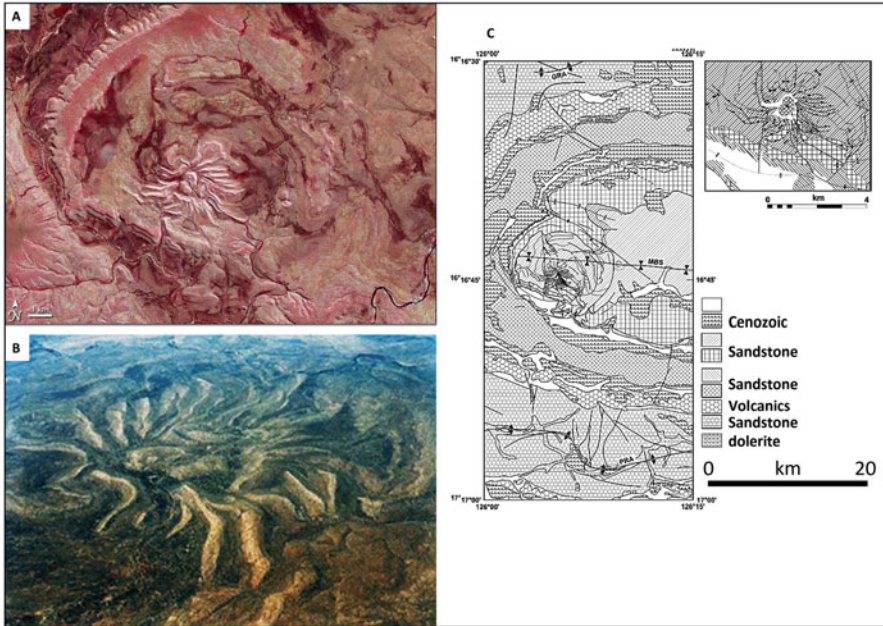


Fig. 4.16 Spider impact structure. (a) Satellite image (NASA) (<http://earthobservatory.nasa.gov/IOTD/view.php?id=8677>); (b) Aerial photograph; (c) Geological map (Geology of the Spider structure (WA), mapped by E.M. Shoemaker and C.S. Shoemaker, 1984–1985. Shoemaker and Shoemaker 1996). (AJES with permission)

outward-plunging radial folds along the southeast flank of the uplift and duplication of strata by over-thrusting toward the centre of the uplift (Dunster et al. 2014). The uplift is associated with intense brecciation of Hatches Creek Group sandstone close to the centre of the structure. The structure is overlain by flat-lying middle Cambrian sediments, suggesting the structure formed between the Palaeoproterozoic and the early Cambrian.

4.1.11 Spider ($D \sim 11\text{--}13\text{ km}$)

The Spider structure features a central uplift approximately 0.5 km in diameter surrounded by multiple clockwise and anti-clockwise thrust faults over an area about 13x11 km large (Figs 4.16a, b), signifying centripetal deformation. The thrust faults displace arenite to quartzite beds of the lower Proterozoic Pentecoste Formation. The recognition of shatter cones (Harms et al. 1980) established the impact origin of the structure. Shoemaker and Shoemaker (1988, 1996) regarded the feature

as a deeply eroded complex impact structure with a 0.5 km central dome surrounded by the displaced thrust sheets, with possible extension to a 20 km diameter. The structure was imaged by the Space-borne Radar displaying the thrust sheets and dome but not the outermost limits of deformation (McHone et al. 2002). In view of the asymmetry of the thrust faults a low-angle impact from the north or northwest has been invoked (Shoemaker and Shoemaker 1996). Abels (2005) suggested the asymmetry may in part be related to a pre-existing topography of the impacted terrain. The older age limit of the Spider impact is constrained by the Palaeoproterozoic target rocks. Abels (2005) suggested the impact postdates gentle folding at about 900 Ma and pre-dates regional glacial erosion and deposition at ~600 Ma, suggesting a Neoproterozoic age.

4.1.12 Goyder (D~9–12 km)

The Goyder impact structure is located in a terrain underlain by the Mesoproterozoic Roper Group, northern McArthur Basin (Haines 1996, 2005; Haines et al. 1999; Dunster et al. 2014). The feature is expressed as a nearly-circular structural uplift of ~3 km McHone et al. 2002 diameter with an outer ring of Hodgson Sandstone forming a hilly region 1.5 km in diameter (Fig. 4.17a). The centre is marked by a positive TMI anomaly (Fig. 4.17c). The structure includes radially-faulted fractured and striated sandstone and mudstone of the Arnold Sandstone and overlying Jalboi Formation, attesting to centripetal deformation. Shatter cones up to 50 cm-long with axes oriented parallel to the bedding and shock-induced planar deformation features occur at the centre of the structure (Fig. 4.17d). The 300 to 400 m wide outer ring of Hodgson Sandstone consists of fractured, brecciated and disintegrated arenite mostly dipping tangentially outwards, constituting relics of a central uplift. The original rim diameter is likely of 9 km to 12 km diameter. Age constraints on the impacts include the age of the target rocks at <1325 Ma, post-impact Cretaceous land surface and undeformed sediments.

4.2 Buried Impact Structures

The advent of geophysical surveys on the Australian continent, including Total Magnetic Intensity (TMI) surveys, Bouguer anomaly studies and deep crustal seismic transects allowed the discovery of a number of large asteroid impact structures and likely to probable impact structures onshore and offshore the Australian continent. These include Woodleigh (120 km; ~359 Ma), Gnargoo (75 km; Lower Permian – upper Cretaceous), Tookoonooka (55–65 km;

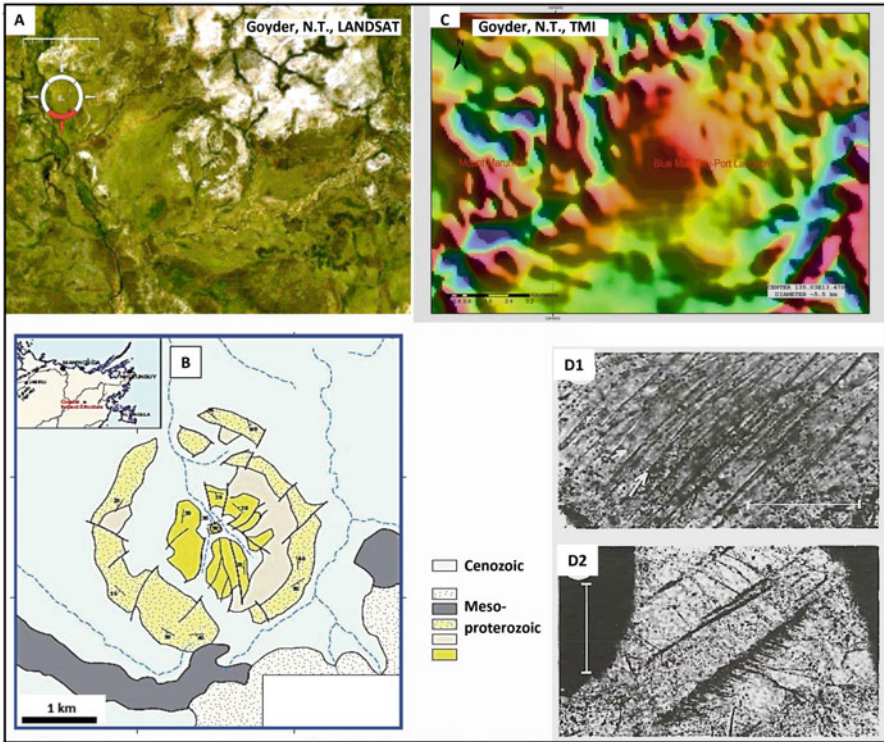


Fig. 4.17 Goyder impact structure. (a) Satellite view (Google Earth; CNES Spot Image 2014) (https://commons.wikimedia.org/wiki/Category:Impact_craters_of_Australia#/media/File:Goyder_crater.jpg); (b) Geological sketch map, after Haines (1996) (NTGS with permission). (c) Goyder, Total Magnetic Intensity (GA creative commons); (d) Photomicrographs of planar deformation features in quartz grains in sandstone from the center of the Goyder impact structure. Scale bar = 100 μm (Haines 1996; GA Creative Commons)

~125 Ma), Talundilly (~84 km; ~125 Ma), Mount Ashmore (near-100 km; end-Eocene) and Warburton twin structures (>400 km; end-Carboniferous). Criteria for recognition of buried impact structures are based on detailed studies of the Chicxulub structure (170 km; 64.98 ± 0.05 Ma), Chesapeake Bay (~85 km; 35.5 ± 0.3 Ma), the former displaying unique structural architecture where pre-impact structural ridges are intersected and truncated by the outer ring of the circular structure. Seismic reflection data outline circular central uplift domes, basement plugs and rim synclines. Circular seismic tomography anomalies indicate low velocity columns under both the Woodleigh and Warburton impact structures, hinting at deep crustal fracturing.

4.2.1 Warburton East ($D \sim < 200$ km)

The Eastern Warburton Basin, northeast South Australia, features major geophysical anomalies, including a magnetic high of near-200 nT centred on a ~25 km-wide magnetic low (b100 nT), interpreted in terms of a magmatic body below 6 km depth (Glikson et al. 2013) (Figs. 3.7a, 3.7bA, C). A distinct seismic tomographic low velocity anomaly may reflect its thick (9.5 km) sedimentary section, high temperatures and possible deep fracturing. Scanning electron microscope (SEM) analyses of granites resolves microbreccia veins consisting of micron-scale particles injected into resorbed quartz grains. Planar and sub-planar elements in quartz grains occur in granites, volcanics and sediments of the >30,000 km-large eastern Warburton Basin. The PDFs consist of multiple intersecting planar to curved sub-planar elements with relic lamellae less than 2 μm wide with spacing of 4–5 μm and are commonly re-deformed, displaying bent and wavy patterns accompanied by fluid inclusions. Transmission Electron Microscopy (TEM) analysis displays relic narrow ≤ 1 μm -wide lamellae and relic non-sub grain boundaries where crystal segments maintain optical continuity. Extensive sericite alteration of feldspar suggests hydrothermal alteration to a depth of ~500 m below the unconformity which overlies the PDF-bearing Warburton Basin terrain. Interpretations include (A) tectonic–metamorphic deformation and (B) impact shock metamorphism producing planar deformation features. A 4–5 km uplift of the Big Lake Granite Suite during ~298–295 Ma is consistent with missing of upper Ordovician to Devonian strata and possible impact rebound. The occurrence of circular seismic tomography anomalies below the east Warburton Basin (Saygin and Kennett 2010, 2012), the west Warburton Basin and the Woodleigh impact structure signifies a potential diagnostic nature of circular tomographic anomalies, supporting an impact origin.

4.2.2 Warburton West ($D < 200$ km)

Geophysical anomalies in the Warburton West Basin include magnetic, gravity and low-velocity seismic tomography anomalies (Glikson et al. 2015) (Figs. 3.7a). Quartz grains from arenite core samples contain intra-crystalline lamellae in carbonate–quartz veins (Fig. 3.7bB, D) and in clastic grains similar to those reported earlier from arenites, volcanic rocks and granites from the Warburton East Basin (Glikson et al. 2013). Universal Stage measurements of quartz lamellae from drill cores are mostly curved and bent either due to tectonic deformation or re-deformation of impact-generated planar features during crustal rebound or/and post-impact tectonic deformation. Seismic tomography low-velocity anomalies in both Warburton West Basin and Warburton East Basin suggest fracturing of the crust to depths of more than 20 km. In the Warburton West Basin a large magnetic body of SI (susceptibility index) = 0.030 is modelled below ~10 km, with a large positive gravity anomaly offset to the north of the magnetic anomaly. The magnetic anomalies in the Warburton East and West sub-basins are

interpreted in terms of (1) presence of deep seated central mafic bodies; (2) deep crustal fracturing and (3) removal of Devonian and Carboniferous strata associated with rebound of a central uplift consequent on large asteroid impact. Further tests of the Warburton structures require deep crustal seismic transects.

4.2.3 *Woodleigh (D = 120 km)*

The buried Woodleigh impact structure, Carnarvon Basin, Western Australia (120 km; ~360 Ma) (Iasky et al. 2001; Mory et al. 2000; Glikson et al. 2005a, b; Uysal et al. 2001), displays significant analogies with the Chicxulub impact structure in terms of its multiring features and intersection of older structural ridges (Fig. 3.8a). Thus the outer ring of the Woodleigh impact structure intersects the Ajana and Wandagee gravity ridges. Seismic-reflection data and a drill hole (Woodleigh-1) indicate a central ~37 km-diameter granitoid basement plug. Seismic evidence indicates an upper diameter of 120 km and a lower diameter at greater depth. A sharp seismic low-velocity tomography anomaly (Saygin and Kennett 2010, 2012) coincides with the ~120 km-diameter circular structure (Fig. 3.8b). The circular fault patterns include outer normal faults dipping toward the center and inner thrust faults around the central uplift, consistent with patterns in other impact structures (Ries crater, Chesapeake Bay). Planar deformation features (PDFs) are well developed in the granitoid central core (Fig. 3.8c) with the majority of planar sets being oriented parallel to {10–13} and lesser abundance to {10–12}. Some sets are parallel to the basal plane {0001} and {10–11}, consistent with lower pressures about 5–10 GPa (Fig. 3.8c, d).

4.2.4 *Talundilly (84 km)*

The Talundilly structure (Longley 1989; Gorter and Glikson 2012), located 328 km northeast of Toookoonooka, in the Eromanga Basin of southwest Queensland, is manifested on seismic reflection transections as an 84 km-large anomaly which disrupts the early Cretaceous Wyandra Sandstone located between the Cadna Owie and Bulldog Shale formations. The seismic anomaly coincides with a prominent aeromagnetic (TMI) high centrally located within a near-circular seismic anomaly (Fig. 4.18). The structure consists of a raised central area with radial faults extending from the central high, an annular synform with disrupted seismic elements dipping at low angles towards the central uplift, and an outer faulted rim. Talundilly-1 well located about 30 km northwest of the structural peak intersected arenite which contains quartz grains with planar deformation features (Fig. 4.19a, b, c). Drilling has obtained cores containing shock metamorphic quartz and comminuted

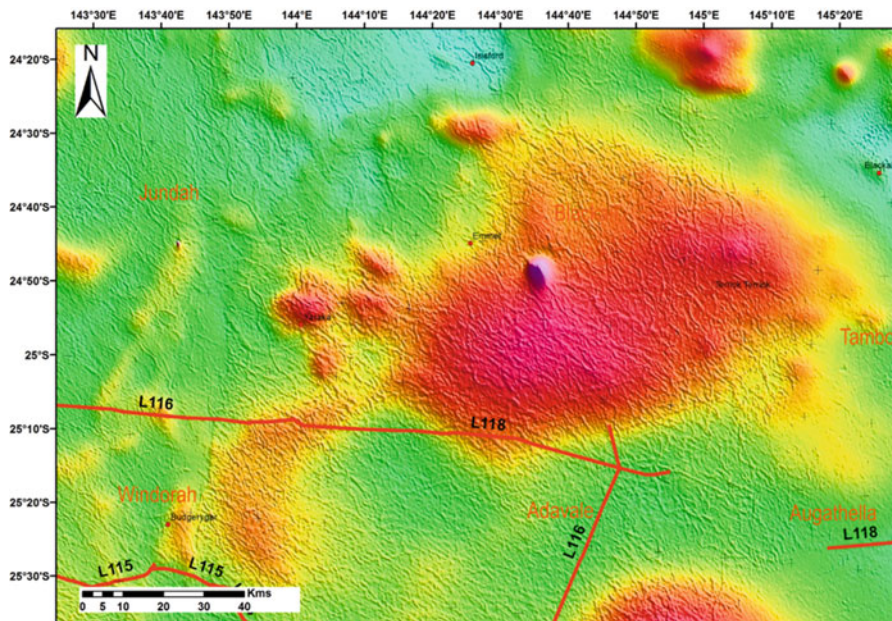


Fig. 4.18 Total Magnetic Intensity of the Talundilly buried impact structure. The red lines represent deep seismic transects (GA Creative Commons)

microbreccia (Fig. 4.19d). The age of the structure, as determined from seismic correlation and sparse palynology, is estimated as ~ 125 Ma, coinciding with the age of Tookoonooka and a marine transgression.

4.2.5 Tookoonooka ($D \sim 55$ km)

The ~ 66 km-diameter Tookoonooka impact structure (Gorter et al. 1989; Gostin and Theriault 1997; Bron and Gostin 2012), buried below ~ 900 m thick Cretaceous and Tertiary sediments of the Eromanga Basin, southwest Queensland, is expressed by weak drainage signatures (Fig. 4.20a). On seismic sections the structure consists of a concentric pattern of anticlines and synclines surrounding a ~ 22 km-wide complex central dome marked by a magnetic high (Fig. 4.20b) and a central gravity low (Fig. 4.20c). The age of the impact corresponds to the Barremian–Aptian boundary at 125 ± 1 Ma. Drilled Lower Cretaceous units (basal Wyandra Sandstone, Cadna Owie Formation) contain impact melt breccia with PDF-bearing quartz grains {10–12}, {11–22}, {21–31} and {11–21}, confirming an impact origin (Gostin and Theriault 1997; Bron and Gostin 2012). The clasts contain accretionary and melt components and lithic and mineral grains derived from the target rocks and the basement.

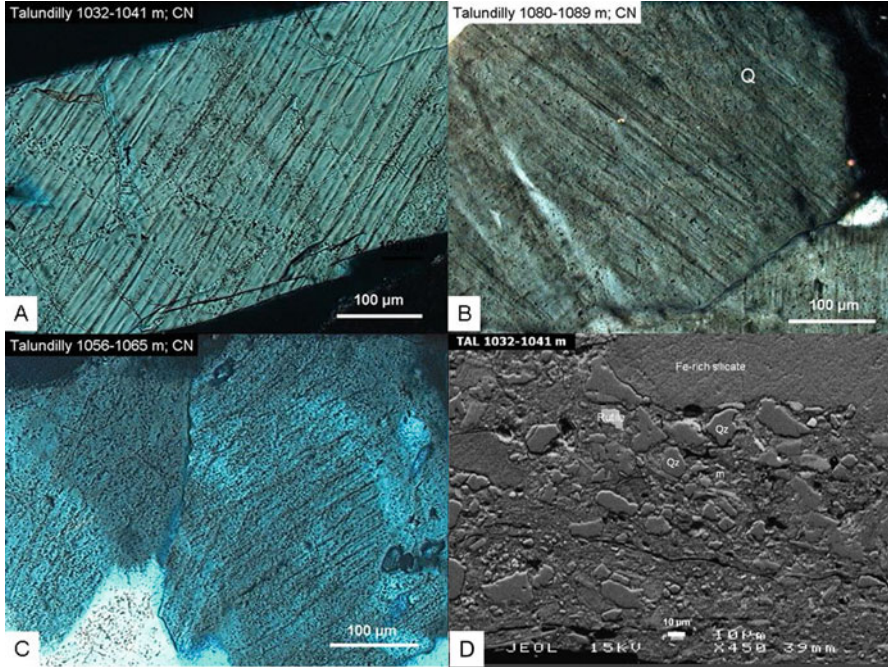


Fig. 4.19 Talundilly buried impact structure. (a–c) Planar deformation features in quartz. Plane polarized light (Gorter and Glikson 2012; AJES, with permission); (d) Microbreccia (SEM Backscatter image).(AJES with permission)

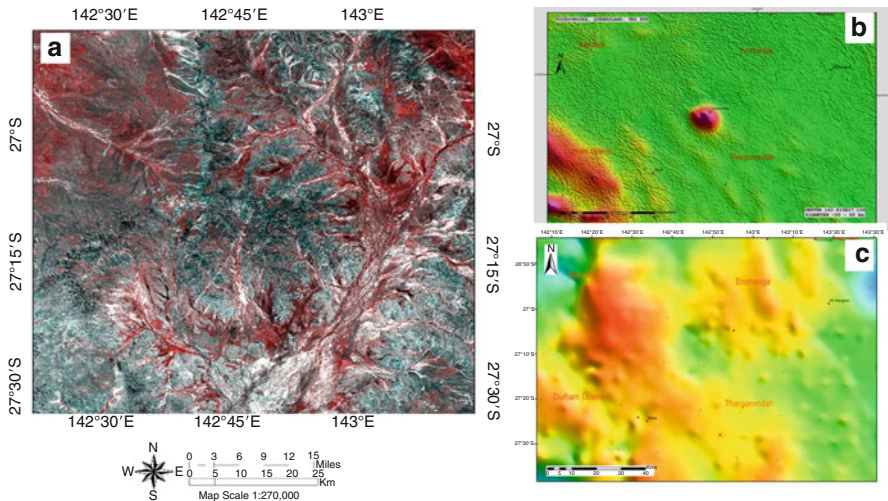


Fig. 4.20 Tookoonooka buried impact structure. (a) LANDSAT image, displaying a roughly circular drainage pattern; (Courtesy Roberto de Souza Filho); (b) Total magnetic intensity image; (c) Bouguer anomaly image (b and c – GA Creative Commons)

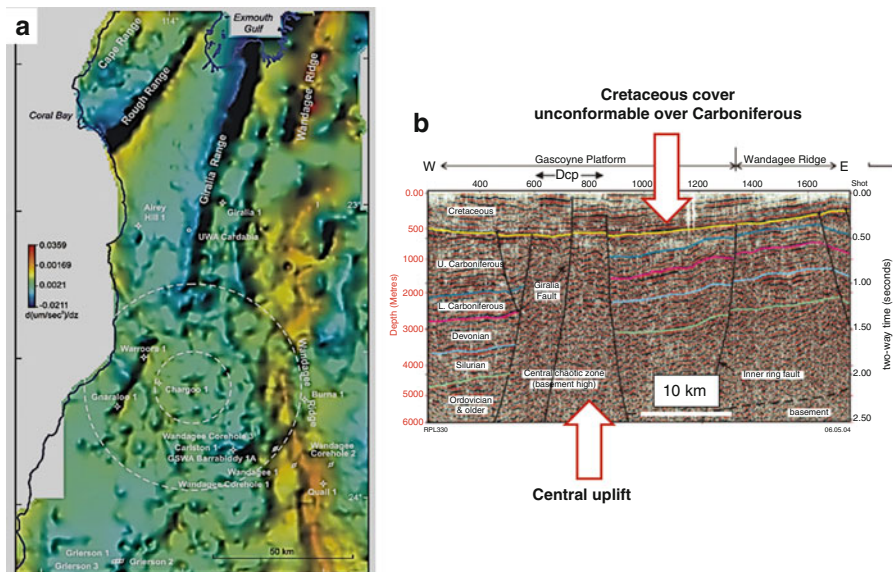


Fig. 4.21 Gnargoo probable buried impact structure (Iasky and Glikson 2005). **(a)** 1st vertical derivative Bouguer anomaly image, displaying the intersection of the Giralia Range by the circular perimeter of Gnargoo; **(b)** A seismic reflection cross section displaying the central uplift and the unconformable Cretaceous cover. (AJES with permission)

4.2.6 Gnargoo ($D \sim 75$ km)

The Gnargoo buried structure located about 500 m below Cretaceous strata features structural elements remarkably identical to those of the Woodleigh impact structure, located about 275 km to the south (Iasky and Glikson 2005). The analogies include a circular Bouguer anomaly ~ 75 km in diameter surrounding a central uplifted plug marked by a weakly defined inner 10 km-diameter circular Bouguer anomaly (Fig. 4.21a). The outer ring intersects the N–S Bouguer anomaly lineament of the Giralia Range. It includes a ~ 28 km-diameter layered sedimentary dome of Ordovician to Lower Permian strata, surrounding a cone-shaped, central uplift plug of 7–10 km diameter. Seismic-reflection data indicate a minimum central structural uplift of 1.5 km (Fig. 4.21b). An interpretation of the Gnargoo structure in terms of a plutonic or volcanic caldera is unlikely as these features display less regular geometry, nor are volcanic rocks known in the onshore Gascoyne Platform. An interpretation of Gnargoo as a salt dome is unlikely as no extensive evaporite units are known in the Southern Carnarvon Basin. The close similarities of Gnargoo to the Woodleigh impact structure are regarded as convincing evidence for their similar origin. The age of Gnargoo is constrained between the deformed Lower Permian target rocks and unconformably overlying Lower Cretaceous strata.

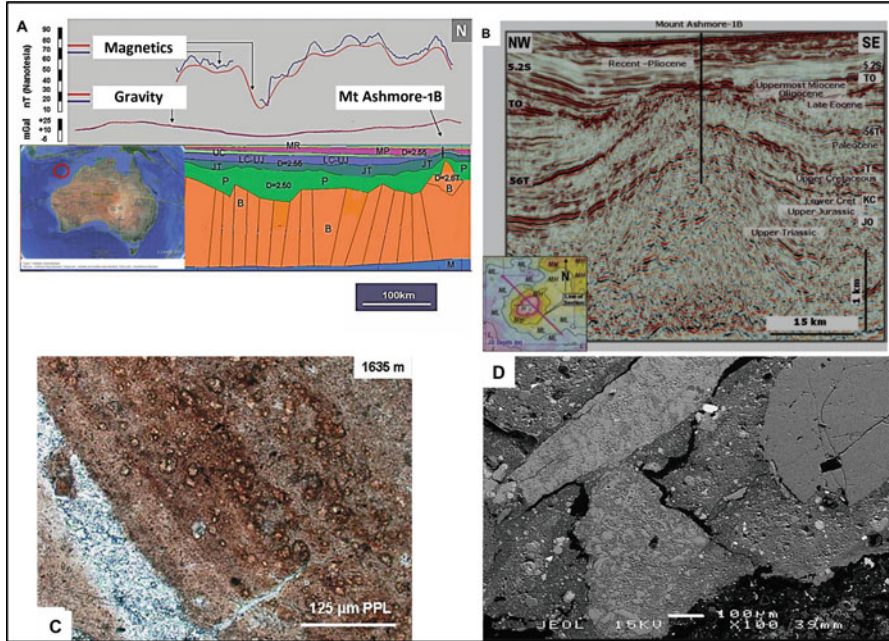


Fig. 4.22 Mount Ashmore probable impact structure (Glikson et al. 2010); (a) Isopach map of the Ashmore Platform and Browse Basin; (b) NW-SE seismic reflection traverse through the Mount Ashmore dome, showing the location of the Mount Ashmore-1B drill hole; (c) MA-1B core: Flow-textured microbreccia, with resorbed carbonate and quartz grains, injected by microcrystalline quartz veins; (d) MA-1B core: Microbreccia displaying a range of fragment sizes, including an intact quartz grain at the top right (AJES with permission)

4.2.7 Mount Ashmore (>50 km)

The Mount Ashmore buried dome, west Bonaparte Basin, Timor Sea (Glikson et al. 2010) (Fig. 4.22a, b), is unconformably overlain by a major pre-Oligocene post-Late Eocene unconformity and underlain by a ~6 km-deep-seated basement expressed by gravity and magnetic anomalies. The dome is approximately 50 km in diameter and the overall structure is estimated as larger than 100 km in diameter. Seismic reflection data displays chaotic deformation at the core of the dome, including centripetal kinematic deformation patterns (Fig. 4.22b). Lower Oligocene to Lower Jurassic well intersections reveal micro-brecciation, comminuted and flow-textured fluidization of altered sedimentary material (Fig. 4.22c, d). The microbreccia is dominated by aggregates of poorly diffracting micrometer to tens of micrometers-scale to sub-millimeter particles, including relic sub-planar fractured quartz grains, carbonate, barite, apatite and K-feldspar. No volcanic material or evaporite sediments were encountered, militating against interpretations of the

structure in terms of magmatic intrusion or salt diapirism models which are also inconsistent with strong gravity and magnetic anomalies consistent with a basement high below the dome. An impact model is consistent with the chaotic structure of the dome-structured core, centripetal sense of deformation, micro-brecciation and fluidization of the Triassic to Eocene rocks. The lack of shock metamorphic effects such as PDF, impact melt or coesite may be attributed to the attenuation of shock by high volatile pressure and the plastic nature of the carbonate-shale sediments. The Mount Ashmore dome is likely contemporaneous with a Late Eocene impact cluster (Popigai: $D \sim 100$ km, 35.7 ± 0.2 Ma; Chesapeake Bay: $D \sim 85$ km, 35.3 ± 0.1 Ma).

4.2.8 Yallalie ($D \sim 12$ km)

The Yallalie 12 km-diameter multi-ring buried impact structure, about 200 km north of Perth, Western Australia, is well expressed on magnetic and gravity images (Figs. 4.23a, b) (Dentith et al. 1992, 1999). The impact, which excavated Mesozoic rocks, is expressed at the surface as a weak circular topographic depression. Seismic data indicates deformation extending approximately 2 km below surface, including a central uplifted region 3–4 km in diameter (Dentith et al. 1999). Aeromagnetic data indicate five concentric ring anomalies, likely expressing magnetised impact melt or post-impact hydrothermal deposits, corresponding to faults and surrounding a single

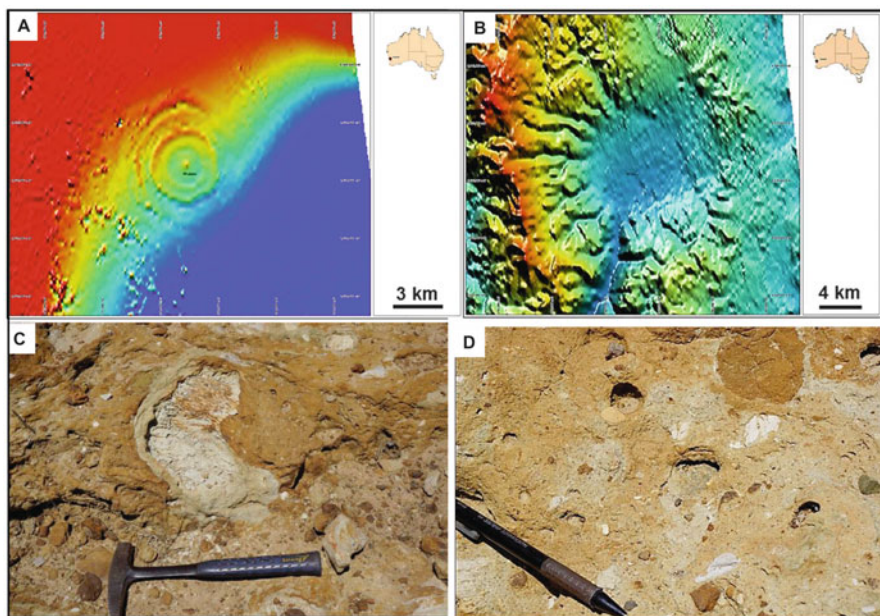


Fig. 4.23 Yallalie buried impact structure (Dentith et al. 1992, 1999). (a) Total magnetic intensity image; (b) Shaded Digital Elevation image; (c & d). Surface ejecta breccia (Courtesy G. Boxer) (http://members.iinet.net.au/~gboxer/4_Yallalie.html)

magnetic peak (Hawke 2003). Drilling indicate Pliocene lacustrine sediments to depth of 177 metres, overlying Cretaceous strata with an angular unconformity (Dentith et al. 1999). Planar fractures in quartz occurring between 430 and 460 metres depth are consistent with weak impact-induced shock. Allochthonous ejecta containing clasts up to 2 metres large occur ~4 km from the southwestern rim of the structure (Bevan et al. 2004) (Fig. 4.23c, d). The age of the impact is considered to approximate the Cretaceous Santonian to Campanian (Haines 2005).

4.2.9 Lake Raeside ($D \sim 11$ km)

Airborne total magnetic intensity data suggest an outline of an 11 km-diameter crater north of Lake Raeside, west of Leonora, Western Australia (Fig. 4.24a, b), consistent with a significant thickness of shock-metamorphosed breccia suggestive of the existence of an impact structure (Glikson et al. 2016). Drilling 60 km west of Leonora in 2008 intersected >95 m of poorly consolidated granitoid-dominated

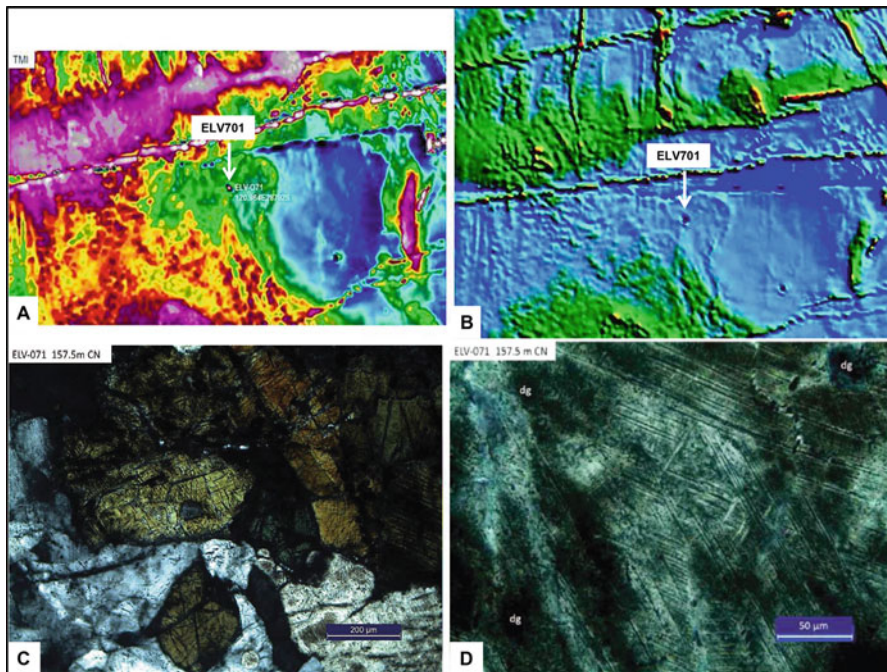


Fig. 4.24 Lake Raeside impact crater (Glikson et al. 2016). (a) Total magnetic intensity image, showing the location of drill hole ELV-701; (b) TMI image showing the half TMI circle to the east and north interpreted as the rim of the crater; (c) Planar deformation features in amphibole in the ELV701 core; (d) Planar deformation features in a quartz grain in the ELV701 core (With permission AJES)

breccia at the base of a Cenozoic paleochannel beneath Lake Raeside. The breccia, initially interpreted as a kimberlite, is composed of poorly consolidated fragments of granitic gneiss, felsite and metamorphosed mafic rock within a matrix of fine to medium-grained breccia. Microscopic examination revealed quartz grains displaying well-developed planar deformation features (PDFs) dominated by the {1013} planar set (Fig. 4.21c, d), diaplectic silica glass and diaplectic plagioclase glass. These features constitute the diagnostic hallmarks of shock metamorphism owing to high velocity impact of a large meteorite or asteroid.

4.3 Meteoritic Impact Craters

Due to the stability and antiquity of extensive land surfaces in the central and western parts of the Australian continent many small to medium size meteorite craters have been preserved while, on the other hand, poor outcrop, crater filling and weathering render their identification difficult. In several instances the identification of meteoritic iron fragments helped distinguish meteorite craters from morphological depressions.

4.3.1 *Goat Paddock (D~6 km)*

The Goat Paddock crater, western Proterozoic Kimberley Basin, is a ~5 km-diameter forms a rugged terrain and a depression (Harms et al. 1980; Milton and Macdonald 2005) (Fig. 4.25a–c) originally studied by Roberts et al. (1965), with an impact origin confirmed by melt breccia, silica glass, suevite, shatter cones (Fig. 4.25d) and shock metamorphism in quartz. The bedrock–breccia contact is sharp to gradual, including upturned bedrock and breccia resting over little-disturbed bedrock. Drilling indicates the crater is in-filled by ~200 meter lacustrine sediments dated by pollen as of Early Eocene age (Harms et al. 1980). Elongation of the crater in a N-S direction may suggest oblique meridional-oriented impact. Drill holes sited at the centre and midway out to the crater wall intersect shocked sandstone at depths of ~210 meter (Milton and Macdonald 2005; Haines 2005). Shatter coned clasts are incorporated in the breccia. The crater is partially filled by younger sediments, including bedded conglomerate grading inward to sand, silt and mudstone toward the centre.

4.3.2 *Liverpool (D~1.6 km)*

The circular Liverpool crater, northeast coast of the Northern Territory (Fig. 4.26), excavated in the Palaeoproterozoic Gumarrirri Sandstone, is located between

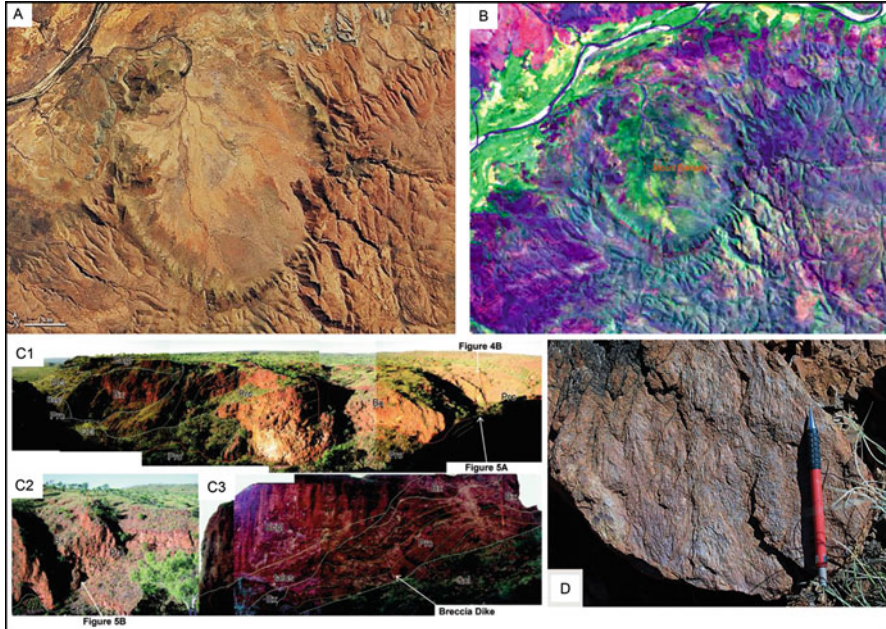


Fig. 4.25 Goat Paddock impact structure (Milton and Macdonald 2005). (a) LANDSAT image; (b) LANDSAT RGB741 image; (c1) Photomosaic of the northeast side of gorge in the east-southeast sector of Goat Paddock exhibiting relationships of disturbed bedrock (Prc) and impact breccia; (c2) Closer view of part of C1; (c3) Photomosaic of the north side of gorge entering Goat Paddock. Overturned bedrock is overlain above and crater-ward by impact breccia, both in turn overlain by post-crater talus and Eocene conglomerate. (d) Shatter cone from Goat Paddock impact crater. (AJES with permission)

the McArthur Basin and overlying Arafura Basin, displaying a raised rim ~1.6 km in diameter. (Rix 1965; Brett et al. 1970; Guppy et al. 1971). Subsequent investigations (Carson et al. 1999; Shoemaker and Shoemaker 1997; Shoemaker et al. 2005) indicate upturned target rocks and two distinct breccia units forming the outer circular ridge. Clasts in the allogenic breccia range from sand-sized to blocks several metres across, denoted as the Liverpool Breccia (Carson et al. 1999). A unit of undeformed sedimentary rocks is located within the ring of Liverpool Breccia, resting with sharp contact on the allogenic breccia. Asymmetries in the shape of the crater and the thickness of the suggest a low-angle impact from the southwest (Shoemaker and Shoemaker 1997). The age of the impact is constrained by the Palaeoproterozoic target rocks and post-impact likely Cretaceous sediments. The high degree of preservation of the crater suggests Liverpool is perhaps the world's oldest well-preserved simple impact crater (Haines 2005).



Fig. 4.26 Liverpool impact structure (Shoemaker et al. 2005). An oblique aerial photograph taken from the north. The white ring of resistant rock is allogenic breccia, which is cut by several small streams. The outer diameter of the ring of allogenic breccia measures ~ 1.6 km. (AJES with permission)

4.3.3 Darwin ($D \sim 1.2$ km)

The Darwin Crater (Ford 1972) forms a circular depression ~ 1.2 km in diameter (Fig. 4.27) located in Silurian metasediments in western Tasmania, identified in the course of a search for the source of Darwin glass distributed over 4400 km² of western Tasmania (Fudali and Ford 1979; Howard 2003; Howard and Haines 2004; Haines 2005). Gravity measurements indicate the depression is filled by a lens of lower density materials up to 230 m thick (Fudali and Ford 1979; Richardson 1991). Drilling intersected <60 m of mid-Pleistocene and younger lacustrine sediments overlying matrix-supported breccia containing rare Darwin glass fragments (Howard 2003; Howard and Haines 2004). An impact origin for Darwin Crater is supported by a trend of increasing size and abundance of glass fragment towards the crater (Fudali and Ford 1979; Howard and Haines 2004). The age of Darwin Crater is correlated with the 816 ± 7 year $^{40}\text{Ar}/^{39}\text{Ar}$ age of the Darwin glass (Haines 2005). Geochemical and isotopic studies show a close affinity between the glass, the stratigraphic units that host the crater, and crater fill breccia (Howard 2003; Howard and Haines 2004). However, as the volume of

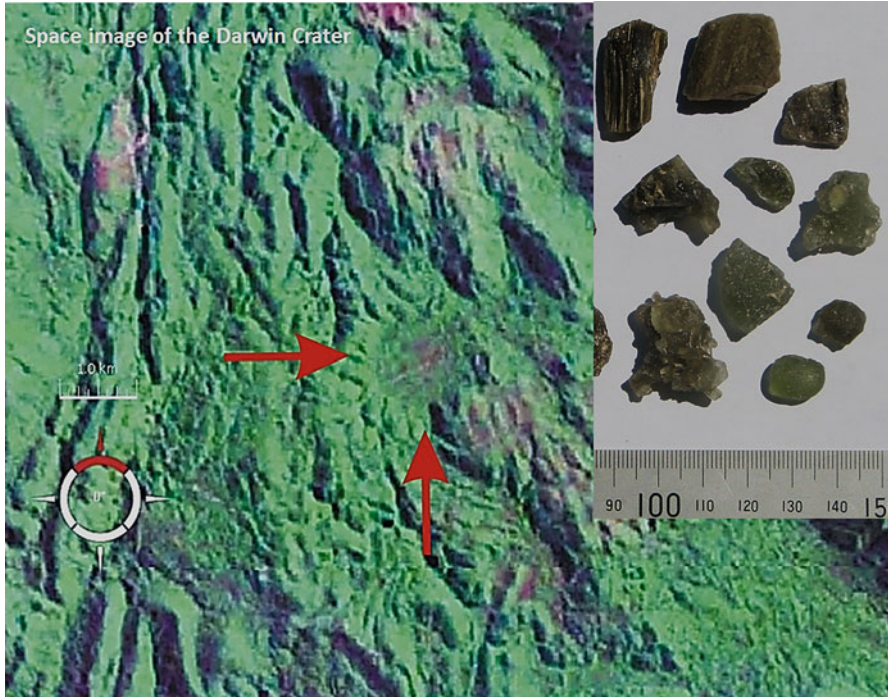


Fig. 4.27 Space image of the Darwin Crater, Southwestern Tasmania the Darwin Crater (https://en.wikipedia.org/wiki/Darwin_Crater#/media/File:Darwin_Crater_Landsat.jpg); Inset: tektites from (https://en.wikipedia.org/wiki/Darwin_glass#/media/File:Darwin_glass.jpg) (Public Domain)

widely dispersed Darwin glass exceeds that of the Darwin Crater Howard (2003) and Howard and Haines (2004) suggest a volatile-rich target.

4.3.4 Wolfe Creek ($D \sim 0.88$ km)

Wolfe Creek Meteorite Crater, with a diameter of ~ 880 meters (Fig. 4.28), located in northern Western Australia (Reeves and Chalmers 1949; Guppy and Matheson 1950; McNamara 1982), has been confirmed by scattered iron meteorite fragments (group IIIAB), decomposed iron oxide shale balls (La Paz 1954; Taylor 1965; Bevan 1996) and impact glass (Shoemaker et al. 2005). Target rocks consist of Devonian sandstone (Hawke 2003) in part overturned around the rim (Shoemaker and Shoemaker 1985). The crater floor lies ~ 50 m below the rim which rises on average about 35 m above the plain. From geophysical data the depth below surface to true crater floor varies from 120 m (O'Neill and Heine 2005) to 320 m (Hawke 2003). The distribution of meteoritic fragments and impact glass suggests oblique impact from the northeast (Shoemaker and

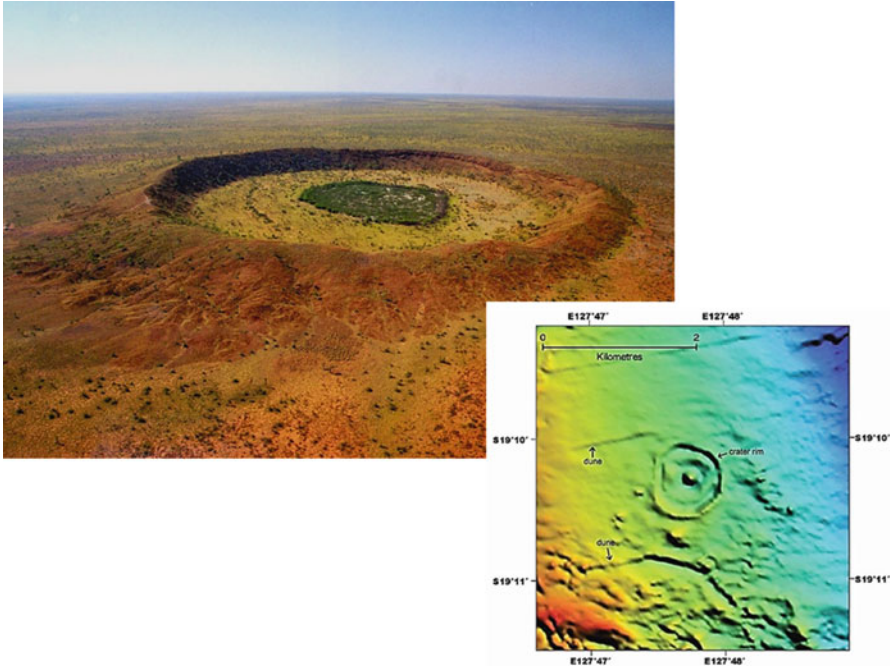


Fig. 4.28 Wolfe Creek crater, Western Australia. Wolfe Creek, oblique air photograph, by Dainis Dravins – Lund Observatory, Sweden; (with permission); inset: airborne magnetic image (Shoemaker et al. 2005) (AJES with permission)

Shoemaker 1985; Shoemaker et al. 2005; O’Neill and Heine 2005). The impact event is dated as ~300,000 years by $^{36}\text{Cl}/^{10}\text{Be}$ and $^{41}\text{Ca}/^{36}\text{Cl}$ methods, indicating the residence age of the meteorite (Shoemaker et al. 1990) (Haines 2005).

4.3.5 Hickman ($D\sim 0.36$ km)

The morphologically well-preserved Hickman Crater with a mean diameter of 260 meters (Fig. 4.29a, b), located in the Ophthalmia Range, Hamersley Basin, north Western Australia, ~36 km north of Newman, is excavated in the Paleoproterozoic Woongarra Rhyolite and the overlying Boolgeeda Iron Formation (Glikson et al. 2008). Rhyolite at the crater’s rim exhibits widespread shatter features injected by veins of goethite bound by sharply defined zones of hydrous alteration (Fig. 4.29d), interpreted in terms of forceful injection of aqueous iron-rich solutions, probably reflecting high-pressure hydrothermal activity by heated iron-rich ground water. Petrography of the rhyolite indicates possible incipient intracrystalline dislocations in quartz (Fig. 4.29c). The Boolgeeda Iron Formation, which crops out on the

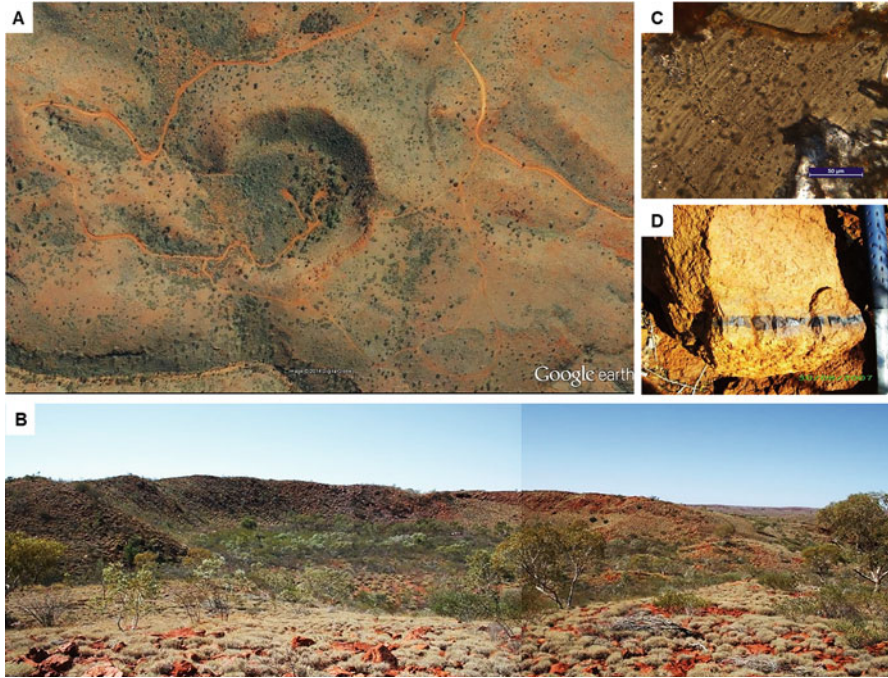


Fig. 4.29 Hickman impact crater (Glikson et al. 2008). (a) Space Google Earth image; (b) Surface photo-mosaic (courtesy A.H. Hickman); (c) incipient planar deformation features in quartz; (d) Goethite vein in felsic hypabyssal rocks (AJES with permission)

southern rim of the crater, displays brecciation and mega-brecciation superposed on fold structures typical of the banded iron-formations in the region. The iron-enrichment of the fractured rhyolite is attributed to a hydrothermal system affecting both the Boolgeeda Iron Formation and the Woongarra Rhyolite, and localised to the area of the crater. A minor north–south asymmetry of the crater, and an abundance of ejecta up to about 300 m northwest and northeast of the crater, suggest high-angle impact from the south. Drilling at the centre of the crater intersected melt-bearing breccia showing strong enrichment in Ni, Co, Au and PGE with respect to the basement and infilling sediments (Haines 2014). PGE inter-element ratios in the breccia are closer to meteorites than to average continental crust. The high Ni level is consistent with an iron meteorite projectile. The lack of shock metamorphism and unusually high meteoritic component of the breccia may be explained by significant atmospheric deceleration of a relatively small projectile prior to impact. A youthful age of the structure, probably Late Pleistocene (10^4 – 10^5 years) is indicated by damming of the drainage of a south-southeast-flowing creek by the southern crater rim. (Glikson et al. 2008).

4.3.6 Boxhole ($D \sim 0.17$ km)

The Boxhole crater of 170 meters diameter (Fig. 4.30a, b), located ~ 180 km north-east of Alice Springs, is estimated as 5400 ± 1500 years-old from ^{14}C isotope, was discovered in 1937 by Joe Webb and Cecil Madigan who identified nickel-bearing iron fragments, breccia (Fig. 4.30c) and ferruginous shale balls. The crater, excavated in Proterozoic schist and gneiss, has a raised rim displaying inverted stratigraphy (Shoemaker et al. 2005). The meteorite of group IIIAB medium octahedrite, includes an 82 kg fragment (Bevan 1996) and Ni-Fe spherules (Hodge and Wright 1973). A suggestion that Boxhole and Henbury may represent a paired fall (Milton 1972) has not been confirmed. Two different age determinations were reported for the Boxhole meteorite impact: A ^{14}C terrestrial exposure age of $5.4 \pm 1.5 \cdot 10^3$ years (Kohman and Goel 1963), and a $^{10}\text{Be}/^{26}\text{Al}$ exposure age of $\sim 30 \cdot 10^3$ years for quartz ejecta (Shoemaker et al. 1990) (Haines 2005).

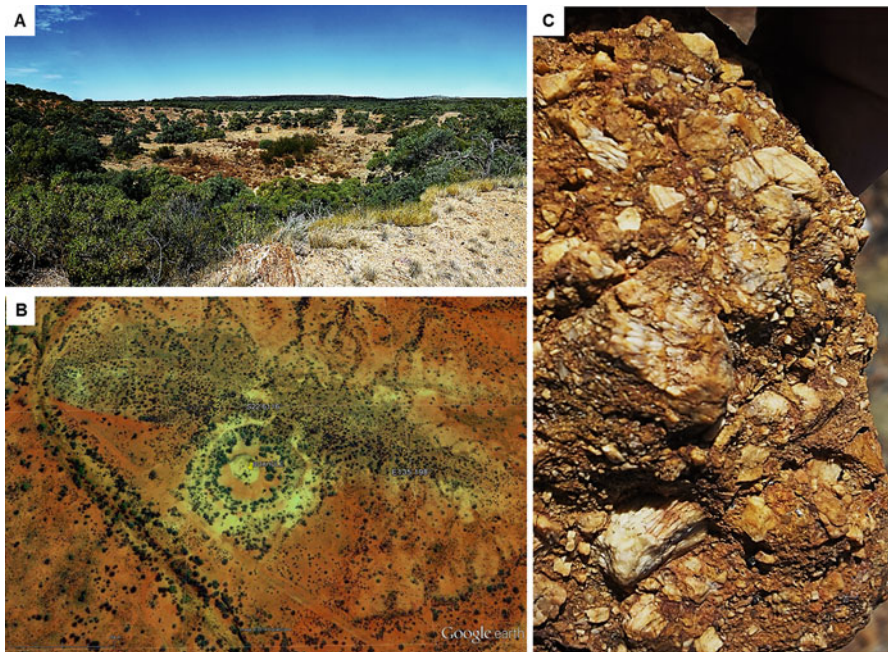


Fig. 4.30 Boxhole crater, central Australia; (a) A surface view of the crater; (b) A vertical Google Earth view (https://commons.wikimedia.org/wiki/Category:Impact_craters_of_Australia#/media/File:Boxhole_meteorite_crater.jpg); (c) Rim breccia (Courtesy of D. Hamacher)

4.3.7 Henbury Craters

The 13 or 14 Henbury crater field (Fig. 4.31a–d) is located in Neoproterozoic sandstone and mudstone of the Amadeus Basin strewn with iron meteorite fragments of Group IIIAB medium octahedrite (Bevan 1996) (Fig. 4.31f) and droplets of black impact glass. Craters including explosion craters and fragmentation pits have diameters range from 6 to 180 meters (Fig. 4.31a–d), the largest being an elongated double crater (Milton 1972). The larger craters are bowl-shaped with overturned flaps containing deformed sandstone (Fig. 4.21e) around the rims (Milton 1972), with one crater displaying a well-developed downrange ejecta ray. The crater field is clearly the result of atmospheric breakup of a projectile travelling with an oblique trajectory from the southwest (Passey and Melosh 1980). Based on the cosmogenic ^{14}C terrestrial age of the meteorite the age of the Henbury craters is interpreted as 4200 + 1900 years (Kohman and Goel 1963). There is a suggestion the impact event is recorded in the oral traditions of the local Aboriginal tribe (Haines 2005).

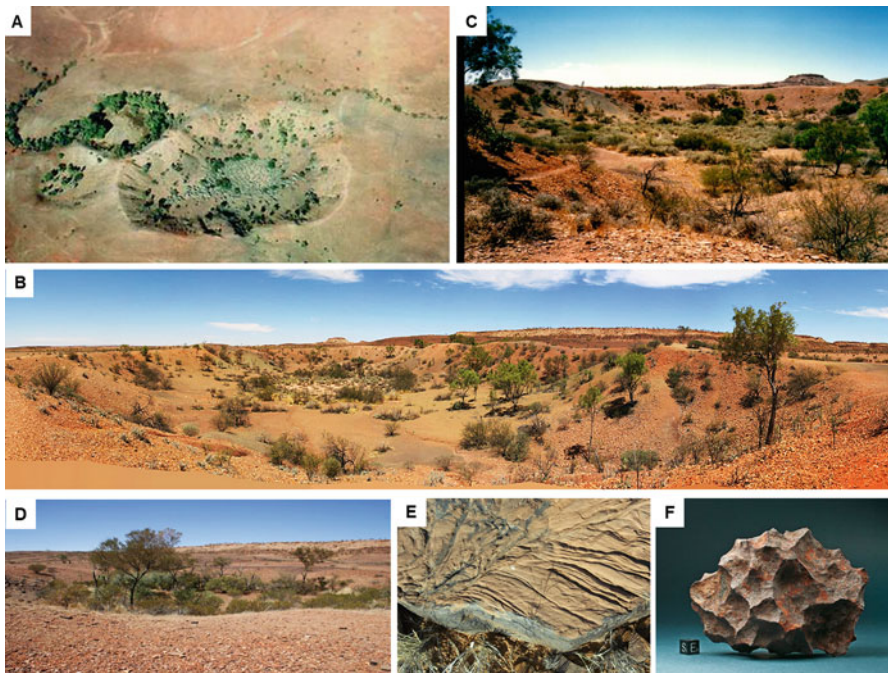


Fig. 4.31 Henbury impact craters. (a). An aerial view of the 3 larger craters. Twelve craters formed at the surface 4700 years ago; (b & c). Photographs of the largest crater (https://en.wikipedia.org/wiki/Henbury_Meteorites_Conservation_Reserve#/media/File:Henbury_Crater.jpg); (d) A photograph of one of the smaller craters (courtesy D. Hamacher); (e) Deformation features at the crater rim; (f) A meteorite fragment (https://commons.wikimedia.org/wiki/File:Henbury_Meteorite.jpg)

References

- Abels A (2005) Spider impact structure, Kimberley Plateau, Western Australia: interpretations of formation mechanism and age based on integrated map-scale data. *Aust J Earth Sci* 52:653–663
- Beere GM (1983) The Piccaninny structure – a cryptoexplosive feature in the Ord Basin, East Kimberly. Geological Survey of Western Australia Record 1983/6
- Bevan A (1996) Meteorites recovered from Australia. *J R Soc of West Aust* 79(1):33–42
- Bevan A, Hough R, Hawke (2004) Morphology and origin of an allochthonous breccia near the Yallalie structure, Western Australia: evidence for subaqueous impact? *Geol Soc Aust Abstr* 73:227
- Boxer (2014) Grant boxer webpages. <http://members.iinet.net.au/~gboxer/Index.html>
- Brett R, Guppy DJ, Milton DJ (1970) Two circular structures of impact origin in Northern territory Australia. *Meteorit* 5:184
- Bron KA, Gostin V (2012) The Tookoonooka marine impact horizon Australia: sedimentary and petrologic evidence. *Meteorit Planet Sci* 47:296–318
- Brown AR (1973) A detailed seismic study of Gosses Bluff, Northern territory, Bureau of Mineral Resources Report 163. Australian Government Publishing Service, Canberra
- Bunting JA, de Laeter JR, Libby WG (1980) Evidence for the age and cryptoexplosive origin of the Teague ring structure Western Australia. *Geol Surv W Aust Ann Rev* 1980:81–85
- Butler H (1974) The Lake Teague ring structure Western Australia: an astrobleme? *Search* 5:536–537
- Carson LJ, Haines PW, Brakel A, Pietsch BA, Ferenczi PA (1999) Millingimbi, Northern territory, 1:250 000 geological series explanatory notes SD53–2, Northern territory geological survey, Darwin
- Crook KA, Cook PJ (1966) Gosses Bluff diaper, cryptovolcanic structure, or astroblemes. *J Geol Soc Aust* 13:495–516
- Darlington V et al (2016) The Lawn Hill annulus: an Ordovician meteorite impact into water-saturated dolomite. <https://researchonline.jcu.edu.au/47631/>
- Dentith MC, Bevan AWR, McInerney KB (1992) A preliminary investigation of the Yallalie Basin: a buried 15 km diameter structure of possible impact origin in the Perth Basin, WA. *Meteoritics* 27:214
- Dentith MC, Bevan AWR, Backhouse J, Featherstone WE, Koeberl C (1999) Yallalie: a buried structure of possible impact origin in the Perth Basin, West Aust. *Geol Mag* 136:619–632
- Dunster JN, Haines PW, Munson TJ (2014) Meteorites and impact structures in the Northern territory. *Northern Territory Geol Surv Rec* 2014:007
- Ford RJ (1972) A possible impact crater associated with Darwin glass. *Earth Planet Sci Lett* 16:228–230
- Fudali RF, Ford RJ (1979) Darwin glass and Darwin crater: a progress report. *Meteoritics* 14:283–296
- Glikson AY (1969) Geology of the outer zone of the Gosses Bluff crypto-explosion structure, Northern Territory. *Bur Min Resour Rec.* 1969/42
- Glikson AY (2008) Field evidence of Eros-scale asteroids and impact-forcing of Precambrian geodynamic episodes, Kaapvaal (South Africa) and Pilbara (Western Australia) Cratons. *Earth Planet Sci Lett* 267:558–570
- Glikson AY, Eggins S, Golding S, Haines P, Iasky RP, Mernagh TP, Mory AJ, Pirajno F, Uysal IT (2005a) Microchemistry and microstructures of hydrothermally altered shock-metamorphosed basement gneiss, Woodleigh impact structure, Southern Carnarvon Basin, Western Australia. *Aust J Earth Sci* 52:555–573
- Glikson A, Mory AJ, Iasky R, Pirajno F, Golding S, Uysal IT (2005b) Woodleigh, Southern Carnarvon Basin, Western Australia: history of discovery late Devonian age and geophysical and morphometric evidence for a 120 km-diameter impact structure. *Aust J Earth Sci* 52:545–553

- Glikson AY, Hickman AH, Vickers J (2008) Hickman Crater, Ophthalmia Range, Western Australia: evidence supporting a meteorite impact origin. *Aust J Earth Sci* 55:1107–1117
- Glikson AY, Jablonski D, Westlake S (2010) Origin of the Mount Ashmore structural dome west Bonaparte basin Timor Sea. *Aust J Earth Sci* 57:411–430
- Glikson AY, Uysal IT, Fitz Gerald JD, Saygin E (2013) Geophysical anomalies and quartz microstructures, Eastern Warburton Basin, North-east South Australia: tectonic or impact shock metamorphic origin? *Tectonophysics* 589:57–76
- Glikson AY, Meixner AJ, Radke B, Uysal IT, Saygin E, Vickers J, Mernagh TP (2015) Geophysical anomalies and quartz deformation of the Warburton West structure, central Australia. *Tectonophysics* 643:55–72
- Glikson AY, Hickman AH, Evans NJ, Kirkland CI, Jung-WP RR, Romano S (2016) A new 3.46 Ga asteroid impact ejecta unit at Marble Bar, Pilbara Craton, Western Australia: a petrological, microprobe and laser ablation ICPMS study. *Precamb Res* 279:103–122
- Gorter JD, Glikson AY (2012) Talundilly Western Queensland Australia: geophysical and petrological evidence for an 84 km-large impact structure and an early cretaceous impact cluster. *Aust J Earth Sci* 59:51–73
- Gorter JD, Gostin VA, Plummer P (1989) The Tookoonooka structure: an enigmatic sub-surface feature in the Eromanga basin its impact origin and implications for petroleum exploration In: O’Neil BJ (ed) *The Cooper and Eromanga basins Australia: Proceedings of the Cooper and Eromanga Basins conference Adelaide*, pp 441–456
- Gostin VA, Therriault AM (1997) Tookoonooka: a large buried early Cretaceous impact structure in the Eromanga basin of southwestern Queensland Australia. *Meteorit Planet Sci* 32:593–599
- Gostin VA, Zbik M (1999) Petrology and microstructure of distal impact ejecta from the Flinders Ranges, Australia. *Meteorit Planet Sci* 34:587–592
- Gostin VA, Haines PW, Jenkins RJF, Compston W, Williams IS (1986) Impact ejecta horizon within late Precambrian shales, Adelaide Geosyncline, South Australia. *Science* 233:198–200
- Gradstein FM, Ogg JG, Smith AG, Bleeker W, Laurens LJ (2004) A new geologic timescale with special reference to Precambrian and Neogene. *Episodes* 72:83–100
- Grey K, Walter MR, Calver CR (2003) Neoproterozoic biotic diversification: snowball earth or aftermath of the Acraman impact? *Geology* 31:469–472
- Guppy DJ, Matherson RS (1950) Wolfe Creek meteorite crater, Western Australia. *J Geol* 58:30–36
- Guppy DJ, Brett R, Milton DJ (1971) Liverpool and strangways craters, Northern territory; two structures of probable impact origin. *J Geophys Res* 76:5387–5393
- Haines PW (1996) Goyder impact structure, Arnhem land, Northern territory. *AGSO J Aust Geol Geophys* 16:561–566
- Haines PW (2005) Impact cratering and distal ejecta: the Australian record. *Aust J Earth Sci* 52:481–507
- Haines PW (2014) Collaborative scientific drilling at Hickman Crater. *GSWA extended abstracts 2014, GSWA Record 2014/2*, p. 1–4
- Haines PW, Rawlings DJ (2002) The Foelsche structure, Northern territory, Australia: an impact crater of probable Neoproterozoic age. *Meteorit Planet Sci* 37:269–280
- Haines PW, Therriault AM, Kelly SP (1999) Evidence for mid-Cenozoic(?) low-angle multiple impacts in South Australia. *Meteorit Planet Sci* 34(Suppl):A49–A50
- Haines P, Sweet I, Mitchell K (2012) The Cleanskin structure. 75th annual meteoritical society meeting. <https://www.lpi.usra.edu/meetings/metsoc2012/pdf/5176.pdf>
- Harms JE, Milton DJ, Ferguson J, Gilbert DJ, Harris WK, Golby B (1980) Goat Paddock cryptoexplosion crater, Western Australia. *Nature* 286:704–706
- Hawke PJ (2003) Some ring-like magnetic anomalies in impact structures and their possible causes. 3rd international conference on large meteorite impacts conference, August 2003, Nordlingen, Germany, abstract 4064
- Hill AC, Grey K, Gostin VA, Webster LJ (2004) New records of late neoproterozoic Acraman ejecta in the officer basin. *Aust J Earth Sci* 51:47–51
- Hodge PW, Wright FW (1973) Particles around Boxhole meteorite crater. *Meteoritics* 8:315–320

- Howard KT (2003) Geochemical systematics in Darwin impact glass. *Meteorit Planet Sci* 38 (Suppl):A47
- Howard KT, Haines P (2004) Fire in the sky above SW Tasmania: the Darwin meteorite impact. *Geological Society of Australia Abstracts* 73:235
- Iasky RP, Glikson AY (2005) Gnargoo: a possible 75 km-diameter post-early Permian–pre-cretaceous buried impact structure Carnarvon Basin Western Australia. *Aust J Earth Sci* 52:577–586
- Iasky RP, Mory AJ, Blundell KA (2001) The geophysical interpretation of the Woodleigh impact structure Southern Carnarvon Basin. *West Aust Geol Surv of West Aust Rep* 79
- Kohman TP, Goel PS (1963) Terrestrial ages of meteorites from cosmogenic ^{14}C . In: *Radioactive dating*. International Atomic Energy Agency, Vienna, pp 395–311
- La Paz L (1954) Meteoritic material from the Wolf Creek, Western Australia, meteorite crater. *Meteoritics* 1:200–203
- Longley IM (1989) The Talundilly anomaly and its implications for hydrocarbon exploration of Eromanga astrolems. In: O’Neil BJ (ed), *The Cooper and Eromanga Basins, Australia: Proceedings of the Cooper and Eromanga Basins Conference*, Adelaide, pp 473–490. Petroleum Exploration Society of Australia, Society of Petroleum Engineers, Australian Society of Exploration Geophysicists (SA Branches)
- Macdonald FA, Mitchell K (2003) Amelia Creek, Northern Territory, Australia: a 20×12 km oblique impact structure with no central uplift. *Impact Cratering: Bridging the Gap Between Modelling and Observations*, February 2003, Houston, Texas, p 47. Lunar and Planetary Institute Contribution 1155
- Macdonald F, Mitchell K (2004) New possible, probable, and proven impact sites in Australia. *Geol Soc Aust Abstr* 73:239
- Macdonald FA, Wingate MTD, Mitchell K (2005) Geology and age of the Glikson impact structure, Western Australia. *Aust J Earth Sci* 52:641
- Madigan CT (1937) The Boxhole crater and the Huckitta meteorite (central Australia). *Trans Proc R Soc S Aust* 6:187–190
- McHone JF, Greeley R, Williams KK, Blumberg DG, Kuzmin RO (2002) Space shuttle observations of terrestrial impact structures using SIR –C and X–SAR radars. *Meteorit Planet Sci* 37:407–420
- McNamara K (1982) Wolf Creek Crater. Western Australian Museum/Advance Press, Perth
- Milton DJ (1968) Structural geology of the Henbury meteorite craters, Northern Territory, Australia. *Geological Survey professional paper* 599-C
- Milton DJ, Macdonald FA (2005) Goat Paddock, Western Australia: an impact crater near the simple – complex transition. *Aust J Earth Sci* 52:691–698
- Milton DJ, Sutter JF (1987) Revised age for the Gosses Bluff impact structure, Northern territory, Australia, based on $^{40}\text{Ar}/^{39}\text{Ar}$ dating. *Meteoritics* 22:281–289. *y & Geophysics* 16, 453 – 486
- Milton DJ, Barlow DJ, Brett R, Brown A, Manwaring EA, Moss FJ, Sedmik E, Van Son J, Young A (1972) Gosses Bluff impact structure, Australia. *Science* 175:1199–1207
- Milton DJ, Glikson AY, Brett R (1996a) Gosses Bluff—a latest Jurassic impact structure, central Australia. Part 1: geological structure, stratigraphy, and origin. *AGSO Journal of Australian Geological structure stratigraphy and origin*. *AGSO J Aust Geol Geophys* 16:453–486
- Milton DJ, Barlow DJ, Brett R, Brown A, Manwaring EA, Moss FJ, Sedmik E, Van Son J, Young A (1996b) Gosses Bluff—a latest Jurassic impact structure, central Australia. Part 2: seismic, magmatic, and gravity studies. *AGSO J Aust Geol Geophys* 16:487–527
- Mory AJ, Iasky RP, Glikson AY, Pirajno F (2000) Woodleigh Carnarvon basin, Western Australia: a new 120 km-diameter impact structure. *Earth Planet Sci Lett* 177:119–128
- Nininger HH, Huss GI (1960) The unique meteorite crater at Dalgarganga, Western Australia. *Mineral Mag* 32:619–639

- O'Neill C, Heine C (2005) Reconstructing the Wolfe Creek Meteorite impact: deep structure of the crater and effects on target rock. *Aust J Earth Sci* 52:699–710
- Passy QR, Melosh HJ (1980) Effects of Atmospheric Breakup on Crater Field Formation. *Icarus* 42:211–233
- Pirajno F (2005) Hydrothermal processes associated with meteorite impact structures: the evidence from three Australian examples and implications for economic resources. *Aust J Earth Sci* 52:587–605
- Pirajno F, Glikson AY (1998) Shoemaker impact structure Western Australia (formerly Teague ring structure). *Celest Mech Dyn Astron* 69:25–30
- Pirajno F, Hawke P, Glikson AY, Haines PW, Uysal T (2003) Shoemaker impact structure Western Australia. *Aust J Earth Sci* 50:775
- Plescia JB (1999) Gravity signature of Teague Ring impact structure, Western Australia. *Geol Soc Am Spec Pap* 339:165–175
- Plescia JB (2006) Kelly West impact structure. *Lunar Planet Sci XXXVII*(2006)
- Reeves F, Chalmers RO (1949) The Wolf Creek crater. *Aust J Sci* 11:145–156
- Richardson RG (1991) Geophysical surveys of Darwin crater. *Geophys Down Under* 13:13–14
- Rix P (1965) Milimimbi, Northern Territory, 1:250 000 Geological Series Explanatory Notes SD53–2. Bureau of Mineral Resources, Canberra
- Roberts HG, Halligan R, Gemuts I (1965) Geology of the Mount Ramsay 1:250 000 sheet area, E/52–9, Western Australia. Bureau of Mineral Resources Record 1965/156
- Salisbury JA, Tomkins AG, Schaefer BF (2008) New insights into the size and timing of the Lawn Hill impact structure: relationships to the Century Zn-Pb deposit. *Aust J Earth Sci* 55:587–603
- Saygin E, Kennett BLN (2010) Ancient seismic tomography of the Australian continent. *Tectonophysics* 481:116–125
- Saygin E, Kennett BLN (2012) Crustal structure of Australia from ambient seismic noise tomography. *J Geophys Res* 117:B01304
- Shoemaker EM, Shoemaker CS (1985) Impact structures of Western Australia. *Meteoritics* 20:754–756
- Shoemaker EM, Shoemaker CS (1986) Connolly Basin: a probable eroded impact crater in Western Australia. *Lunar Planet Sci Conf XVII*:797–798
- Shoemaker EM, Shoemaker CS (1988) The Spider impact structure, Western Australia. *Geol Soc Am Abstr Programs* 20:147
- Shoemaker EM, Shoemaker CS (1996) The Proterozoic impact record of Australia. *Aust Geol Surv Org J Aust Geol Geophys* 16:379–398
- Shoemaker EM, Shoemaker CS (1997) Notes on the geology of Liverpool Crater, Northern Territory, Australia. *Lunar and Planetary Science Conference XXVIII*, abstract 1662
- Shoemaker EM, Shoemaker CS, Nishiizumi K, Kohl CP, Arnold J, Klein J, Fink D, Middleton R, Kubik PW, Sharma P (1990) Ages of Australian meteorite craters; a preliminary report. *Meteoritics* 25:409
- Shoemaker EM, Macdonald FA, Shoemaker CS (2005) Geology of five small Australian impact craters. *Aust J Earth Sci* 52:529–544
- Spray JG, Kelley SP, Dence MR (1999) The Strangways impact structure, Northern territory, Australia: geological setting and laser probe $^{40}\text{Ar}/^{39}\text{Ar}$ geochronology. *Earth Planet Sci Lett* 172:199–211
- Stewart A, Mitchell K (1987) Shatter cones at the Lawn Hill circular structure, northwestern Queensland; presumed astrobleme. *Aust J Earth Sci* 34:477–485
- Sweet IP, Haines PW, Mitchell K (2005) The Matt Wilson structure: record of an impact event of possible Early Mesoproterozoic age, Northern territory. *Aust J Earth Sci* 52:675–689
- Taylor SR (1965) The Wolf Creek iron meteorite. *Nature* 208:944–945
- Tonkin PC (1973) Discovery of shatter cones at Kelly West near Tennant Creek, Northern territory, Australia. *J Geol Soc Aust* 20:99–102

- Uysal T, Golding SD, Glikson AY, Mory AJ, Glikson M (2001) K–Ar evidence from illitic clays of a Late Devonian age for the 120 km diameter Woodleigh impact structure, southern Carnarvon Basin, Western Australia. *Earth Planet Sci Lett* 192:281–289
- Wallace MW, Gostin VA, Keays RR (1990) Spherules and shard-like clasts from the late Proterozoic Acraman impact ejecta horizon, South Australia. *Meteoritics* 25:161–165
- Wallace MW, Gostin VA, Keays RR (1996) Sedimentology of the Neoproterozoic Acraman impact-ejecta horizon, South Australia. *AGSO J Aust Geol Geophys* 16:443–451
- Williams GE (1986) The Acraman impact structure; source of ejecta in late Precambrian shales, South Australia. *Science* 233:200–203
- Williams GE, Gostin VA (2005) The Acraman – Bunyeroo impact event (Ediacaran), South Australia, and environmental consequences: 25 years on. *Aust J Earth Sci* 52:607–620
- Williams GE, Schmidt PW (2015) Low paleolatitude for the late Cryogenian interglacial succession, South Australia: paleomagnetism of the Angepena Formation, Adelaide Geosyncline. *Aust J Earth Sci* 62:243–253
- Williams GE, Wallace MW (2003) The Acraman asteroid impact, South Australia: magnitude and implications for the late Vendian environment. *J Geol Soc Lond* 160:545–554
- Williams GE, Schmidt PW, Boyd DM (1996) Magnetic signature and morphology of the Acraman impact structure, South Australia. *AGSO J Aust Geol Geophys* 16:431–442
- Yeates AN, Crowe RWA, Towner RR (1976) The Veevers Crater; a possible meteoritic feature. *BMR J Aust Geol Geophys* 1:77–78
- Youles IP (1976) Mount Toondina impact structure. *Geol Surv S Aust Q Geol Notes* 60:10–12
- Zummersprekel H, Bischoff L (2005) Remote sensing and geographic information system analyses of the Strangways impact structure, Northern territory. *Aust J Earth Sci* 52:621–630

Chapter 5

Ring and Dome Features, Possible and Probable Impact Structures



Abstract Circular drainage patterns, round lakes and oval depressions may provide hints of possible underlying ring or dome structures, requiring field tests or drilling where no outcrop occurs (Grieve RAF, Pilkington M, Aust Geol Surv J Aust Geol Geophys 16:399–420, 1996; Glikson AY, Uysal IT, Earth-Sci Rev 125:114–122, 2013). Structural domes and near-circular fold structures may initially be mistaken for impact structures, as are basins of approximately circular or slightly elongate pattern and plutonic domes such as oval granite intrusions, laccoliths and gabbro plugs. In orogenic belts, domes may be produced by compression and associated folding, including folding fold sets with different trends producing domes at the culminations of crossing anticlines. Diapirs are cored by relatively low-density rocks or magma, an example being granite domes rising in response to the gravity instability of the granitic magma relative to the denser country rocks. Circular drainage patterns, round lakes and oval depressions may provide hints of possible underlying ring or dome structures, requiring field tests or drilling where no outcrop occurs (Grieve RAF, Pilkington M, Aust Geol Surv J Aust Geol Geophys 16:399–420, 1996; Glikson AY, Uysal IT, Earth-Sci Rev 125:114–122, 2013). Structural domes and near-circular fold structures may initially be mistaken for impact structures, as are basins of approximately circular or slightly elongate pattern and plutonic domes such as oval granite intrusions, laccoliths and gabbro plugs. In orogenic belts domes may be produced by compression and associated folding, including folding fold sets with different trends producing domes at the culminations of crossing anticlines. Diapirs are cored by relatively low-density rocks or magma, an example being granite domes rising in response to the gravity instability of the granitic magma relative to the denser country rocks.

5.1 Structural Elements of Circular Features Suggestive of an Impact Origin

This paper documents 43 exposed and buried ring structures many of which of unknown origin but some of possible to probable impact origin (Figs. 5.1, 5.2, 5.3, 5.4, 5.5, 5.6, 5.7, 5.8, 5.9, 5.10, 5.11, 5.12, 5.13, 5.14, 5.15, 5.16, 5.17a, 5.17b, 5.17c, 5.18, 5.19 and 5.20). Structural elements suggestive of an impact origin include:

1. Intersections of older structures by external rings of the ring feature, as displayed for example by the Chicxulub impact structure (Sharpton et al. 1996), the Woodleigh impact structure (Fig. 3.8) (Gliksion et al. 2005a, b), the Gnargoo probable impact structure (Fig. 4.21) (Iasky and Gliksion 2005; Gliksion and Uysal 2013) and the Shoemaker impact structure (Pirajno et al. 2003) (Figs. 4.5 and 4.6). Whereas

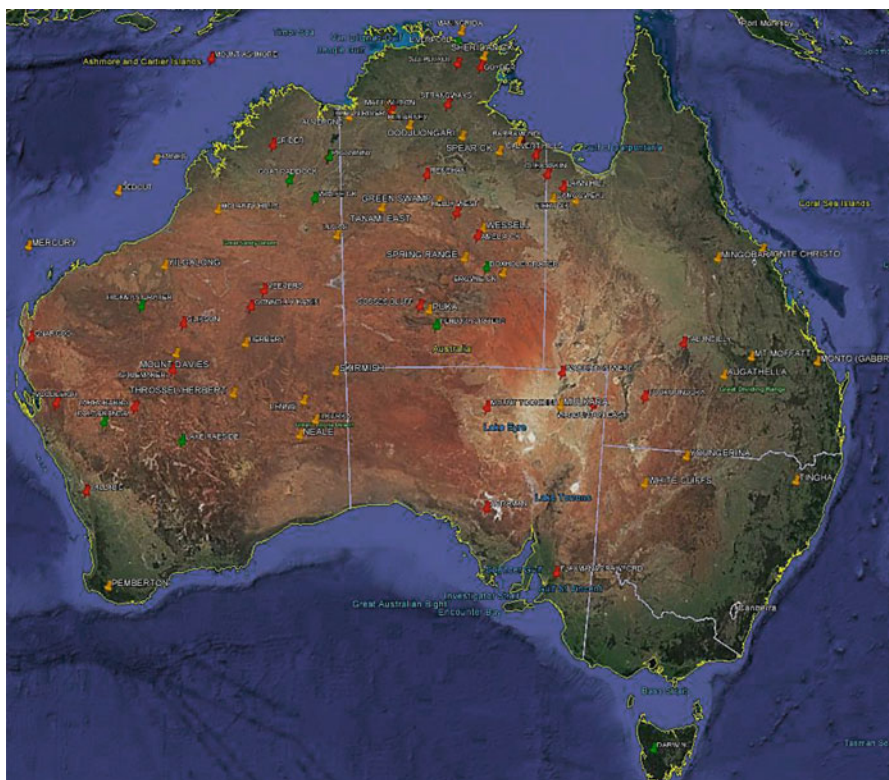


Fig. 5.1 Distribution of confirmed impact structures and ring and dome features of undetermined origin, igneous origin and possible to probable impact origin on the Australian continent and continental shelf. Red pins – confirmed impact structures; green pins – confirmed impact craters; orange pins – features of undetermined, igneous and possible to probable impact origin (Elsevier, with permission)

structurally discordant intersections are also displayed by volcanic diatremes, igneous plugs and salt domes, a presence of a central uplift core or dome fringed by a ring syncline is consistent with diagnostic features of impact structures;

2. The central uplifts of impact structures are well defined in seismic reflection sections where the uplift is commonly associated with inward-verging thrust faults, as in the Woodleigh impact structure (Iasky et al. 2001) (Fig. 3.8) and the Spider impact structure (Abels 2005) (Fig. 4.16).
3. An intersection of the top of the dome or a basement uplift by unconformably overlying post-impact sediments is typical of impact structures, as demonstrated in the Woodleigh (Fig. 3.8), Gnargoo (Fig. 4.21), Mount Ashmore (Fig. 4.22) and Tookoonooka (Fig. 4.20) structures. Post-impact isostatic vertical movements are indicated where the central uplift pierces through the unconformity, as in the Mount Ashmore structure (Fig. 4.22).

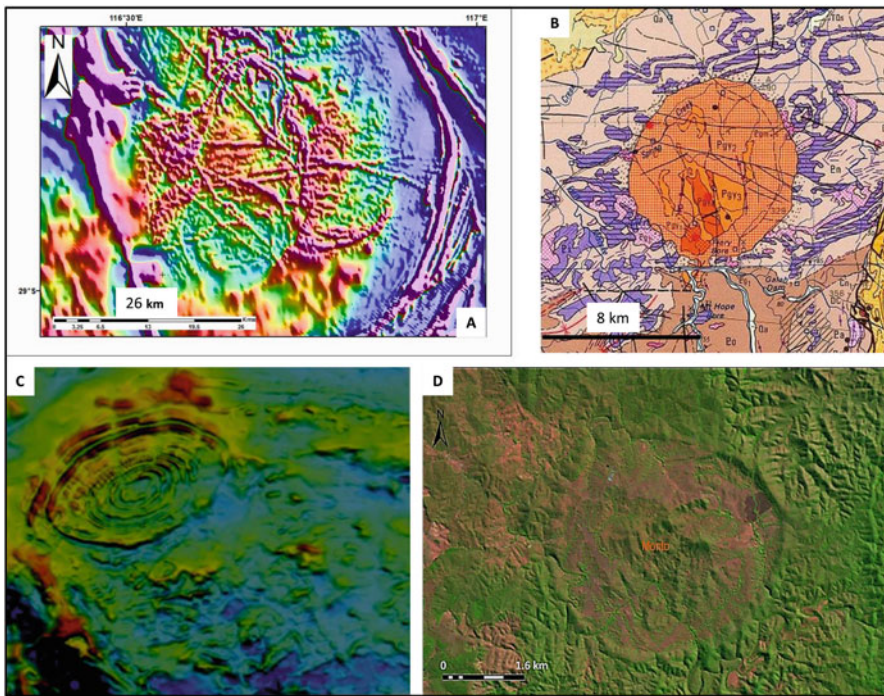


Fig. 5.2 Plutonic ring and dome structures: (a) Total magnetic intensity image of *Windinie Hills* circular granite, Yalgoo Goldfield, Murchison Province, Western Australia (GA Creative Commons); (b) Geological map of the *Yataga* Granodiorite, northern Queensland (GA Creative Commons); (c) TMI image of the Saturn mafic-ultramafic magnetite-bearing multi-ring intrusion, Giles Complex, Blackstone region, Western Australia (Maier et al. 2014; GSWA with permission); (d) Google Earth image of the Monto, Goondicum gabbro plug, NE Queensland. (Elsevier, with permission)

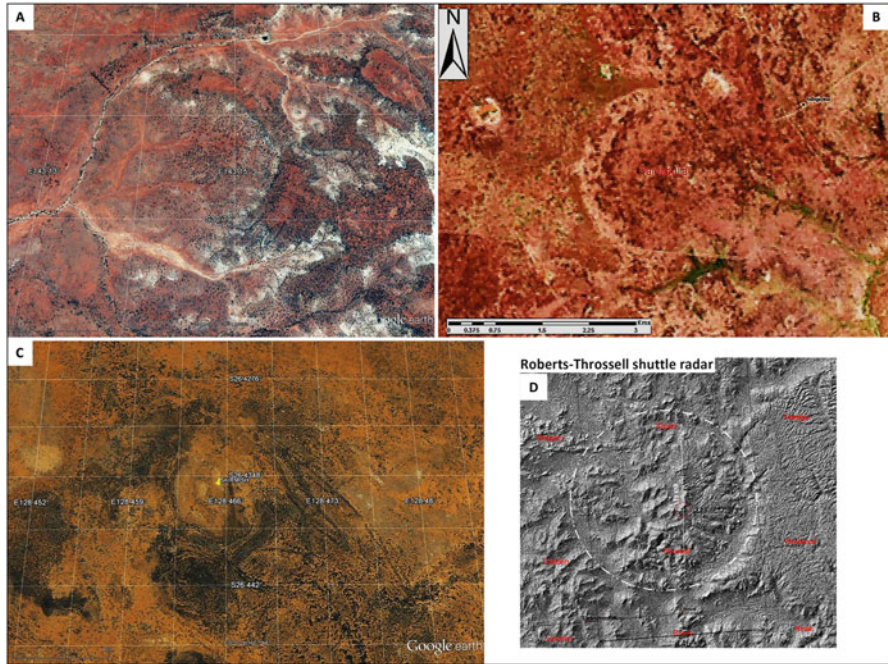


Fig. 5.3 (a) Google Earth image of the White Cliffs semi-circular morphological feature, western New South Wales; (b) The Youngerina circular drainage feature, northern New South Wales; (c) Google Earth image of the Skirmish feature, Western Australia; (d) Shuttle Radar image of the Throssell-Roberts half circular feature. The thin discontinuous white circle demarcates the approximate limits of the apparent feature (GA Creative Commons; Elsevier, with permission)

Where the core of the structure consists of sedimentary strata, a structural dome is outlined containing chaotically disrupted core zones which display a loss of seismic markers associated with mega-brecciation, as in the Mount Ashmore probable impact structure (Glikson and Vickers 2010). By contrast to thrust faults around and within central core zones, ring synclines and outer rims of impact structures display inward-dipping normal faults. These structural patterns represent centripetal and upward block movements involving compression around the uplifted core or plug and inward collapse of the crater rim, evident in the Woodleigh, Gnargoo and Talundilly structures. In addition, some impact structures and probable impact structures display uplift of crystalline basement below impacted sediments, as in the Woodleigh impact structure (Jasky et al. 2001; Glikson et al. 2005a, b), the Mount Ashmore probable impact structure (Glikson and Vickers 2010) and as magnetic highs at the centres of the Warburton impact structures (Glikson et al. 2013, 2015).

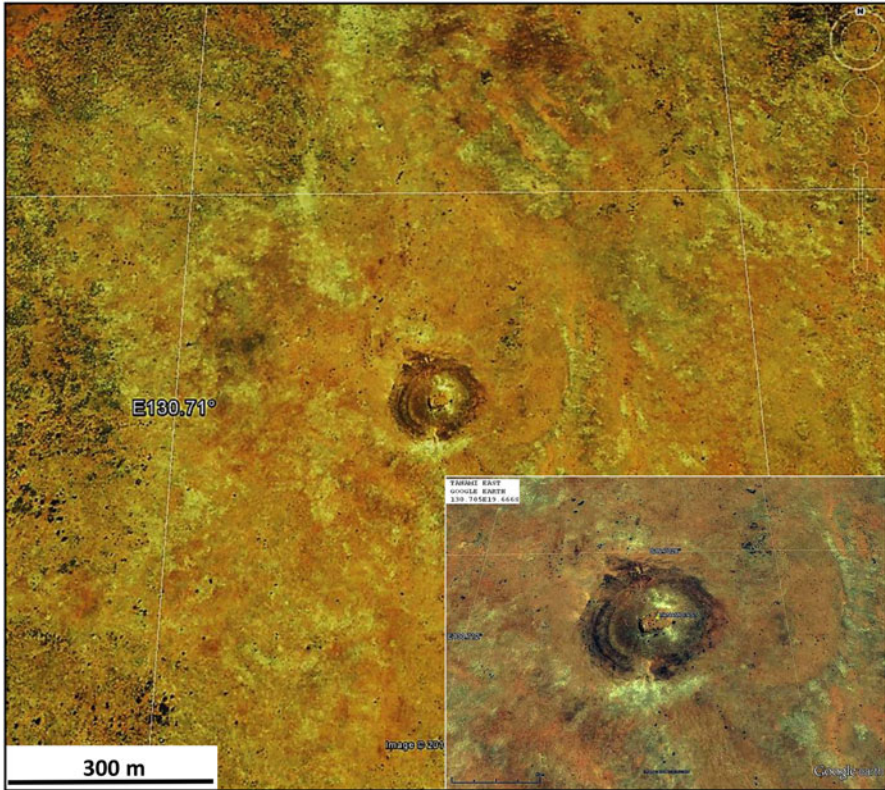


Fig. 5.4 Google Earth image of the Tanami East probable impact structure. Note the triple rings of the central dome and the faint outlines of an outer rim (Google Earth)

5.2 Morphological and Buried Ring Features

The geological antiquity of Australian land surfaces, in particular platform sediment and volcanic cover over Precambrian cratons in central and western parts of the continent, allows preservation of a range of circular features, including morphological and drainage rings, circular lakes, volcanic craters, tectonic domes, oval granite bodies, mafic igneous plugs (Fig. 5.2), salt diapirs, and magnetic, gravity and seismic anomalies of unknown origin. The criteria applied for recognition of asteroid impact structures and meteorite craters from geophysical evidence (Grieve and Pilkington 1996; Shoemaker and Shoemaker 1996; Glikson and Uysal 2013; Glikson et al. 2013, 2015) and from petrological evidence for shock metamorphism (French 1998; French and Koeberl 2010) allow identification of at least 38 impact structures and very likely impact structures on the Australian continent and surrounding continental shelf (Gorter 1998; Haines 2005; Bevan et al. 2012; Dunster et al. 2014; World Impacts Database 2016) (Table 4.1).

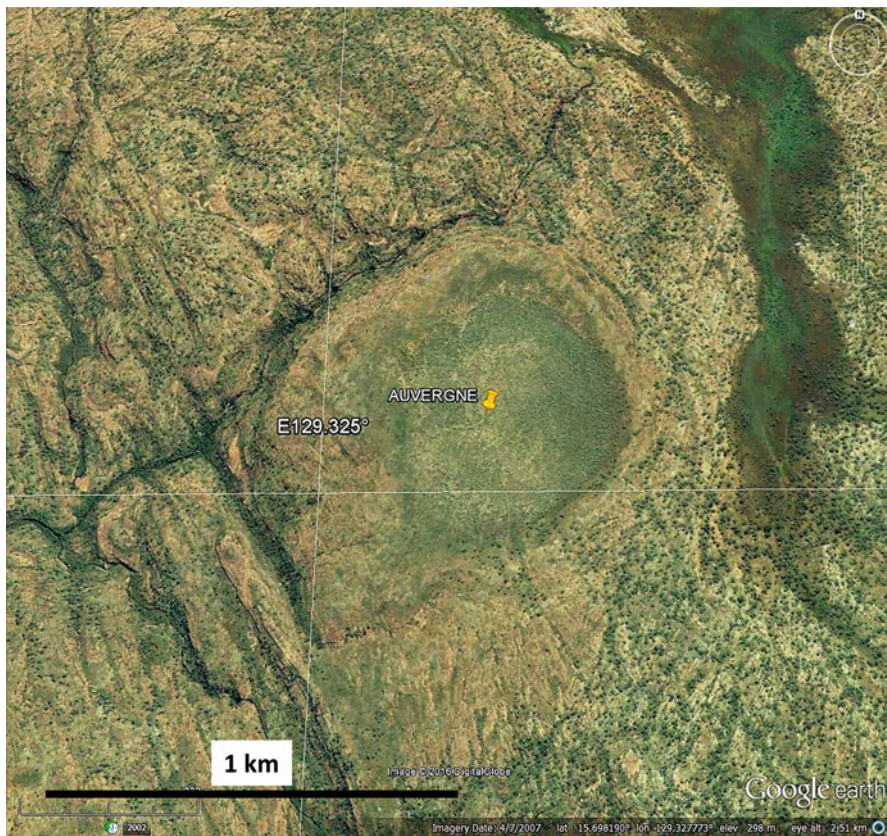


Fig. 5.5 Google Earth image of the Auvergne sub-rounded depression, Northern Territory (Google Earth)

Australian ring, dome and crater features include 43 features many of which are of possible to probable impact origin, to be tested by field investigations and/or drilling. Exposed structures include features consistent with impact structures, such as circular crater-like morphological patterns which may intersect pre-existing linear structural features, central morphological highs and unique thrust and fault patterns. Buried circular features include circular single or multi-ring TMI patterns, circular TMI quiet zones, corresponding gravity patterns, low velocity and non-reflective seismic zones. Discrimination between impact structures and igneous plugs, volcanic caldera and salt domes may require field work and/or drilling.

Examples of exposed crater-form features containing some elements consistent with, but unproven to be of, impact origin (Table 5.1) include White Cliffs (Fig. 5.3a), Youngerina, (Fig. 5.3b), Skirmish (Fig. 5.3c), Tanami East (Fig. 5.4), Auvergne (Fig. 5.5), Fiery Creek (Fig. 5.6), Tingha (Fig. 5.7), Monte Christo (Fig. 5.8), Mount Moffatt (Fig. 5.9), Lucas (Fig. 5.10).

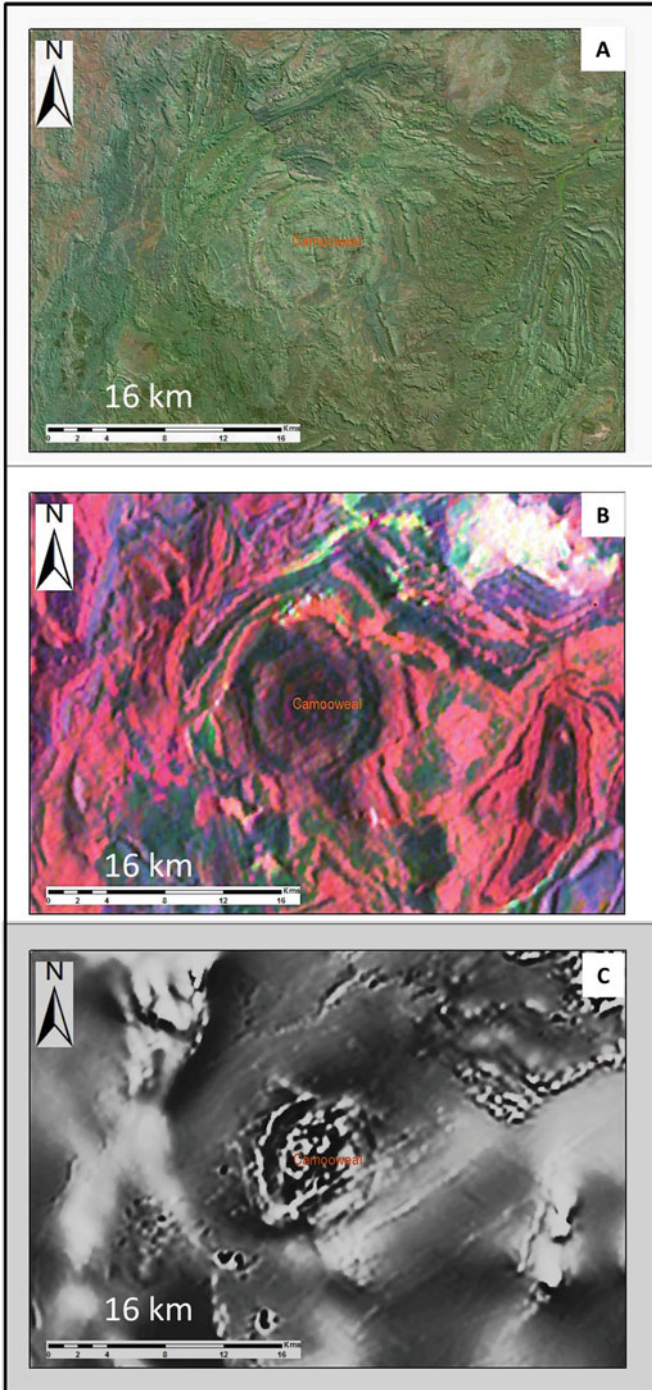


Fig. 5.6 Fiery Creek structure, Queensland: (a) Landsat-TM; (b) K-Th-U radiometric image; (c) Total Magnetic Intensity (Google Earth and GA Creative Commons; Elsevier with permission)

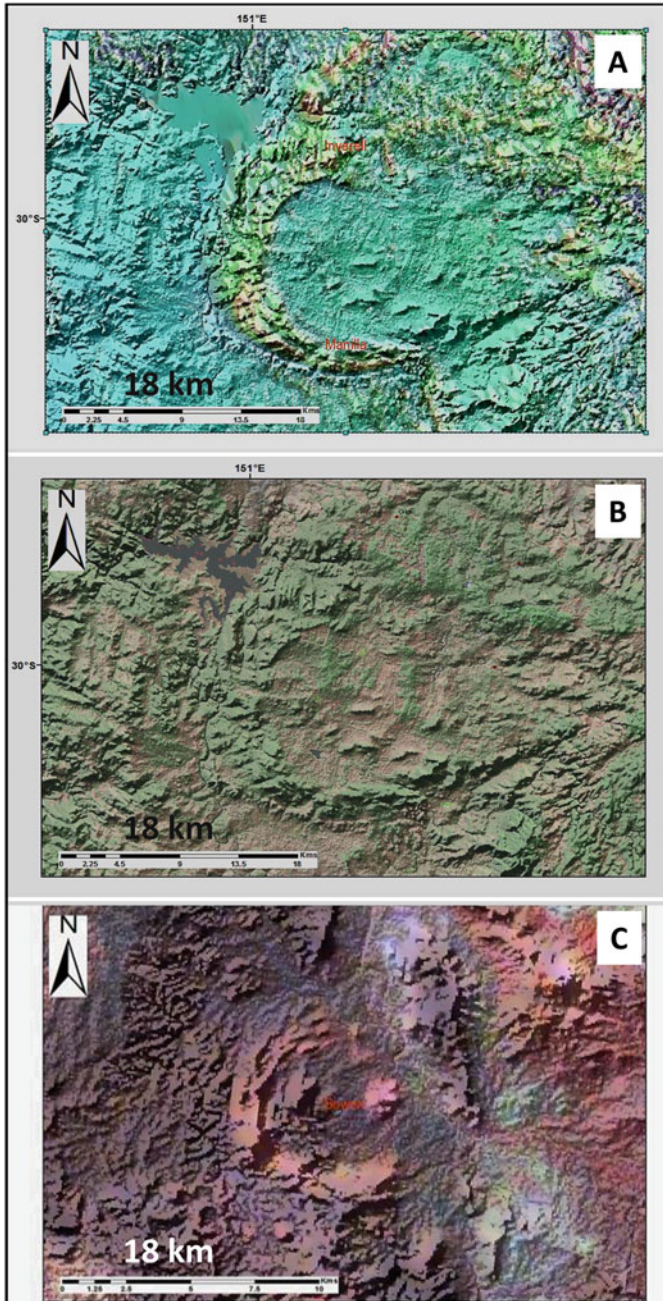


Fig. 5.7 *Tingha* ring feature. (a) superposed TMI and shuttle radar; (b) superposed Landsat-TM and shuttle radar; (c) combined K-Th-U radiometric image and shuttle radar; (GA Creative commons; Elsevier with permission)

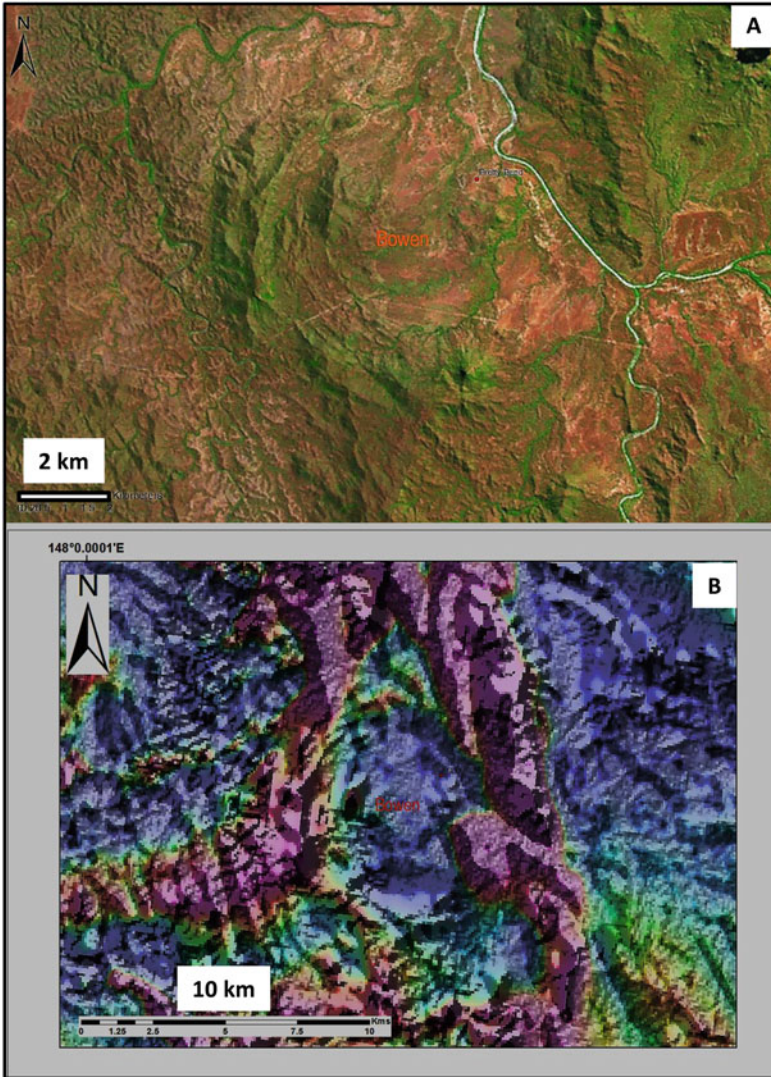


Fig. 5.8 Monte Christo ring feature: (a) Combined Google Earth image and shuttle radar; (b) Combined shuttle radar and TMI radiometric image (GA Creative Commons; Elsevier with permission)

Examples of TMI ring features of buried structures some of which are likely impact structures (Table 5.1) include Camoowel (Fig. 5.11a, b), Killarney (Fig. 5.11c, d), Neale (Fig. 5.12a), Herbert (Fig. 5.12b), Lennis (Fig. 5.12c), Ilkurka (Fig. 5.12d), Oodjuongari (Fig. 5.13a), Wessell (Fig. 5.13b), Calvert Hills (Fig. 5.13c), Mount Davies (Fig. 5.13d), Renehan (partly exposed) (Fig. 5.14a), McLarty Hills (Fig. 5.14b), Augathella (Fig. 5.14c), Green Swamp Well (Fig. 5.14d), Pemberton (Fig. 5.15).

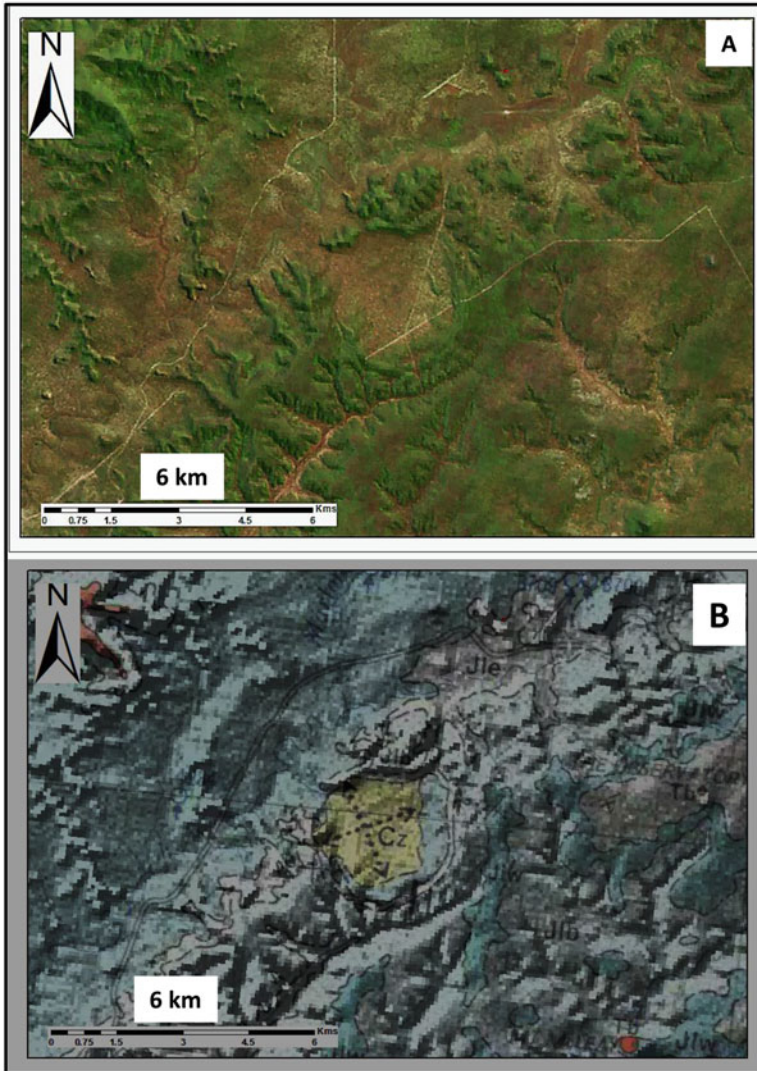


Fig. 5.9 Mount Moffatt ring feature: (a) Combined Google Earth and shuttle radar image; (b) superposed geological map and shuttle radar image (GA Creative Commons; Elsevier with permission)

The origin of large circular TMI and gravity pattern such as the Diamantina River drainage feature (Glikson et al. 2016b) (Fig. 5.16) the multiple TMI ring pattern of the Deniliquin-Booligal (Figs. 5.17a, 5.17b and 5.17c) and the Coompana geophysical anomaly (Fig. 5.18) remain unresolved.

Compared with frequency distribution patterns of extra-terrestrial impact structures worldwide, the Australian record displays a relatively a common occurrence of large impact structures and relative depletion in small impact structures and craters,

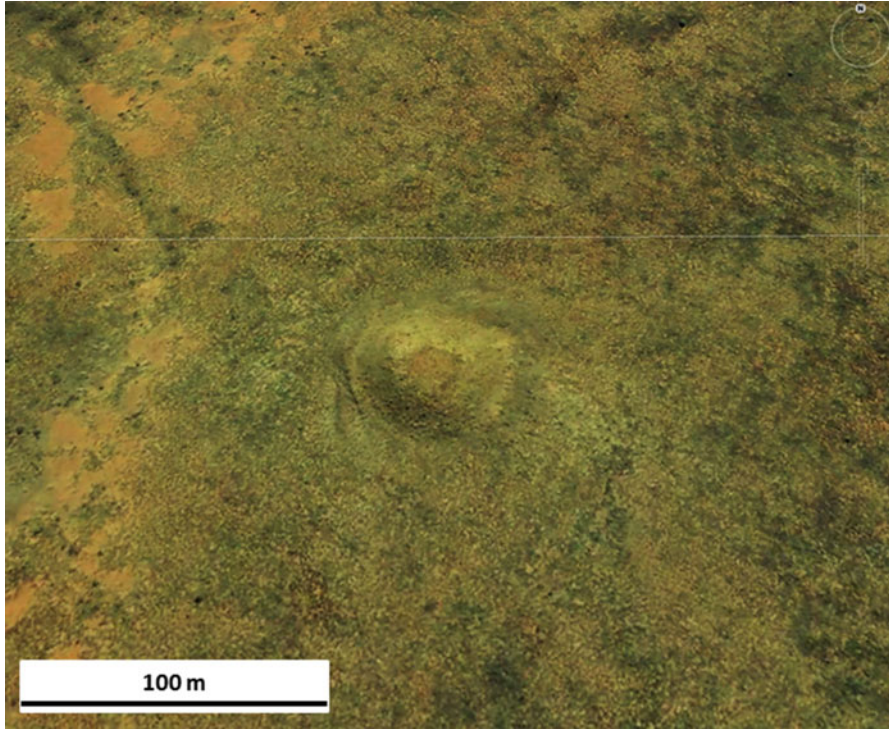


Fig. 5.10 Google Earth image of *Lucas/Yam Hill*, Western Australia. Note the apparent multiple rings

accounted for by the better preservation of large structures at deep crustal zones as compared to the erosion of small craters, and a good geophysical coverage of large parts of the continent.

The role of circular structures in the evolution of the Australian continent was highlighted by E.S.T. O’Driscoll (in Claoue-Long 2017). A classic example of a circular drainage feature is the *Diamantina* drainage ring feature, west of Winton, north-western Queensland (Fig. 5.16) constituting an example of a near perfectly circular drainage ring associated with geophysical features, including TMI, Bouguer anomalies and deep seismic transects (Glikson et al. 2016a). The *Diamantina* ~120 km-diameter ring feature is manifested by a near-360 degrees circular drainage pattern, radial creeks and a coincident radiometric (K-Th-U) pattern. A western subducted TMI arc with a ~110 km diameter is offset by ~30 km eastward from the western rim of the drainage ring. Bouguer anomaly data shows gravity low near the centre of the ring structure, but no outer circular pattern. Two recent seismic transects indicate a moderately reflective to weakly reflective crust below flat lying strata of the Jurassic–Cretaceous Eromanga and Permian–Triassic Galilee basins,

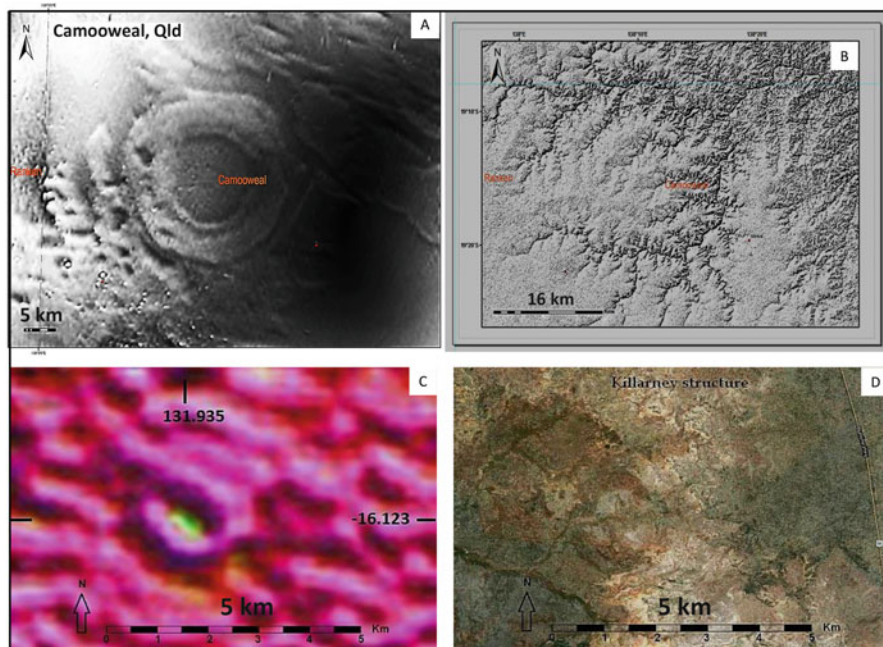


Fig. 5.11 (a) TMI image of the Camooweal buried multi-ring feature; (b) Shuttle Radar image of the Camooweal area overlying the TMI ring feature; (c) TMI image of the Killarney feature, Northern Territory; (d) Google Earth image of the Killarney feature, Northern Territory (GA Creative Commons; Elsevier with permission)

and above a usually well-defined $\sim 39\text{--}45$ km-deep Moho. An approximately ~ 100 km-wide seismically non-reflective to weakly reflective zone overlapping the *Diamantina* ring feature separates crust of different seismic reflection character on either side. The nature of the seismic non-reflective crust is unknown. A potential interpretation of the ring structure in terms of asteroid impact cannot be confirmed or rejected given the present state of knowledge, owing to the near-30 km depth of the seismically non-reflective zone along the transects; and the shift of the TMI part ring zone relative to the circular drainage expression of the *Diamantina* ring feature. A test of the nature and origin of the *Diamantina* ring feature requires a cored drill hole near the centre of the TMI ring structure.

The *White Cliffs* half-ring morphological feature (Fig. 5.3a) forms an approximately ~ 2 km-diameter half-circle ring fringed to the north, east and east-southeast by 2–3 meters thick terraces formed by ferricrete and silcrete capping of likely Cretaceous strata. The laterite and weathered rocks are estimated as 100–200 metres thick, are incised to the northwest and southwest by creeks, and are centred by a near-flat depression. Possible traces of a western rim accompanied by drainage are seen. The base of the low cliffs to the east and north is marked by white eroded material. Samples from the underlying white rock consist of foliated to non-foliated quartz-clay siltstone. No clear TMI signature is associated with this semicircular feature.

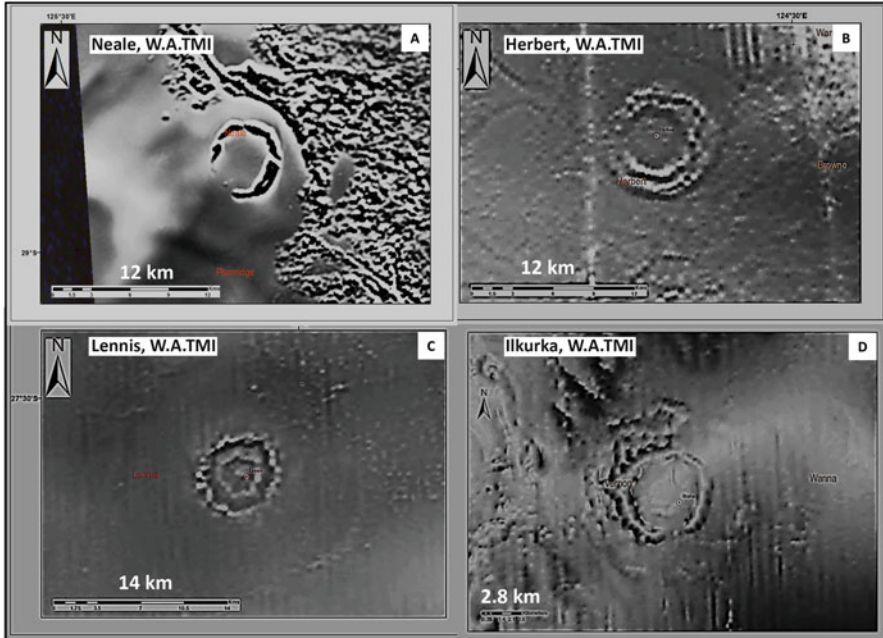


Fig. 5.12 (a) Neale TMI multi-ring structure; (b) Herbert TMI multi-ring structure; (c) Lennis triple ring TMI structure; (d) Ilkurka double ring structure (GA Creative Commons; Elsevier with permission)

Other examples of circular drainage rings include the *Youngerina* ring feature (Fig. 5.3b), which constitutes a ~ 2.8 km-diameter morphological ring demarcated by a light rim and associated with a K-Th-U high and a TMI low. No distinct gravity feature is apparent. The *Skirmish* feature, eastern Western Australia, (Fig. 5.3c) (Haines 2005), is a ~ 2 km diameter circular structural anomaly with outward dips resembling an eroded central uplift of a complex impact structure. The feature is situated in otherwise uniformly dipping Early Neoproterozoic Townsend Quartzite. (F. Pirajno, pers. Com., 2017) observed a ring of strongly fractured outwardly dipping quartzite with possible shatter cleavage, surrounding a central sand covered region. Petrographic examination reveals common grain fracturing consistent with, but not uniquely diagnostic of, low shock levels. No evidence of igneous or diapiric intrusion is evident and the feature is considered a possible eroded central uplift of a larger ~ 6 km complex impact structure of post-Early Neoproterozoic age (Haines 2005).

The *Throssell-Roberts* half-ring topography feature (Fig. 5.3d) is an apparent eastern half-circle feature of ~ 140 km-diameter weakly expressed on shuttle radar images straddling the Roberts and Throssell 1:250,000 Sheet areas, including an apparent central ring, corresponding to the radiometric K-Th-U image. The TMI image displays semi-circular features within the limits of the morphological features. Little correspondence is observed with the gravity pattern.

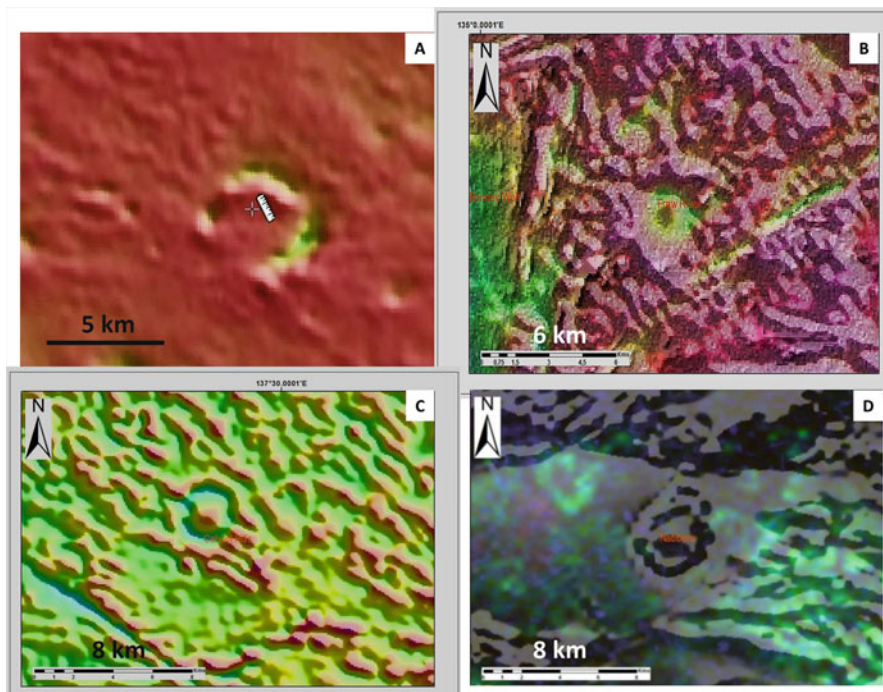


Fig. 5.13 (a) Oodjuongari TMI feature; (b) Wessell TMI feature; (c) Calvert Hills feature; (d) Mount Davies combined TMI and shuttle radar image (GA Creative Commons; Elsevier with permission)

Tanami East, Northern Territory (Fig. 5.4) constitutes a central outcrop with a diameter of approximately 150 meters surrounded by multiple rings up to ~600 meters in diameter. The outcrop consists of Middle Cambrian sediments, including dolomite with chert nodules, dolomitic siltstone, sandstone and claystone and is fringed by at least 3 external rings.

Auvergne, Victoria Basin, Northern Territory (Fig. 5.5). A morphological ring features constitutes a well-defined ~1.1 km diameter sub-rounded depression surrounded by sandstone and quartz sandstone conglomerate cliffs of the Neoproterozoic Bullo River Sandstone (838 ± 80 – 739 ± 30 Ma). The ring is truncated in its WSW flank by a NNW-striking shear zone and on the eastern flank by a NNE-trending fault. A small radiometric K-anomaly is indicated at the centre of the structure. No volcanic rocks are associated with the structure. Subject to field tests the discordant nature of the structure relative to the regional trends and the sub-circularity of a central depression render the Auvergne ring structure a potential target for a search of diagnostic shock metamorphic features.

Fiery Creek, Northwest Queensland (Fig. 5.6): The *Fiery Creek* dome structure constitutes a prominent morphological ring feature with an inner northeast diameter of ~10 km and an outer quiet TMI zone defining a structure about ~19 km in diameter formed in Lower Proterozoic arenites of the Myally Beds (quartzite,

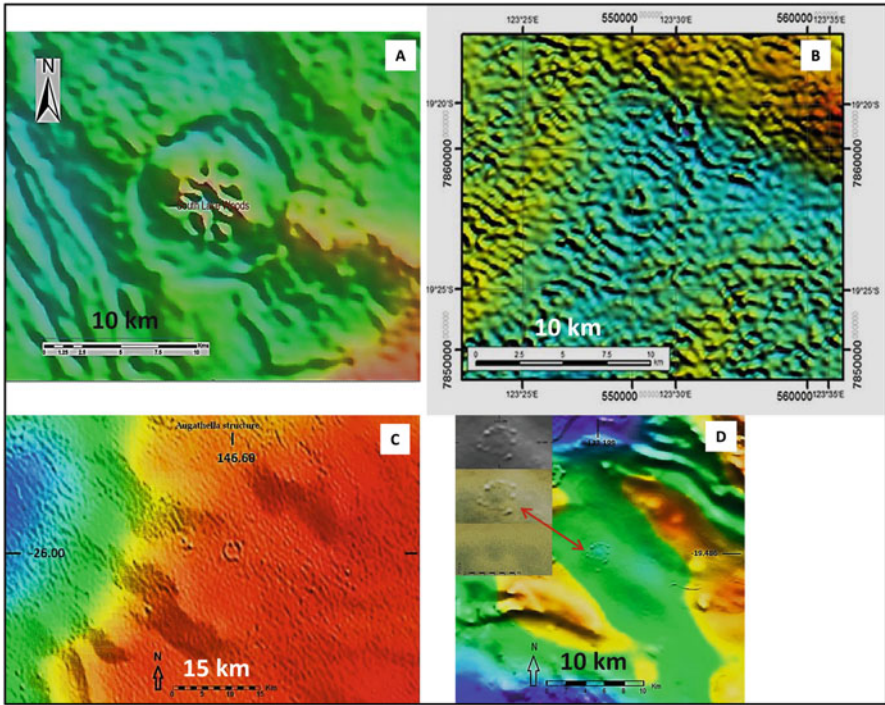


Fig. 5.14 (a) The Renehan probable impact structure, displaying a TMI ring pattern including a partly exposed central dome; (b) McLarty Hills TMI multi-ring feature; (c) Augathella TMI multi-ring feature; (d) Green Swamp Well TMI feature (GA Creative Commons). Images b, c and d processed by klajnik krisztián (Elsevier with permission)

sandstone, siltstone, conglomerate, volcanics. The circular structure corresponds to a gravity low and is well manifested on the K-Th-U image displaying distinctly low levels of the radioactive elements. The intersection of NNW structural trends by the circular feature is consistent with features of impact structures such as *Woodleigh* and *Shoemaker*. The occurrence of a quiet magnetic mantle around the central dome is analogous to similar TMI-quiet circular mantles observed around some proven impact structures, including *Yarrabubba*, *Acraman*, and *Shoemaker*. However Shoemaker and Shoemaker 1996 did not find evidence of impact in the rocks.

Tingha, Northern New South Wales (Fig. 5.7): The Tingha ring feature constitutes a ~21 km-diameter circular body consisting of a core of the Tingha Adamellite (Uralla Plutonic Suite) and mantle of Late Permian granites. The structure is well manifested on TMI and Radiometric images, the latter representing different K-Th-U ratios in the granitoids. Pending further field tests including a search for shock metamorphic features, the structure is regarded as a zoned igneous plug, conceivably a basement uplift of an impact structure?

Monte Christo, Northeast Queensland (Fig. 5.8): The ~8 km topographic ring/crater feature coincides with a TMI low fringed by N-S trending TMI ridges. The

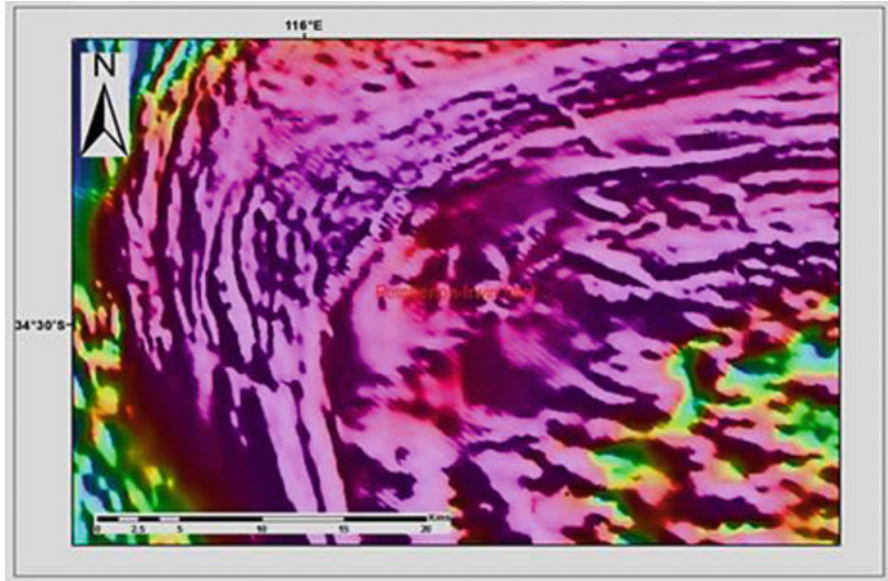


Fig. 5.15 A. The Pemberton TMI feature, Albany-Fraser belt, Western Australia (GA Creative Commons)

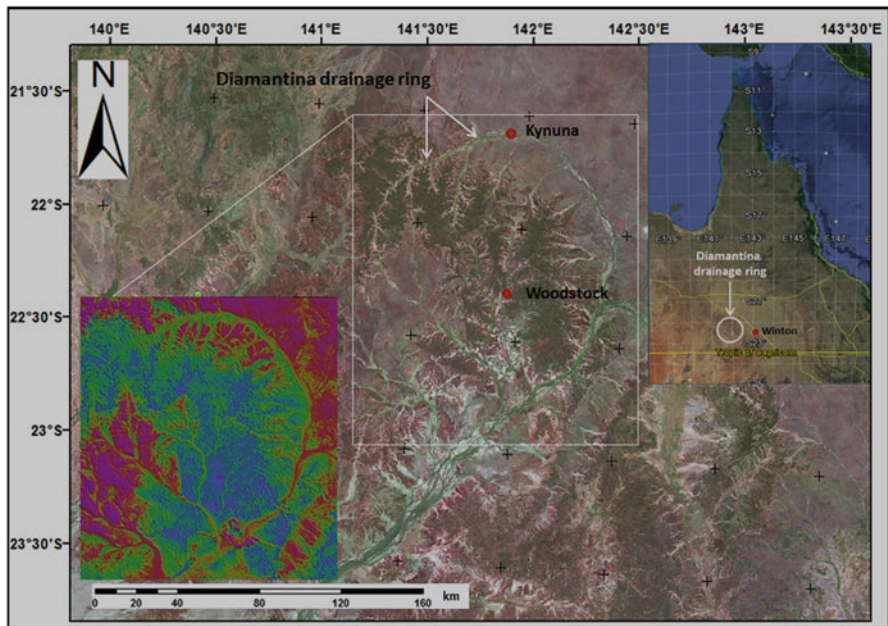


Fig. 5.16 The *Diamantina* River circular ring, western Queensland: Location and K-Th-U radiometric image. After Glikson et al. (2016a) (Google Earth: AJES with permission)

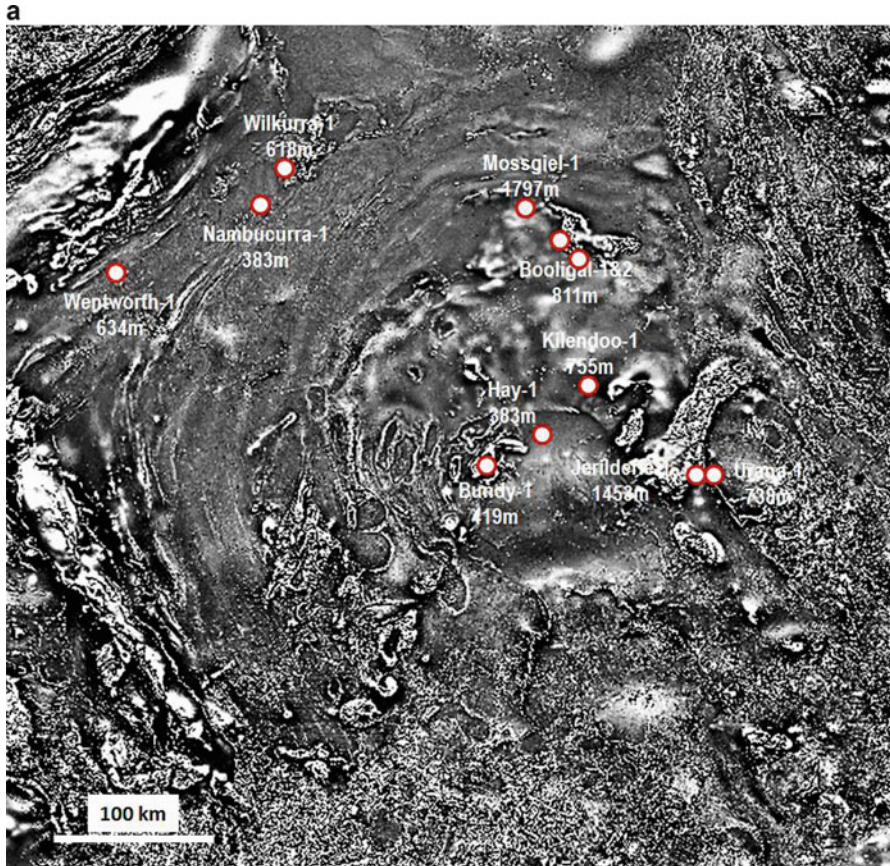


Fig. 5.17a TMI features of the Deniliquin-Booligal ring structure, New South Wales and Victoria (GA Creative Commons; Elsevier with permission)

ring is cored by Lower Cretaceous igneous units including granodiorite and adamellite and is surrounded by Upper Carboniferous diorite, quartz diorite, tonalite, gabbro, granodiorite, rare adamellite, norite, monzonite, granite (Stephen Johansen, [pers.com.](http://pers.com), 2012). The core consists of much more mafic hornblende quartz diorite or tonalite and is deeply weathered and poorly exposed. The aplitic granite at the rim of the ring structure displays concentric shearing and is topographically elevated relative to the granite-occupied central depression, possibly reflecting silicification of the sheared aplite. The aplite displays higher K-U-Th levels than the internal granite. The ring feature is likely to represent a circular magmatic intrusion emplaced in a sheared Upper Carboniferous igneous complex. Such Cretaceous intrusions become increasingly common toward the coast to the northeast of the Bowen Basin. According to R. Bultitude pers. Com. 2015) the feature consists of granitic rocks ranging from hornblende-biotite granodiorite to leucocratic biotite syenogranite, all almost certainly of early Cretaceous age. The nearest

b

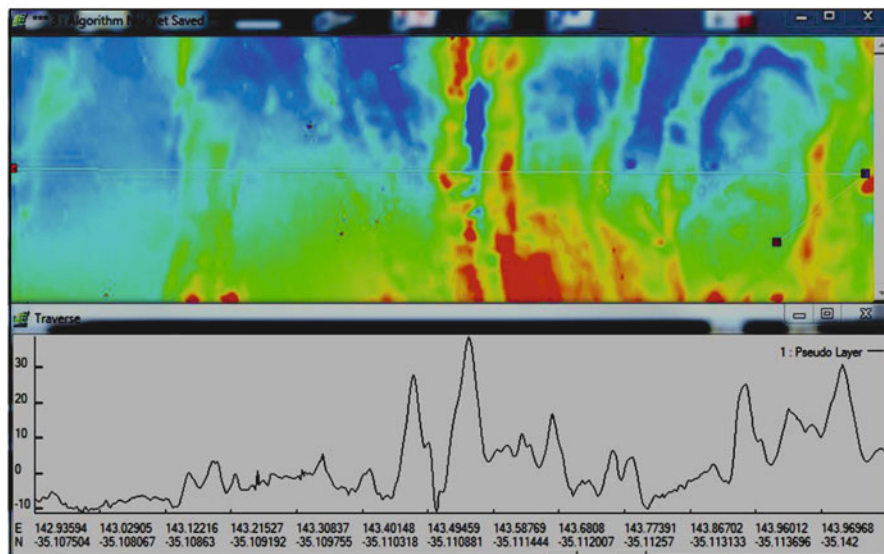


Fig. 5.17b Deniliquin-Booligal structure. NW-SE TMI traverse (GA Creative Commons; Elsevier with permission)

c

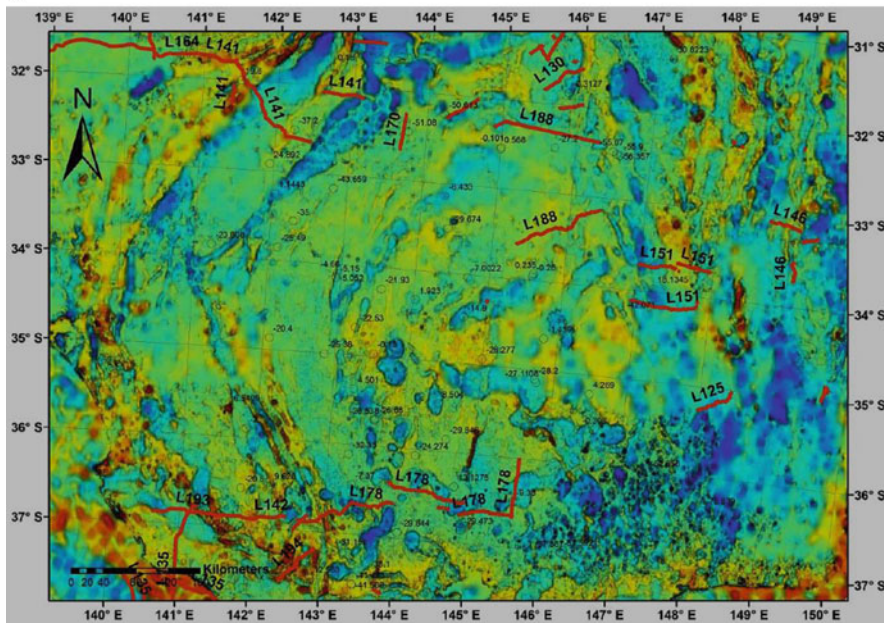


Fig. 5.17c Deniliquin-Booligal structure. Bouguer gravity anomalies. Red lines represent deep seismic transects (GA Creative Commons; Elsevier with permission)

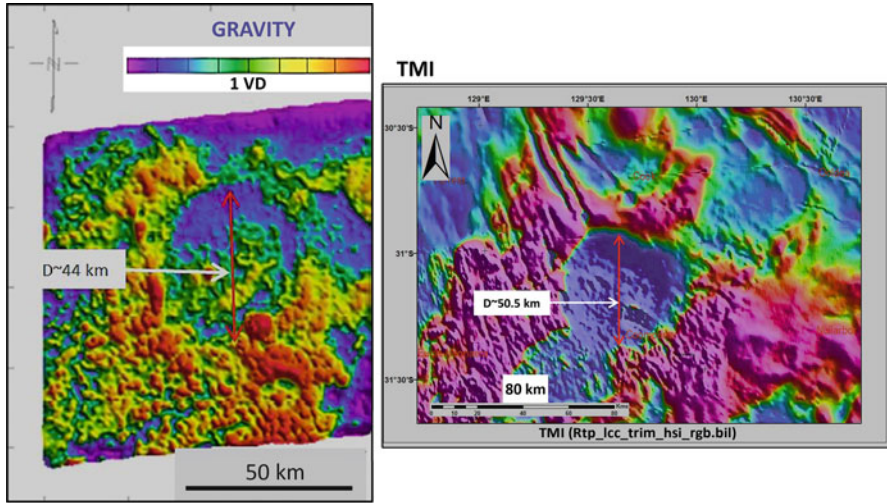


Fig. 5.18 (a) Gravity and (b) TMI images of the Coompana anomaly, Eucla Basin, South Australia (GA Creative Commons; Elsevier with permission)

Cretaceous volcanics are in the Proserpine region >50 km to the east. The origin of the *Monte Christo* ring feature requires field search for diagnostic textural features, possibly of shock metamorphic nature.

Mount Moffatt Carnarvon National Park, Queensland (Fig. 5.9): The feature constitutes a somewhat NS-elongated crater ~2.8–2.5 km in diameter, surrounded by a circular ridge consisting of Lower Jurassic sandstones displaying an overall NW to NNW structural trend. No corresponding TMI or gravity features are observed.

Lucas/Yam Hill, Western Australia (Fig. 5.10) is a ~70–80 meters-diameter circular multiring knob of Permian-Triassic sediments, featuring a central ~20 meters crater, surrounded by a > 220 meters-diameter ring consisting of Tertiary calcrete. LANDSAT images suggest a weakly defined external ring approximately ~400–500 meters in diameter.

5.3 Magnetic and Gravity Ring Anomalies

Circular TMI anomalies offer critical evidence in the search for buried impact structure, provided discrimination can be made between anomalies induced by mafic/ultramafic igneous plugs, magnetite-bearing granitoids, salt diapirs such as the Woolnough Hills salt dome and impact structures (Haines 2005). An example of a multiring mafic-ultramafic intrusion is the Saturn Intrusion in the western part of the Giles Complex, Western Australia (Fig. 5.2c). Where the outer TMI and gravity

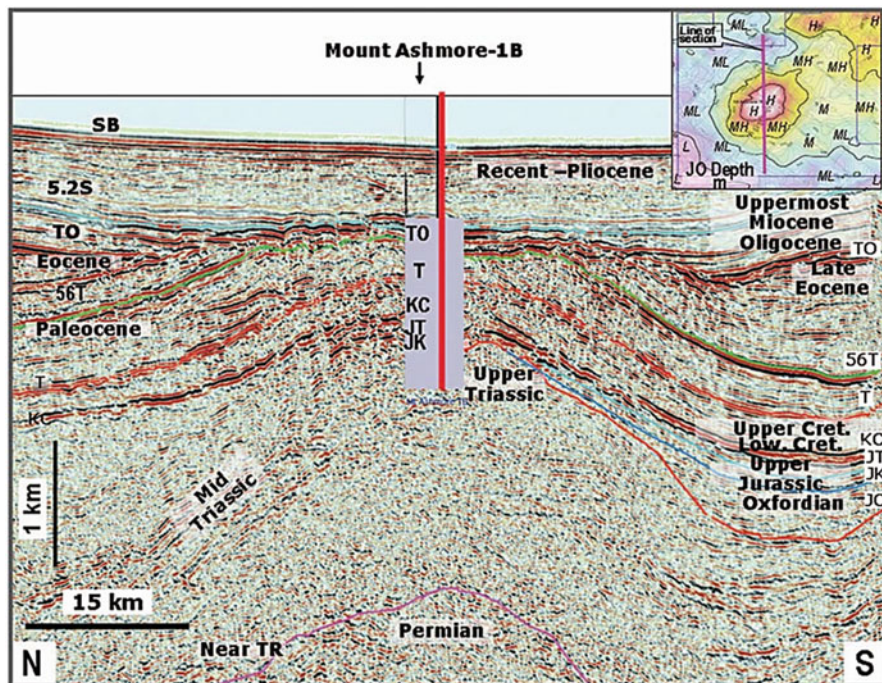


Fig. 5.19 The *Mount Ashmore* dome. A north–south seismic section displaying an overall structural tilt to the south, a steep-flanked inner dome and a well-expressed Late Eocene unconformity which sharply truncates Eocene strata. The isopach map indicates the depth to Oxfordian strata. Note vertical exaggeration (AJES with permission)

rings intersect pre-existing structural trends, as in the instances of the Woodleigh and Shoemaker impact structures, a possible interpretation in terms of impact is enhanced. An example is the McLarty Hills buried TMI multi-ring anomaly, Canning Basin, Western Australia (Fig. 5.14b). Typically exposed and buried impact structures may display TMI signatures of such as radial dykes, as in the Sudbury offset dikes, Ontario (Lightfoot et al. 1997). Disruptions of flat-lying basalts detected on aeromagnetic images may in some instances express uplifted and deformed by impact structures, such as in the Foelsche and Glikson impact structures detected thanks to the circular deformation of magnetic layers of the *Antrim* Plateau Volcanics and equivalents (Haines 2005).

Aeromagnetic data reveal a significant number of TMI ring and multiring anomalies ranging from 8 to 30 km in diameter. An example is the *Camooweal* (Fig. 5.11a, b), which appears to be a pre-existing annular depression with central circular topographic high that was selectively infilled by basalt flows. *Renehan* reveals a radially folded central zone central to a sub circular region of depressed

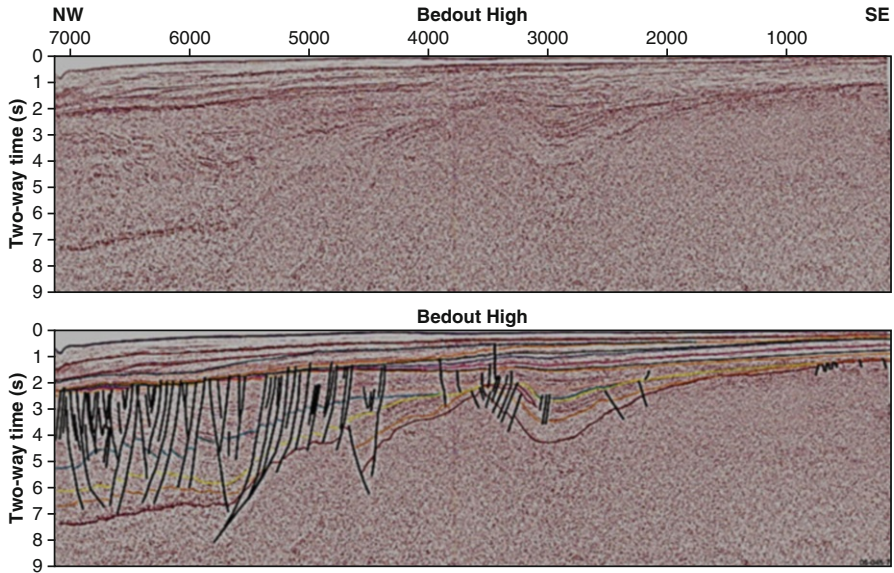


Fig. 5.20 A NW-SE seismic section through the Bedout dome, offshore Pilbara coast, Western Australia. S-15 1994 AGSO multichannel seismic line s120-04. This interpretation shows the central uplift of the Bedout structure deforming end-Permian (dark blue line) and older sequences (pre-Permian, orange dashed line, and top Precambrian basement, red dashed line), overprinted by younger faults associated with late-Triassic to mid-Jurassic rifting. The “pre-Permian strata” are inferred only from seismic character, yet appear to show uplift with the basement. These reflectors are carried from wells in the adjacent onshore Canning basin. (Müller et al. 2005) (Elsevier with permission)

magnetic response (Haines 2005). The *Camooweal* structure, Georgina Basin, is expressed by a well pronounced 21 km-diameter TMI triple-ring pattern (Fig. 5.11a) which corresponds to gravity, radiometric K-Th-U, and Shuttle-Radar images expressing concentric and radial drainage features (Fig. 5.11b). The structure underlies the Camooweal Dolomite of Lower Cambrian or uppermost Proterozoic age, consisting of dolomite with chert nodules and some arenite beds. The TMI image displays a 360 degrees triple ring pattern superposed on a SE-dipping TMI gradient where northern and eastern sectors are superposed on and intersect WNW lineaments (Fig. 5.11). The central ~10 km diameter zone constitutes a quiet magnetic zone or depression and corresponds to a broadly circular gravity high and to a well-defined ~140 degrees circular drainage ring fed by outward radiating creeks (Fig. 5.11b) representing an original morphological elevation of a central dome. The above features of the Camooweal TMI ring structure are consistent with those of a buried impact structure. (Grieve and Pilkington 1996). The low radiometric values of the drainage pattern suggest the creeks are occupied with winnowed quartz-dominated alluvium depleted in K, U and Th relative to the central dome.

Delicate multi-ring TMI ring and multi-ring patterns are identified by close spaced (20 and 40 meters) patterns such as at Connolly Basin, Western Australia, the McLarty Hills multi-ring (Fig. 5.14b), Augathella ring, Queensland (Fig. 5.14c) and Green Swamp Well, NT (Fig. 5.14d) (Table 5.1).

The *Neale* TMI circular feature, northeast of the Fraser Range, Western Australia (Fig. 5.12a), forms a somewhat NS-elongated (NS – 6 km-diameters; EW – 5 km-diameter) ring structure surrounded by a ~1.5–4 km wide subdued TMI rim. The geological map suggests the structure intersects Proterozoic granite overlain by Cambrian volcanics. The structure coincides with a gravity low, very likely suggestive of a ~10 km-diameter impact structure. The ring structure intersects a NW-trending lineament, probably a fault, and is superposed on an uneven TMI relief. The central magnetic ring of the *Neale* structure may represent a central uplift accentuated by up-folded basaltic sheet whereas the outer quiet zone may represent an outer ring syncline. The geology of the basement in the vicinity of the *Neale* ring structure remains subject to further interpretation. The *Neale* ring structure is likely to represent a potential buried impact structure. To the west of *Neale* is a near-360 degrees circular feature of yet unresolved origin, possibly a granite plug. To the north is a magnetically quiet NS-elongated area of unknown nature.

A three-ring TMI anomaly defines the ~16 km-diameter multiring *Herbert* structure (Fig. 5.12b), Camooweal Sheet, north-western Queensland. Two circular magnetic anomalies occur in the western Officer Basin, including *Lennis* 20 km in diameter (Fig. 5.12c) and *Ilkurka* ~12 km in diameter (Fig. 5.12d), both displaying magnetic signature characteristic of impact structures. Gravity data coverage in the area (GA national grid of 11 km) is too coarse to verify an impact-like gravity signature. The two most northern of these structures were investigated by CRA as possible kimberlitic or lamproite igneous intrusions by shallow drilling, but intrusions were not discovered. CRA interpreted the ring features as possible up-doming and ring fracturing with the circular magnetic anomaly being caused by tholeiitic flood basalts (Table Hill Volcanics). However, the dimensions of these structures are larger than those of typical alkaline igneous intrusions, and drilling on the annular magnetic high anomaly of the northern structure verified highly dipping beds, consistent with deformation caused by a central uplift from an impact. The largest magnetic anomaly was drilled by five shallow drill holes by CRA and intrusions were not discovered. No samples from these drill holes have been recovered.

Herbert (Fig. 5.12b) Western Australia is a multi-ring TMI feature including ~16, 8, and 5 km diameter magnetic rings underlying Cenozoic sediments of the Officer Basin, Western Australia, covered by quartz sand, rock fragments, clay, silt, colluvium and minor alluvium in the Herbert 1:250,000 Sheet. The Cenozoic sediments overlie Cambrian to Cretaceous sediments overlying a Proterozoic basement located at a depth to magnetic basement of >4500 meters. The 360 degrees multi-ring TMI anomaly is strongly suggestive of a buried impact structure. Another example is the *Oodjuongari* Structure, Northern Territory (Fig. 5.13a) (Gorter et al., unpublished report), expressed on aeromagnetic data and poor quality seismic reflection profiles, is interpreted as a possible impact crater concealed by superficial Cainozoic strata. From the regional

Table 5.1 43 Ring, dome and crater structures of unknown, possible or probable impact origin

Name	Long/Lat	province	Diameter (km)	Age	Notes	References
Augathella	146.60E/26.00S	Charleville, Qld	3	Devonian to Lower Cretaceous?	Buried TMI ring	K. Klajnik, pers. com. 2017
Auvergne	129.328E/15.698S	Victoria Basin, NT	≥1.1	Post-739 Ma?	Sub-rounded depression, discordant to the regional structure; unknown origin	This report
Balfour Downs feature	120.14E 22.40,S	East Pilbara, WA	~4		TMI ring anomaly Unknown origin	K. Klajnik, pers.com.
Bedout	118.94E/17.97S	Off Pilbara Coast, WA	~200	251.1 ± 4	Seismic dome capped by unconformity	Gortler (1996) and Becker et al. (2004)
Coompana	129.35E/31.10S	SW South Australia	44-50	Pre-Eocene	Gravity and TMI circular anomaly	GA and SADME surveys
Camooweal	138.204E/19.245S	Georgina Basin, Qld	≥21	Post-Cretaceous	TMI and drainage signatures; probable impact structure	Haines (2005)
Cummins Range craters	127.3898E/18.887S	Kimberley	4 craters: the largest: ~38 × 28m		Small craters	BMR Record 1966/218 (Dow and Taylor 1966)
Delamere	131.175E/15.775S	Victoria Basin, NT	4.5	4.6NSx4.4EW	Elliptical morphological ring of Antrim Plateau volcanics/ Possible impact structure	A. Whittaker, pers. com.
Eurowie Creek	136.007E/22.45S	East NT	1	Post-Cambrian	TMI anomaly	Dunster et al. (2014)
Fiery Creek	139.228E/19.222S	NW Qld	19	Post-lower Proterozoic	Morphological, TMI, gravity and K-Th-U data consistent with impact	Shoemaker and Shoemaker (1996)

(continued)

Table 5.1 (continued)

Name	Long/Lat	province	Diameter (km)	Age	Notes	References
Green Swamp Well, NT	133.20E 19.48S	NT	3		structure but no evidence for impact was detected. TMI ring; Small depression	K. Klajnik pers. com. 2017
Gulpullyul, NT	134.001'E 13.316S,	McArthur Basin, NT	0.5–0.8	1600–1500	Probable impact structure, structure and drainage features	Plumb (2005) and Dunster et al. (2014)
Haines	120.7E 6.9S	Timor Sea, offshore Canning Basin	2.5	Post-Eocene	Seismic disturbance	Jones et al. (2010)
Herbert	124.394E 25.056S	Officer Basin, WA	8.5–9.0	Post-Cambrian	TMI ring; probable buried impact crater	Haines (2005)
Ikybon River	131.02E 15.174S	Antrim Plateau volcanics, NT	3.67 × 2.79	Post 513 Ma	Morphological ring/crater, TMI and radiometric features. Possible impact structure	A. Whitaker, pers. com.
Ilkurka	127.426E 28.354S	Officer Basin, WA	≥12	Tertiary	TMI ring; probable impact structure	Iasky and Glikson (2004)
Killarney	131.948E 16.159S	Victoria Basin, NT	1–1.5		Several TMI and LANDSAT ring features.	klajnik krisztián, pers. Com.
Lennis	126.945E 27.56S	Officer Basin, WA	≥20	Tertiary	TMI ring; Likely buried impact structure	Iasky and Glikson (2004)
Lucas/Yam Hill	128.7163E 20.8418S	Canning Basin, WA	>0.22–0.5	Post-Triassic	Round hill, origin unknown	This paper
Manningrida	134.242E 11.802S	Offshore, NT	8	Post-Neoproterozoic	TMI feature, Probable impact structure	Haines (2005)
McLarty Hills	123.46E 19.375S	Canning Basin, W.A.	~10	Post-late Ordovician	Multiring TMI	K. Klajnik pers.com. 2017

Mercury	114.33E19.66S	Timor Sea	30 +	Late Cretaceous	Gravity feature	Gorter (1998) and Haines (2005)
Mingobar	145.91E21.08S	NE Qld	>15	late Middle Devonian		Gorter (1998)
Monte Christo	148.116E20.404S	NE Qld	≥8	Post-lower Cretaceous	topographic ring	S. Johansen, pers. Com.2012
Monto (Goondicum Gabbro)	151.4194E24.863S	Qld	≥6.5	Early Cretaceous	Gabbro plug	Huemer 2013, pers. com.
Mount Davies	121.1104E25.217S	Nabberu Basin, WA	4–5	post 1460 Ma	TMI multiple ring. Probable impact structure	This paper
Mount Moffatt	147.913E25.082S	Cararvon National Park, Qld	≥2.5–2.8	Post-Paleozoic	topographic ring	This paper
Mulkara	138.878E27.705S	Eromanga Basin, SA	≥9	Mesozoic	Geophysical feature	Plescia (1999)
Neale	125.637E28.946S	Fraser Range, WA	≥6	Post-Cambrian	TMI ring; probable impact structure	This paper
Oodjuongari	134.2E16.637S	McArthur Basin	~5	Post-Early Cambrian	TMI ring; probable impact structure	Gorter et al. (unpublished)
Pemberton	116.051E34.557S	Albany-Fraser, WA	5	Post-Paleozoic	Magnetic anomaly	
Puka	132.708E24.0S	Palm Valley, Amadeus Basin, NT	0.28	Post-Palaeozoic	Bowl shaped crater, no impact deformation observed	Dunster et al. (2014) and Hamacher and Norris (2009)
Sheridan Creek	135.1101E13.079S	NE Northern Territory	≥3	Post-Mesoproterozoic	TMI anomaly	Dunster et al. (2014)
Skirmish	128.466E26.435S	WA	≥6	Post early Neoproterozoic	topographic ring	Haines (2005)

(continued)

Table 5.1 (continued)

Name	Long/Lat	province	Diameter (km)	Age	Notes	References
Spear Creek	135.83E17.26S	Carpentaria Basin	0.6–1.0	Post-Cretaceous	Topographic, K-Th-U and TMI ring	K. Mitchell, pers. Comm.
Spring Range	134.3E 21.85S	Georgina Basin, NT	0.3	Post-Cambrian	Possible impact structure	Haines (1989) and Dunster et al. (2014)
Tanami East	130.714E19.703S		~600 m	Post-Cambrian	Possible impact structure	This paper
Throssell-Roberts	123.63E27.08S	East Yilgarn	<140		Apparent Eastern half circle and central uplift on shuttle-radar	This paper
Tingha	151.114E30.004S		≥21	Post late Permian	topographic ring	This paper
Youngerina	145.08E29.522S	North NSW	≥2.8		Morphological, radiometric and TMI ring	This paper
Wessell	135.081E20.608S	Davenport Ranges, NT	2.5	Proterozoic or Post-Proterozoic	TMI ring; possible impact structure	Dunster et al. (2014)
White Cliffs	143.1450E30.785S	W NSW	≥2		topographic half ring	This paper
Yilgalong	120.893E;21.4817S	East Pilbara	18.2 × 17.5	Quaternary	Probable impact crater	Williams (2007)

geology, the age of the possible impact is considered as post Cambrian based on the interpretation of the Cambrian Tindal Limestone within the interpreted impact structure.

Relatively weakly manifested circular TMI signatures are displayed by the *Wessell* feature, Davenport Ranges, Northern Territory, a 2.5 km doughnut-shaped aeromagnetic low coincident with a topographic low or crater. The feature is pronounced in the 1st Vertical Derivative magnetic data (Fig. 5.13b) and has been noted as a geophysical anomaly by Arafura Resources and as a possible impact structure by Macdonald and Mitchell (2004). Pre-existing structures include highly folded Proterozoic dolerites and siltstones. Similar features are displayed by the *Calvert Hills* probable impact structure (Fig. 5.13c). The *Calvert Hills* structure, identified by Peter Haines from aeromagnetic images, aerial photos and ASTER imagery, possibly represents an exhumed impact crater partly exposed in otherwise flat-lying rocks of the McArthur Basin (Dunster et al. 2014; Macdonald and Mitchell 2004). Aeromagnetic images show a circular magnetic low 4 km in diameter, disrupting the high frequency signature of the magnetic Gold Creek Volcanics. Radial and circumferential folding is consistent with impact deformation. The structure is considered of likely impact origin and inferred as of late Palaeoproterozoic to earliest Mesoproterozoic age. A semicircular drainage pattern may indicate isostatic uplift of ~ 11 diameter zone. Another example is the *Sheridan Creek* circular structure noted by Haines (2005) (Dunster et al. 2014), a ring like positive aeromagnetic anomaly, 3 km in diameter, hosted by Mesoproterozoic rocks and disrupting a reversely magnetised dolerite sill. The source of the anomaly is buried beneath younger cover, constituting a possible impact structure in view of its resemblance to aeromagnetic signature of known impact structures such as Foelsche.

Weakly defined TMI features include the *Mulkara* feature, Eromanga Basin, South Australia, a geophysical feature defined by a TMI high located in flat-lying Mesozoic sedimentary rocks of the Eromanga Basin. The structural anomaly was initially identified from seismic surveys and first reported by Flynn (1989), who considered the feature to be a 9 km diameter simple bowl-shaped crater within a broader disturbed zone. Subsequent gravity studies indicate a gravity low at the centre of the structure leading Plescia (1999) to reinterpret the feature as a complex crater with a diameter of ~ 20 km and a central peak ring with diameter of 9 km. The geophysical anomaly is in part overlapped by semi-circular topographic expression. A petroleum exploration well, Crater-1, was drilled about halfway between centre and rim in 1993, but did not provide definitive information on the origin of the structure (Gorter 1998). The age of the structure is interpreted as 105 ± 3 Ma based on seismic and stratigraphic evidence (Flynn 1989). If an impact origin is correct, impact occurred into an active sedimentary basin, which subsequently buried the crater.

A potential impact structure has been suggested for the *Pemberton* feature, a roughly circular magnetic quiet zone approximately 10 km-diameter within the linear TMI ridges which form the hinge of an ENE to SSE-flexure of the Albany Fraser high-grade metamorphic terrain, indicated by John Myers (pers. Comm.) (Fig. 5.15). In this area the linear TMI features are markedly disrupted and subdued, yielding the appearance of an apparent circular feature. The subdued ~ 10 km-diameter sub-oval region is located between two terrains distinguished by

contrasting TMI and gravity characteristics. The northern terrain consists of mostly linear though undulated TMI features forming a large flexure and forms a gravity high. The southern terrain appears to be dominated by both linear and fractured features which occur at high angles to the linear northern and western terrain and form a gravity low. The southern and northern terrains are weakly distinguished on shuttle radar image and less so on radiometric images. The southern terrain is dominated by granitoids whereas the northern terrain is more heterogeneous.

5.4 Large Geophysical Multi-ring Features

A large >400 km-diameter TMI and gravity multi-ring structure in southern New South Wales, the *Deniliquin-Booligal* structure (D-B structure) (Figs. 5.17a, 5.17b and 5.17c), studied in detail by A.N. Yeates (pers. com.), has been tested for the possibility of an impact origin. Circular magnetic lineaments define a > 130 degrees multi-ring pattern with an approximate diameter of ~430 km NE-SW and ~415 km NW-SE. The concentric ring structure is truncated in the northeast and in the southeast by the Bootheragandra Fault which separates the D-B ring structure from the NS-trending Omeo Zone of the Snowy Mountains fold belt. The TMI rings are well expressed in the western part of the structure and are truncated at about 15–20 degrees by a major NNW-trending ~290 km-long linear magnetic anomaly (<565 nT). The truncation of the D-B ring structure magnetic ridges suggests the ring structure predates the Cambrian-Ordovician Delamerian orogenic belt defined as the Stawell Zone by Hallett et al. (2005).

The centre of the D-B concentric TMI structure is occupied by a ~125 km diameter-large magnetic zone showing relatively smooth magnetic pattern with TMI values ranging between –46 nT and +157 nT. This zone is surrounded by markedly circular TMI patterns which attain an overall width of ~124 km in the northwest and ~115 km in the southwest. Cross sections through the north-western and north-eastern sectors of the circular TMI and gravity rings display fine circular ridge and trough zones (Figs 5.17a, 5.17b and 5.17c). TMI values of this zone in the northwest range between –2.5 nT and 62 nT. This markedly lineated annular zone is fringed to the northwest and the southwest by an arcuate up to 70 km-wide TMI trough with values as low as –43 nT. The outer TMI troughs are fringed in the southwest and the northwest by strongly magnetic linear zones where TMI values reach ~300–560 nT.

The overall circular ridge pattern which characterizes the Deniliquin-Booligal TMI ring structure is overprinted by younger magnetic anomalies, including:

1. Probable granitic intrusions showing narrow well-defined magnetic outlines overprinted on the DB anomalies.
2. Probable volcanic formations suggested by sharp magnetic signatures.

Probable granitic intrusions are expressed as well defined annular features, in particular in the south-western part of the D-B ring. Irregular high-amplitude strongly magnetic features superposed on the D-B ring may constitute sub-horizontal volcanic units, cf. a ~110 km-long NNE-trending strongly magnetic anomaly of ~198 nT, a ~45 km-long NW-trending body and irregular NNW-trending anomalies (A.N. Yeates, pers. Comm.). A search for shock metamorphic textures in basement drill hole (Fig. 5.17a) (Glikson, unpublished results) has not yielded positive results.

The basement for the Eucla Basin, South Australia, southwestern South Australia (Fig. 5.18), displays a number of circular gravity and TMI anomalies, the largest of which is the *Coompana* structure, with a diameter of ~44 km as defined by a gravity anomaly (Fig. 5.18a) and a strong TMI anomaly (Fig. 5.18b). The TMI feature is generated by a strong reverse remanent magnetization (Foss et al. 2016a, b). A small subsidiary magnetic ring is located on the south-eastern rim of the structure. The main magnetic anomaly is well correlated with the negative gravity anomaly, suggesting that the material generating the main magnetic anomaly has a relatively low density. In view of the highly magnetic nature of the Coompana anomaly its origin from a granite body is open to question. The effects of mafic volcanics intersected in marginal bore holes at depth of 302–340 m (CD-1, KN-1) (Foss et al. 2016a) are uncertain. An interpretation in terms of an impact structure needs to be tested by a drill hole near the centre of the anomaly.

A type example of a probable impact structure is *Gnargoo* (Fig. 4.21) 75 km-diameter structure which occurs in the northernmost Carnarvon Basin, Western Australia, identified from seismic and gravity datasets displaying close similarities to *Woodleigh* (Fig. 3.8), *Gnargoo* was interpreted by Iasky and Glikson (2004) as a possible complex impact structure. The age of the *Gnargoo* structure is constrained between the Early Permian age of deformed rocks and unconformably overlying undeformed Lower Cretaceous strata (Iasky and Glikson 2004, 2005).

The Mount Ashmore seismic dome (Figs. 4.22 and 5.19) (Glikson and Vickers 2010), described earlier, constitutes a classic case where seismic data including a dome intersected by an unconformity suggests a likely impact structure, as confirmed by drilling, providing clues for investigation of similar seismic anomalies such as the *Bedout* structure off shore the Pilbara, Western Australia. A major controversy has been raised in connection with this seismic dome (Fig. 5.20) which consists of Permian volcanics and sediments truncated unconformably by Cretaceous sediments. The dome was proposed to be a possible impact structure by Gorter (1996, 1998) due to the discordant relations between the dome and overlying sediments as revealed in a seismic transect, typical of eroded central uplift structures. $^{40}\text{Ar}/^{39}\text{Ar}$ dating of feldspar from the breccia in Lagrange-1 well gives an age of 251.1 ± 4 Ma, approximately coincident with the Permian – Triassic boundary. Becker et al. (2004) claimed to have identified shock metamorphosed impact breccia in samples from the drill hole, inferring a possible impact crater ~200 km large. However, other analyses of *Bedout-1* core samples found no evidence of shock metamorphism and reinterpreted the breccia as an altered mafic volcanic breccia (Renne et al. 2004; Glikson 2004; Wignall et al. 2004).

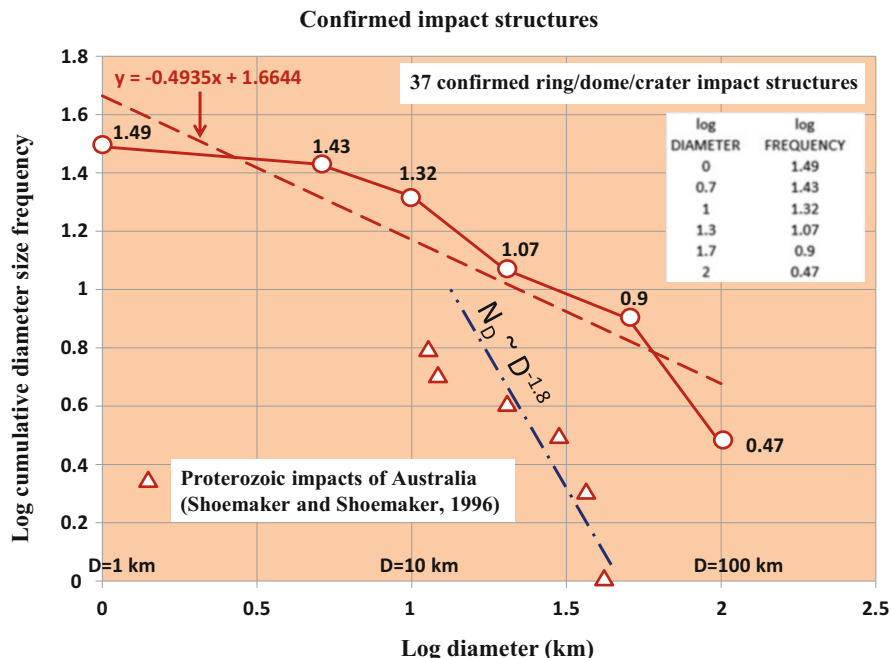


Fig. 5.21 Log cumulative size distribution vs log diameter of confirmed and probable impact structures on the Australian continent. Red open circles – Australian impact structures; discontinuous line – regression; triangles – six Proterozoic impacts (Shoemaker and Shoemaker 1996). $N_D \sim D^{-1.8}$. The cumulative size distribution of terrestrial impact structures according to Grieve and Shoemaker (1994) for structures larger than 20 km in diameter (Elsevier with permission)

5.5 Distribution Patterns of Ring and Dome Features

Estimates of the temporal cratering flux are complicated by the difficulty in determining the age of impact structures (Jourdan et al. 2012). Based on crater size vs cumulative frequency plots for post-LHB (Late Heavy Bombardment) (3.95–3.85 Ga) in the Earth–Moon system (Barlow 1990; Shoemaker and Shoemaker 1996) (Figs. 5.21 and 5.22) estimated the present crater formation rate as $5.9 \pm 3.5 \times 10^{-15} \text{ km}^{-2} \text{ year}^{-1}$ for craters of diameter $D \sim 20 \text{ km}$. This estimate is consistent with the $\sim 20 \text{ km}$ diameter crater production rate of $6.3 \pm 3.2 \times 10^{-14} \text{ km}^{-2} \text{ y}^{-1}$ for the last 120 years based on impact structures in Europe and North America (Grieve and Shoemaker 1994), which is higher than the crater flux estimated for the post-3.2-Ga lunar crater record. Based on the above cratering size-frequency rates it was estimated approximately 450 craters of diameter $\geq 100 \text{ km}$ were produced on Earth since $\sim 3.8 \text{ Ga}$ (Glikson 2001). The preferential preservation of large impact craters, arising from the presence of deep crater root zones at mid-crustal levels, as well as the detection of large impact structures on geophysical maps, allows estimates of the minimum impact flux.

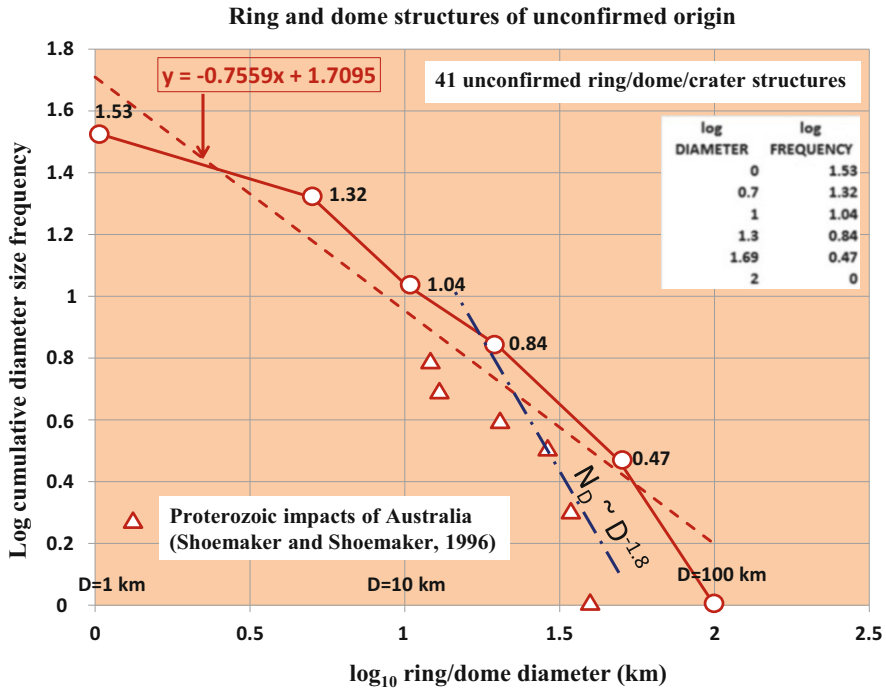


Fig. 5.22 Log cumulative size distribution vs log diameter of Australian ring, dome and crater features of unknown origin. Red open circles – ring, dome and craters; discontinuous line – regression; triangles – six Proterozoic impacts (Shoemaker and Shoemaker 1996). $N_D \sim D^{-1.8}$. The cumulative size distribution of terrestrial impact structures according to Grieve and Shoemaker (1994) for structures larger than 20 km in diameter (Elsevier with permission)

Shoemaker and Shoemaker (1996) showed that the cumulative size-frequency distribution of six Australian Proterozoic impact structures (Fig. 5.21) is consistent with the flux of Earth-crossing asteroids and long-period comets. Plots of cumulative size frequency of 38 confirmed Australian impact structures (Table 5.1) for the range of diameters of 10–100 km fall approximately parallel to this trend (Fig. 5.21) while the cumulative size frequency of craters <5 km in size peters out, which is likely due to the higher rate of erosion and removal of small craters. A similar size frequency distribution and petering out of small craters applies to plot of 43 ring and dome structures of unconfirmed origin (Fig. 5.22). Compared with frequency distribution patterns of extra-terrestrial impact structures $N_D \sim D^{-1.8}$ (Grieve and Shoemaker 1994), the Australian trend display a relatively more common occurrence of large impact structures and depletion in small impact structures, a trend explained by the better preservation of large as compared to small structures.

The oldest asteroid impacts on the Australian continent are represented by ejecta fallout units intercalated with sedimentary units in the Pilbara Craton, Western Australia, including ejecta units dated at 3.47, 3.46, 2.63, 2.57, 2.56 and 2.48 Ga (Lowe and Byerly 1986; Simonson 1992; Glikson et al. 2016a). However, since the originating impact sites may have pre-existed at locations removed from the present position of the Australian continent, these impact are not considered in the present paper. Detailed field research of Australian impact structures by Eugene and

Caroline Shoemaker during the 1980s and 1990s have recovered a wealth of impact observations, including the *Teague Lake* (renamed as *Shoemaker*), *Spider*, *Kelly West*, *Strangways* and *Lawn Hill*. Comprehensive documentation and analysis of the Australian impact record was presented by Haines (2005), for the Northern Territory by Dunster et al. (2014) and for Western Australia Bevan (1996) and Boxer (2014).

Many of the 43 rings, domes and crater features indicated in this paper (Table 5.1) display structural attributes consistent with an impact origin, including high degrees of circularity of multiple ring features. The agreement between diameter vs cumulative diameter plots of these features with impact trends (Fig. 5.22) is consistent with this observation. The preservation of impact structures and of ring and dome features depends on the extent to which these structures are exposed, eroded, shallow-buried or deeply buried, complicating estimates of their original diameters. The difficulty in precise age determinations of impact events (Jourdan et al. 2012), renders estimates of impact age frequencies uncertain. Examples are the contrasts between (1) deeply buried relatively well dated Phanerozoic impact structures such as Woodleigh, Talundilly, Tookoonooka and Yallalie, and (2) deeply eroded poorly dated impact structures such as Yarrabubba, Shoemaker, Strangways and Spider (Table 4.1).

References

- Abels A (2005) Spider impact structure, Kimberley Plateau, Western Australia: interpretations of formation mechanism and age based on integrated map-scale data. *Aust J Earth Sci* 52:653–663
- Barlow NG (1990) Estimating the terrestrial crater production rate during the late heavy bombardment period. *Lunar Planet Inst Contrib* 746:4–7
- Becker L, Poreda RJ, Basu AR, Pope KO, Harrison TM, Nicholson C, Jasky IR (2004) Bedout: a possible end-Permian impact Crater offshore of Northwestern Australia. *Science* 304:1469–1476
- Bevan A (1996) Meteorites recovered from Australia. *J R Soc West Aust, Roy Soc West Aust* 79:33–42
- Bevan A, Bunting J, Freeman M (2012) Western Australian impact craters Field Excursion 20–9 August 2012. <http://museum.wa.gov.au/sites/default/files/Met-FT-2012.pdf>
- Boxer (2014) Grant boxer webpages. <http://members.iinet.net.au/~gboxer/Index.html>
- Clauue-Long JC (2017) O’Driscoll’s Lineament Map of Australia. Geoscience Australia. <https://data.gov.au/dataset/odriscoll-lineament-maps-of-australia>
- Dow DB, Taylor B (1966) Probable meteorite craters near Cummins Range, Kimberley Region, Western Australia. *Bur Miner Resour Record* 1966/218
- Dunster JN, Haines PW, Munson TJ (2014) Meteorites and impact structures in the Northern territory. *Northern Territory Geological Survey Record* 2014–007
- Flynn M (1989) The Cooper and Eromanga basins Australia. In: O’Neil B (ed) *Australian society of exploration geophysicists*. Australian Society of Exploration Geophysicists, Sydney, pp 431–439
- Foss C (2015) Coompana Airborne Magnetic and Radiometric Survey. Gov. S. Aust. Dept State Development http://www.minerals.statedevelopment.sa.gov.au/_data/assets/pdf_file/0007/276235/Foss_Coompana_magnetics_presentation_May_2016.pdf
- Foss C, Reed G, Keeping T, Wise T, Dutch R (2016a) Inversion of an anomaly due to multiple magnetizations: an example from the Coompana survey, South Australia. *CSIRO Mineral*

- Resources and Geological Survey of South Australia <https://library.seg.org/doi/abs/10.1190/segam2016-13972845.1>
- Foss C, Reed G, Keeping T, Wise T, Dutch R (2016b) Looking into a 'Blue Hole' – Resolving magnetization and structure from the complex negative coompana anomaly, South Australia. ASEG-PESA 25th Geophys Conference & Exhibition, Adelaide
- French BM (1998) Traces of catastrophe—a handbook of shock metamorphic effects in terrestrial meteorite impact structures. *Lunar Planet Sci Inst Contrib* 954:120
- French BM, Koeberl C (2010) The convincing identification of terrestrial meteorite impact structures: what works what doesn't and why. *Earth Sci Rev* 98:123–170
- Glikson AY (2001) The astronomical connection of terrestrial evolution: crustal effects of post-3.8 Ga mega-impact clusters and evidence for major 3.2 ± 0.1 Ga bombardment of the Earth–Moon system. *J Geodynamics* 32:205–229
- Glikson AY (2004) Early Precambrian asteroid impact-triggered tsunami: excavated seabed debris flows exotic boulders and turbulence features associated with 3.47–2.47 Ga-old asteroid impact fallout units, Pilbara Craton, Western Australia. *Astrobiology* 4:1–32
- Glikson AY, Uysal IT (2013) Geophysical and structural criteria for the identification of buried impact structures, with reference to Australia. *Earth Sci Rev* 125:114–122
- Glikson AY, Vickers JW (2010) Asteroid impact connections of crustal evolution. *Aust J Earth Sci* 57:79–95
- Glikson AY, Eggins S, Golding S, Haines P, Iasky RP, Mernagh TP, Mory AJ, Pirajno F, Uysal IT (2005a) Microchemistry and microstructures of hydrothermally altered shock-metamorphosed basement gneiss, Woodleigh impact structure, Southern Carnarvon Basin, Western Australia. *Aust J Earth Sci* 52:555–573
- Glikson A, Mory AJ, Iasky R, Pirajno F, Golding S, Uysal IT (2005b) Woodleigh, Southern Carnarvon Basin, Western Australia: history of discovery late Devonian age and geophysical and morphometric evidence for a 120 km-diameter impact structure. *Aust J Earth Sci* 52:545–553
- Glikson AY, Uysal IT, Fitz Gerald JD, Saygin E (2013) Geophysical anomalies and quartz microstructures, Eastern Warburton Basin, North-east South Australia: Tectonic or impact shock metamorphic origin? *Tectonophysics* 589:57–76
- Glikson AY, Meixner AJ, Radke B, Uysal IT, Saygin E, Vickers J, Mernagh TP (2015) Geophysical anomalies and quartz deformation of the Warburton West structure, central Australia. *Tectonophysics* 643:55–72
- Glikson AY, Hickman AH, Evans NJ, Kirkland CI, Jung-WP RR, Romano S (2016a) A new 3.46 Ga asteroid impact ejecta unit at Marble Bar, Pilbara Craton, Western Australia: a petrological, microprobe and laser ablation ICPMS study. *Precamb Res* 279:103–122
- Glikson A, Korsch RJ, Milligan P (2016b) The Diamantina River ring feature, Winton region, western Queensland. *Aust J Earth Sci* 63:653–666
- Gorter JD (1996) Speculation on the origin of the Bedout high—a large, circular structure of pre-Mesozoic age in the offshore Canning Basin, Western Australia. *PESA News*, October/November 1996:32–34
- Gorter JD (1998) The petroleum potential of Australian Phanerozoic impact structures. *APPEA Journal* 1998:159
- Grieve RAF, Pilkington M (1996) The signature of terrestrial impacts. *Aust Geol Surv J Aust Geol Geophys* 16:399–420
- Grieve RAF, Shoemaker EM (1994) The record of past impacts on Earth. In: Gehrels T (ed) *Hazards due to comets & asteroids*. The University of Arizona Press, Tucson, pp 417–462
- Haines PW (1989) Probable impact structure near Barrow Creek, Northern territory. *Aust J Earth Sci* 36:135–137
- Haines PW (2005) Impact cratering and distal ejecta: the Australian record. *Aust J Earth Sci* 52:481–507
- Hallett M, Vassallo J, Glen J, Webster S (2005) Murray–Riverina region: an interpretation of bedrock Palaeozoic geology based on geophysical data. *Q Note Geol Surv NSW* 118:1–16

- Hamacher DW, Norris RP (2009) Australian aboriginal geomythology: eyewitness accounts of cosmic impacts? The University of Texas Press. Volume XXII, p 51
- Iasky RP, Glikson AY (2004) New possible buried impact structures in the Carnarvon and Officer Basins, Western Australia. *Geol Soc Aust Abst* 73:235
- Iasky RP, Glikson AY (2005) Gnargoo: a possible 75 km-diameter post-early Permian–pre-Cretaceous buried impact structure Carnarvon Basin Western Australia. *Aust J Earth Sci* 52:577–586
- Iasky RP, Mory AJ, Blundell KA (2001) The geophysical signature of the Woodleigh impact structure Southern Carnarvon basin, Western Australia. *Geol Surv West Aust Report* 79
- Jones AT, Gorter D, Kennard M (2010) Haines Structure: a probable Eocene complex impact structure in the offshore Canning Basin, Western Australia. *Aust J Earth Sci* 57:567–576
- Jourdan F, Reimold WU, Deutsch A (2012) Dating terrestrial impact structures. *Elements* 8:49–53
- Lightfoot PC, Naldrett AJ, Morrison G (1997) Sublayer and offset dikes of the sudbury igneous complex—an introduction and field guide. Ontario Geological Survey, Open File Report 5965, 37 p
- Lowe DR, Byerly GR (1986) Early Archaean silicate spherules of probable impact origin, South Africa and Western Australia. *Geology* 14:83–86
- Macdonald FA, Mitchell K (2003) Amelia Creek, Northern Territory, Australia: a 20x12 km oblique impact structure with no central uplift. In: *Impact cratering: bridging the gap between modelling and observations*, February 2003, Houston, Texas, p 47. Lunar and Planetary Institute Contribution 1155
- Macdonald FA, Mitchell K (2004) New possible, probable, and proven impact sites in Australia. *Geol Soc Aust Abst* 73:239
- Maier WD, Howard HM, Smithies RH, Yang S, Barnes S-J, O'Brien H, Huhma H, Gardoll S (2014) Mafic-ultramafic intrusions of the Giles Event, Western Australia: petrogenesis and prospectivity for magmatic ore deposits. *Geological Survey Western Australia Report* 134, p 82
- Müller RD, Goncharov A, Kristi A (2005) Geophysical evaluation of the enigmatic Bedout basement high, offshore northwest Australia. *Earth Planet Sci Lett* 237:265–284
- Pirajno F, Hawke P, Glikson AY, Haines P, Uysal T (2003) Shoemaker impact structure, Western Australia. *Aust J Earth Sci* 50:775–796
- Plescia JB (1999) Gravity signature of Teague Ring impact structure, Western Australia. *Geol Soc Am Spl Pap* 339:165–175
- Plumb KA (2005) Gulpuliyul structure: a possible impact structure of Mesoproterozoic age in western Arnhem Land, Northern territory. *Aust J Earth Sci* 52:665–673
- Renne et al (2004) Is Bedout an impact crater? Take 2. *Science* 306:610–612
- Sharpton VL, Martin LE, Carney JL, Lees S, Ryder G, Schuraytz BC, Sikora P, Spudis PD (1996) A model of the Chicxulub impact basin based on the evaluation of geophysical data well logs and drill core samples. *Geol Soc of Am Spl Pap* 307:55–74
- Shoemaker EM, Shoemaker CS (1996) The Proterozoic impact record of Australia. *Aust Geol Surv Org J Aust Geol Geophys* 16:379–398
- Simonson BM (1992) Geological evidence for an early Precambrian microtektite strewn field in the Hamersley Basin of Western Australia. *Geol Soc Am Bull* 104:829–839
- Wignall PB, Thomas B, Willink R, Watling J (2004) The Bedout Crater—no sign of impact. *Science* 306:609
- Williams IR (2007) *Geology of the Yilgalong 1:100 000 sheet, Explanatory notes*. Geological Survey of Western Australia, Perth
- World Impacts Database (2016) <http://www.passc.net/EarthImpactDatabase/>

Chapter 6

Asteroids and Crustal Evolution



Abstract Uniformitarian models for the early Earth take little or no account of repeated impacts of asteroid clusters and their effects on crust and mantle. However a growing body of evidence exists for multiple impacts by bodies on the scale of tens of kilometer during $\sim 3.47\text{--}2.48$ Ga, likely accounting at least in part for mafic-ultramafic volcanism produced by mantle rebound and melting events, consistent with the original suggestion by Green (Earth Planet Sci Lett 15:263–270, 1972, Precambrian plate tectonics. Elsevier, Amsterdam, pp 469–489, 1981). Further, the juxtaposition of at least four impact ejecta units with the fundamental unconformity between granite-greenstone terrains and semi-continental deposits in both the Barberton Greenstone Belt and the Pilbara Craton about $\sim 3.26\text{--}3.227$ Ga constitutes a primary example for the tectonic and magmatic effects of asteroid impact clusters in the Archaean, supporting Lowe and Byerly (Did the LHB end not with a bang but with a whimper? 41st Lunar Planet Science Conference 2563pdf, 2010) suggested extension of the late heavy bombardment (LHB).

6.1 Significance of Archaean Impacts

The lunar cratering record contains evidence for pre-Nectarian (pre-3.9 Ga) to Nectarian (about 3.85 Ga), whereas terrestrial records for this era, defined as Hadean, include high-grade metamorphic rocks (to ~ 4.0 Ga) and detrital or xenocrystic zircons (to ~ 4.4 Ga). The oldest Archaean terrains include banded granite gneiss such as in Greenland, Labrador, Slave and Superior Provinces of the Canadian Shield, Finland, South Africa, India, Western Australia and Brazil. To date equivalents of the $\sim 3.95\text{--}3.85$ Ga asteroid bombardment of the Moon (Late Heavy Bombardment – LHB) (Ryder 1990), which formed the lunar Mare, have not been identified. Whether the LHB constitutes a distinct temporal episode or represents a tail end of continuous bombardment has been questioned by some (Lineweaver and Norman 2008). Elucidation of the size-frequency of asteroid impacts (Fig. 6.1) and the growing body of isotopic age data for the geological record (Figs. 6.2 and 6.3), initially of Rb–Sr isochron ages and subsequently U–Pb zircon studies (Compston et al. 1986; Compston and Kröner 1988; Nelson 2008; O’Reilly et al. 2008;

Earth-crossing asteroids - impact incidence, size frequency and energy release (after D. Morrison, NASA, 2002)

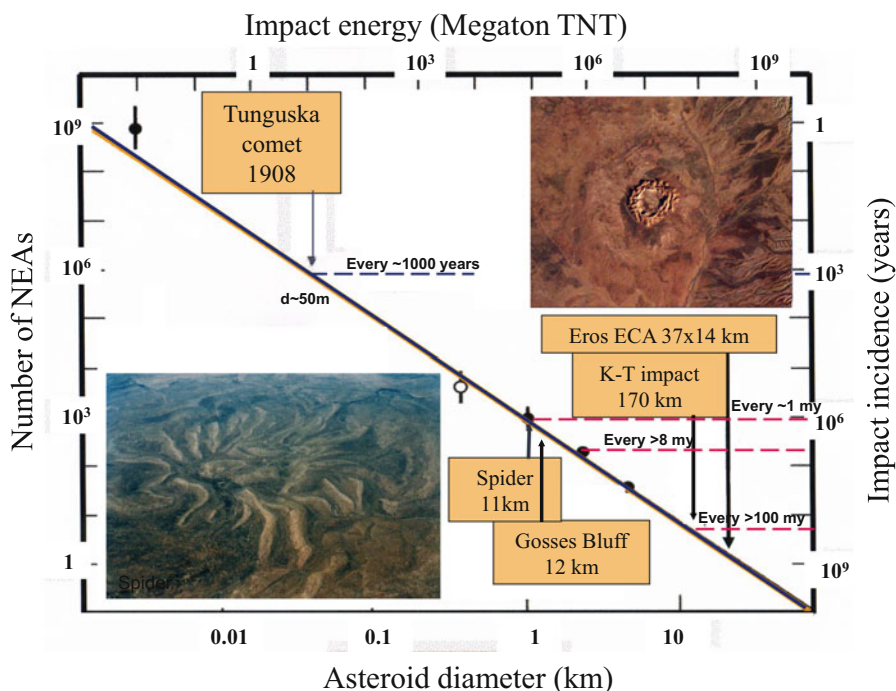


Fig. 6.1 Power-law fit to the average impact frequency for the whole Earth as a function of impact energy in megatons of TNT. Examples of impacts on different scales are shown for the Tunguska comet (Siberia), Spider impact structure (Kimberley, northern Australia), Gosse Bluff impact structure (NASA), the KT boundary impact and potential impact by the asteroid Eros (After Morrison 2006, NASA) (https://commons.wikimedia.org/wiki/Category:Spider_crater#/media/File:Spider_crater_zentrale_Kimberley-Region.jpg, https://commons.wikimedia.org/wiki/Category:Gosse_Bluff_crater#/media/File:Gosse_Bluff_Northern_Territory_Australia.jpg)

Valley 2008), allows the definition of distinct Archaean peak ages some of which correlate with impact episodes (Fig. 6.3). Such peak thermal events coinciding with asteroid bombardment periods, including 3.46–3.47 Ga, 3.24–3.26 Ga and 2.56–2.63 Ga (Fig. 6.3), militate for regional to global thermal events associated with large asteroid impacts.

Early SIAL crustal models have been advocated in part on the basis of the discovery of pre-volcanic zircons in greenstone belts (Compston et al. 1986) and of detrital zircons up to 4.4 Ga in the Narryer Terrain of the Yilgarn Craton, Western Australia (Harrison et al. 2005). The sial basement paradigm was questioned by other authors (Folinsbee et al. 1968; Goodwin 1974; Card 1990) who regarded andesite volcanics and intercalated sediments in-folded within Archean gneiss as ancient analogues of circum-Pacific island arc–trench systems. Geochemical

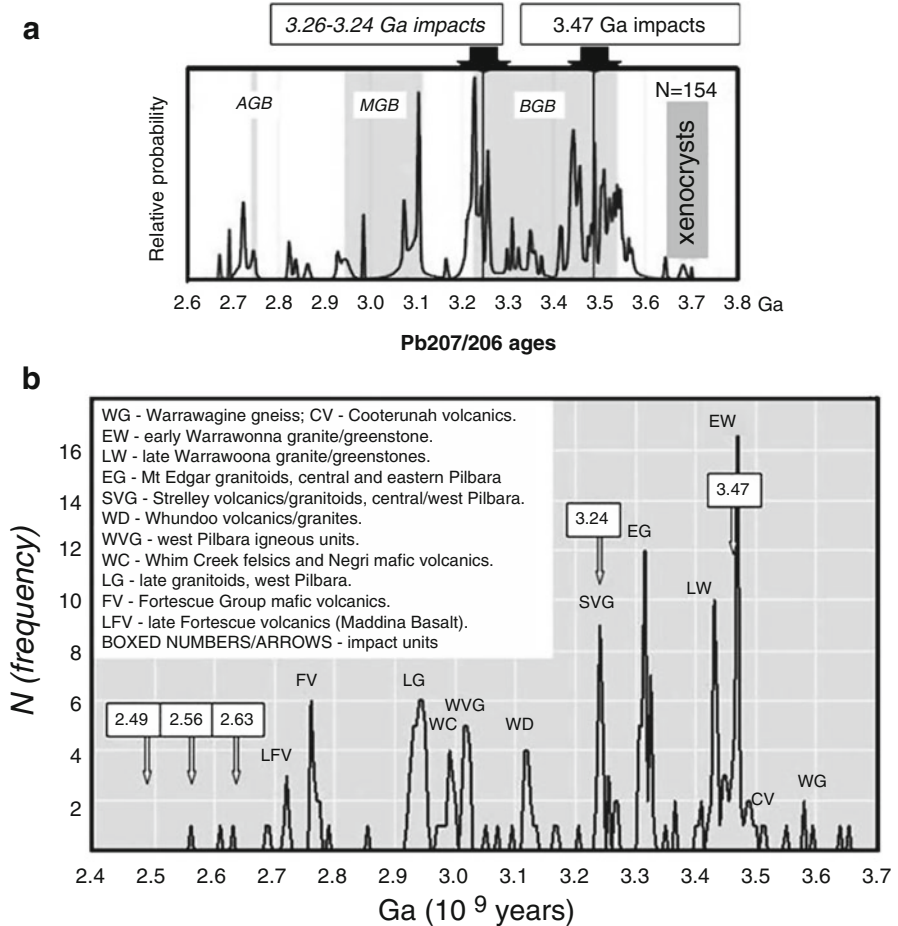


Fig. 6.2 Frequency distribution of U–Pb zircon ages in the eastern part of the Kaapvaal Craton, South Africa and frequency distribution of U–Pb ages from the Pilbara Craton, Western Australia. Boxed ages represent observed impact events in the Pilbara and Kaapvaal Cratons (After Glikson and Vickers 2006) (EPSL with permission)

evidence and isotopic data including initial $^{143}\text{Nd}/^{144}\text{Nd}$ and $d^{176}\text{Hf}$ data (McCulloch and Bennett 1994; Kamber 2007; Valley 2008) were increasingly interpreted in terms of plate tectonic models (Naqvi 1976; Tarney et al. 1976; Glikson 1972, 1984, 1999; Card 1990; Kröner et al. 1996). However, in so far as Earth was affected by the late Heavy Bombardment (LHB) during and before 3.95–3.85 Ga, which is inevitable in view of the effects of the LHB on the Moon and other terrestrial planets (Ringwood 1986), the early crust most likely consisted of a mixture of material, namely partial melts of the mantle and products of re-melting of mantle material (Green and Ringwood 1967). Such assemblages could consist of felsic volcanics, felsic hypabyssal rocks and anorthosites, some of

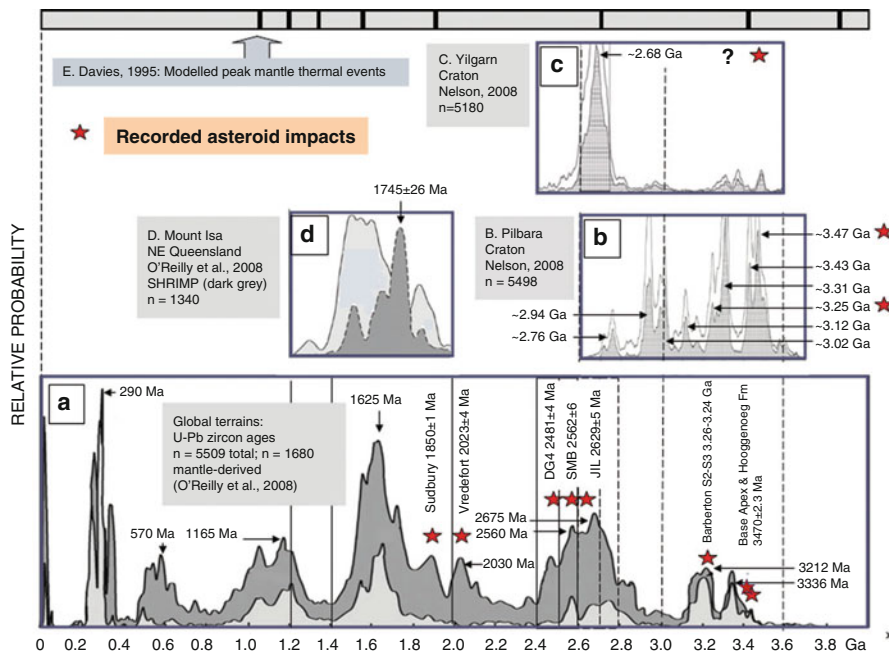


Fig. 6.3 Isotopic U-Pb zircon age frequency distribution (relative probability) diagrams. (a) Global (after O'Reilly et al. 2008). (b) Pilbara Craton, Western Australia (after Nelson 2008). (c) Yilgarn Craton, Western Australia (after Nelson 2008). (d) Northwest Queensland (after Nelson 2008). (e) Model mantle thermal events (Davies 1995). Stars represent recorded large asteroid impacts. Impact ages are located above stars; histogram peaks are indicated by horizontal arrows (After Glikson and Vickers 2010) (AJES with permission)

which may be represented by the oldest banded gneiss units. Interpretations of the terrestrial zircon record in terms of a Hadean felsic continental crust suffer from a major sampling bias in favor of preservation of resistant zircon grains vs the absence of labile mafic detrital material, rendering the overall composition of the pre-4.0 Ga Earth crust uncertain.

Considerations of the effects of asteroid impacts require a perspective on models of Archaean crustal evolution. A long-standing divergence between models of the early Archaean and the Hadean hinges on whether the early crust consisted (A) mostly felsic rocks (SIAL) (Hunter 1974; Oversby 1976; Bridgwater and Collerson 1976; Moorbath 1977; Windley 1977; Hickman 1981; Hamilton 2003; Harrison et al. 2005; Watson and Harrison 2005); (B) continuous recycling of SIAL crust affecting secondary depression of $^{87}\text{Sr}/^{86}\text{Sr}$ (Ri) values through isotopic exchange with the mantle (zone refining) (Armstrong 1968); or (C) a mafic SIMA oceanic-like crust (Engel 1966; Glikson 1971, 1972). A range of Archean models assume extensive continental crust (Oversby 1976; Baragar and McGlynn 1976; Archibald et al. 1978; Harrison et al. 2005), modified plate-tectonic regimes (Tarney et al. 1976; Windley 1977; Card 1990; Condie 1995; Smithies et al. 2003), and

mantle-plume-based models (Smithies et al. 2005; Van Kranendonk et al. 2007). As highlighted by Hamilton 1998, 2003 these models require tests of alternative or additional factors underlying Precambrian tectono-thermal events. Principal differences between ancient and modern volcanic and sedimentary environments include the vertical accumulation in greenstone belts of more than 10 km-thick volcanics and sediments over time spans as long as 300 Ma, for example from about ~3.5 to ~3.2 Ga in the Pilbara Craton and Kaapvaal Craton (Poujol et al. 2003; Hickman 2004; Hickman and Van Kranendonk 2004; Van Kranendonk et al. 2007). These relations are inconsistent with the lateral accretion of ophiolite–turbidite wedges over shorter time spans in circum-Pacific island arc–trench chains (Hamilton (1998, 2003). A distinction between Archaean and Phanerozoic geo-tectonics is the dome-pattern structure of granite–greenstone terrains referred to as ‘*gregarious batholiths*’ (Macgregor 1951). As distinct from the near-continuous accretion of circum-Pacific ophiolite–turbidite wedges (Hamilton 1998), Archaean magmatic pulsations constituted distinct temporal episodes.

The role of large impacts constitutes a factor capable of explaining some of the major differences between Archaean and modern crustal models. The evidence indicated above for likely relationships between the multiple 3.26–3.24 Ga impacts, related unconformities and plutonic events in the Barberton greenstone belt, and contemporaneous unconformities and megabreccia units in the Pilbara Craton, as well as the appearance of ferruginous sediments above impact fallout units (Table 1.1), signifies extensive mafic volcanism following impacts (Glikson and Vickers 2006; Glikson and Hickman 2014), underpinning the significance of impacts in Archaean crustal evolution.

It has been suggested by Lowe and Byerly (2010) that the Archaean asteroid bombardment can be regarded as an extension of the LHB on Earth. A cluster consisting of at least three asteroid impacts dated as 3.47–3.46 Ga has been studied in the Barberton and Pilbara terrains, overlapping the early Imbrian lunar period (Lowe and Byerly 1986; Lowe et al. 2003; Glikson 2004, 2006). Lunar impacts associated with Mare volcanism about ~3.2 Ga (early Eratosthenian) (Fig. 1.12) correlate with a large impact cluster which affected Archaean mafic-ultramafic crust and associated TTG (tonalite-trondhjemite-granodiorite) plutons, triggering abrupt uplift of this crust and forming small continental nuclei such as are documented in the eastern Kaapvaal Craton, South Africa, and the Pilbara Craton, northwestern Australia.

Studies of the Barberton greenstone belt, Eastern Transvaal and Swaziland (Viljoen and Viljoen 1969; Anhaeusser 1973), interpret the 10 km-thick sequence of the 3.55–3.26 Ga Onverwacht Group as ancient oceanic crust. The sequence consists of pillowed Mg-rich quench basalts, peridotitic lavas and intrusive dolerite and gabbro intercalated with thin units of quartz- and feldspar-rich tuff and chert. Trace-element studies by Sun and Nesbitt (1978) showed the production of these Mg-rich lavas required high degrees of melting of the early mantle under high geothermal gradients. The common presence of supracrustal enclaves within granitoid gneiss and U–Pb and Sm–Nd evidence for sialic precursors of meta-sediments has led to a ‘chicken and egg’

impasse. Some enclaves contain isotopic $^{207}\text{Pb}/^{206}\text{Pb}$ and $d^{143}\text{Nd}$ indices suggesting derivation from or contamination by older granitoids, an example being zircons in volcanic and sedimentary units of the Kalgoorlie greenstone belts, Western Australia (Compston et al. 1986).

The spatial and temporal association of the 3.26–3.24 Ga asteroid impact cluster at the top of the >10 km-thick mafic–ultramafic volcanic sequence of the Onverwacht Group and at the base of a turbidite/felsic volcanic sequence of the Fig Tree Group, and correlated olistostrome and deeply incised arenites in the Pilbara Craton, as well as associated plutonic magmatism, provide evidence of strong vertical movements, rifting and development of vertically dislocated terrains (Glikson and Vickers 2010). As indicated by the onset of the Mapepe Formation at 3258 Ma and of the Pincunah Hill Formation immediately above 3235 Ma, the documented field and isotopic age relationships indicate an overall overlap with the Barberton impacts. The onset of vertical movements and high-energy sedimentation, reflecting uplift, exposure and erosion of granitoids, was triggered at different regions at different points in time. The intrusion of major plutonic granitoids in both the Kaapvaal Craton and the Pilbara Craton within the period about 3.27–3.23 Ga overlaps the ages of the S2–S4 impact units and related tectonic events. The coincidence of these events with the top boundary of the predominantly mafic–ultramafic crust of the Onverwacht (including the Mendon Formation) and Warrawoona (including the Sulphur Springs Formation) indicates the fundamental break between SIMA-dominated and SIAL-dominated crust constituted a major tectono-magmatic event in Archaean history. Mass balance calculations based on Ir and Cr levels (Kyte et al. 2003; Shukolyukov et al. 2000) and thermodynamic-based correlations of microkrystite spherule sizes of 1–4 mm-diameter (O’Keefe and Aherns 1982; Melosh and Vickery 1991) suggest that the S2–S4 units resulted from impact by asteroids on the scale of 20–50 km-diameter, implying terrestrial impact basins some 300–800 km in diameter (Glikson 2005). The Fe–Mg-rich composition of the Barberton spherules and the relative scarcity, although not absence, of shocked quartz in the Archaean impact units (Rasmussen and Koeberl 2004) suggest these impact basins largely formed in simatic/oceanic regions of the Archaean Earth. From geochemical and isotopic evidence (McCulloch and Bennett 1994) such crust occupied over 80% of the Earth surface before ~3.0 Ga.

In view of the difficulty in visual detection of the small microkrystite spherules in the field and in drill cores it is estimated that no more than 1 in 10 of such units have been identified to date. Furthermore, an estimate of the stratigraphic gaps between isotopically dated units in the Pilbara Craton by A.H. Hickman (pers. com., 2017) (Table 6.1) suggests a time gap of approximately ~330 Ma. Compared to the total isotopic age range of the supracrustal sequences (3515–2943 = 572 Ma) this would suggest preservation of about 58 percent of the age sequence, further reducing the probability of discovery of the impact record. Based on the above it is tentatively suggested the original impact incidence in the Archaean Pilbara Craton was about an order of magnitude higher than the record of 17 impact events identified to date (Table 2.1), with implications for the effects of asteroid impacts on the Archaean crust.

Table 6.1 Temporal gaps between stratigraphic units in the Pilbara Craton, Western Australia (A. Hickman, pers com. 2017)

Stratigraphy	Youngest date (Ma)	Sample	Oldest date (Ma)	Sample	Gap (Ma)	Unconformity	Notes
Bookinarra Group	2943 ± 7	144,261	2964 ± 6	142,949	27	Unconformable on Whim Ck Gp	
Croydon Group	>2931 ± 5	141,977	<3015 ± 9	136,899		No known contact	
Whim Creek Group	2991 ± 12	UWA	3009 ± 4	141,936	7	Unconformity	Could be as old as 3066 Ma
Gorge Creek Group	3016 ± 13	142,842	3022 ± 12	127,330	90	Unconformity	Possible ≡ BIF deposition in NE Pilbara
Whundo Group	3112 ± 6	W193	3128 ± 4	N4325		No known contact	
Soanesville Group	3176 ± 3	180,098	<3228 ± 6	168,908	>7	Unconformity	
Sulphur Springs Group	3235 ± 3	94,002	3255 ± 3	60,925	60	Unconformity	Leilira Formation deposited
Wyman Formation	3315 ± 4	94,003	3525 ± 3	94,754	10	Conformable?	
Euro Basalt	3335 ± 3	168,999	3350 ± 3	178,042			Two dates on chert in Euro Basalt
Panorama Formation (upper)	3424 ± 16	169,008	3434 ± 5	142,952	74	Unconformity	Strelley Pool Formation deposited
					10	Unconformity	AB and PF (lower) locally eroded to zero

(continued)

Table 6.1 (continued)

Stratigraphy	Youngest date (Ma)	Sample	Oldest date (Ma)	Sample	Gap (Ma)	Unconformity	Notes
Panorama Formation (lower)	3444 ± 3	100,511	3449 ± 3	94,770			
Apex Basalt	3449 ± 3	94,770	3458 ± 2	100,507	0	Conformable	No dates on Apex Basalt
Duffer Formation and Mount Ada Basalt	3458 ± 2	100,507	3474 ± 7	142,975	9	Unconformity	Marble Bar Chert Member deposited
McPhee and Dresser Formations	3477 ± 2	148,498	3481 ± 3	180,070	3	Conformable?	Maximum age of Dresser Fm uncertain
Coonterunah Subgroup and North Star Basalt	3498 ± 2	168,995	3515 ± 3	70,601	34	Unconformity?	Maximum age c. 3530 Ma

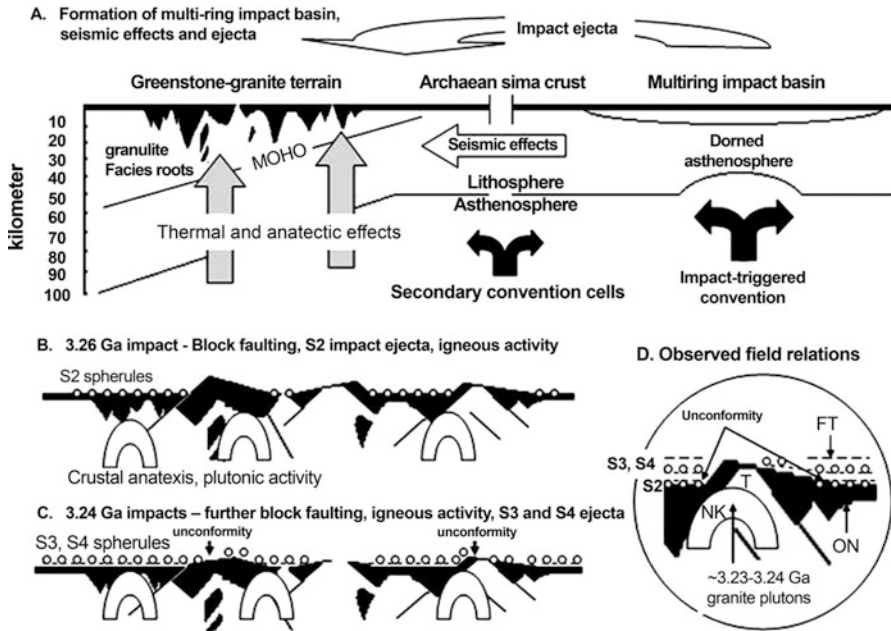


Fig. 6.4 Model (not to scale) portraying the principal stages in multiple 3.26 and 3.24 Ga impacts in an oceanic region of the Archean Earth and their geodynamic consequences, including formation of oceanic impact maria, mantle rebound and volcanic activity, ensuing rearrangement of mantle convection patterns, seismic activity affecting pre-existing granite-greenstone nuclei (microcontinent), faulting, uplift, erosion and formation of unconformities, anatexis at the roots of sial nuclei and rise of granitoid magmas. **(a)** ~3.26 Ga: formation of a multi-ring impact basin by a ~20 km asteroid, seismically triggered faulting, mantle rebound and onset of a new convection cell, thermal and anatexis effects across the asthenosphere–lithosphere boundary below sial nuclei. **(b)** ~3.26 Ga: Block faulting in sial nuclei, rise of anatexis granites, settling of S2 ejecta spherules, preservation of S2 spherules preserved below-wave-base environments. **(c)** ~3.24 Ga: S3 and S4 impacts, ejecta fallout and preservation in below-wave-base environments, further faulting, block movements and rise of plutonic magmas. **(d)** Schematic representation of observed field relationships between the ~3.55–3.26 Ga mafic–ultramafic volcanic Onverwacht Group (ON), intrusive early tonalites and trondjemites (T), 3.26–3.24 Ga granites (NK), S2 ejecta, unconformity, S3, S4 ejecta, and the Fig Tree Group sediments (FT) (After Glikson and Vickers 2010) (AJES with permission)

A model portraying the principal stages in multiple 3.26 and 3.24 Ga impacts in an oceanic region of the Archean Earth and their geodynamic consequences, including formation of oceanic impact maria, mantle rebound and volcanic activity, ensuing rearrangement of mantle convection patterns, seismic activity affecting pre-existing granite/greenstone sial nuclei (microcontinent), faulting, uplift, erosion and formation of unconformities, anatexis at the roots of sial nuclei and rise of granitoid magmas, is portrayed in Fig. 6.4, including the following stages: **(A)** ~3.26 Ga: formation of a multi-ring impact basin by a ~20 km-large asteroid, seismically triggered faulting, mantle rebound and onset of a new convection cell,

thermal and anatectic effects across the asthenosphere–lithosphere boundary below sial nuclei. (B) ~3.26 Ga: Block faulting in sial nuclei, rise of anatectic granites, settling of ejecta spherules and their preservation below-wave-base environments; (C) ~3.24 Ga: impacts, ejecta fallout and preservation in below wave-base environments, further faulting, block movements and rise of plutonic magmas.

6.2 Significance of Proterozoic and Phanerozoic Impacts

Compared with frequency distribution patterns of extra-terrestrial impact structures ND ~ D-1.8 (Grieve and Shoemaker 1994), the Australian trend display a relatively more common occurrence of large impact structures and depletion in small impact structures, a trend explained by the better preservation of large as compared to small structures (Figs. 5.20 and 5.21). The ages of several asteroid impact structures on the Australian continent (Haines 2005), commonly assigned to the Proterozoic on the basis of broad stratigraphic constraints remain undetermined (Table 4.1). These structures include in order of size: Yarrabubba (30–70 km; Proterozoic); Strangways (25–40 km; <642 Ma); Shoemaker (~29–30 km; <568 Ma); Amelia Creek (~20 × 12 km; <1640 Ma), Cleanskin (~15 km; <1400 Ma); Spider (11–13 km; 900–600 Ma); Goyder (9–12 km; ~1325 Ma); Kelly West (8–20 km; <1640 Ma); Foelsche (~6 km; Neoproterozoic); Matt Wilson (5.5 km; Neoproterozoic); Calvert Hills (>4 km; post-Mesoproterozoic) and Liverpool (1.6 km; Neoproterozoic). By contrast to the more precise stratigraphic and isotopic age definitions of Archaean impact ejecta units and Phanerozoic impacts, the lack of precise ages for likely Proterozoic impacts precludes detailed analysis of the temporal significance of Proterozoic impacts.

The ~580 Ma-old Acraman impact (Fig. 4.2) and its Bunyerroo ejecta equivalent in South Australia constitutes an exception event in terms of its size, estimated as 90 km, and the excellent preservation of its ejecta fallout deposits (Figs. 2.15 and 2.16). The associated extinction and radiation of Acritarch fauna (Grey et al. 2003) (Fig. 2.17) renders this event the oldest known mass extinction of species caused by an asteroid impact. The relations between Phanerozoic mega- impacts and mass extinction of species are less well established. Thus the ^{40}Ar - ^{39}Ar Ordovician (472+/-8 Ma) age reported for impact-related melt particles of the Lawn Hill structure (D = 18–20 km) (Darlington et al. 2016) is older than the Rhuddanian age (443.8–440.8 Ma) of the extinction (Elewa 2008).

The likely age of the 120 km-large Woodleigh impact structure (Iasky et al. 1998; Mory et al. 2000; Iasky et al. 2001; Glikson et al. 2005; Fig. 3.8) is provided by K–Ar isotope analysis of illite and mixed layered illite – smectite yielding a 359 ± 4 Ma age for basement gneiss (Uysal et al. 2001) coincident with the 359.2 ± 2.5 Ma Devonian – Carboniferous boundary (Gradstein et al. 2004). The Woodleigh impact represents a component of an end-Devonian impact cluster, including Charlevoix Crater (Quebec, Canada; 342 ± 15 Ma; 54 km) and Alamo impact structure (Nevada, ~367 Ma, ~100 km diameter).

A major question emerges in connection with the age of the twin Warburton impact structures (Glikson et al. 2013, 2015; Sects. 4.15, 4.16; Fig. 3.7) A tentative age for the impacts is constrained by the ~291 Ma age of the shock metamorphosed Big Lake Granite. The cooling and rise of these plutons are constrained by the 298 ± 4 Ma age of granite containing quartz with PDFs, and the c. 295 Ma age of overlying glacial sediments determined by pollen (Gatehouse et al. 1995). Whereas major geophysical features including deep crustal seismic tomographic, magnetic and Bouguer anomalies, coupled with planar deformation features (PDF) in quartz studied in drill cores have been identified (Glikson 2013, 2015), neither impact ejecta nor evidence of mass extinction have been identified to date. While a search for ejecta along the Carboniferous-Permian boundary is yet to be undertaken, the absence of paleontological evidence for an end-Carboniferous mass extinction event (Keller 2005) is puzzling in view of combined <400 km size of the Warburton twin impact structures. A possibility that the original age of the Big Lake Granite may be older, and may coincide with the end-Devonian mass extinction event, remains to be tested by further isotopic age studies.

A large post-early Permian pre-Cretaceous probable impact structure is represented by Gnargoo ($D = 75$ km) (Iasky and Glikson 2005) (Fig. 4.21) in the northern Carnarvon Basin, displaying remarkable structural analogies to the Woodleigh impact structure but which postdates Woodleigh as it deforms lower Permian sediments.

Gosses Bluff impact structure, located in the Missionary Plain syncline in central Australia (Milton et al. 1972), constitutes one of the best exposed impact structure in the world (Fig. 7.14) and part of the end-Jurassic cluster which includes Morokweng (70 m; 145.0 ± 0.8 Ma) and Mjølfnir (142.0 ± 2.6 Ma) are also members. The end-Jurassic (Tithonian) constitutes an extinction event when about 20 percent of genera disappeared (Keller 2005). About 13 percent of general disappeared in the Aptian following the 125 Ma Tookoonooka and Talundilly impacts (Keller 2005). A relatively minor extinction event of 10 percent of genera is also associated with the end-Eocene, the approximate age of the Mount Ashmore impact structure (Fig. 4.22 and 5.18). To summarize, a number of Australian impact events including Acraman, Lawn Hill, Woodleigh, Gosses Bluff, Tookoonooka, Talundilly and Mount Ashmore occur at or near to large, moderate or minor mass extinction events.

References

- Anhaeusser CR (1973) The evolution of the early Precambrian crust of southern Africa. *Philos Trans R Soc Lond A273*:359–388
- Archibald NJ, Bettenay LF, Binns RA, Groves DI, Gunthorpe RJ (1978) The evolution of Archaean greenstone terrains Eastern Goldfields Province, Western Australia. *Precambrian Res* 6:103–131
- Armstrong RL (1968) A model of the evolution of strontium and lead isotopes in a dynamic Earth. *Rev Geophys* 6:175–199

- Baragar WRA, McGlynn JC (1976) Early Archaean basement in the Canadian Shield: a review of the evidence, Geological Survey of Canada Paper 14. Geological Survey of Canada, Ottawa
- Bridgwater D, Collerson KD (1976) The major petrological and geochemical characteristics of the 3600 m.y. old Uivak Gneiss from Labrador. *Contrib Mineral Petrol* 54:43–60
- Card KD (1990) A review of the superior province of the Canadian Shield, a product of Archaean accretion. *Precambrian Res* 48:99–156
- Compston W, Kröner A (1988) Multiple zircon growth within early Archean Tonalitic gneiss from the ancient Gneiss Complex, Swaziland. *Earth Planet Sci Lett* 87:13–28
- Compston W, Williams IS, Campbell IH, Gresham JJ (1986) Zircon xenocrysts from the Kambalda volcanics: age constraints and direct evidence of an older continental crust below the Kambalda–Norseman greenstones. *Earth Planet Sci Lett* 76:299–311
- Condie KV (1995) Episodic ages of greenstone: a key to mantle dynamics? *Geophys Res Lett* 22:2215–2218
- Darlington V et al (2016) The Lawn Hill annulus: an Ordovician meteorite impact into water-saturated dolomite. *Meteor. Planet. Sci* 51: 2416–2440
- Davies GF (1995) Punctuated tectonic evolution of the Earth. *Earth Planet Sci Lett* 136:363–380
- Elewa A (2008) Late Ordovician Mass Extinction. p. 252. Springer, Dordrecht
- Engel AEJ (1966) The Barberton mountain land: clues to the differentiation of the Earth, Information circular 27. University of Witwatersrand, Johannesburg
- Folinsbee RE, Baadsgaard H, Cumming GL, Green DC (1968) A very ancient island arc. In: The crust and upper mantle of the Pacific area, American Geophysical Union Monograph 12. American Geophysical Union, Washington, DC, pp 441–448
- Gatehouse CG, Fanning CM, Flint RB (1995) Geochronology of the Big Lake Suite, Warburton Basin, north-east South Australia. *Q Geol Notes Geol Surv S Aust* 128:8–16
- Glikson AY (1971) Primitive Archaean element distribution patterns: chemical evidence and tectonic significance. *Earth Planet Sci Lett* 12:309–320
- Glikson AY (1972) Early Precambrian evidence of a primitive ocean crust and island nuclei of sodic granite. *Geol Soc Am Bull* 83:3323–3344
- Glikson AY (1984) Significance of early Archaean mafic–ultramafic xenolith patterns. In: *Archaean Geochem*, pp. 263–280. Springer, Berlin
- Glikson AY (1999) Oceanic mega-impacts and crustal evolution. *Geology* 27:341–387
- Glikson AY (2004) Early Precambrian asteroid impact-triggered tsunamis: excavated seabed debris flows exotic boulders and turbulence features associated with 3.47–2.47 Ga-old asteroid impact fallout units, Pilbara Craton, Western Australia. *Astrobiology* 4:1–32
- Glikson AY (2005) Geochemical and isotopic signatures of Archaean to early Proterozoic extra-terrestrial impact ejecta/fallout units. *Aust J Earth Sci* 52:785–799
- Glikson AY (2006) Asteroid impact ejecta units overlain by iron rich sediments in 3.5–2.4 Ga terrains Pilbara and Kaapvaal cratons: accidental or cause–effect relationships? *Earth Planet Sci Lett* 246:149–160
- Glikson AY, Hickman AH (2014) Coupled asteroid impacts and banded iron-formations, Fortescue and Hamersley Groups, Pilbara, Western Australia. *Aus J Earth Sci* 61:689–701
- Glikson AY, Vickers J (2006) The 3.26–3.24 Ga Barberton asteroid impact cluster: tests of tectonic and magmatic consequences Pilbara Craton Western Australia. *Earth Planet Sci Lett* 241:11–20
- Glikson AY, Vickers J (2010) Asteroid impact connections of crustal evolution. *Aust J Earth Sci* 57:79–95
- Glikson A, Mory AJ, Iasky R, Pirajno F, Golding S, Uysal IT (2005) Woodleigh, Southern Carnarvon Basin, Western Australia: history of discovery late Devonian age and geophysical and morphometric evidence for a 120 km-diameter impact structure. *Aust J Earth Sci* 52:545–553
- Glikson AY, Uysal IT, Fitz Gerald JD, Saygin E (2013) Geophysical anomalies and quartz microstructures, Eastern Warburton Basin, North-east South Australia: tectonic or impact shock metamorphic origin? *Tectonophysics* 589:57–76

- Glikson AY, Meixner AJ, Radke B, Uysal IT, Saygin E, Vickers J, Mernagh TP (2015) Geophysical anomalies and quartz deformation of the Warburton West structure, central Australia. *Tectonophysics* 643:55–72
- Goodwin AM (1974) Precambrian belts, plumes and shield development. *Am J Sci* 274:987–1028
- Gradstein FM, Ogg JG, Smith AG, Bleeker W, Laurens LJ (2004) A new geologic timescale with special reference to Precambrian and Neogene. *Episodes* 72:83–100
- Green DH (1972) Archaean greenstone belts may include equivalents of lunar maria? *Earth Planet Sci Lett* 15:263–270
- Green DH (1981) Petrogenesis of Archaean ultramafic magmas and implications for Archaean tectonics. In: Kroner A (ed) *Precambrian plate tectonics*. Elsevier, Amsterdam, pp 469–489
- Green DH, Ringwood AE (1967) An experimental investigation of the gabbro to eclogite transformation and its petrological applications. *Geochim Cosmochim Acta* 31:767–833
- Grey K, Walter MR, Calver CR (2003) Neoproterozoic biotic diversification: snowball earth or aftermath of the Acraman impact? *Geology* 31:469–472
- Grieve RAF, Shoemaker EM (1994) The record of past impacts on earth. In: Gehrels T (ed) *Hazards due to comets & asteroids*. The University of Arizona Press, Tucson, pp 417–462
- Haines PW (2005) Impact cratering and distal ejecta: the Australian record. *Aust J Earth Sci* 52:481–507
- Hamilton WB (1998) Archaean magmatism and deformation were not products of plate tectonics. *Precamb Res* 91:143–179
- Hamilton WB (2003) An alternative earth. *Geol Soc Am Today* 13:412
- Harrison et al (2005) Heterogeneous Hadean hafnium: evidence of continental crust by 4.4–4.5 Ga. *Science* 310:1947–1950
- Hickman AH (1981) Crustal evolution of the Pilbara Block. In: Glover JE, Groves DI (eds) *Archaean geology: second international Archaean symposium*, Perth, 1980, Geological society of Australia special publications 7. Geological Society of Australia, Sydney, pp 57–69
- Hickman AH (2004) Two contrasting granite–greenstones terrains in the Pilbara Craton, Australia: evidence for vertical and horizontal tectonic regimes prior to 2900 Ma. *Precambrian Res* 131:153–172
- Hickman AH, Van Kranendonk MJ (2004) Diapiric processes in the formation of Archaean continental crust, East Pilbara Granite–Greenstone Terrain, Australia. In: Eriksson PG et al (eds) *The Precambrian earth: tempos and events in Precambrian Time*, developments in Precambrian geology, vol 12. Elsevier, Amsterdam, pp 118–139
- Hunter DR (1974) Crustal development in the Kaapval craton: part 1 – the Archaean. *Precambrian Res* 1:259–294
- Iasky RP, Glikson AY (2005) Gnargoo: a possible 75 km-diameter post-early Permian–pre-Cretaceous buried impact structure Carnarvon Basin Western Australia. *Aust J Earth Sci* 52:577–586
- Iasky RP, Mory AJ, Shevchenko SI (1998) A structural interpretation of the Gascoyne platform Southern Carnarvon basin West Australia In: Purcell PG, Purcell RR (eds) *The sedimentary basins of West Australia*, Proc Petrol Explor Soc Aust Symp, Perth, pp 589–598
- Iasky RP, Mory AJ, Blundell KA (2001) The geophysical interpretation of the Woodleigh impact structure Southern Carnarvon Basin. *West Aust Geol Surv West Aust Rep* 79
- Kamber B (2007) The enigma of the terrestrial protocrust: evidence for its former existence and the importance of its complete disappearance. In: Condie KC (ed) *Developments in Precambrian geology*, vol 15. Elsevier, Amsterdam, pp 75–89
- Keller G (2005) Impacts volcanism and mass extinction: random coincidence or cause and effect? *Aust J Earth Sci* 52:725–757
- Kröner A, Hegner E, Wendt JI, Byerly GR (1996) The oldest part of the Barberton granitoid-greenstone terrain, South Africa: evidence for crust formation between 3.5 and 3.7 Ga. *Precambrian Res* 78:105–124

- Kyte FT, Shukolyukov A, Lugmair GW, Lowe DR, Byerly GR (2003) Early Archaean spherule beds: chromium isotopes confirm origin through multiple impacts of projectiles of carbonaceous chondrite type. *Geology* 31:283–286
- Lineweaver CH, Norman M (2008) The Bombardment history of the moon and the origin of life on earth. <https://www.mso.anu.edu.au/~charley/papers/LHBASSC2008.pdf>
- Lowe DR, Byerly GR (1986) Early Archaean silicate spherules of probable impact origin, South Africa and Western Australia. *Geology* 14:83–86
- Lowe DR, Byerly GR (2010) Did the LHB end not with a bang but with a whimper? 41st Lunar Planet Science Conference 2563pdf
- Lowe DR, Byerly GR, Kyte FT, Shukolyukov A, Asaro F, Krull A (2003) Characteristics, origin, and implications of Archaean impact-produced spherule beds, 3.47–3.22 Ga, in the Barberton Greenstone Belt, South Africa: keys to the role of large impacts on the evolution of the early Earth. *Astrobiology* 3:7–48
- Macgregor AM (1951) Some milestones in the Precambrian of southern Rhodesia (anniversary address by president). *Proc Geol Soc S Afr* IIV:xxvii–lxxiv
- McCulloch MT, Bennett VC (1994) Progressive growth of the Earth's continental crust and depleted mantle: geochemical constraints. *Geochim Cosmochim Acta* 58:4717–4738
- Melosh HJ, Vickery AM (1991) Melt droplet formation in energetic impact events. *Nature* 350:494–497
- Milton DJ, Barlow DJ, Brett R, Brown A, Manwaring EA, Moss FJ, Sedmik E, Van Son J, Young A (1972) Gosses Bluff impact structure, Australia. *Science* 175:1199–1207
- Moorbath S (1977) Ages, isotopes and the evolution of the Precambrian continental crust. *Chem Geol* 20:151–187
- Morrison D (2006) Asteroid and comet impacts: the ultimate environmental catastrophe. *Philos Trans Roy Soc Lond* 364:2041–2054
- Mory AJ, Iasky RP, Glikson AY, Pirajno F (2000) Woodleigh Carnarvon basin, Western Australia: a new 120 km-diameter impact structure. *Earth Planet Sci Lett* 177:119–128
- Naqvi SM (1976) Physical – chemical conditions during the Archaean as indicated by Dharwar geochemistry. In: Windley BF (ed) *Early history of the earth*. Wiley, London, pp 289–298
- Nelson DR (2008) Geochronology of the Archean of Australia. *Aust J Earth Sci* 55:779–793. 55
- O'Keefe JD, Aherns TJ (1982) Interaction of the Cretaceous/Tertiary extinction bolide with the atmosphere. *Geol Soc Am spec pap* 190:103–120
- O'Reilly SY, Griffin WL, Pearson NJ, Jackson SE, Belousova EA, Alard O, Saeed A (2008) Taking the pulse of the earth: linking crustal and mantle events. *Aust J Earth Sci* 55:983–996
- Oversby VM (1976) Isotopic ages and geochemistry of Archaean acid igneous rocks from the Pilbara, Western Australia. *Geochim Cosmochim Acta* 40:817–829
- Poujol M, Robb LJ, Anhaeusser CR, Gericke B (2003) A review of the geochronological constraints on the evolution of the Kaapvaal Craton, South Africa. *Precambrian Res* 127:181–213
- Rasmussen B, Koeberl C (2004) Iridium anomalies and shocked quartz in a Late Archean spherule layer from the Pilbara Craton: new evidence for a major asteroid impact at 2.63 Ga. *Geology* 32:1029–1032
- Ringwood AE (1986) Origin of the Earth and Moon. *Nature* 322:323–328
- Ryder G (1990) Lunar samples lunar accretion and the early bombardment of the Moon. *EOS Trans Am Geophys Union* 71:313–322
- Shukolyukov A, Kyte FT, Lugmair GW, Lowe DR, Byerly GR (2000) The oldest impact deposits on Earth. In: Koeberl C, Gilmour I (eds) *Lecture notes in Earth science 92: impacts and the early Earth*. Springer, Berlin, pp 99–116
- Smithies RH, Champion DC, Cassidy KF (2003) Formation of Earth's early Archaean continental crust. *Precambrian Res* 127:89–101
- Smithies RH, Van Kranendonk MJ, Champion DC (2005) It started with a plume. *Earth Planet Sci Lett* 238:284–297

- Sun SS, Nesbitt RW (1978) Petrogenesis of Archean Ultrabasic and basic volcanics: evidence from rare earth elements. *Contrib Mineral Petrol* 65(301):325
- Tarney J, Dalziel IWD, DeWit MJ (1976) Marginal basin 'Rocas Verdes' complex from south Chile: a model for Archean greenstone belt formation. In: Windley BF (ed) *Early history of the earth*. Wiley, London, pp 131–146
- Uysal T, Golding SD, Glikson AY, Mory AJ, Glikson M (2001) K–Ar evidence from illitic clays of a Late Devonian age for the 120 km diameter Woodleigh impact structure, southern Carnarvon Basin, Western Australia. *Earth Planet Sci Lett* 192:281–289
- Valley JW (2008) The origin of habitats. *Geology* 36:911–912
- Van Kranendonk MJ, Smithies RH, Hickman AH, Champion DC (2007) Paleo-archaean development of a continental nucleus: the east Pilbara terrain of the Pilbara craton. In: Van Kranendonk MJ, Smithies RH, Bennett VC (eds) *Earth's oldest rocks, Developments in Precambrian geology*, vol 15. Elsevier, Amsterdam, pp 307–337
- Viljoen MJ, Viljoen RP (1969) Archean volcanicity and continental evolution in the Barberton region, Transvaal. In: Clifford JN, Gass JP (eds) *African magmatism and tectonics*. Oliver and Boyd, Edinburgh, pp 29–47
- Watson EB, Harrison TM (2005) Zircon thermometer reveals minimum melting conditions on earliest Earth. *Science* 308:841–844
- Windley BF (ed) (1977) *Early history of the earth*. Wiley, London, pp 289–298

Chapter 7

Asteroids and Associated Mineral Systems



By Franco Pirajno

Abstract In this chapter we discuss hydrothermal and metasomatic processes that have taken place in impact structures, subsequent to the collapse of the transient cavity and the cooling of the melt sheet and melt rocks. Most of what follows is drawn from Pirajno et al. (*Aust J Earth Sci* 50:775–796, 2003), Pirajno (*Aust J Earth Sci* 52:587–620, 2005) and Pirajno and Van Kranendonk (*Aust J Earth Sci* 52:329–352, 2005), particularly for the Australian examples. The flow of hot aqueous solutions commonly results in the formation of mineral deposits. Therefore, knowledge of post-impact hydrothermal activity is important because it may have resulted in economic mineral deposits. The world-class and widely known Sudbury mineral deposits (Ni, Cu, PGE, Pb, Zn, Au) are perhaps the best and most celebrated expression of mineralization directly related to a meteorite impact (Lightfoot, Nickel sulfide ores and impact melts – origin of the Sudbury Igneous Complex. Elsevier, Amsterdam, 662pp, 2016). Several lines of evidence suggest that the giant gold deposits of the Witwatersrand in South Africa may have been reworked or even enhanced by the effects of the large Vredefort impact structure. These cases will be examined briefly in the sections that follow. Hydrothermal circulation systems associated with impact events have been reported from the Ries (Germany), Puchezh-Katunki (Russia), Jämtland (Sweden), Roter Kamm (Namibia), Manson (USA), the above-mentioned Vredefort, Kärdla (Estonia), Sudbury and Houghton (Canada) structures (Newsom et al., *J Geophys Res* 91:E239–E251, 1986; Koeberl et al., *Geoch Cosmo Acta* 53:2113–2118, 1989; Naumov, *Meteoritics* 28:408–409, 1993; Sturkel et al., *Eur J Miner* 10: 589–609, 1998; Ames et al., *Geology* 26: 447–450, 1998; McCarville and Crossey, *Geol Soc Am Sp Pap* 302:347–379, 1996); Grieve and Thierriault, *Annu Rev Earth Planet Sci* 28: 305–338, 2000; Osinski et al., *Meteor Planet Sci* 36:731–745, 2001; Molnár et al., *Econ Geol* 96:1645–1670, 2001; Puura et al., Impact-induced replacement of plagioclase by K-feldspar in granitoids and amphibolites at the Kärdla crater, Estonia. In: Gilmour I, Koeberl C (eds) *Impacts and the early earth*. Springer-Verlag, Berlin, pp 417–445, 2000 and *Geochemistry of K-enriched impactites, based on drillings into the Kärdla Crater, Estonia*. *Geol Soc Am Abs with Programs*, Denver, Oct. 2002, p 341, 2002). Recently, aspects of hydrothermal alteration in the

Chicxulub impact structure have been published in *Meteoritic and Space Science* (Lüders and Rickers, *Meteor Planet Sci* 39:1187–1198, 2004; Zürcher and Kring, *Meteor Planet Sci* 39:1199–1222, 2004; Goto et al., *Meteor Planet Sci* 39:1233–1247, 2004).

7.1 Introduction

Hypervelocity impacts cause melting of the target rocks and form a crater resulting in the conversion of kinetic to thermal energy, which in turn causes thermal perturbations and heat release particularly in the central structural uplifts, which bring near the surface deeper and hotter crust. These thermal effects result in a spectrum of phenomena from partial melting to high-temperature metamorphism and hydrothermal fluid flow. In general, the transformation of kinetic energy into heat will take place mainly at sub-crater levels, where hydrothermal circulation would be focused, although impact-related hydrothermal circulation can extend well below the crater floor to depths of several kilometers (Komor et al. 1988). It is also likely that impact-related hydrothermal fluids can vent at the surface as hot springs and geysers, forming silica-rich deposits (Newsom 1980). The effects of hydrothermal fluid flow would be presumably greatly enhanced if the impact occurs in ocean, where seawater would rush into the heated and fragmented target rocks, as probably was the case for Chicxulub (Goto et al. 2004). The flow of hydrothermal fluids leaves its mark on the rocks through which they pass in the form of new mineral assemblages, with processes that involve cation and H⁺ metasomatism and resulting in hydrothermal alteration. An overview of the economic aspects of impact structures was presented by Reimold et al. (2005).

In this chapter we discuss hydrothermal and metasomatic processes that have taken place in impact structures, subsequent to the collapse of the transient cavity and the cooling of the melt sheet and melt rocks. Most of what follows is drawn from Pirajno et al. (2003), Pirajno (2005) and Pirajno and Van Kranendonk (2005), particularly for the Australian examples. The flow of hot aqueous solutions commonly results in the formation of mineral deposits. Therefore, knowledge of post-impact hydrothermal activity is important because it may have resulted in economic mineral deposits. The world-class and widely known Sudbury mineral deposits (Ni, Cu, PGE, Pb, Zn, Au) are perhaps the best and most celebrated expression of mineralization directly related to a meteorite impact (Lightfoot 2016). Several lines of evidence suggest that the giant gold deposits of the Witwatersrand in South Africa may have been reworked or even enhanced by the effects of the large Vredefort impact structure (Pirajno 2009 and references therein). Both these cases will be examined briefly in the sections that follow. Hydrothermal circulation systems associated with impact events have been reported from the Ries (Germany), Puchezh-Katunki (Russia), Jämtland (Sweden), Roter Kamm (Namibia), Manson (USA), the above-mentioned Vredefort, Kärdla (Estonia), Sudbury and Haughton (Canada) structures (Newsom et al. 1986; Koeberl et al. 1989; Naumov 1993;

Sturkel et al. 1998; Ames et al. 1998; McCarville and Crossey 1996); Grieve and Therriault 2000; Osinski et al. 2001; Molnár et al. 2001; Puura et al. 2000 and 2002). Recently, aspects of hydrothermal alteration in the Chicxulub impact structure (Ames et al. 2004) have been published in *Meteoritic and Space Science* (Lüders and Rickers 2004; Zürcher and Kring 2004; Goto et al. 2004).

7.2 Asteroid and Cometary Impacts and Hydrothermal Circulation

Allen et al. (1982) studied hydrothermally altered melt rocks and breccia from 12 impact structures, including Ries, Manicouagan and Sudbury, and suggested possible analogues at Martian impact sites. These authors recorded dominant assemblages consisting of clay minerals, chlorite, mixed layer illite-chlorite, silica, K-feldspar and zeolites, which they estimate to have formed at low pressures and at temperatures between 100 and 300 °C. Newsom (1980) proposed a model of interaction of water and impact melt sheets. Commonly, impact-related hydrothermal systems result in the remobilization and deposition of sulphides in breccia or fracture zones. Naumov (2002) provided a detailed account of impact-related hydrothermal processes in three major impact structures: Kara, Popigai and Puchezh-Katunki, briefly introduced below, together with other examples.

In the Ries impact structure, hydrothermal alteration minerals include illite, montmorillonite, analcite, calcite, siderite, K-feldspar, quartz, barite and chlorite (Newsom et al. 1986). The Puchezh-Katunki 80-km diameter impact crater (Russia) is characterised by widespread hydrothermal alteration, mainly concentrated within the central uplift, which is composed of brecciated Archaean basement rocks. At this impact site, Naumov (1993) recognized the following hydrothermal assemblages: (1) chlorite + albite + epidote + calcite, associated with andradite garnet, epidote and prehnite in fractures; (2) prehnite + calcite + pyrite, absence of Ca-Fe silicates; (3) zeolites + apophyllite + calcite + anhydrite + pyrite in vugs and fractures. Masaitis and Naumov (1993) modelled the hydrothermal convection for the Puchezh-Katunki structure and suggested that the fluids originated by infiltration of water from a crater lake towards a lens of hot impact breccia and basement rocks. These fluids would have reached the surface along the uplifted margins. Masaitis and Naumov (1993) proposed three stages of hydrothermal activity: (1) an initial stage, with temperatures in the region of 400–500 °C, decreasing downward and outward from the impact site; (2) a main stage, with maximum temperatures of 200–300 °C, and fluids circulating at depths of 2.5–4 km; and (3) a final stage, in which circulation is restricted to the uppermost parts of the basement rocks, with temperatures of 150–100 °C.

Alkali metasomatism at deep levels is followed by a lower temperature hydrothermal regime, which partially obliterates the alkali-rich rocks, but is best manifested at higher levels, possibly because of downward flow of meteoric water-

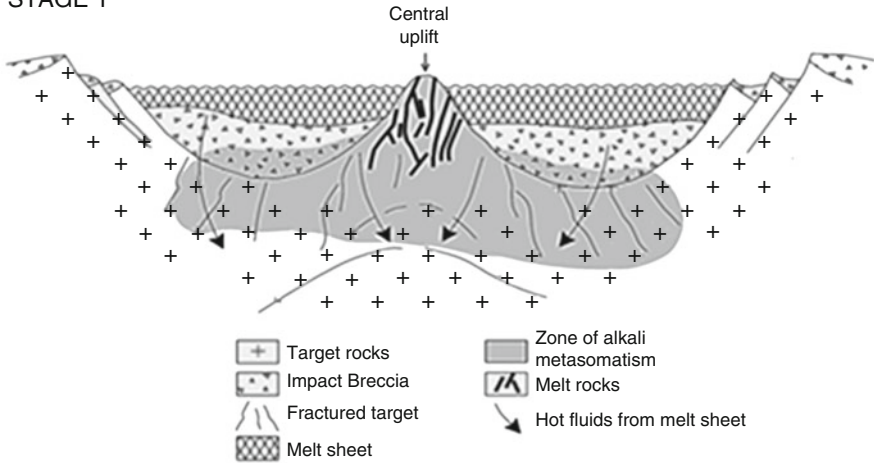
dominated hydrothermal circulation. A view of this lower temperature regime at higher levels is provided by the central uplift of the Woodleigh structure, where the dominant alteration minerals are phyllosilicates with carbonate overprints. Impact-induced alkali metasomatism and the presence of syenite-like rocks in impact structures may be more common than realized. Puura et al. (2000, 2002) studied impact-induced K metasomatism in sub-crater basement granitoids for the Kärddla Crater in Estonia. These authors found strong chemical and mineralogical alteration of the sub-crater lithologies. Chemical alteration includes K enrichment and Na and Ca depletion, whereas the mineralogical alteration results in changes in the structural state of the feldspars (related to K enrichment, Na and Ca removal) and decomposition of hornblende to Fe-rich chlorite and quartz. Puura et al. (2000) concluded that these changes took place as a result of post-impact alteration processes, but that the source of K is unknown. However, the authors also pointed out that geochemical studies of impactites indicate selective mobility of alkalis with loss of K and Na in strongly shocked rocks from large craters. The K and Na lost from shocked rocks could be mobilized, during phases of post-impact hydrothermal action, resulting in the enrichment of the surrounding and/or deeper lithologies. Three possibilities are considered for the selective mobility of alkalis (Puura et al. 2000): (1) impact-induced high temperature hydrothermal system; (2) ultrahigh-temperature and pressure mobilization of fluids; and (3) action of low-temperature post-impact hydrothermal system.

7.3 A Working Model

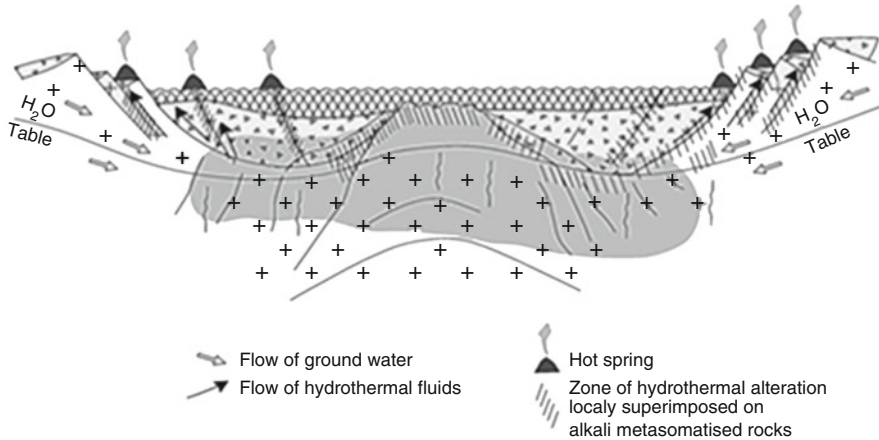
A working model of a hydrothermal system that may develop within, and as a result of meteorite impacts on land is shown in Fig. 7.1. This model schematically shows two stages of the hydrothermal processes, which clearly represent end members of a continuum. In stage 1, hydrothermal fluids are primarily derived from “magmatic” heat supplied by the melt sheet and melt injected into the surrounding target rocks. This is a magmatic-hydrothermal stage during which alkali metasomatism is dominant. This is the stage of highest temperature (probably 500–600 °C) in which mineral reactions result in the formation of K-feldspar and/or albite (potassic and sodic metasomatism), resulting in the modification of protoliths to a rock of syenitic affinity. In addition to the alkali metasomatism previously mentioned for the Kärddla structure, impact-related Ca-Na-K metasomatism has also been well-documented at Chicxulub by Zürcher and Kring (2004). These authors reported the occurrence of the same alteration phases as those found in Shoemaker and Yarrabubba, namely albite, K-feldspar, titanite, diopside-hedenbergite, amphibole, biotite and epidote.

This type of alteration affects the shattered target rocks well below the melt sheet and are best manifested at the lower levels of an impact structure. Progressive cooling of the melt sheet with decaying of the high-temperature magmatic fluid system and inflow of meteoric waters lead to stage 2. In this lower temperature regime (<500 °C), the flow of hydrothermal fluids is dominantly fracture-controlled.

STAGE 1



STAGE 2



FMP774

24.01.05

Fig. 7.1 Model of hydrothermal fluid circulation in impact structure; details in text (After Pirajno 2005)

Much of the thermal energy for this stage could be provided by the hot rocks of the central uplift. The uplifted central peak is therefore especially affected, as is shown in the Woodleigh structure. Quite possibly hot springs discharge at surface, within remnants of the crater, and/or along its walls, with their pathways bearing the signs of the passage of hot solutions, resulting in hydrothermal mineral assemblages that form alteration types like those found in volcanic epithermal systems. These include phyllic, propylitic, argillic, silicification and carbonatization types including mineral phases such as sericite, chlorite, epidote, calcite, hematite, iron carbonates, and quartz. These alteration types overprint the earlier assemblages of the alkali metasomatic stage. Boiling of fluids in the hot spring system forms veins of bladed calcite

within zones dominated by silicified rocks. This may have been the case at Yarrabubba (Figs 4.3 and 4.4). Phase separation is potentially a very important mechanism for the precipitation of metal sulphides and gold. The presence of hot springs also constitutes an ideal environment for microbial life, and this too may lead to metal precipitation by biologically mediated processes.

The activity of a hydrothermal system in impact structures is effectively no different from those formed in magmatic settings, except perhaps in terms of duration. The largest impacts (e.g. Vredefort, Sudbury, Chicxulub) would have had hydrothermal systems operating for long periods of time (100 s of thousands of years; Rowe et al. 2004), whereas hydrothermal activity in smaller impacts is likely to be short-lived. It is estimated that melt pools can provide the heat source necessary to drive hydrothermal circulation systems for some 100,000 years (Kring 1995; McCarville and Crossey 1996). The depth extent of hydrothermal flow is also related to the size of the impact structure. Depths of 2–4.5 km have been recognized by Naumov (1993), whereas a depth of 5 km has been estimated for the 80-km diameter Puchezh-Kantunki impact crater (Pevzner et al. 1992; Zürcher and Kring 2004). In this light, it is also possible that for the larger impacts (mega-impacts; e. g. Vredefort, Sudbury) the thermal effects could spatially extend well beyond the crater's limits, with impact-induced fluids circulating in pre-existing fractures and faults in country rocks and around the crater.

7.4 Mineral Deposits and Impact Structures

The inception of impact-induced hydrothermal activity may have important consequences in terms of ore formation or modification of existing mineralization. There is already a substantial body of evidence to suggest that economically important mineral deposits owe their existence, directly or indirectly, to impact events. A review of economic mineral deposits associated with impact structures can be found in Reimold et al. (2005), who also provided a list of all impact structures that are associated with mineral systems and hydrocarbons. A key paper detailing the economic potential of impact structures is that of Grieve and Masaitis (1994), who classified impact-associated ore deposits, as progenetic, syngenetic and epigenetic, as briefly described below.

Progenetic mineral deposits are those that existed before the impacting event, but subsequently modified during and after the impact. Examples are: (1) the Fe and U ores at the Ternovka structure (age 375 Ma, 15–18 km diameter) in the Ukraine; (2) U ore at the Carswell structure (age 115 Ma, 39 km diameter) in Canada; (3) Au and U associated with the Vredefort multi-ringed structure. In Australia, a possible example of redistribution of ore minerals as a result of impact-related hydrothermal fluids is provided by MVT type sulphide deposits around the Shoemaker structure.

Fluid inclusions data from these deposits exhibit increasing temperatures towards the impact structure (Pirajno et al. 2003).

Syngenetic deposits are those that are formed as a direct consequence of the impact, either during or soon afterwards. They include magmatic type Cu-Ni-PGE and diamonds. The best known example is above-mentioned Sudbury Igneous Complex with its world-class Ni-Cu sulphide deposits (Naldrett 2002; Lightfoot 2016). The high pressure of shock metamorphism (greater than 30 GPa) can produce diamonds from pre-existing carbon in the target rocks, such as graphite and coal. Impact diamonds are known from a number of localities. These include the Kara (68 Ma and 65 km-diameter) and Popigai (35.7 Ma and 100 km-diameter) structures in Russia; the Ries crater in southern Germany. The Popigai impact-formed diamonds are polycrystalline, not of industrial quality, but they are harder than mantle-derived diamonds (Koeberl et al. 1997). The Ries crater is 24 km in diameter and was formed 15 Ma ago; here the occurrence of diamond and lonsdaleite (a polymorph of diamond) and silicon carbide was reported by Hough et al. (1995). A speculative corollary is that, since most mantle-derived diamonds are known to be approximately 3.3 Ga old (e.g. Phillips et al. 1989), could it be that they may be associated with Eo-Archaeon mega-impacts?

Epigenetic deposits form as a result of hydrothermal circulation within and around the structure, caused by cooling of impact melt sheets or by related magmatic activity. Examples of hydrothermal ores are numerous. They include Pb, Zn, Ag and Ba at Siljia in Sweden (Johansson 1984), Serpent Mound, USA, and Cu, Zn, Pb, Au at Vermilion in the Sudbury structure. Also in the Sudbury structure, a number of Zn-Cu-Pb massive sulphides deposits can be ascribed to post-impact hydrothermal activity (see Naldrett 2002 and references therein; Golightly 1984). Hildebrand and Pilkington (2002) on the basis of seismic and aeromagnetic data suggested that the floor of the Chicxulub crater may contain exhalative sulphide deposits and calculated a possible metalliferous concentration of 50×10^6 Mt. It is interesting to note that Zürcher and Kring (2004) likened the Chicxulub hydrothermal system to that which is characteristic of Fe oxide-Cu-Au-REE deposits, such as Olympic Dam in South Australia.

Included in epigenetic deposits are hydrocarbon occurrences related to the formation of impact basins with restricted sedimentation. This is because impact events induce considerable fracturing, thus enhancing the permeability of the target rocks, which may result in the formation of oil and gas traps. The Ames buried structure (450 Ma, 14 km diameter in Oklahoma, USA) contains important reserves of hydrocarbons (Carpenter and Carlson 1992; Donofrio 1998). The 25 km-diameter Steen River impact structure in Canada has an estimated 3 billion barrels of oil along the rims of the structure (Grieve 2003). Chicxulub offshore has reserves of 30 billion barrels. In Queensland, Australia, the 55 km-diameter Tookoonooka structure also contains hydrocarbons (Gorter 1998). Impact structures associated with productive oil fields are found in the Cretaceous Avak (Alaska) and the late Cambrian Newporte structures (Kirschner et al. 1992; Forsman et al. 1996).

In the sections that follow, examples of epigenetic and progenetic deposits in which the hydrothermal activity is linked with impact events are described.

7.5 The Sudbury Hydrothermal System

Sudbury (Ontario, Canada) is an 1850 Ma deformed impact structure whose original diameter was about 140 km (Melosh 1989; other estimates consider diameters of 200–250 km, Dressler and Sharpton 1999). Sudbury or more accurately the Sudbury Igneous Complex is probably best known for its mineral wealth, which includes world-class Ni-Cu ores as well as a number of Zn-Cu-Pb massive sulphides deposits (see Naldrett 2002 and references therein; Golightly 1984; Lightfoot 2016).

Ames et al. (1998) recognized regional-scale semi-conformable hydrothermal alteration in the Sudbury structure, more specifically in the Onaping Formation, which represents crater-fill rocks (Fig. 7.2). This alteration is pervasive and consists of silicification, albitization, chloritization, calcitization and complex phases of feldspathization (microcline, hyalophane and celsian). The authors linked this alteration to a basin-wide hydrothermal circulation, which resulted in the formation of the

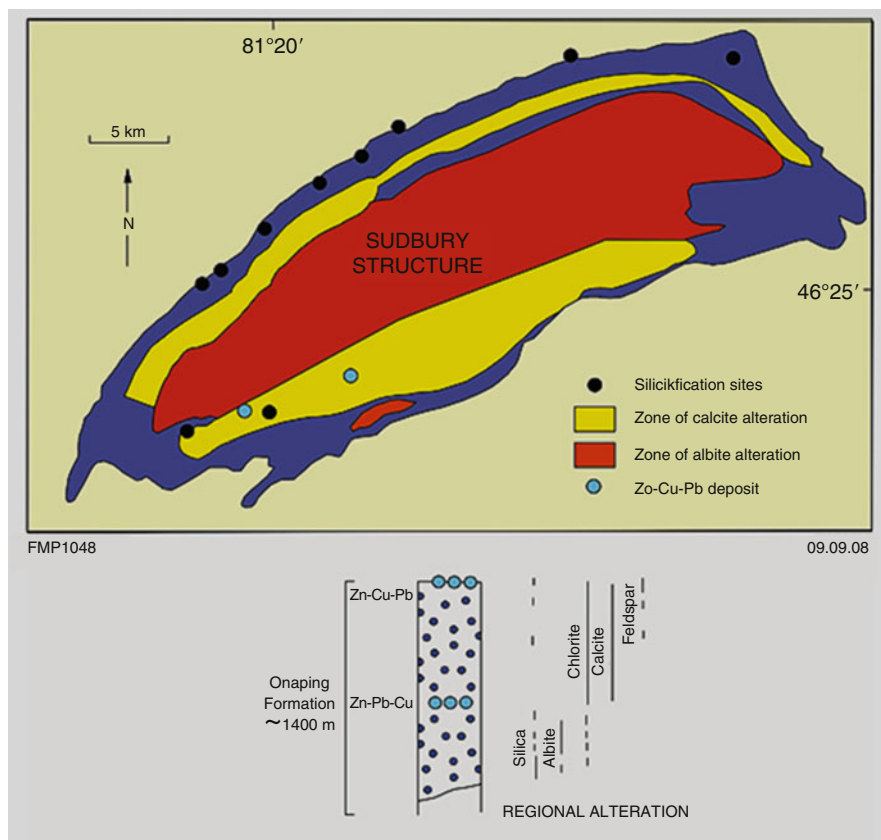


Fig. 7.2 Outline of the Sudbury impact structure showing distribution of mineral deposits and alteration zones (After Molnár et al. 2001)

above-mentioned Zn-Cu-Pb massive sulphide deposits (Fig. 7.2). On the basis of geochronological data Ames et al. (1998) argued that this extensive alteration lasted from tens to hundreds of thousand years and is related to conductive heat loss of the Sudbury Igneous Complex. The authors concluded that this comparatively short-lived impact-induced hydrothermal system resulted in the alteration zones and mineralization similar to the VHMS of volcanic terranes.

Molnár et al. (2001), based on a systematic fluid inclusion study of samples along the contacts of the Sudbury Igneous Complex with the North Range footwall rocks, recognized that post-impact hydrothermal processes were responsible for vein type Cu-Ni-PGE mineralization. These authors established at least three stages of hydrothermal activity. Early stage high temperature (>400 °C) fluids resulted in hydrothermal assemblages of epidote-quartz-actinolite-chlorite, which form vein selvages, where Cu, Ni and PGE occur as veins and disseminations. A second stage of hydrothermal activity is characterized by carbonic-aqueous fluids (at least two coexisting fluids; 20–26 wt% and 6–12 wt% NaCl equivalent), which caused the formation of carbonate-epidote-actinolite-chlorite veins, overprinting the earlier assemblage. These fluids also precipitated Cu, Ni, Bi sulphides and native silver. Fluid inclusions indicate that these fluids boiled at about 300–350 °C, during uplift from 6 km to 3–4 km. A final stage of hydrothermal activity was dominated by aqueous solutions (20–40 wt% salinity) with temperatures of between 150 and 250 °C. These late fluids were channeled along fractures more or less parallel to the Sudbury Igneous Complex and footwall contacts. They formed late veinlets containing chalcopyrite-epidote-quartz-chlorite. However, Molnár et al. (2001) related this late stage hydrothermal activity to a tectonothermal event linked to the emplacement of dykes at 1.24 Ga.

7.6 The Lockne Impact Structure

This 455 Ma structure in central Sweden was formed in a marine environment, with seawater depths of about 200 m, with the final crater being at a depth of 500 m (Sturkel et al. 1998). The 13.5-km diameter Lockne structure provides an excellent example of an impact structure in which hydrothermal processes took place in a marine setting and with seawater as the source of the fluids.

Sturkel et al. (1998) conducted a comprehensive study of fluid inclusions and stable isotopes from drill core samples. The Lockne impact breccia and the fractured basement contain cavities filled with hydrothermal minerals which include calcite, quartz, chalcopyrite, pyrite, galena and zeolites, as well as solid bitumen. At least three phases of fluid activity are recognized in fluid inclusion trapped in quartz crystals (phase 1), calcite and sulphides (phase 2) and late calcite (phase 3). Gaseous inclusion in quartz consist of CH₄ and other hydrocarbons, whereas aqueous inclusions in sulphides and calcite contain CaCl₂-NaCl-H₂O, with salinities ranging from 28.8 to 20.5 wt % NaCl equivalent. Temperatures of liquid-vapour homogenization range from 77 to 218 °C, with most values between 100 and 180 °C. Fluid inclusion

studies of samples collected from outcrops also showed the presence of $\text{CaCl}_2\text{-NaCl-H}_2\text{O}$ -rich solutions, which homogenize between 136 and 169 °C. The presence of CH_4 in the fluid inclusions is interpreted by the authors as the result of organic-rich clay in the Cambrian shales of the target which were thermally altered and decomposed by impact-heated basement rocks to form hydrocarbons and CH_4 -rich fluids. Sulphides have $\delta^{34}\text{S}$ values ranging from +1 to +5.5‰. The authors suggested that the S was largely derived from the fractured mafic volcanic basement. $\delta^{13}\text{C}$ determinations for the hydrothermal calcite yielded values of -2 to 14‰, suggestive of a mixed marine and organic source.

Sturkel et al. (1998) concluded that the impact-induced hydrothermal convection system of the Lockne structure was short lived and low-temperature, but nevertheless capable of generating sulphides and hydrocarbons.

7.7 The Vredefort Meteorite Impact and the Case for Witwatersrand Gold

The greatest concentration of gold in the world is in the Witwatersand Basin (Witwatersrand Supergroup), South Africa (Fig. 7.3), where in the order of 50,000 tonnes of Au have been mined between 1886 and 2004, or about 40% of all the gold mined in recorded history (Frimmel et al. 2005). Overviews of the geology of the Witwatersrand are provided by Frimmel et al. (2005) and Law and Phillips (2005). The Witwatersrand Supergroup is subdivided into the West Rand (older) and Central Rand (younger) Groups, overlying the Dominion Group and all lying on a basement of Archaean granite-greenstone rocks (Kaapvaal Craton). The Witwatersrand rocks are predominantly clastic sediments, which include the ore-bearing braided fluvial conglomerates. The maximum ages of the West Rand and Central Rand Groups provided by detrital zircons are 2914 ± 8 Ma and 2902 ± 13 Ma, respectively. Xenotime dating yielded a minimum age of 2780 ± 3 Ma for the Central Rand Group. The exceptional Au endowment of the Witwatersrand goldfields has fascinated geologists for well over a century. Ideas on the origin of the “Wits gold” span the full range from placer (alluvial, lacustrine delta and even marine), to placer subsequently modified through hydrothermal circulation (modified placer model) to purely hydrothermal and other genetic models. Enter the catastrophic event of a meteorite impact to add to the complicated and fascinating geological history of this part of the world, where the largest layered intrusion with the largest Cr and Pt deposits in the world and the basin with largest Au accumulation in the world occur in the same region: the Kaapvaal Craton.

The Witwatersrand goldfield is generally considered a palaeo-placer deposit, based on evidence provided by the presence of detrital uraninite and pyrite (buckshot pyrite), studies of detrital zircons showing that detrital gold and pyrite have pre-sedimentation ages and the fact that most gold is associated with fluvial conglomerates. However, gold is also found redistributed in microfractures and

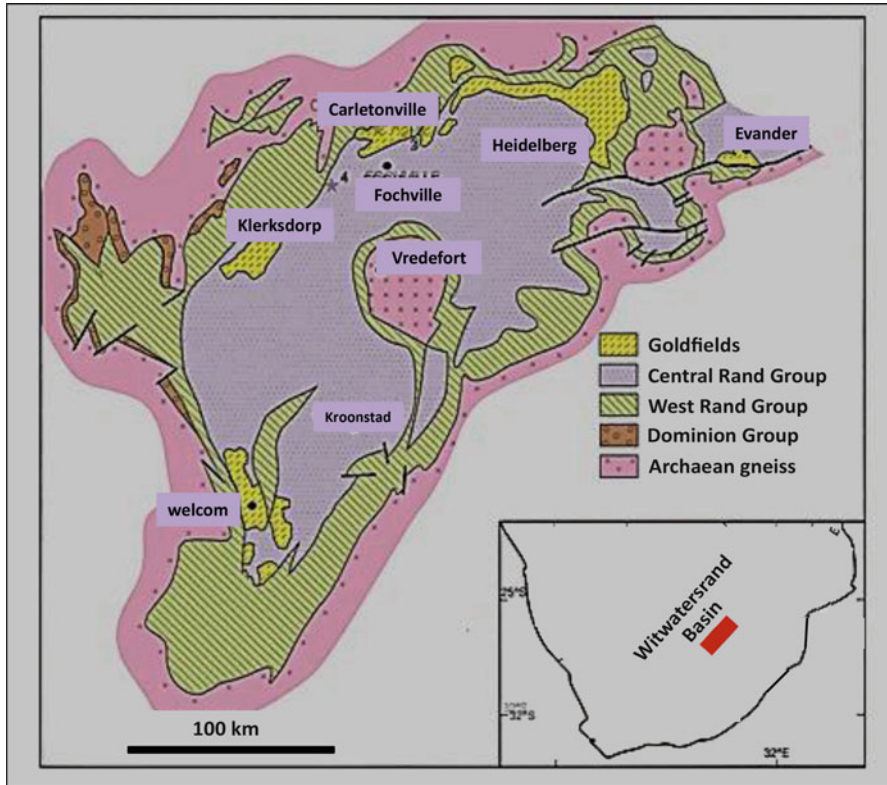


Fig. 7.3 Simplified map of the gold fields of the Witwatersrand Basin (South Africa) and position of the Vredefort Dome (After Reimold et al. 1999)

associated with hydrothermal minerals and this is now taken to signify that the original placers were subsequently modified by hydrothermal activity (modified paleo-placer model). Frimmel and co-workers suggested that the uniqueness of the Witwatersrand goldfields is linked to strong reworking of sediments, shed from rapidly exhumed greenstone belts containing orogenic and perhaps also porphyry-epithermal systems (as suggested by the presence of blue opalescent quartz in the conglomerates), by braided rivers and streams in a region that must have been devoid of vegetation and with intense chemical weathering under an acidic and anoxic Archaean atmosphere. The palaeo-placer model was challenged by Neil Phillips in a series of papers published from 1987 onward (e. g. Phillips 1987, 1988), presenting arguments for a role of metamorphic fluids in the genesis of the Au mineralization. Law and Phillips (2005) reiterated the viability of the hydrothermal model pointing out that regional metamorphism with peak temperatures of 300–400 °C generated mineral assemblages including pyrophyllite, chloritoid, chlorite, muscovite and pyrite and that this metamorphism extended for up to 300 km around the basin

margins. Furthermore, the extent of this regional metamorphism coincides with the distribution of the gold mineralization. Hydrothermal $\text{CO}_2\text{-H}_2\text{S}$ aqueous fluids carrying Au would have been introduced along thrust faults and controlled by bedding-parallel fracture networks and unconformity surfaces. Critical to the hydrothermal replacement model is the timing of the metamorphism and associated hydrothermal alteration. Law and Phillips (2005) considered the thermal effects of the 2.05 Ga Bushveld Igneous Complex and of the 2.02 Ga Vredefort Dome, as possible candidates for Au remobilization in the Witwatersrand Basin. In addition, due consideration should also be given to the heat generated by the 2.7 Ga Ventersdorp igneous province (Ventersdorp Supergroup; an 8-km thick succession of dominantly sub-aerially erupted tholeiitic basalts, komatiites, andesites and pyroclastics; see Pirajno 2000 and references cited therein).

The Vredefort Dome in South Africa is an 80-km-wide central uplift of a large impact structure with a possible original diameter of 300 km. Remarkably, and perhaps not coincidentally, the Vredefort structure is at the centre of the Witwatersrand Basin (Figs. 7.3 and 7.4). Reimold (1995), Reimold and Gibson (1999) and Gibson and Reimold (2001) have described the impact origin of the Vredefort structure, which is one of the largest and the oldest known terrestrial impact structure. An excellent and well-illustrated book on the Vredefort structure was published by Reimold and Gibson (2005). The core of the Dome consists of pre-3.1 Ga granitic and gneissic rocks, supracrustals and mafic rocks. These are further subdivided into an inner zone of leucogneisses (Inlandsee Leucogranofels) and an outer zone of granitic rocks. The central uplift of the Dome represents rocks of the upper and mid crust. The core is surrounded by collars of rocks of the Transvaal, Ventersdorp and Witwatersrand Supergroups. These volcano-sedimentary successions are nearly

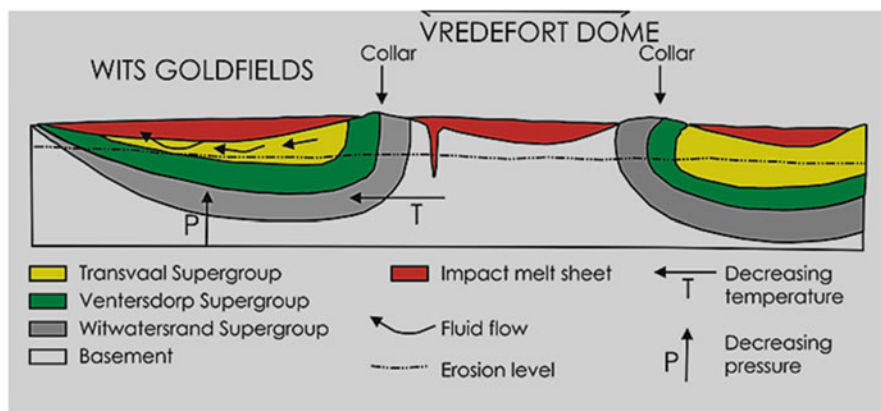


Fig. 7.4 Idealized cross-section of the Witwatersrand Basin and Vredefort Dome, with hydrothermal fluid flow generated by the impact event. Heat from the overlying melt sheet and the hot central uplift (Vredefort Dome) powered the circulation of hydrothermal fluids. The highest shock pressures and temperatures were in the central uplift, decreasing away from it, as shown by the arrows (After Reimold et al. (2005). See also Fig. 11.1)

vertical or overturned, and form a regional rim synclinorium around the Dome. In the core of the synclinorium is the mafic-ultramafic Losberg Complex, whereas alkali and mafic igneous complexes are present near and along the contact between the Ventersdorp and Transvaal Supergroups. Rocks around the Vredefort Dome are metamorphosed to lower greenschist facies (about 350 °C and 2–3 kbar). The metamorphic grade increases towards the dome, so that the corresponding greenschist, amphibolite and granulite facies are concentrically arranged around it.

The greenschist facies zone, in the outer collar pelites of the Transvaal Supergroup, is characterized by chloritoid, biotite, chlorite and muscovite. The amphibolite facies zone lies between the rocks of the upturned collar and the core of the Dome. The collar rocks include pelite, quartzite, and banded iron-formations of the Witwatersrand Supergroup, and basaltic lavas of the Dominion Group and the Ventersdorp Supergroup. Amphibolite facies minerals are: biotite, muscovite, chlorite, cordierite, andalusite, garnet and staurolite, all of which form various assemblages, depending on the composition of the precursor material. In the core, which is made up of Archaean rocks, mafic xenoliths contain an upper amphibolite facies assemblage, consisting of hornblende + biotite + plagioclase + quartz. The granulite facies zone is between the Outer Granite Gneiss and the Inlandsee Leucogranofels. This zone is poorly defined, due to the intense structural disruption caused by the impact event. Nevertheless, Gibson and Stevens (1998) recognized within pelitic stromatic migmatites, coarse-grained garnet, cordierite and orthopyroxene. In mafic rocks, the assemblage that characterizes the granulite facies is represented by clinopyroxene + hornblende + plagioclase + magnetite ± orthopyroxene. Although, the high-grade metamorphic assemblages detailed above were affected by a post-impact retrograde event, Gibson and Stevens (1998) were able to filter out retrograde assemblages, and recognised peak metamorphic reactions, which define an anticlockwise P-T path for the amphibolite facies, with peak temperatures of around 570–600 °C at pressures of 4–4.5 kbar. The anticlockwise P-T path for granulite facies rocks is estimated to have reached peak temperatures in excess of 900 °C, marking the transition from spinel + quartz to garnet + sillimanite, at pressures of 4–5 kbar. Textural evidence suggests that metamorphic peak conditions occurred prior to the impact event, although current geochronological data are unable to distinguish between the two events (U-Pb zircon age of 2017 ± 5 Ma in granulite facies rocks, and 2023 ± 4 Ma for the impact event). Nevertheless, estimates of pre- and post-impact geothermal gradients indicate that these had elevated values. The pre-impact prograde metamorphism of the Vredefort Dome, could be related to the emplacement of the Bushveld Igneous Complex at about 2.05–2.06 Ga, which predated the impact by approximately 30 Ma.

Thus, the Witwatersrand was subjected to at least two important metamorphic-hydrothermal events. One is pre-impact, as discussed above and documented by Phillips and co-workers, the other is post-impact with metamorphic grades decreasing away from the Vredefort Dome. Grieve and Masaitis (1994) suggested that the Witwatersrand Au-U ores, which are distributed in a semicircular fashion around the Vredefort structure, owe their preservation and present-day exposure, to the down-dropped annular ring away

from the central uplifted core. Reimold et al. (1999) carried out petrographic and geochemical studies of the pseudotachylite breccia in the fault zones of the Witwatersrand Basin, where they are associated with gold and uranium mineralization. This pseudotachylite breccia is related to the Vredefort impact event and were found to have acted as major channels for hydrothermal fluids that resulted in the remobilization of Au, U and base metals along the fault zones. Along these lines, Hayward et al. (2003) suggested that the Vredefort impact had a direct influence on the distribution of the Witwatersrand gold mineralization. These authors contended that Vredefort-related post-impact metamorphism, driven by the heat energy of the melt sheet and the uplift of deep crustal rocks, caused the hydrothermal remobilization of the gold, at least on a small scale, along late brittle fractures in sulphides, quartz and zircons. Here the gold is associated with prograde chlorite. In conclusion, the Witwatersrand Au mineral system is of the progenetic type in the classification of Grieve and Masaitis (1994) and its preservation was largely due to the Vredefort impact. Whereas a post-impact hydrothermal overprint of the Witwatersrand rocks is yet to be proven, there are indications of hydrothermal activity at about 2.0 Ga (e. g. Gibson and Reimold 1999). At least two thermal events are recognized in the Vredefort Dome. The first is linked with the Bushveld magmatism at around 2.06 Ga, causing greenschist facies metamorphism. The second was centered on the Dome and was caused by the uplift of hot rocks, due to the impact's shock wave. This thermal event may have attained temperatures ranging from 1000 to 1400 °C in the Dome and of 300 to 500 °C in the Witwatersrand rocks (Reimold et al. 2005). Hydrothermal circulation associated with this event extended to the areas of Au mineralization on the northwestern margin of the Basin. There is evidence that some ore textures in the Witwatersrand Au were formed during post-impact times, such as widespread brittle deformation, pseudotachylite breccia and Au remobilization (Reimold et al. 2005 and references cited therein). It is envisaged that the high temperatures in the central uplift and the region of the surrounding collar, powered hydrothermal circulation that extended throughout the Witwatersrand Supergroup, resulting in the redistribution of Au (Fig. 7.4).

7.8 Australian Examples of Impact-Related Hydrothermal Activity

In the following we describe three Australian impact structures, which exhibit evidence of post-impact hydrothermal fluid flow, namely the Shoemaker structure (Pirajno 2002; Pirajno et al. 2003), the Woodleigh (Mory et al. 2000 and 2001) and Yarrabubba impact structures (Macdonald et al. 2003) (Fig. 7.5). Petrographic observations of altered impactites from Shoemaker, Woodleigh and Yarrabubba allow some insights into complex but widespread hydrothermal and metasomatic processes that are associated with meteorite impacts on land. The present day

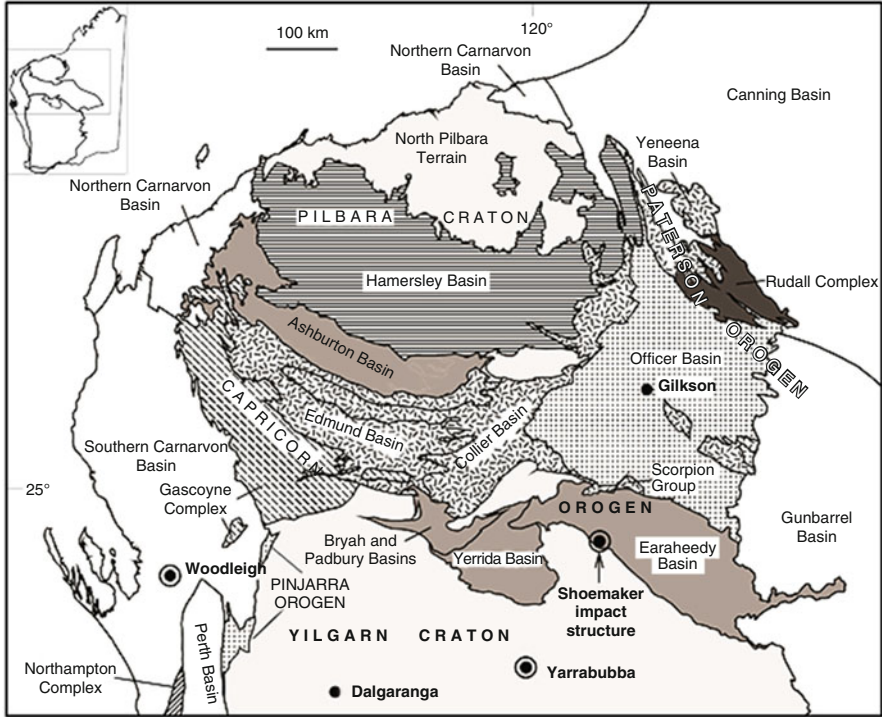


Fig. 7.5 Location of three major impact structures in Western Australia: Shoemaker, Yarrabubba and Woodleigh

outcrops of these three structures represent levels of exposure ranging from deep (Yarrabubba, Shoemaker) to nearer the surface (Woodleigh). Woodleigh is a buried structure, but, as suggested from the interpretation of geophysical data (Iasky et al. 2001), its level could be higher than the other two. Assuming that this is correct then a generalized sequence of time-space alteration events can be reconstructed. At the deepest level (Yarrabubba and Shoemaker) complete replacement of a granitic protolith takes place by processes of alkali metasomatism, similar to magmatic-hydrothermal systems associated with non-orogenic granite systems, resulting in rocks of syenitic appearance. Alkali metasomatism at deep levels is followed by a lower temperature hydrothermal regime, which partially obliterates the alkali rocks, but is best manifested at higher levels, probably because of downward flow of the hydrothermal circulation. A view of this lower temperature regime at higher levels is provided by the central uplift of the Woodleigh structure, where the dominant alteration minerals are phyllosilicates with carbonate overprints.

7.9 Shoemaker Impact Structure

The Shoemaker impact structure, with a diameter of about 30 km, is located on the southern edge of the Palaeoproterozoic Earraheedy Basin, which overlies the northern margin of the Archaean Yilgarn Craton (Fig. 7.5). Details of the geology and geochemistry of the Shoemaker structure are provided in Pirajno (2002) and Pirajno et al. (2003). The structure is topographically well-defined by two concentric rings of low hills that interrupt the continuity of the west-northwest-trending Frere Range. The target rocks consist of strata that are shallowly dipping to the northeast (about 10–15°), including essentially un-deformed and un-metamorphosed sedimentary rocks of the Earraheedy Group, overlying Archaean granite-greenstone basement of the Yilgarn Craton. Basement granitic rocks are only exposed within the eastern part of the central structure, on the inside of the inner ring of the Shoemaker impact structure. These granitic rocks are grouped under the name of Teague Granite. The central and the western parts of the inner structure are entirely covered by Quaternary lake sediments and sand dunes (Fig. 7.6). However, aeromagnetic data indicate that granitic rocks (possibly monzogranite) and greenstone rocks are present beneath these surficial deposits, representing the northern continuation of the Yilgarn Craton beneath the sedimentary cover of the Earraheedy Basin. The presence of diagnostic impact indicators, suggest that granitic rocks and greenstones form an impact-induced central structural uplift and possibly the basement core of the original crater. This central uplift has a diameter of about 12 km. The eastern side of the structural uplift is characterized by high total magnetic intensity (TMI), hydrothermal alteration and the only exposures of the granitic rocks (Teague Granite). The TMI pattern suggests not only that the upper parts of the original impact structure were eroded away, but also that the entire structure is probably tilted towards the east.

The age of the Shoemaker impact is not resolved, because of thermal and tectonic resetting of the isotopic systems of the target rocks at 1670–1620 Ma (reactivation of the Capricorn Orogen; Tyler 2005), 1070 Ma (age of a large igneous province in the region; Wingate et al. 2004) and ca 550 Ma (age of the 560 Ma Petermann Orogeny; Scrimgeour et al. 1999). The magmatic age of the Teague Granite is Archaean (2648 ± 8 Ma; Nelson 1999), which is within the range of other granitic rocks in the Yilgarn Craton (Smithies and Champion 1999). Bunting et al. (1980) obtained two whole-rock Rb-Sr isochron ages of 1630 and 1260 Ma from samples Teague Granite. Pirajno et al. (2003) reported K-Ar and $^{39}\text{Ar}/^{40}\text{Ar}$ determinations on K-feldspar and illite-smectite separates also from the Teague Granite. The $^{39}\text{Ar}/^{40}\text{Ar}$ system yielded unreliable results, only providing broad constraints as to a maximum age (<1300 Ma). The K-Ar system gave two ages: 694 ± 25 Ma and 568 ± 20 Ma for K-feldspar and illite-smectite separates, respectively. It was concluded that the 568 ± 20 Ma K-Ar age determined on illite could represent either resetting due to the Peterman Orogeny, or the formation of illite as a result of post-impact hydrothermal activity.

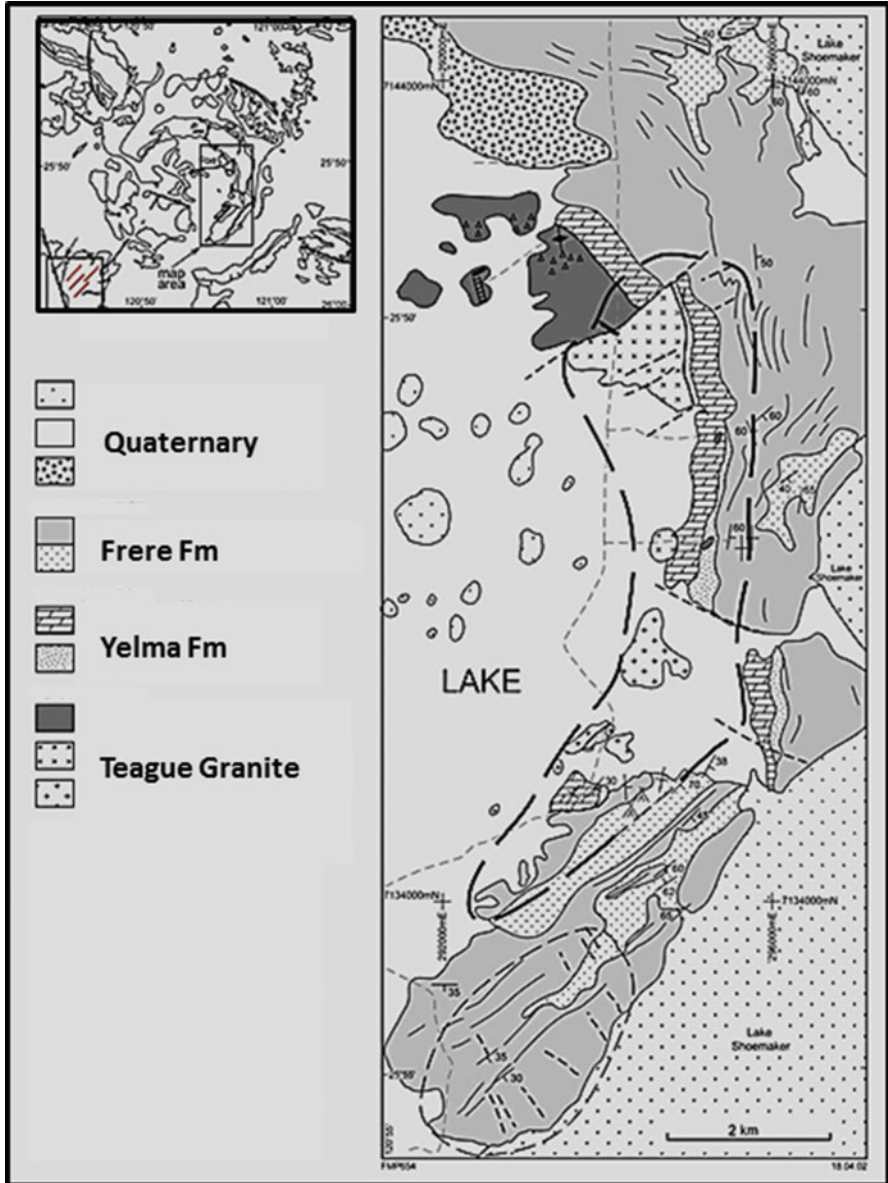


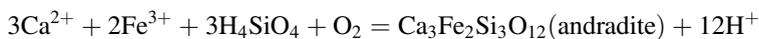
Fig. 7.6 Simplified geological map of the eastern inner ring of the Shoemaker structure, showing the extent of hydrothermal alteration, silica pods and shatter cone localities. Inset shows full extent of the impact structure; the smaller square in the bottom left corner of the inset shows northeast trending quartz veins, which were formed as a result of impact-related hydrothermal activity (After Pirajno 2002)

7.10 Hydrothermal Alteration

In the Shoemaker impact structure the effects of impact energy-induced hydrothermal circulation within the impact aureole are evident in the Teague Granite and in rocks of the Yelma and Frere formations (Earaheedy Group) exposed in the eastern inner ring. The extent of the hydrothermal alteration in the eastern rim of the structure is shown in Fig. 7.6. Outcrops of Teague Granite in the east and southeast are fractured, hydrothermally altered and partially to pervasively silicified. The rocks of the Teague Granite were studied as part of a regional investigation of felsic alkaline rocks of the Yilgarn Craton by Johnson (1991), who concluded that the granitic rocks that outcrop in the Shoemaker structure were modified by alkali metasomatism resulting in a granitoid of syenitic composition. Johnson's conclusion was confirmed in subsequent studies (Pirajno and Glikson 1998; Pirajno 2002; Pirajno et al. 2003), in which the Teague Granite was subdivided into three units: syenite, quartz syenite and a leucocratic alkali feldspar granite.

The syenite is medium-grained and pink to brick-red in color, and it contains up to 55% orthoclase phenocrysts and up to 15% zoned alkali pyroxene (sodic hedenbergite or aegirine-augite), with albite (~25%) as small grains forming a groundmass. Accessories include green fibrous amphibole, zircon and andradite garnet. The quartz-syenite is also medium-grained, pink to brick-red in color, fractured and characterized by a distinct polygonal and granoblastic texture, and is transitional to the syenite. This rock is dominated by euhedral to subhedral albite and quartz, roughly in equal proportions, overprinted by perthitic microcline crystals. Accessory minerals include alkali pyroxene (aegirine-augite or sodic hedenbergite), actinolite-tremolite, zircon and titanite. The leucocratic alkali feldspar granite is coarse- to medium-grained, locally brecciated, and consists an assemblage quartz + K-feldspar (microcline) ± albite ± biotite ± sericite. Where it is least altered, it contains about 30% by volume quartz, 40% albite and 30% K-feldspar. Generally, this granitic rock has a cataclastic to mylonitic fabric and/or brecciated texture. Unlike the syenitic rocks, the overall texture of the leucocratic granite is distinctly cataclastic. This cataclastic deformation suggests that this type of Teague Granite is a remnant of an original Archaean, which underwent deformation during the impact event.

The leucocratic alkali feldspar granite is probably the result of stages of silicification of the Teague Granite. This silicification was in places pervasive, whereby the granitic rock is almost entirely replaced by quartz (silica flooding). In places, fibrous amphibole (actinolite-tremolite) infills micro-fractures in the rock and in a network of cracks in andradite garnet crystals that are locally present in the Teague Granite. Andradite garnets have also been found in hydrothermally altered rocks in the Manson impact structure for which a reaction of the type given below is postulated (McCarville and Crossey 1996):



Greenstone enclaves in the Teague Granite are cut by quartz-albite veinlets, associated with selvages of diopside. All these features are evidence that hydrothermal minerals were precipitated during phases of post-impact hydrothermal activity. Some of the mineral phases associated with this hydrothermal activity are illustrated in Fig. 7.7.

A tentative paragenetic sequence based on textural relationships and assuming that the mineral assemblages observed replaced those of an original granite (? monzogranite) is shown in Fig. 7.8. The three columns in Fig. 7.8 indicate mineral assemblages that are present in the Teague Granite and in greenstone xenoliths

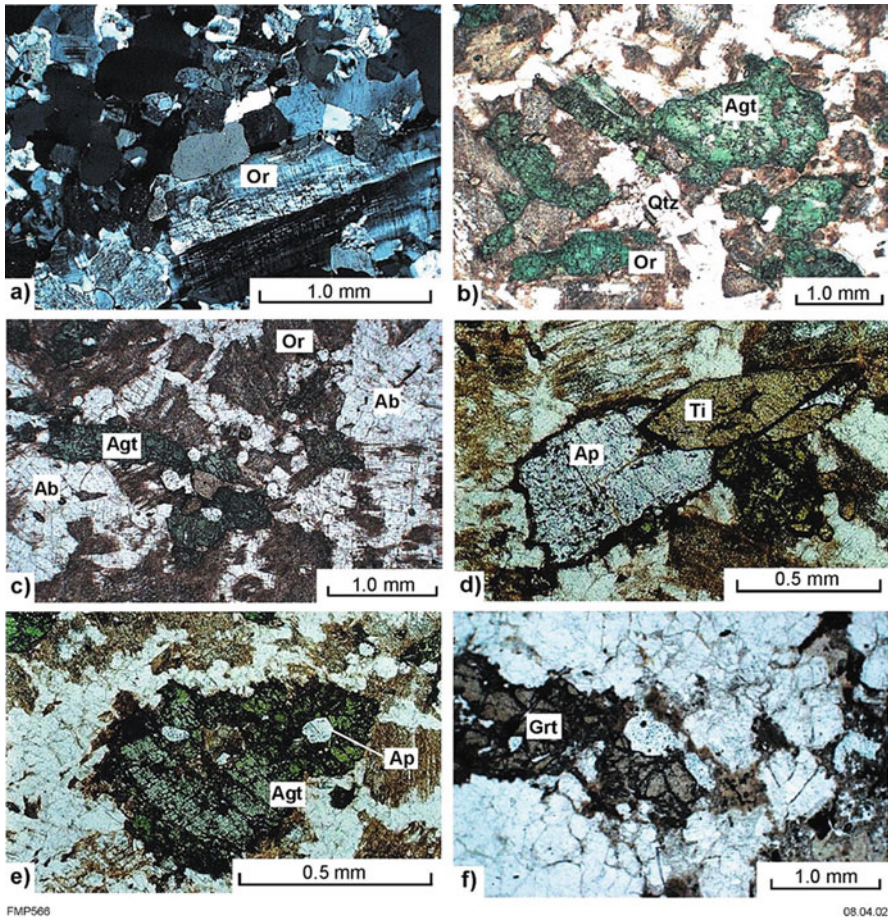


Fig. 7.7 Photomicrographs showing mineralogical assemblages of the Teague Granite (syenite): (a) orthoclase (Or) phenocryst in a matrix of quartz-albite; (b) orthoclase (Or), aegirine-augite (Agt) and quartz (Qtz); (c) orthoclase (Or), aegirine-augite (Agt) and albite (Ab) assemblage; (d) apatite (Ap) and titanite (Ti) crystal; (e) aegirine-augite crystal (Agt) with apatite (Ap) inclusion; (f) garnet (Grt) crystal associated with a quartz-albite assemblage. **a**, with cross polars; **b, c, d, e** and **f** in plane polarized light, **a** with crossed polars (After Pirajno 2002)

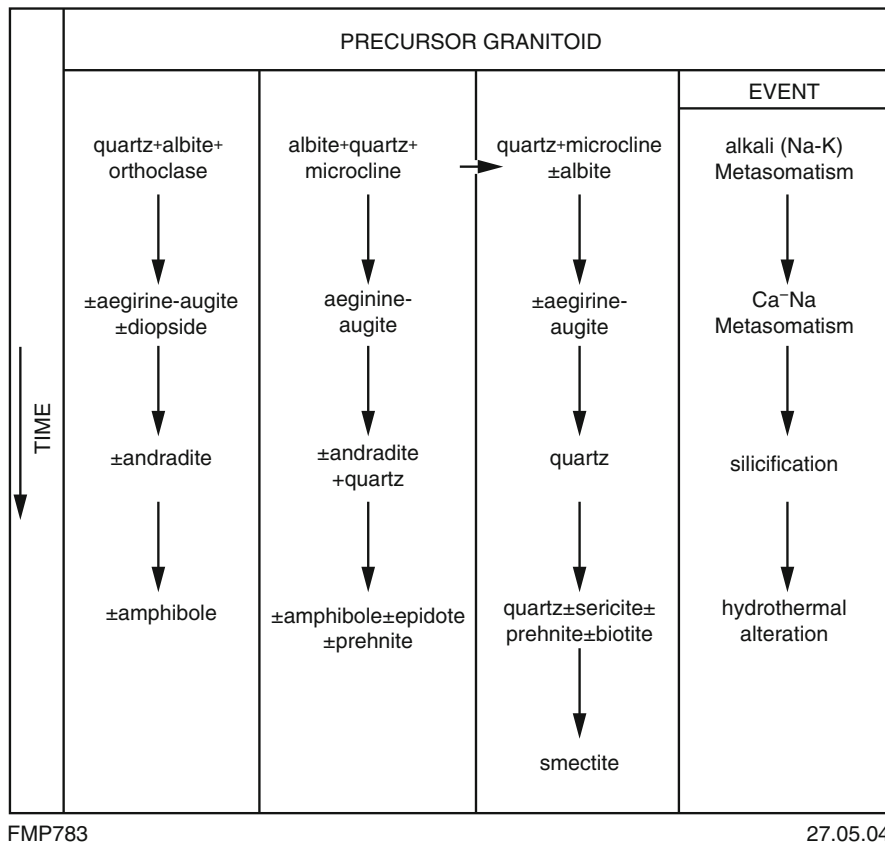


Fig. 7.8 Mineral assemblages and a tentative paragenetic sequence of the Teague Granite (After Pirajno 2002)

within it. It is not known whether or not these represent different protolith compositions. It can be concluded, however, that the protolith(s) was completely modified by an early Na-K-Ca metasomatic process, followed by hydrous alteration with deposition of silica and phyllosilicate phases.

The petrography and overall chemistry of the Teague Granite shows that it is of syenitic affinity and alkaline composition, with the mineral assemblages and textural relationships suggesting that it is derived from alkali metasomatism of a precursor granitoid (Johnson 1991; Pirajno 2002). The syenitic rocks of the Teague Granite are strongly enriched in Na₂O, K₂O, Rb, Sr, Y, Zr, Nb, Ba, and REE compared to high-Ca granite and alkaline rocks of the Yilgarn Craton. The REE patterns of the Teague Granite are similar to the average alkaline rocks of the Yilgarn Craton (Witt and Davy 1997). However, the syenite is enriched in REE by almost one order of magnitude compared to the average Yilgarn alkaline rock, whereas the leucocratic alkali granite shows REE depletion. The quartz syenite is close to the average

Yilgarn syenite (Witt and Davy 1997). The strong REE enrichment of the Teague Granite syenite, compared to average Yilgarn Craton high-Ca granite, confirms that the precursor granitoid was modified by alkali alteration.

Pervasive silicification affected rocks of the Yelma Formation (Sweetwaters Well Member), whilst the granular iron formation of the Frere Formation exhibit cross-cutting quartz veining and are partially silicified. In the same area, pods of chert and jasperoidal quartz are present along the eastern margin of the central uplift (Fig. 7.6). The chert consists mainly of brecciated microcrystalline quartz cemented by chalcedonic quartz. Open spaces are filled with euhedral quartz crystals. These chert pods are interpreted to have formed by precipitation from hydrothermal fluids that circulated along faults and fractures in the eastern sector of Shoemaker impact structure.

To the southwest of Shoemaker impact structure a number of northeast-trending milky white quartz veins are associated with, and parallel to northeast and north-northeast-trending fractures in hornblende quartz-monzonite granite (see inset of Fig. 7.6). The attitude of the veins and associated fractures suggests a pattern that converges towards the centre of Shoemaker impact structure. The quartz veins post-date the hornblende quartz-monzonite that was emplaced at 2664 ± 4 Ma (Nelson 1999) and again are evidence of unusual hydrothermal activity in the area. Other Archaean granitic rocks in the region do not display the same intensity and regular pattern of quartz veins and fractures. It is therefore concluded that the northeast-trending fractures are impact-related and that their local infilling with quartz may have resulted from impact-induced circulation of hydrothermal fluids.

It is likely that the meteorite impact that created the Shoemaker impact structure formed a melt sheet which, together with impact-released heat in the central uplift, gave rise to a hydrothermal convection system within and around the central uplift zone. The melt sheet would have acted as a magma-like heat source within the crater structure and would have formed several hot springs in the crater and surrounding areas. Fluid channels and degassing pipes have been reported from the Ries impact crater in Germany (Newsom et al. 1986). Hydrothermal pods are present in the annular structures associated with the Houghton impact structure in Canada that have been interpreted as hydrothermal pipe structures (Osinski et al. 2001). Similarly, the pods of quartz-jasperoidal material that are present along structural breaks in the eastern rim of the Shoemaker impact structure may be the eroded remnants of fluid channels that fed thermal springs.

7.11 Yarrabubba Impact Structure

The Yarrabubba impact structure, a recent discovery (Macdonald et al. 2003), is situated about 100 km southeast of Meekatharra in Western Australia in Archaean granite-greenstone rocks of the Yilgarn Craton (Fig. 7.5). The structure is highly eroded and no readily visible topographic or geological expression can be discerned, except for an elliptical zone (15 km long axis) of low magnetic signature roughly

centred around the Barlangi Granophyre and shocked granitic rocks (Yarrabubba Granite). Within this magnetic low and surrounding the main outcrop of the Barlangi Granophyre (discussed below), is a circular high-frequency magnetic anomaly, about 2 km in diameter. An east-west-trending linear magnetic anomaly, interpreted as a mafic dyke, traverses the zone of low magnetic signature and is assumed to be of post-impact age (Fig. 7.9).

Macdonald et al. (2003) reported on the age constraints of the Yarrabubba structure, largely based on field, and limited and inconclusive U-Pb SHRIMP dating of xenocrystic zircons from the Barlangi Granophyre. These zircons yielded ages of around 2715 Ma. Dating carried out by the Geological Survey of Western Australia (D. R. Nelson, unpublished data) revealed two populations of xenocrystic zircons in the

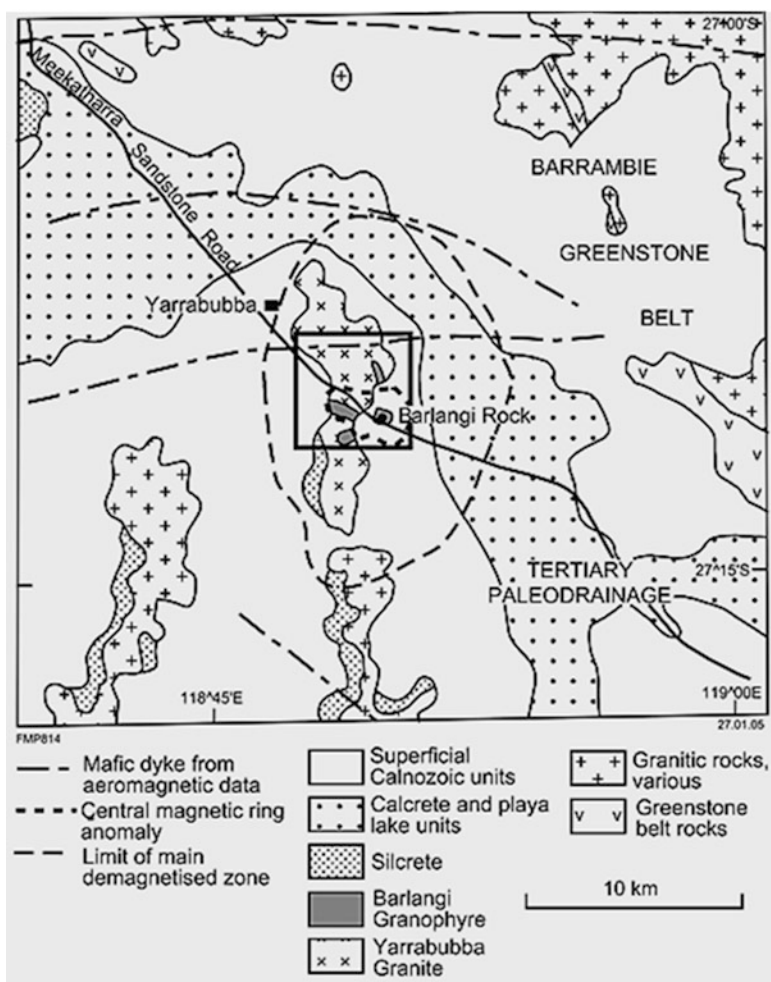


Fig. 7.9 Simplified geological map of Barlangi area (After Pirajno 2005)

Barlangi Granophyre, which yielded ages of 2689 ± 7 and 2647 ± 11 Ma). In situ ultraviolet laser Ar-Ar dating was reported in Pirajno (2005) for one pseudotachylite sample that had been altered to sericite. A weighted mean of the 7 youngest ages yielded an Ar-Ar age of 1134 ± 26 Ma (95% confidence). However, the Ar-Ar pseudotachylite age may possibly reflect a younger resetting or partial resetting age, as a result of the alteration of the original pseudotachylite material to sericite, or a later thermal event. Macdonald et al. (2003) concluded that a Proterozoic age for Yarrabubba is indeed likely and this is supported by the observation that the central region of the structure is cut by the above-mentioned east-trending dyke, assumed to be of Proterozoic age, as are most east-trending dykes in the Yilgarn Craton.

The rock type that enabled the recognition of the Yarrabubba structure is the Barlangi Granophyre (Fig. 7.10). This is a pink-brown rock containing xenocrysts and lithic fragments of granite. In thin section the Barlangi granophyre exhibits typical K-Na-feldspar-quartz granophyric intergrowths, as well as silica spherules and nucleation textures indicative of rapid quenching. Macdonald et al. (2003) interpreted the Barlangi Granophyre as an impact melt injected along a fault or fracture. As mentioned previously, large impact structures generate impact melts, which generally collect within the crater and/or form sill-like and dyke-like igneous bodies that penetrate into the basement below the crater floor (French 1998). The REE and normalized trace element abundance patterns of the Barlangi Granophyre and the Yarrabubba Granite are almost identical and this confirms that the granophyre was formed by melting of granitic target rocks. The Barlangi Granophyre is surrounded by shocked granitic rocks (Yarrabubba Granite) displaying classic shatter cones and pseudotachylite veins. Petrographic work on the Yarrabubba Granite revealed common quartz grains with multiple sets of planar deformation features (PDFs). Pseudotachylites form injection veins, locally showing flow-banded micro- to cryptocrystalline quartz and sericite aggregates with plastically deformed shapes (lithic fragments).

Petrographic work revealed evidence of post-impact hydrothermal fluid flow in both the Yarrabubba Granite and the Barlangi Granophyre. The most conspicuous features of this hydrothermal circulation can be seen in the Yarrabubba Granite and include veins of bladed calcite (Fig. 7.11a) similar to those found in volcanic epithermal systems. Bladed calcite, commonly replaced by quartz, is indicative of boiling of CO₂-bearing fluids. Reddish-brown alkali feldspar granite of the Yarrabubba Granite consists of a granoblastic aggregate of K-feldspar and quartz (Fig. 7.11b–d). In places, the Yarrabubba Granite appears modified by coarsening and absence of FeMg silicates and exhibits cross-cutting veins of K-feldspar. This rock is interpreted as representing the complete replacement of a granitic protolith, similar to that observed in the syenitic rocks of the Teague Granite in the Shoemaker structure. Fluorite + biotite and chlorite + prehnite occur as veinlets (Fig. 7.11b–d) cutting through the granoblastic aggregate of K-feldspar and quartz of the Yarrabubba Granite. Macdonald et al. (2003) recognized that the presence of K-feldspar (microcline) and albite together with muscovite is indicative of strong K metasomatism. These authors also suggested that the central demagnetized zone

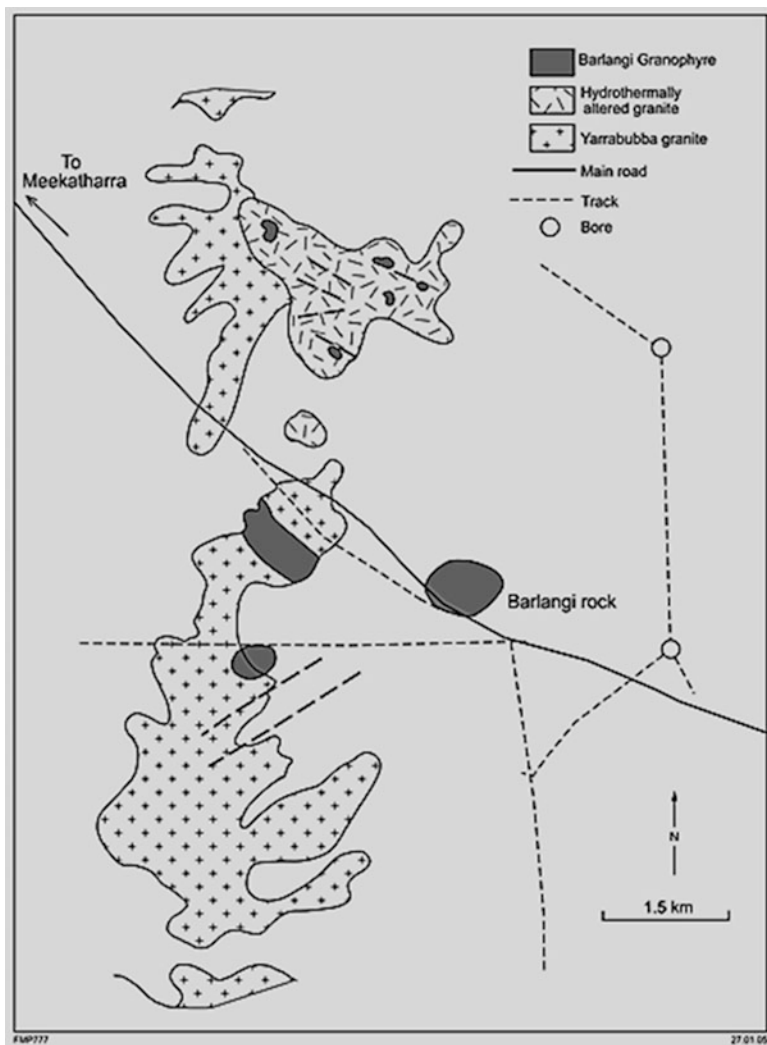


Fig. 7.10 Altered or modified granite cut by a reddish-brown K-feldspar vein possibly due to potassic metasomatism (After Pirajno 2005)

may be the effect of this metasomatism, which resulted in the destruction of Fe-bearing mineral phases. As also observed for the Shoemaker structure, these assemblages suggest that an early alkali metasomatism was followed by hydrous fluids that infiltrated fractures in the metasomatically altered target rocks. Pervasive sericitic alteration and green mica overprint the granophyric textures in the Barlangi Granophyre.

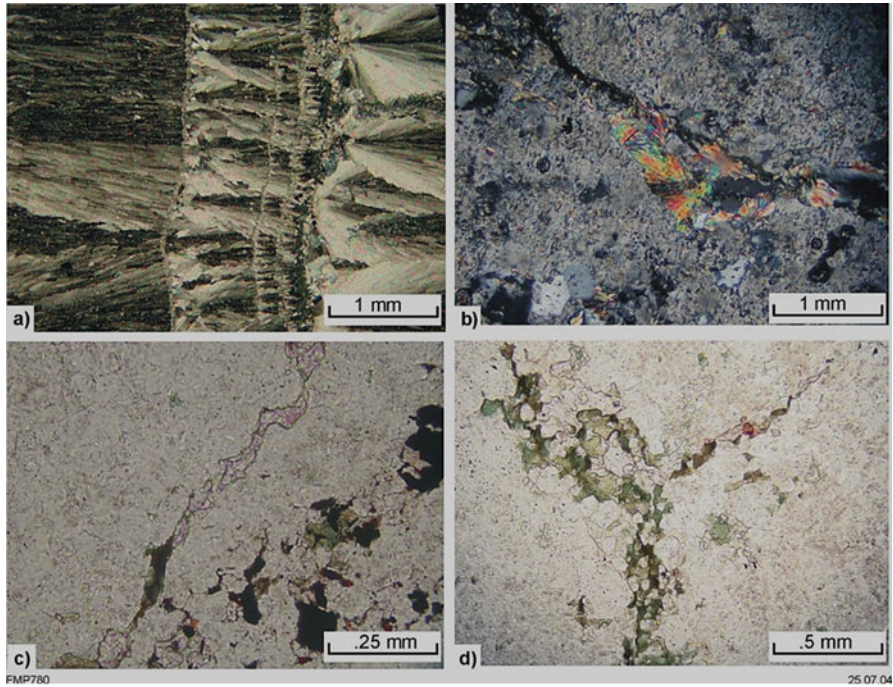


Fig. 7.11 Photomicrographs showing (a) aggregates of bladed calcite crystals (crossed polars); (b, c and d) syenitic like Yarrabubba Granite composed of a granoblastic aggregate of K-feldspar and quartz is cut by a vein of prehnite and lesser chlorite (b), a vein containing green biotite and fluorite (c) and veins of chlorite (d); b at crossed polars, c and d in plane polarised light

7.12 Woodleigh Impact Structure

Woodleigh structure is a buried, multi-ring impact structure, approximately 160 km south-southeast of Carnarvon, east of Shark Bay (Fig. 7.5; Mory et al. 2000, 2001). The structure was first identified as a possible impact crater in late 1997, during a geological review of the Gascoyne Platform, from the coincidence of shallow granitic rocks in a drill hole over the centre of a circular gravity anomaly (Fig. 7.12). The hole was later deepened to verify the impact interpretation. The new Woodleigh 1 core shows extremely well preserved shock metamorphic features in granitic rocks, including veins of pseudotachylite, breccia, and planar deformation features, thereby providing indisputable evidence of an impact origin. Subsequently, a second drill hole (Woodleigh 2A) was sunk 13 km to the west to sample the crater-infill section (Fig. 7.13). Woodleigh 2A intersected a substantial thickness of para-conglomerate, overlain by lacustrine strata of the Woodleigh Formation. The para-conglomerate contains lithic fragments of shocked granitic rocks and sandstone, and is interpreted as the re-working of shocked

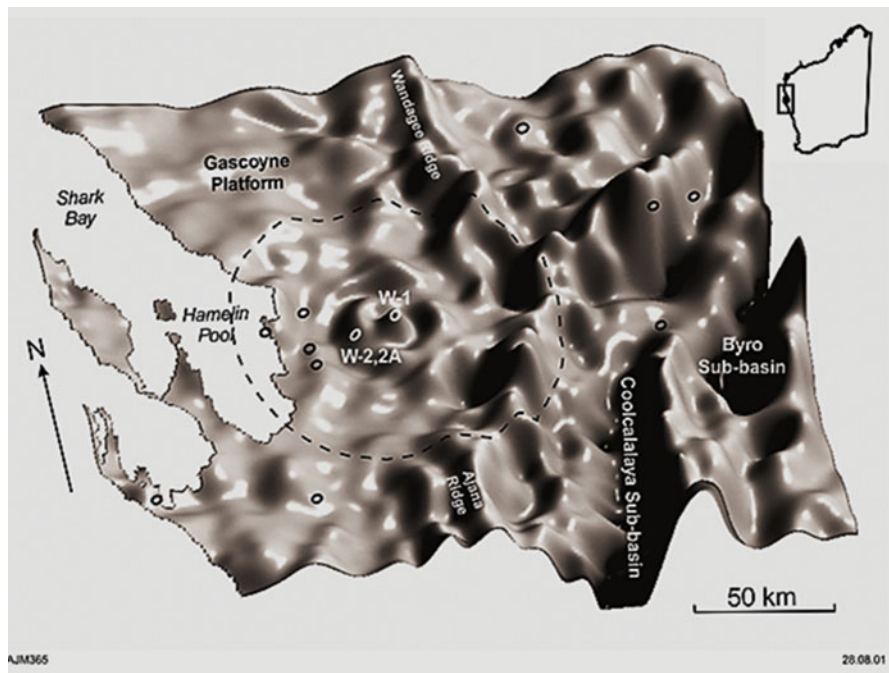


Fig. 7.12 Woodleigh impact structure: isometric view of first vertical derivative of the Bouguer gravity (After Mory et al. 2001); small circles indicate position of drill holes and the dashed line shows the inferred extent of the structure

material that filled the impact crater. The Woodleigh Formation probably represents a later crater-lake fill. The structure is most clearly shown on the first vertical derivative of the Bouguer gravity as a series of annular ridges and troughs (Fig. 7.12). The central gravity ‘high’, about 25 km in diameter, is interpreted as the central uplift of the impact. The adjacent gravity ‘trough’ probably corresponds to a ring syncline filled with strata similar to those in Woodleigh 2A. The diameter of the Woodleigh structure remains controversial. Estimates range from a maximum of 120 km (Mory et al. 2000; Glikson et al. 2005) to 60–70 km (Reimold et al. 2003).

Gravity and seismic data indicate that the structure is asymmetric with basement east of the central peak being about 2 km shallower than to the west. The asymmetry is interpreted as due to tilting during Early Cretaceous. Initial studies constrain the age of the Woodleigh impact to between Early Permian and Early Jurassic (290–200 Ma). K–Ar isotope dating of clay minerals within shocked granitic rocks from Woodleigh 1, and from transported shocked material in Woodleigh 2A have yielded ages clustering around 359 Ma (Uysal et al. 2001, 2002), near the Devonian–Carboniferous boundary.

The extensively fractured and brecciated granitic rocks cored in Woodleigh 1 show clear evidence of post-impact hydrothermal alteration and sulphide mineralization. This is shown by the presence of mineral phases, such as albite, quartz,

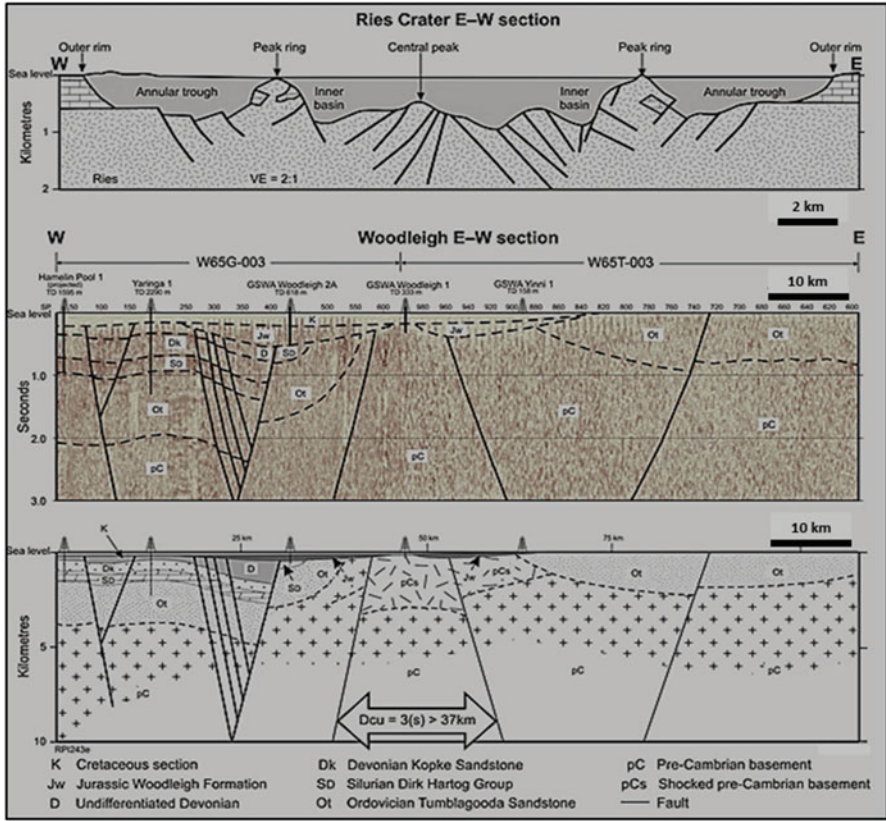


Fig. 7.13 Woodleigh impact structure: seismic reflection east-west cross section and geological interpretation, compared with a section of the Ries impact structure in Germany (After Glikson et al. (2005 and references cited therein) (AJES with permission))

muscovite, illite, chlorite and calcite, which overprint the primary and/or impact-modified mineralogy and infill micro-fractures (Fig. 7.14a, b). Uysal et al. (2001) reported on the occurrence of illitic clays and their textural relationships, which indicate that these clays represent phases precipitated from hydrothermal fluids and are not pre-existing clay minerals. Furthermore, the presence of abundant fluid inclusions (liquid and liquid + gas) within impact-related microstructures (Fig. 7.13c) is evidence that substantial volumes of fluids circulated through the impact-modified target rocks. Sulphides that have been recognized by reflected light optical microscopy include pyrite, marcasite and chalcopyrite. Typically, these sulphides fill micro-fractures in the silicate matrix and in pre-existing ore minerals, such as ilmenite. Examples are shown in Fig. 7.14d, e.

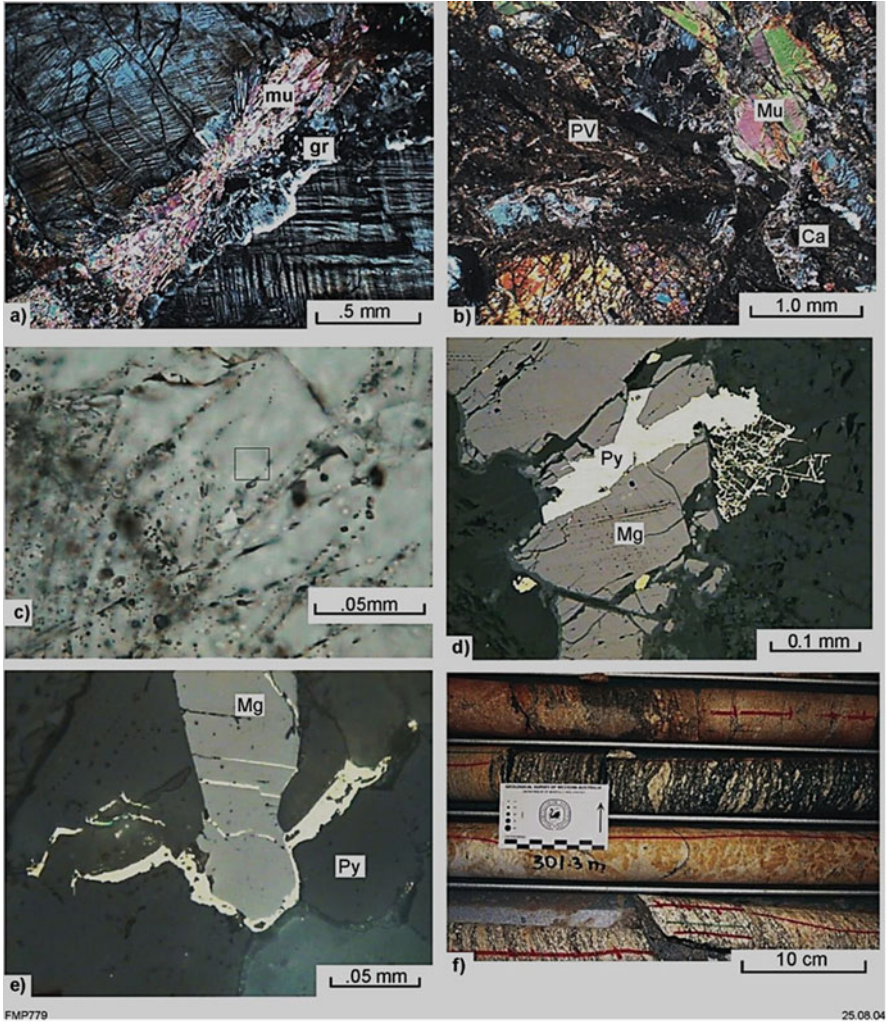


Fig. 7.14 (a) photomicrographs taken with crossed polars, showing sheaves of muscovite (mu) overprinting granophyric material (gr) at the boundary between quartz (with PDFs) and microcline; (b) photomicrographs taken with crossed polars, pseudotachylite veinlet (PV) displaced by a late micro-fracture and overprinted by calcite (Ca), there are also large muscovite (Mu) crystals in the brecciated groundmass material; (c) photomicrographs taken with crossed polars, showing PDFs in quartz decorated with fluid inclusions, boxed area shows a two-phase inclusion; (d) reflected light photomicrograph showing magnetite (Mg), cut by pyrite (Py), associated with fine pyrite filling a network of micro-fractures and chalcopyrite blebs (at margins of the magnetite); (e) reflected light photomicrograph showing magnetite (Mg) and pyrite filling small fractures in silicate minerals and the magnetite; (f) core (about 301 m) of shocked granitoid rock with yellow-brown (rusty) patches and brecciated biotite-gneissic granite

Hydrothermal alteration is especially common in samples that are extensively fractured and/or have pseudotachylite veinlets. Textural relationships gleaned from petrographic work suggest a possible alteration paragenesis, as follows: quartz + albite + muscovite or sericite \pm epidote \pm silica flooding \pm calcite.

The pervasive shock-thermal alteration has produced distinctly re-constituted leucocratic medium-grained granitic rocks with rust-colored patches (Fig. 7.14f). Magmatic biotite, where present, exhibits kink bands, edge resorption, and concordant to transgressive pseudotachylite veins; locally PDFs are also present. Fresh and un-deformed biotite may be the product of post-impact potassic alteration. Some of the pseudotachylite veinlets show devitrification features characterised by nucleation of quartz and alkali feldspar (usually microcline) with a spherulitic appearance and/or granophyric texture. Isolated corundum crystals locally replace feldspar, suggesting re-concentration of alumina as a refractory element. Accessory phases in the shocked granitic include zircon, monazite and apatite, whereas post-impact hydrothermal alteration effects include calcite veinlets, pyrite growth in pseudotachylite veins and micro-fractures, epidote, and fine sericite aggregates replacing shocked feldspar grains.

Both in Woodleigh 1 and 2A altered zones in shocked quartz and feldspars take on a reddish-brown color due to oxidation of iron and the presence of numerous fluid inclusions. Woodleigh 1 shows features of melt devitrification, which involves nucleation of quartz and alkali feldspar (generally microcline) and results in a spherulitic and/or a granophyric texture. The spherulitic texture is more common and generally consists of blebs, or roundish bodies of quartz and feldspar.

Major and trace element analyses of core samples from Woodleigh 1 were reported by Mory et al. (2001). These were used to show if changes can be detected in the chemistry of the target rocks (central uplift granite). The data were normalized against average granite, in absence of comparable granites in the region. Results indicate that while the lithophile and chalcophile trace metals (Pb, Sn, W, Mo, Bi, Ag, Sb, Zn, Cu, Au) vary by factors in the range of 0.1 to 10 times relative to average granite. Siderophile trace metals, however, are strongly enriched (V, 6–20 times; Cr, up to 30 times; Co, 10–50 times; Ni, up to 120 times). Major elements show moderate to strong K₂O enrichment, associated with depletions in SiO₂, Na₂O, TiO₂, MgO and P₂O₅ (Mory et al. 2001).

7.13 Concluding Remarks

The possibility of hydrothermal ore deposits, directly or indirectly related to impacts is a good catalyst to encourage geoscientists to investigate impact-induced hydrothermal systems. There is by now overwhelming evidence of hydrothermal fluid circulation powered by the heat generated by meteorite impacts. The heat engine is provided by either the melt sheet of large impact structures and/or the hot sections of the central

uplift. This is probably followed by the influx of meteoric fluids into the highly fractured rocks, which also make available an ideal reservoir for hydrocarbons. The role of the Vredefort large impact structure in the development of the Witwatersrand Au mineralization remains uncertain, mainly because of the difficulty in separating the metamorphic-hydrothermal signatures of two or even three thermal events that affected the region at around 2.05–2.0 Ga. Up till now, impact-related hydrothermal activity has been studied in comparatively large impact structures, all of which have a central uplift. More recently, however, Glikson et al. (2008) have shown that a low-temperature hydrothermal system can be activated in a simple (no central uplift) small-diameter impact structures.

References

- Allen CC, Gooding JL, Keil K (1982) Hydrothermally altered impact melt rock and breccia: contributions to the soil of Mars. *J Geophys Res* 87:10083–10101
- Ames DE, Watkinson DH, Parrish RR (1998) Dating of a regional hydrothermal system induced by the 1850 Ma Sudbury impact event. *Geology* 26:447–450
- Ames DE, Kjarsgaard IM, Pope KO, Dressler B, Pilkington M (2004) Secondary alteration of the impactite and mineralization in the basal tertiary sequence, Yaxcopoil-1, Chicxulub impact crater, Mexico. *Meteor Planet Sci* 39:1145–1167
- Buffetaut E, Koeberl C (eds) (2002) *Geological and biological effects of impact events*. Springer, Berlin
- Bunting JA, De Laeter JR, Libby WG (1980) Evidence for the age and cryptoexplosive origin of the Teague ring structure. *Geol Surv West Aust Ann Rep* 1980:125–129
- Carpenter BN, Carlson R (1992) The Ames impact crater. *Oklahoma Geol Surv* 52:208–223
- Donofrio RR (1998) North American impact structures hold giant field potential. *Oil and Gas J* 96:69–83
- Dressler BO, Sharpton VL (eds) (1999) *Large meteorite impacts and planetary evolution II*. *Geo Soc Am Sp Pap* 339
- Forsman NF, Gerlach TR, Anderson NL (1996) Impact origin of the Newport structure, Williston Basin, North Dakota. *Am Ass Petrol Geol Bull* 80:721–730
- French BM (1998) *Traces of catastrophe – a handbook of shock-metamorphic effects in terrestrial meteorite impact structures*. *Lunar Planet Ins Contr* 954, Houston, Texas, 120pp
- Frimmel HE, Groves DI, Kirk J, Ruiz J, Chesley J, Minter WEL (2005) The formation and preservation of the Witwatersrand goldfields, the world's largest gold province. *Econ Geol* 100th Ann Vol: 769–97
- Gibson RL, Reimold WU (1999) Significance of the Vredefort Dome for metamorphic-mineralization studies in the Witwatersrand Basin. *Miner Petr* 66:25–53
- Gibson RL, Reimold WU (2001) *The Vredefort impact structure, South Africa – the scientific evidence and a two-day excursion guide*. Council Geosc S Afr Memoir 92
- Gibson RL, Stevens G (1998) Regional metamorphism due to non-orogenic cratonic magmatism. *Geol Soc London Sp Publ* 138:121–135
- Gilmour I, Koeberl C (2000) *Impacts and the early Earth*. Springer, Berlin, 448pp
- Glikson A (1998) Eugene Shoemaker and the impact paradigm in Earth and planetary science. *Celest Mech Dyn Astron* 69:1–7
- Glikson A, Mory AJ, Iasky RP, Pirajno F, Golding SD, Uysal LT (2005) Woodleigh, Southern Carnarvon Basin, Western Australia: history of discovery, Late Devonian age, and geophysical and morphometric evidence for a 120 km-diameter impact structure. *Aust J Earth Sci* 52:545–553

- Glikson A, Hickman A, Vickers J (2008) Hickman Crater, Ophthlamia Range, Western Australia: evidence supporting a meteorite impact origin. *Aust J Earth Sci* 55:1107–1117
- Golightly JP (1984) The Sudbury Igneous Complex as an impact melt: evolution and ore genesis. *Ontario Geol Surv Sp Vol 5*:105–118
- Gortler JD (1998) The petroleum potential of Australian Phanerozoic impact structures. *APPEA J* 38:159–187
- Goto K, Tada R, Bralower TJ, Hasegawa T, Matsui T (2004) Evidence for ocean water invasion into the Chicxulub crater at the cretaceous/tertiary boundary. *Meteor Planet Sci* 39:1233–1247
- Grady MM, Hutchinson R, McCall GJH, Rothery DA (eds) (1998) Meteorites: flux with time and impact effects. *Geol Soc London Sp Publ* 140
- Grieve RAF (2003) Extraterrestrial triggers for resource deposits. *Ext Abs Appl Earth Sci* 112(2): B145–B147
- Grieve RAF, Masaitis VL (1994) The economic potential of terrestrial impact craters. *Int Geol Rev* 36:105–151
- Grieve RAF, Theriault A (2000) Vredefort, Sudbury and Chicxulub: three of a kind? *Annu Rev Earth Planet Sci* 28:305–338
- Hayward CL, Reimold WU, Robb LJ, Gibson RL (2003) The Witwatersrand gold deposit, South Africa: an impact-modified metamorphosed placer. In: McDonald I, Annel AE, Bevins RE, Boyce AJ, Brabham PJ, Butler IB, Herrington RJ, Polya DA (eds), *World Class Mineral Deposits, Extended Abstracts, The Geological Society's 2003 Fermor Flagship Meeting*, B147–B148
- Hildebrand AR, Pilkington M (2002) Crater floor exhalative (Crafex) sulphide deposits at the Chicxulub crater, Yucatan, Mexico. *Lunar Planet Sci XXXIII*:2031
- Hough RM, Gilmour I, Pillinger CT, Arden JW, Glikes KWR, Yuan J, Milledge HJ (1995) Diamond and silicon carbide of impact melt rock from the Ries crater. *Nature* 378:41–44
- Iasky R, Mory AJ, Blundell K (2001) The geophysical interpretation of the Woodleigh impact structure, southern Carnarvon Basin, Western Australia. *Geol Surv West Aust Report* 79
- Johansson Å (1984) Geochemical studies on the Boda Pb-Zn deposit in the Siljan astrobleme, central Sweden. *Geol Fören Stockh Förh* 106:15–25
- Johnson GI (1991) The petrology, geochemistry and geochronology of the felsic alkaline suite of the eastern Yilgarn block, Western Australia: PhD thesis (unpublished), University of Adelaide, p 192
- Kirschner CE, Grantz A, Mullen MW (1992) Impact origin of the Avak structure, Arctic Alaska and genesis of the Barrow gas fields. *Am Ass Petrol Geol Bull* 76:651–679
- Koeberl C, Henkel H (eds) (2005) *Impact tectonics*. Springer, Berlin, 552pp
- Koeberl C, Fredrikson K, Göttinger M, Reimold WU (1989) Anomalous quartz from the Roter Kamm impact crater, Namibia: evidence for post impact hydrothermal activity? *Geochim Cosmochim Acta* 53:2113–2118
- Koeberl C, Masaitis VL, Shafranovsky GI, Gilmour I, Langenhorst F, Schrauder M (1997) Diamonds from the Popigai impact structure, Russia. *Geology* 25:967–970
- Komor SC, Valley JW, Brown PE (1988) Fluid-inclusion evidence for impact heating at the Siljan Ring, Sweden. *Geology* 16:711–715
- Kring DA (1995) The dimension of the Chicxulub impact crater and impact melt sheet. *J Geophys Res* 100:16 979–16 989
- Law JDM, Phillips GN (2005) Hydrothermal replacement model for Witwatersrand gold. *Econ Geol* 100th Ann Vol: 799–811
- Lightfoot P (2016) *Nickel sulfide ores and impact melts – origin of the Sudbury Igneous Complex*. Elsevier, Amsterdam, 662pp
- Lüders V, Rickers K (2004) Fluid inclusion evidence for impact-related hydrothermal fluid and hydrocarbon migration in Cretaceous sediments of the ICDP-Chicxulub drill core Yax-1. *Meteor Planet Sci* 39:1187–1198
- Macdonald FA, Bunting JA, Cina SE (2003) Yarrabubba – a large, deeply eroded impact structure in the Yilgarn Craton, Western Australia. *Earth Planet Sci Lett* 213:235–247

- Masaitis VL, Naumov MV (1993) Puchezh-Katunki impact crater: preliminary model of hydrothermal circulation system. *Meteor* 7:390–391
- McCarville P, Crossey LJ (1996) Post-impact hydrothermal alteration of the Manson impact structure. *Geol Soc Am Sp Pap* 302:347–379
- Melosh HJ (1989) *Impact cratering – a geologic process*. Oxford University Press, Oxford, 246pp
- Molnár F, Watkinson DH, Jones PC (2001) Multiple hydrothermal processes in footwall units of the North Range, Sudbury Igneous Complex, Canada, and implications for the genesis of vein-type Cu-Ni-PGE deposits. *Econ Geol* 96:1645–1670
- Mory AJ, Iasky RP, Glikson AY, Pirajno F (2000) Woodleigh, Carnarvon Basin, Western Australia: a new 120 km-diameter impact structure. *Earth Planet Sci Lett* 177:119–128
- Mory AJ, Pirajno F, Glikson AY, Coker J (2001) GSWA Woodleigh 1, 2, and 2A well completion report: Woodleigh impact structure, Southern Carnarvon Basin, Western Australia. *Geol Surv West Aust Record* 2001/6
- Naldrett AJ (2002) From impact to riches: evolution of geological understanding as seen at Sudbury, Canada. *GSA Today* 13:4–10
- Naumov MV (1993) Zonation of hydrothermal alteration in the central uplift of the Puchezh-Katunki astrobleme. *Meteoritics* 28:408–409
- Naumov MV (2002) Impact-generated hydrothermal systems: data from Popigai, Kara and Puchezh-Katunki impact structures. In: Plado J, Pesonen LJ (eds) *Impacts in precambrian shields*. Impact studies series. Springer, Berlin, pp 117–171
- Nelson DR (1999) Compilation of geochronology data 2000. *Geol Surv West Aust Record* 1999/2
- Newsom HE (1980) Hydrothermal alteration of impact melt sheets with implications for Mars. *Icarus* 44:207–219
- Newsom HE, Graup G, Sowards T, Keil K (1986) Fluidization and hydrothermal alteration of the suevite deposit at the Ries Crater, West Germany, and implications for Mars. *J Geophys Res* 91: E239–E251
- Osinski GR, Spray JG, Lee P (2001) Impact-induced hydrothermal activity within the Haughton impact structure, arctic Canada: generation of a transient, warm, wet oasis. *Meteor Planet Sci* 36:731–745
- Pevzner LA, Kirjakov AF, Vorontsov AK, Masaitis VL, Mashchak MS, Ivanov BA (1992) Vorotilovskaya drillhole; first deep drilling in the central uplift of large terrestrial impact crater. 23rd Lunar Planetary Science Conference, Houston, Abstract volume, pp 1063–1064
- Phillips GN (1987) Metamorphism of the Witwatersrand gold fields: conditions during peak metamorphism. *J Meta Geol* 5:307–322
- Phillips GN (1988) Widespread fluid infiltration during metamorphism of the Witwatersrand gold fields: generation of chloritoid and pyrophyllite. *J Metamorph Geol* 6:311–332
- Phillips D, Onstott TC, Harris JW (1989) $^{40}\text{Ar}/^{39}\text{Ar}$ laser-probe dating of diamond inclusions from the Premier kimberlite. *Nature* 340:460–462
- Pirajno F (2000) *Ore deposits and mantle plumes*. Kluwer Academic Publ, Dordrecht
- Pirajno F (2002) Geology of the Shoemaker impact structure, Western Australia. *Geol Surv West Aust Rep* 82
- Pirajno F (2005) Hydrothermal processes associated with meteorite impact structures: evidence from three Australian examples and implications for economic resources. *Aust J Earth Sci* 52:587–620
- Pirajno F (2009) *Hydrothermal processes and mineral systems*. Springer, Dordrecht, p 1250
- Pirajno F, Glikson AY (1998) Shoemaker impact structure, Western Australia. *Celest Mech Dyn Astron* 69:25–30
- Pirajno F, Van Kranendonk MJ (2005) Review of hydrothermal processes and systems on Earth and implications for martian analogues. *Aust J Earth Sci* 52:329–352
- Pirajno F, Hawke P, Glikson AY, Haines P, Uysal T (2003) Shoemaker impact structure, Western Australia. *Aust J Earth Sci* 50:775–796
- Puura V, Kärki A, Kirs J, Kirsimäe K, Kleesment A, Konsa M, Niin M, Plado J, Suuroja K, Suuroja S (2000) Impact-induced replacement of plagioclase by K-feldspar in granitoids and

- amphibolites at the Kärđla Crater, Estonia. In: Gilmour I, Koeberl C (eds) *Impacts and the early Earth*. Springer, Berlin, pp 417–445
- Puura V, Koeberl C, Kärki A, Juvonen R, Konsa Plado JM, Suuroja K, Kirs J, Huber H (2002) Geochemistry of K-enriched impactites, based on drillings into the Kärđla Crater, Estonia. *Geol Soc Am Abs with Programs*, Denver, Oct. 2002, p 341
- Reimold WU (1995) Impact cratering – a review, with special reference to the economic importance of impact structures and the southern African impact crater record. *Earth Moon Planets* 70:21–45
- Reimold WU, Gibson RL (1999) Geology and evolution of the Vredefort impact structure, South Africa. *J Afr Earth Sci* 23:125–162
- Reimold WU, Gibson RL (2005) Meteorite impact! The danger from space and South Africa's mega-impact – the Vredefort structure. Chris van Rensburg Publ Pty Ltd, Johannesburg
- Reimold WU, Koeberl C, Fletcher P, Killick AM, Wilson JD (1999) Pseudotachylite breccias from fault zones in the Witwatersrand Basin, South Africa: evidence of autometasmatism and post-brecciation alteration processes. *Miner Petr* 66:25–53
- Reimold WU, Koeberl C, Hough R, McDonald I, Bevan A, Amare K, French BM (2003) Woodleigh impact structure: shock petrography and geochemical studies. *Meteor Planet Sci* 7:1109–1130
- Reimold WU, Koeberl C, Gibson RL, Dressler BO (2005) Economic mineral deposits in impact structures: a review. In: Koeberl C, Henkel H (eds) *Impact tectonics*. Springer, Berlin, pp 479–552
- Rowe AJ, Wilkinson JJ, Coles BJ, Morgan JV (2004) Chicxulub: testing for post-impact hydrothermal input into the Tertiary ocean. *Meteor Planet Sci* 39:1223–1231
- Scrimgeour IR, Close DF, Edgoose CJ (1999) Peterman ranges SG52–7 explanatory notes. Northern Territory Geol Surv Dept Mines and Energy
- Smithies RH, Champion DC (1999) Late Archean felsic alkaline igneous rocks in the Eastern Goldfields, Yilgarn Craton, Western Australia: a result of lower crustal delamination? *J Geol Soc Lond* 156:561–579
- Sturkel FF, Broman C, Forsberg P, Torsander P (1998) Impact-related hydrothermal activity in the Lockne impact structure, Jämtland, Sweden. *Eur J Miner* 10:589–609
- Tyler IM (2005) Australia: Proterozoic. In: Selley RC, Cocks LRM, Plimer IR (eds) *Encyclopedia of geology*, vol 1. Elsevier, Oxford, pp 208–221
- Uysal IT, Golding S, Glikson AY, Mory M, Glikson M (2001) K-Ar evidence from illitic clays of a Late Devonian age for the 120 km diameter Woodleigh impact structure, southern Carnarvon Basin, Western Australia. *Earth Planet Sci Lett* 192:281–289
- Uysal IT, Golding S, Glikson AY, Mory M, Glikson M, Iasky RP, Pirajno F (2002) Reply to Comment on: K-Ar evidence from illitic clays of a Late Devonian age for the 120 km diameter Woodleigh impact structure, southern Carnarvon Basin, Western Australia. *Earth Planet Sci Lett* 201:253–260
- Wingate MTD, Pirajno F, Morris PA (2004) Warakurna large igneous province: a new Mesoproterozoic large igneous province in west-central Australia. *Geology* 32:105–108
- Witt WK, Davy R (1997) Geology and geochemistry of Archaean granites in the Kalgoorlie region of the Eastern Goldfields, Western Australia: a syn-collisional tectonic setting? *Precamb Res* 83:133–183
- Zürcher L, Kring DA (2004) Hydrothermal alteration in the core of the Yaxcopoil-1 borehole, Chicxulub impact structure, Mexico. *Meteor Planet Sci* 39:1199–1222

Index

A

- Acid rain, 10
- Acraman impact structure, 84–85
- Adelaide rift complex (ARC), 55
- Aegirine-augite
 - and albite, orthoclase, 191
 - crystal, 191
 - and quartz, orthoclase, 191
- Age vs. diameter of global impact structures, 16
- Albany-Fraser belt, 138
- Albany Fraser high-grade metamorphic terrain, 149
- Albite, 176
 - aegirine-augite and, 191
- Alkali metasomatism, 175–176, 187, 196
- Alkaline rocks, of Yilgarn Craton, 192
- Alkali-rich rocks, 175
- Amadeus Basin, 95
- Amelia Creek impact structure, 91–94
- Amor class asteroids, 2
- Amphibolite facies, 185
- Amygdales, 40
- Anorthosites, 159
- Antarctic Chert Member, 33, 34
- Antarctic Creek Chert Member, 37
- Apatite
 - aegirine-augite crystal with, 191
 - crystal, 191
- Aplitic granite, 139
- Apollo class asteroids, 2
- Apollo missions (1963–1972), 10
- Arafura Basin, 111
- ARC, *see* Adelaide rift complex (ARC)
- Archaean basement rocks, 175
- Archaean crustal evolution, 161
- Archaean granitic rocks, 193
- Archaean greenstone belt, 32
 - sediments in, 13
- Archaean impacts
 - ejecta, 22–23
 - Hadean to early, 10–21
 - to proterozoic impact ejecta/fallout units and impact structures, 35–36
 - significance of, 157–166
- Archaean Pilbara Craton, 162
- Archaean-Proterozoic boundary stratigraphy, 41
- Archean Earth and geodynamic consequences, 165
- Arenite-turbidites, Bouma-type cycle, 48
- Asteroid
 - and cometary impacts, 175–176
 - compositional diversity of, 6
 - Earth-crossing, 158
 - impacts identification, criteria, 21–25
 - Near Earth asteroids (NEA), 2, 3
 - orbits, 2
 - in space and time, 1–9
 - See also* specific types of asteroid
- Asteroid belt, 4
 - origin, 5–6
- Astronomical units (AU), 2
- Aten class asteroids, 2
- AU, *see* Astronomical units (AU)
- Augathella TMI multiring feature, 137
- Auvergne, 136
- Auvergne sub-rounded depression, Earth image, 128

B

- Banded iron-formation, 115
 - of Gorge Creek Group, 40
- Barberton Greenstone Belt (BGB), 17–19, 21, 161
 - East Kaapvaal shield, South Africa, 32
 - impact spherule-bearing units (S1–S3) in, 39
 - stratigraphic units of, 34
- Barberton Mountain Land, 13
- Barangí area, geological map, 194
- Barangí Granophyre, 85, 194–196
- Basalts
 - flat-lying, 142
 - tholeiitic flood, 144
- Bedout dome, 143
- Bee Gorge, massive spherule-rich layers of east of, 50
- BGB, *see* Barberton Greenstone Belt (BGB)
- Biotite, igneous, 73
- Black chimneys, 10
- Bladed calcite, 195
- Boolgeeda Iron Formation, 114–115
- Bootheragandra Fault, 150
- Bouguer anomaly study, 66, 100
- Bouma-type cycle arenite-turbidites, 48
- Bowen Basin, 139
- Boxhole meteoritic impact crater, 116
- Breccia
 - chert, 38
 - granitic rocks, 198
 - melt, 65
 - multiple veins of, 44
 - pseudotachylite, 64
- Bunyeroo 580 Ma impact ejecta, 53–55
- Buried impact structures, 100–101
 - Gnargoo, 106
 - Lake Raeside, 109–110
 - Mount Ashmore, 107–108
 - Talundilly, 103–105
 - Tookoonooka, 104–105
 - Warburton East, 102
 - Warburton West, 102–103
 - Woodleigh, 103
 - Yallalie, 108–109
- Buried ring features, morphological and, 127–141
 - Augathella TMI multiring feature, 137
 - Calvert Hills feature, 136
 - Camooweal buried multi-ring feature, 134
 - Deniliquin-Booligal ring structure, 139, 140
 - Diamantina River circular ring, 138
 - Fiery Creek dome structure, 136
 - Fiery Creek ring feature, Queensland, 129

- Green Swamp Well TMI feature, 137
 - Herbert TMI multi-ring structure, 135
 - Ilkurka double ring structure, 135
 - Lennis triple ring TMI structure, 135
 - McLarty Hills TMI multi-ring feature, 137
 - Monte Christo ring feature, 131, 137, 141
 - Mount Moffatt ring feature, 132
 - Neale TMI multi-ring structure, 135
 - Oodjuongari TMI feature, 136
 - Pemberton TMI feature, 138
 - Renehan probable impact structure, 137
 - Skirmish ring feature, 135
 - Throssell-Roberts half-ring topography feature, 135
 - Tingha ring feature, 130, 137
 - Wessell TMI feature, 136
 - White Cliffs half-ring morphological feature, 134
 - Youngerina ring feature, 135
- Bushveld magmatism, 186

C

- Calcite crystals, 197
- Calisto, Valhalla on, 7
- Calvert Hills structure, 136, 149
- Cambrian volcanics, 144
 - Cambrian Antrim Plateau Volcanics, 90
- Camooweal, 142
 - buried multi-ring feature, 134
 - structure, 143
 - TMI ring structure, 143
- Canning basin, 143
- Carawine Dolomite (CD), 46
 - Camooweal Dolomite of Lower Cambrian, 143
 - impact, 41–46
- Carawine Dolomite spherule bearing mega-breccia (CDMB), 44
 - origin, 44
- Carbonaceous (C-type) chondrites, 4
- Carboniferous–Permian boundary, 167
- Carboniferous–Permian Cooper Basin, 70
- Camraron Basin, 74, 103, 151
- CD, *see* Carawine Dolomite (CD)
- CDMB, *see* Carawine Dolomite spherule bearing mega-breccia (CDMB)
- Cenozoic sediments, 144
- Ceres, 5
- c.3.3–3.227 Ga, impact-correlated units, 39–41
- Chert, 39, 43
 - breccia, 38
 - Marker Chert (MC), 40
- Chesapeake Bay, 68

- Chicxulub, Yucatan Peninsula (Mexico), 66–68
 impact structure, 23
- Chondritic fragments, 10
- Clay minerals, 73
- Cleanskin impact structure, 92–93, 95
- c.3460 Ma Impacts, 37–39
- c.3472 Ma Impacts, 32–37
- Cobalt, in microkrystite, 38
- Collar rocks, 185
- Cometary impacts, 175–176
- Comets, 4, 5
 Shoemaker-Levy, fragments of, 6, 7
 Wilde-2 from stardust spacecraft
 240 km-across., 6
- Continental crust estimation, 14
- Coompana structure, 151
- Corundum crystals, 201
- Cosmic dust, 10
 accretion of, 10
- Cosmic radiation, 10
- Craft's gamma-ray spectrometer, 7
- Crater, 12
 on Australian continent and continental
 shelf, 81–83
 crater diameter, 14
 crater-form features, 128
 simple, 17
See also Meteoritic impact crater
- Cretaceous–Paleocene boundary, 68
- Cretaceous sediments, 151
- Crustal metamorphism, endogenic, 18
- Crystal
 aegirine-augite, 191
 calcite, 197
 corundum, 201
 garnet, 191
- Crystal-vitroclastic suevite, 69
- C-type asteroid, 4, 8
- D**
- Dales Gorge (DGS4) c.2.48 Ga spherule layer,
 50–53
- Darwin meteoritic impact crater, 112–113
- Deniliquin-Booligal ring structure (D-B ring
 structure), 139, 140, 150
 TMI ring structure, 150
- Deposits, *see specific types of deposits*
- Devonian sandstone, 113
- Diamantina River circular ring, 138
- Diamantina River drainage feature, 132–134
- Diamictite, tsunami-generated, 38
- Dolomite, 10
- Dome
 Bedout dome, 143
 features, distribution pattern, 152–154
 Fiery Creek dome structure, 136
 Mount Ashmore dome, 142, 151
 orogenic belts, 21
 Plutonic ring and dome structure, 125
 seismic, 151
 Upheaval Dome, Utah, 17
 Vredefort Dome, South Africa, 184, 185
- Duffer Formation, 33
- E**
- Earaheedy Basin, 188
- Early Neoproterozoic Townsend Quartzite, 135
- Earth
 Late Heavy Bombardment impact on, 13
 Late Heavy Bombardment of, 10, 14
 Near Earth asteroids (NEA), 2, 3
 surface, 9
- Earth-crossing asteroids, 158
- Earth Impact Database, 14
- Earth–Moon system, 11, 13, 152
- Eastern Hamersley Basin, geological map, 45
- Eastern Transvaal, Barberton Greenstone Belt
 (BGB), 32
- Eastern Warburton Basin, 71, 102
- East Hamersley Basin, 44
- East Kaapvaal shield (South Africa), Barberton
 Greenstone Belt (BGB), 32
- Ediacaran palynomorphs, 55
- Electron-microprobe (EMP), 38
- Endogenic crustal metamorphism, 18
- Epigenetic deposits, 179
- Epithermal system, volcanic, 177
- Eromanga Basin, 149
- Eros, 7
- Eucla Basin, 151
- European Space Agency's probe, 8
- Explosion-type craters, 14
- F**
- Feldspar granite, leucocratic alkali, 190
- Feldspar-hosted planar deformation features, 73
- Felsic hypabyssal rocks, 159
- Felsic igneous rocks, 10
- Felsic volcanics, 159
- Fe-rich spherule rims, 38
- Ferruginous sediments, 22–23
- Ferruginous shale (FS), 20
- Ferruginous siltstone (FS), 40

Fiery Creek structure, Queensland, 129, 136
 Fire layer, turbidites, 49
 Flat-lying basalts, 142
 Fragmental deposits, 20
 Frere Formation, 193

G

Garnet crystal, 191
 Geological antiquity, of Australian land surfaces, 127
 Geophysical anomalies, in Warburton West Basin, 102–103
 Geophysical multi-ring features, 150–152
 Georgina Basin, 143
 Giant gold deposits, 174
 Glikson impact structure, 93–94, 96
 Globotruncana contusa, 68
 Gnargoo impact structure, 23, 106, 151
 Gneissic rocks, 184
 Goat Paddock meteoritic impact crater, 110, 111
 Gold Creek Volcanics, 149
 Gold deposits, 174
 Gorge Creek Group, 40
 banded iron formation of, 40
 Gosses Bluff impact structure, 94–97, 158, 167
 Goyder impact structure, 100, 101
 Granite
 aplitic, 139
 leucocratic alkali feldspar, 190
 Yarrabubba Granite, 195, 197
 See also Teague Granite
 Granite-greenstone rocks, of Yilgarn Craton, 193
 Granitic rocks, 184, 188
 Archaean, 193
 brecciated, 198
 shocked, 194
 Gravity ring anomalies, magnetic and, 141–150
 Gravity, total magnetic intensity and, 141–142
 Greenstone rocks, 188
 Greenstone xenoliths, 191
 Green Swamp Well TMI feature, 137
 Gregarious batholiths, 161

H

Hadean, to early Archaean impacts, 10–21
 Hayabusa spacecraft, 7
 Heat engine, 201–202
 Henbury meteoritic impact crater, 117
 Herbert structure, 144

Hickman meteoritic impact crater, 114–115
 High-pressure minerals, stability curves for, 18
 Hydrothermal activity
 impact-related, 186–187
 stages, 175
 Hydrothermal alteration, 190–193, 201
 Hydrothermal circulation, 174–176, 186
 Hydrothermal fluid, 176
 Hydrothermal fluid flow, 174, 176, 184
 effects of, 174
 in impact structure, model, 177
 Hydrothermal ores, 179
 deposits, 201
 Hydrothermal pods, 193
 Hydrothermal replacement model, 184
 Hydrothermal system, 174
 activity of, 178
 Sudbury, 180–181
 working model, 176–178
 Hypervelocity impacts, 174

I

ICPMS, *see* Inductively Coupled Plasma Mass Spectrometry (ICPMS)
 Igneous biotite, 73
 Igneous rocks, felsic, 10
 Ilkurka double ring structure, 135
 Illitic clays, 199
 Impact origin
 ring, dome and crater structures of
 unknown, possible/ probable,
 145–148
 structural elements of circular features
 suggestive of, 124–127
 Impact-related hydrothermal activity, 186–187
 Impact structures, 80–83
 Acraman, 84–85
 Amelia Creek, 91–94
 Cleanskin, 92–93, 95
 Glikson, 93–94, 96
 Gosses Bluff, 94–97
 Goyder, 100, 101
 Kelly West, 97–99
 Lawn Hill, 88–91
 mineral deposits and, 178–179
 Shoemaker, 86–89
 spider, 99–100
 Strangways, 89–92
 Yarrabubba, 85–87
 See also Buried impact structures
 Inductively Coupled Plasma Mass Spectrometry (ICPMS), 38

- Iron formation, 40
 Isotopes, Sm–Nd, 14
 Isotopic U–Pb zircon age frequency distribution, 160
- J**
 Jeerinah c.2.63 Ga impact layer (JIL), 41–46
 Jupiter
 comet Shoemaker-Levy 9 fragments impacting, 6, 7
 moons, 7
 Jurassic–Cretaceous Eromanga basin, 133
- K**
 Kaapvaal Craton, sediments in, 17
 Kalgoorlie greenstone belt, 162
 Kelly West impact structure, 97–99
 K-feldspar, 34, 53, 61, 176, 195–197
 Kinetic energy
 conversion to thermal energy, 174
 transformation of, 174
- L**
 Lake Raeside impact structure, 109–110
 Lamellae
 metamorphic deformation, 24
 planar deformation features in quartz, 24, 25
 Laptev Sea, 68
 Large geophysical multi-ring features, 150–152
 Late Heavy Bombardment (LHB), 157
 of Earth, 10, 14
 effects of, on Moon, 159
 impact on Earth, 13
 Lunar post, 14
 Lawn Hill impact structure, 88–91
 Leilira formation, 40
 Lennis triple ring TMI structure, 135
 Leucocratic alkali feldspar granite, 190
 LHB, *see* Late Heavy Bombardment (LHB)
 Liverpool meteoritic impact crater, 110–112
 Lockne impact structure, 181–182
 Lucas/Yam Hill, Western Australia, 133, 141
 Lunar craters, 10
 Lunar impact history, 12
 Lunar post-Late Heavy Bombardment (LHB), 14
 Lutetia, Rosetta’s OSIRIS images of, 8
- M**
 Maastrichtian–Danian boundary, 68
 Maastrichtian sediments, 68
 Mafic rocks, 185
 Mafic volcanics effect, 151
 Mafic volcanism, 20
 Magmatic biotite, 201
 Magmatic-hydrothermal stage, 176
 Magmatism, Bushveld, 186
 Magnetic and gravity ring anomalies, 141–150
 Magnetic anomalies
 in Warburton East Basin, 72, 102–103
 in Warburton West Basin, 102–103
 Magnetic Gold Creek Volcanics, 149
 Maniitsoq, South Greenland, 61–62
 Mantle thermal events model, 160
 Marble Bar Chert Member (MBCM), 37, 38
 Marble Bar greenstone belt, stratigraphy and isotopic ages of, 34
 Mare basins, 12
 Mare Orientale, on Moon, 8
 Marker Chert (MC), 40
 Mars
 impact structures on, 7
 surface, 9
 MBCM, *see* Marble Bar Chert Member (MBCM)
 McArthur Basin, 89, 100, 111, 149
 McLarty Hills TMI multi-ring feature, 137
 MDL/Qz, *see* Metamorphic Deformation Lamellae (MDL/Qz)
 Mega-breccia
 outcrops, 69
 tsunami, 41–46
 Mega-clasts, 52
 Melt breccia, 65, 90
 Melt fraction, 90
 Melt rock, 64
 Melt sheet, 193, 201–202
 Mercury
 cratered surface of, 8
 surface, 9
 Mesoproterozoic rocks, 149
 Mesoproterozoic sediments, 89
 Mesozoic rocks, 108
 Metallic (M-type) asteroid, 4
 Metamorphic Deformation Lamellae (MDL/Qz), 24
 Metamorphism, 14, 184
 endogenic crustal, 18
 shock, 64, 179
 of Vredefort Dome, 185
 Metasomatic process, 174
 Metasomatism, alkali, 175–176, 187, 196
 Metavolcanic rocks, 40

- Meteoritic impact crater, 110
 Boxhole, 116
 Darwin, 112–113
 Goat Paddock, 110, 111
 Henbury, 117
 Hickman, 114–115
 Liverpool, 110–112
 Wolfe Creek, 113–114
- Microbreccia, multiple veins of, 44
- Microkrystite, 25
 cobalt levels in, 38
 impact spherule, 19, 38
 nickel levels in, 38, 42–43
 of spherule marker bed, 48
- Microkrystite spherule, 34, 42
 in chert and arenite intercalations, 37
 layer of, 41
 rich sediments, 50
- Millimetre-scale spherulitic textures, 50
- Mineral deposits
 distribution of, 180
 and impact structures, 178–179
 progenetic, 178
 Sudbury, 174
- Mineral system, Witwatersrand gold,
 182–186
- Missionary Plain syncline, 167
- Monte Christo ring feature, 131,
 137, 141
- Moon
 asteroid bombardment of, 157
 effects of Late Heavy Bombardment on, 159
 face of, 11
 Mare Orientale on, 8
 stratigraphy of, 12
 surface, 9
- Mount Ada Basalt, 33
- Mount Ashmore dome, 142, 151
- Mount Ashmore impact structure, 23, 107–108,
 126
- Mount Davies combined TMI and shuttle radar
 image, 136
- Mount Moffatt Carnarvon National Park,
 Queensland, 141
- Mount Moffatt ring feature, 132
- M-type asteroid, 4, 8
- Mulkara feature, 149
- Multi-ring features
 Augathella TMI mul-tiring feature, 137
 Camooweal buried, 134
 geophysical, 150–152
 McLarty Hills TMI, 137
- MVT type sulphide deposits, 178
- N**
- Nanobes, 10
- NASA
 Deep Impact probe, 7–8
 global map, 15
 Lunar events, 12
 wide-field infrared survey explorer (WISE),
 3
- NEA, *see* Near Earth asteroids (NEA)
- Neale ring structure, 144
- Neale TMI circular feature, 144
- Neale TMI multi-ring structure, 135
- Near Earth asteroids (NEA), 2, 3, 5
- NEAR Shoemaker mission, 6–7
- Neoproterozoic Bullo River Sandstone, 136
- NEOWISE project, 3
- Nickel, in microkrystite, 38, 42–43
- O**
- Olistostrome, 40
- Onaping Formation, 65, 180
- Oodjuongari structure, 144
- Oodjuongari TMI feature, 136
- Oort cloud, 1, 5
- Orbits, asteroid, 2
- Ore deposits, hydrothermal, 201
- Ore minerals, 178
- Orogenic belts domes, 21
- Orthoclase
 aegirine-augite and albite, 191
 aegirine-augite and quartz, 191
 phenocryst, 191
- P**
- Palaeo-placer deposit, 182
- Palaeo-placer model, 183
- Palaeoproterozoic Earraheedy Basin, 188
- Palaeoproterozoic Gumarrimbang Sandstone,
 110–111
- Paleoarchean asteroid impact, 39
- Palynomorphs, Ediacaran, 55
- Paraburdoo c. 2.57 Ga spherule layer (PSL),
 46–47
- PDF, *see* Planar deformation features (PDF)
- PDF/Qz, *see* Planar deformation features in
 quartz (PDF/Qz)
- Pemberton feature, 149
- Pemberton TMI feature, 138
- Penokean orogeny, 65
- Permian Pedirka Basin, 70
- Permian–Triassic Galilee basin, 133

PGE, *see* Platinum Group Element (PGE)
 Phanerozoic impacts, significance of, 166–167
 Phenocryst, orthoclase, 191
 Pilbara Craton, Western Australia, 19–20, 153, 160
 geological sketch map of, 33
 olistostrome and banded iron formations, 40
 sediments in, 17
 temporal gaps between stratigraphic units in, 163–164
 Pilbara granite-greenstone Craton, 32
 Pincunah Hill Formation, 162
 Plagioclase melting, 61
 Planar deformation features (PDF), 13, 21, 43, 61, 70, 195
 feldspar-hosted, 73
 Planar deformation features in quartz (PDF/Qz), 24
 lamellae, 24, 25
 Planets surfaces, 9
 Platinum Group Element (PGE), 49
 Pliocene lacustrine sediments, 109
 Plutonic granitic activity, 20
 Plutonic ring and dome structure, 125
 Plutons, tonalite-trondhjemite-granodiorite, 161
 Poolwana Basin, 72
 Popigai impact-formed diamonds, 179
 Popigai, Siberia, 68–70
 Post-LHB asteroids, 14
 Precambrian cratons, 127
 Precambrian tectono-thermal events, 161
 Principal Lunar craters, 10–11
 Procellarum region, 11
 Progenetic mineral deposits, 178
 Proterozoic age, for Yarrabubba, 195
 Proterozoic impacts, significance, 166–167
 Proterozoic impact structure, 153
 Proterozoic Kimberley Basin, 110
 Proterozoic Pentecoste Formation, 99
 Pseudotachylite, 64, 195
 breccia, 64
 Pseudotachylite veinlet (PV), 200
 PSL, *see* Paraburdo c. 2.57 Ga spherule layer (PSL)
 Puchezh-Katunki 80-km diameter impact crater, 175, 178
 PV, *see* Pseudotachylite veinlet (PV)
 Pyroclastic rocks, 40
 Pyrolite model, 49

Q
 Quartz syenite, 192–193
 Quiet Zone, 48

R

Radiation, cosmic, 10
 Renhan probable impact structure, 137, 142–143
 Rhyolite, 114
 Rhythmic turbidites, 48
 Ries crater, 179
 Ries impact structure, 175
 Ring features
 distribution patterns of, 152–154
 Monte Christo ring feature, 131, 137, 141
 Mount Moffatt ring feature, 132
 Skirmish ring feature, 135
 Tingha ring feature, 130, 137
 Youngerina ring feature, 135
 See also Buried ring features; Multi-ring features
 Rocks
 alkaline, 192
 alkali-rich, 175
 collar, 185
 felsic hypabyssal, 159
 felsic igneous, 10
 granitic, 188, 193
 brecciated, 198
 greenstone, 188
 melt, 64
 mesoproterozoic, 149
 mesozoic, 108
 metavolcanic, 40
 pyroclastic, 40
 shattered target, 176
 shocked granitic, 194
 syenitic, 192, 195
 volcanic, 39
 Vredefort granitic, 64
 Witwatersrand, 182
 See also specific types of rocks
 Rosetta (spacecraft), 8

S

Sedimentary strata, 23
 Sediments
 in Archaean greenstone belts, 13
 cretaceous, 151
 ferruginous, 22–23
 in Kaapvaal Craton, 17
 Maastrichtian, 68
 in Pilbara Craton, 17
 See also specific types of sediments
 Seismic dome, 151
 Seismic markers, 126
 Seismic tomography anomalies, 101

- Seismic velocity tomography, Warburton twin impacts, 71
- Seismic zone, turbidites, 49
- Shatter cones, 64, 65, 91, 97
- Shattered target rocks, 176
- Sheridan Creek circular structure, 149
- Shocked granitic rocks, 194
- Shock metamorphism, 64, 179
- Shock-thermal alteration, 201
- Shoemaker impact structure, 23, 86–89, 187–190, 193
- Shoemaker-Levy comet, fragments of, 6, 7
- SIAL crustal models, 158
- SIC, *see* Sudbury igneous complex (SIC)
- Siderophile elements, 49
- Silicate minerals, 7
- Siliceous (S-type) asteroid, 4, 7
- Silicification, 190, 193
- Skirmish ring feature, 135
- SMB, *see* Spherule marker bed (SMB)
c. 2.56 Ga Layer
- Sm–Nd isotopes, 14
- Solar disc, 1
- Solar nebula, chondritic fragments and cosmic dust in, 10
- Solar system, formation, 2
- Solar wind, 7
- Southern Carnarvon Basin, 106
- Space and time, asteroids in, 1–9
- Spherule, 18, 38
microkrystite (*see* (Microkrystite spherule))
- Spherule layer
Dales Gorge (DGS4) c.2.48 Ga, 50–53
Paraburdoo c. 2.57 Ga, 46–47
- Spherule marker bed (SMB) c. 2.56 Ga Layer, 47–50
- Spider impact structure, 23, 99–100
- SSG, *see* Sulphur Springs Group (SSG)
- Steen River impact structure, Canada, 179
- Strangways impact structure, 89–92
- S-type asteroid, 4, 7
- Sudbury hydrothermal system, 180–181
- Sudbury igneous complex (SIC), 65, 66, 179–181
- Sudbury impact structure, 180
geological sketch map of, 65
- Sudbury mineral deposits, 174
- Sudbury, Ontario, 65–66
- Suevite, 65
- Sulphides, 199
- Sulphur Springs area, Pilbara Craton, 40
- Sulphur Springs Group (SSG), 39, 40
- Surfaces, planets, 9
- Syenite, 190–193
- Syenitic rocks, of Teague Granite, 192, 195
- Syngenetic deposits, 179
- T**
- Table Hill Volcanics, 144
- Tagamite, 69
- Talundilly impact structure, 23, 103–105
- Tanami East impact structure, 127, 136
- Teague Granite, 86–87, 89, 188, 190
chemistry of, 192
greenstone enclaves in, 191
mineral assemblages and a tentative paragenetic sequence of, 192
mineralogical assemblages of, 191
REE patterns of, 192
silicification of, 190
syenitic rocks of, 192, 195
- Teague impact structure, 86–88
- Thermal effects, 174
- Thermal energy, 174
- Tholeiitic flood basalts, 144
- Throssell-Roberts half-ring topography feature, 135
- Tingha ring feature, 130, 137
- Titanite crystal, 191
- Tonalite-trondhjemite-granodiorite (TTG) plutons, 161
- Tookoonooka impact structure, 104–105, 179
- Total Magnetic Intensity (TMI) anomalies, 141, 144
Camooweal TMI ring structure, 143
and gravity, 141–142
Neale TMI circular feature, 144
ring structure, 150
surveys, 100
- Transmission electron microscopy (TEM), PDF/Qz lamellae, 24, 25
- Transvaal Supergroup, 185
- Triassic Simpson Basin, 70
- Trojan asteroid belt, 1
- Tsunami
deposits, 20
layer, turbidites, 49
megabreccia, 41–46
origin of spherule marker bed, 48
- Tsunami-generated diamictite, 38
- Tsunami zone (TZ), 48
- Turbidites
fire layer, 49
seismic zone, 49
tsunami layer, 49
- TZ, *see* Tsunami zone (TZ)

U

- Umbrian Apennines, Italy, 68
- Upheaval Dome, Utah, 17
- Uplift, 23
 - of impact structures, 125

V

- Valhalla, on Calisto, 7
- Venus, surface, 9
- Vesta, 5
- Victoria Basin, 136
- Volcanics, 22–23
 - Cambrian, 144
 - Cambrian Antrim Plateau Volcanics, 90
 - epithermal systems, 177
 - felsic, 159
 - Gold Creek Volcanics, 149
 - Mafic, 151
 - Magnetic Gold Creek Volcanics, 149
 - rock, 39
 - Table Hill Volcanics, 144
 - terranes, 181
 - varioles, 40
- Volcanism, mafic, 20
- Vredefort, South Africa, 62–64
 - dome, 184, 185
 - granitic rocks, 64
 - meteorite impact structure, 182–186
 - Vredefort Granophyre, 63–64

W

- Warburton East Basin
 - impact structure, 102
 - magnetic anomalies in, 72, 102–103
- Warburton impact structure, 167
- Warburton Twin Structures, South Australia, 70–73

Warburton West Basin, 72

- impact structure, 102–103
- magnetic anomalies in, 102–103
- Wessell TMI feature, 136
- White Cliffs
 - Earth image, 126
 - half-ring morphological feature, 134
- Wide-field infrared survey explorer (WISE), 3
- Windinie Hills, 125
- WISE, *see* Wide-field infrared survey explorer (WISE)
- Wittenoom formation, 47
- Witwatersand Basin, South Africa, 63, 182–184
- Witwatersand Gold, South Africa, 182–186
- Witwatersand rocks, 182
- Witwatersand Supergroup, 182
- Wolfe Creek meteoritic impact crater, 113–114
- Woodleigh Formation, 197, 198
- Woolleigh impact structure, 23, 24, 73–75, 103, 126, 151, 166, 187, 197–201
- Woongarra Rhyolite, 115

Y

- Yallalie impact structure, 108–109
- Yarrabubba Granite, 195, 197
- Yarrabubba impact structure, 85–87, 187, 193–197
- Yarrabubba, Proterozoic age for, 195
- Yelma Formation, 193
- Yilgarn Craton, 160
 - alkaline rocks of, 192
 - granite-greenstone rocks of, 193
- Youngerina ring feature, 135

Z

- Zn-Cu-Pb massive sulphides deposits, 179–181